TESIS DE LA UNIVERSIDAD DE ZARAGOZA

2025 160

Ana Cristina Millán Placer

Investigating the molecular mode of action of new series of antituberculosis compounds and the role of the Tap efflux pump in persistence and drug tolerance in mycobacteria

Director/es
Ramon Garcia, Santiago
Aínsa Claver, José Antonio

ISSN 2254-7606

Prensas de la Universidad Universidad Zaragoza

Universidad de Zaragoza
Servicio de Publicaciones

ISSN 2254-7606

Universidad Zaragoza
1542

Tesis Doctoral

INVESTIGATING THE MOLECULAR MODE OF ACTION OF NEW SERIES OF ANTITUBERCULOSIS COMPOUNDS AND THE ROLE OF THE TAP EFFLUX PUMP IN PERSISTENCE AND DRUG TOLERANCE IN MYCOBACTERIA

Autor

Ana Cristina Millán Placer

Director/es

Ramon Garcia, Santiago
Aínsa Claver, José Antonio

UNIVERSIDAD DE ZARAGOZA
Escuela de Doctorado

Programa de Doctorado en Bioquímica y Biología Molecular

2023

FACULTAD DE MEDICINA

Departamento de Microbiología, Pediatría, Radiología y Salud Pública

Investigating the molecular mode of action of new series of antituberculosis compounds and the role of the Tap efflux pump in persistence and drug tolerance in mycobacteria

Memoria para optar al grado de Doctor presentada por:

Ana Cristina Millán Placer

Graduada en Biotecnología

Directores:

José Antonio Aínsa Claver

Santiago Ramón-García

Esta tesis doctoral ha sido elaborada en el Departamento de Microbiología, Pediatría, Radiología y Salud Pública de la facultad de Medicina en la Universidad de Zaragoza, dentro del Programa de Doctorado en Bioquímica y Biología Molecular, habiendo sido Ana Cristina Millán Placer beneficiaria de un contrato para la Formación de Profesorado Universitario (FPU) concedido por el Ministerio de Universidades del Gobierno de España (Referencia: FPU 17/01812).

El trabajo ha sido realizado bajo el marco del proyecto de investigación "El fenotipo silente de *Mycobacterium tuberculosis:* persistencia y latencia", con referencia SAF2017-84839-C2-1-R y financiado por el Ministerio de Economía, Industria y Competitividad del Gobierno de España, y de un acuerdo de colaboración entre la Universidad de Zaragoza y la Universidad de British Columbia (Vancouver, Canadá) junto con el "*Center for Drug Research and Development*" (actualmente AdMare BioInnovations) en Vancouver, Canadá.

Parte de los estudios de granuloma incluidos en el Capítulo 2 se han llevado a cabo en una estancia de tres meses realizada en el Swiss Tropical and Public Health Institute (SwissTPH) de Basilea (Suiza), financiada por una beca para estancias de corta duración de la Organización Europea de Biología Molecular (EMBO, referencia 9199).

Agradecer el uso del Servicio General de Apoyo a la Investigación-SAI de la Universidad de Zaragoza y la contribución de los Servicios Científico Técnicos del Instituto Aragonés de Ciencias de la Salud.

INDEX

CHAPTER 2: Evaluation of the activity of butyrophenones and the role of the Tap efflux pump in mycobacteria

Index of figures

Index of tables

List of abbreviations

ABC	Adenosine triphosphate (ATP)-binding cassette
Abs	Absorbance
ADC	Albumin dextrose catalase
ADME	Absorption, distribution, metabolism and excretion
Ag85	Antigen 85
AMK	Amikacin
Amp	Ampicillin
BAC	Bacterial Artifical Chromosome
BCCM	Belgian Co-ordinated Collection of Microorganisms
BCG	Bacilli Calmette-Guérin
BDQ	Bedaquiline
BiNGO	Biological Networks Gene Ontology
bp	base pair
BPaL	Bedaquiline-pretomanid-linezolid
BPaLM	Bedaquiline-pretomanid-linezolid-moxifloxacin
BPD	Bromperidol
BSL	Biosafety Level
BWA	Burrows-Wheeler Aligner
CaMH	Cation-adjusted Müller-Hinton
CaMHB	Cation-adjusted Müller-Hinton broth
CCCP	Carbonyl Cyanide 3-Chlorophenylhydrazone
CDRD	Centre for Drug Research and Development
CF	Cystic fibrosis
CFU	Colony Forming Unit
CFX	Cefadroxil
CFZ	Clofazimine
CLA	Clarithromycin
CLN	Cilastatin
CLSI	Clinical & Laboratory Standards Institute
Cm	Chloramphenicol
CNAG	Centro Nacional de Análisis Genómico
cpm	counts per million
CPZ	Chlorpromazine
CS	Cycloserine
DEG	Differentially expressed gene
DFO	Deferoxamine
DLM	Delamanid
DMSO	Dimethyl sulfoxide
DPR	Domperidone
DR	Drug Resistant
DS	Drug Susceptible
ECM	Extracellular matrix
ECO	Econazole
EDTA	Ethylenediaminetetraacetic acid
EI	Efflux inhibitor

EMA	European Medicine Agency
EMB	Ethambutol
Emis	Emission
Eq.	Equation
ERY	Erythromycin
ESAT-6	6-kDa early secretory antigenic target
EtBr	Ethidium bromide
ETC	Electron Transport Chain
ETH	Ethionamide
FAS-II	Fatty acid synthase type II
FBDD	Fragment-Based Drug Discovery
FBS	Fetal bovine serum
FC	Fold change
FDA	Food and Drug Administration
FIC	Fractional Inhibitory Concentration
FICI	Fractional Inhibitory Concentration Index
FISABIO	Fundación para el Fomento de la Investigación Sanitaria y Biomédica de la Comunidad Valenciana
GATK	Genome Analysis Tool Kit
GO	Gene Ontology
HIV	Human immunodeficiency virus
HTS	High throughput screening
HTSS	High Throughput Synergy Screen
Hyg	Hygromycin
HygR	Hyg resistant
IC_{50}	Inhibitory concentration of 50%
IC_{90}	Inhibitory concentration of 90%
ideR	Iron-dependent regulator
IFN-γ	Interferon-γ
IGRA	Interferon Gamma Release Assay
IMI	Innovative Medicines Initiative
IMP	Imipenem
Indel	Insertion-deletion
INH	Isoniazid
IPTG	Isopropyl-β-D-thiogalactopyranoside
KET	Ketoconazole
Km	Kanamycin
KmR	Km resistant
LB	Luria-Bertani
LDH	Lactate dehydrogenase
LM-PCR	Ligation mediated PCR
LTBI	Latent TB infection
LVX	Levofloxacin
LZD	Linezolid
MATE	Multidrug and toxic compound extrusion
MCC	Methylcitrate cycle
MDR-TB	Multi Drug Resistant TB
MER	Meropenem

MFS	Major Facilitator Superfamily
MGC	Multinucleated giant cells
MIC	Minimal Inhibitory Concentration
MmpL	Mycobacterial membrane protein large
MmpS	Mycobacterial membrane protein small
MoA	Molecular mode of action
MOX	Moxifloxacin
Mtb	*Mycobacterium tuberculosis*
MTBC	*Mycobacterium tuberculosis* Complex
MTBVAC	*Mycobacterium tuberculosis* vaccine
MTT	3-(4,5-dimethylthiazol-2-yl)-2,5-diphenyltetrazolium bromide
NAG	N-acetylglucosamine
ND	not determined
NDH	NADH dehydrogenase
NGM	N-glycolylmuramic acid
NGS	Next generation sequencing
NTM	Non-tuberculous mycobacteria
OADC	Oleic acid albumin dextrose catalase
OD	Optical Density
OXA	Oxacillin
OxPhos	Oxidative phosphorylation
p-adj	Adjusted p-value
PAMPs	Pathogen-associated molecular patterns
PAS	p-aminosalicylic acid
PBMC	Peripheral blood mononuclear cell
PBS	Phosphate buffered saline
PCA	Principal Component Analysis
PCR	Polymerase chain reaction
PDIM	Phthicerol dimycocerosate
PG	Peptidoglycan
PK	Pharmacokinetics
PD	Pharmacodynamics
PMF	Proton motive force
PPD	Purified protein derivative
Pre-XDR-TB	Pre-extensively drug-resistant TB
PRRs	Pattern-recognition receptors
PTD	Pretomanid
PTO	Prothionamide
PZA	Pyrazinamide
qRT-PCR	Quantitative real time PCR
RD1	Region of difference 1
RIF	Rifampicin
RLU	Relative light unit
RNA-seq	RNA-sequencing
RND	Resistance, nodulation and cell division
RpfC	Resuscitation-promoting factor C
RPT	Rifapentine
RR-TB	Rifampicin-resistant TB

RT	Room temperature
SAM	Sequence alignment map
SAR	Structure activity relationship
SD	Standard deviation
SDH	Succinate dehydrogenase
SEM	Standard error of the mean
SI	Selectivity Index
SL-1	Sulfolipid-1
SMR	Small Multidrug Resistance Family
SNP	Single Nucleotide Polymorphism
SPT	Spectinomycin
ss18b	streptomycin-starved 18b strain
ssd	septum site determining protein
STR	Streptomycin
T7SS	Type VII secretion system
tapFR	tap from *Mycolicibacterium fortuitum*
tapTB	tap from *Mycobacterium tuberculosis*
TB	Tuberculosis
TCA	Tricarboxylic acid cycle
TDM	Trehalose dimycolate
TDZ	Thioridazine
TE	Tris-EDTA
TET	Tetracycline
TRD	Terizidone
TST	Tuberculin Skin Test
UBC	University of British Columbia
UZ	University of Zaragoza
VER	Verapamil
WGS	Whole Genome Sequencing
WHO	World Health Organization
XDR-TB	Extensively drug-resistant TB
X-Gal	5-bromo-4-chloro-3-indolyl-β-d-galactopyranoside

Summary

Tuberculosis remains one of the deadliest infectious diseases worldwide. Therefore, there is an urgent need to develop new drugs with novel modes of action effective against multidrug resistant *Mycobacterium tuberculosis* (*Mtb*) strains and to shorten the duration of current anti-tuberculosis therapies. Potential new drugs can come from both *de novo* drug discovery and drug repurposing approaches, as shown in Chapters 1 and 2 of this thesis, respectively.

In **Chapter 1**, the antimicrobial activity of a new chemical series coming from a medicinal chemistry program was characterized against diverse bacteria *in vitro* and *ex vivo*. Then, different approaches were used to elucidate the molecular mode of action of these compounds: (i) standard mutant isolation assays at inhibitory concentrations using *Mtb* wild type; (ii) screening of a *Mycobacterium bovis* BCG transposition library to identify either resistant or susceptible mutants. While resistant mutants were not identified, several susceptible mutants were selected and their drug-sensitive phenotype validated by MIC determination, susceptibility testing on agar plates and time kill assays. Interestingly, three susceptible mutants had the transposon inserted in a gene encoding a transmembrane transport protein related to iron acquisition, suggesting that the MoA of these compounds is related to iron metabolism.

In a synergy screening performed against *Mtb*, these compounds displayed synergism with several anti-TB drugs, indicating a potential role in combination therapy against *Mtb*. Moreover, treatment of *Mtb* with these compounds altered ATP production and O_2 consumption, suggesting that this new chemical series might interfere with energy metabolism.

Transcriptomic studies further supported that these compounds affect both iron metabolism and the oxidative phosphorylation.

In **Chapter 2**, an *in vitro* 3D granuloma model was used to study the antimycobacterial activity of a chemical family of compounds used to treat several psychiatric disorders and shown to be active against *Mtb in vitro* and *ex vivo.* These compounds reduced bacterial viability in the granuloma model, indicating that they are able to penetrate into the granulomas and display activity against dormant mycobacteria.

Taking into consideration the previous association of the Tap efflux pump with drug tolerance and the potential Tap inhibitory activity of these compounds, the role of Tap in mycobacteria was further explored by using the granuloma model and RNA-seq studies. In the granuloma model, the *Mtb* mutant with the *tap* gene disrupted displayed a slight lower replication rate than the wild type strain and developed RIF-tolerant bacteria at a lower rate than the respective parental strain. RNA-seq studies showed that Tap disruption triggers more transcriptional changes in actively replicating bacteria than in non-replicating bacteria, thus suggesting that Tap could be more relevant for replicating bacteria. Moreover, the results obtained by RNA-seq suggested that the absence of Tap in *Mtb* might result in an altered cell wall composition that may compromise its cell wall-associated virulence and render the bacterium more vulnerable to diverse drugs, but mainly cell-wall targeting drugs.

Resumen

La tuberculosis sigue siendo hoy en día una de las enfermedades infecciosas más mortales a nivel mundial. Por ello, es necesario desarrollar nuevos fármacos con mecanismos de acción novedosos que sean eficaces frente a cepas multirresistentes de *Mycobacterium tuberculosis* (*Mtb*), así como acortar la duración de los tratamientos actuales. Estos nuevos agentes antimicrobianos pueden proceder de programas de descubrimiento de nuevos fármacos (*de novo*) o bien del reposicionamiento de fármacos, como se describe en los Capítulos 1 y 2 de esta tesis, respectivamente.

En el Capítulo 1, se caracteriza la actividad de una nueva serie química de compuestos obtenidos mediante un programa de medicina química frente a diversas bacterias, tanto *in vitro* como *ex vivo.* Posteriormente, se utilizan diferentes aproximaciones para elucidar el mecanismo de acción molecular de estos compuestos: (i) ensayos estándar de selección de mutantes resistentes realizados con la cepa silvestre de *Mtb* en presencia de concentraciones inhibitorias del compuesto; (ii) cribado de una banca de mutantes por transposición en *Mycobacterium bovis* BCG para identificar mutantes resistentes o susceptibles a los compuestos. Si bien no se identificaron mutantes resistentes, se seleccionaron varios mutantes susceptibles, cuyo fenotipo de susceptibilidad aumentada se validó mediante ensayos de determinación de la CIM, pruebas de susceptibilidad en placas de agar, y cinéticas de muerte. Encontramos que tres mutantes susceptibles a los compuestos de estudio tienen el transposón insertado en un gen que codifica para una proteína transmembrana implicada en la adquisición de hierro, lo que sugiere que el mecanismo de acción de estos compuestos está relacionado con el metabolismo del hierro.

En un cribado de sinergias realizado frente a *Mtb*, los compuestos de estudio mostraron sinergia con varios fármacos utilizados para el tratamiento de la tuberculosis, lo que sugiere que estos compuestos podrían emplearse en terapia combinada frente a *Mtb*. Además, tras tratar *Mtb* con estos compuestos, se detectó una alteración en los niveles de ATP y en el consumo de O_2, por lo que estos resultados sugieren que estos compuestos podrían interferir con el metabolismo energético.

Finalmente, el análisis transcriptómico realizado indica que estos compuestos afectan tanto al metabolismo del hierro como al metabolismo energético, respaldando los resultados obtenidos previamente.

En el Capítulo 2, se utiliza un modelo de granuloma *in vitro* 3D para estudiar la actividad antimicrobiana de una familia de compuestos químicos utilizados para el tratamiento de diversos trastornos psiquiátricos y con actividad demostrada frente a *Mtb* tanto *in vitro* como *ex vivo.* Estos compuestos redujeron la viabilidad bacteriana en el modelo de granuloma, indicando que estos compuestos son capaces de penetrar en los granulomas y mostrar actividad frente a micobacterias en estado latente.

Puesto que estudios previos han demostrado que estos compuestos actúan inhibiendo Tap, una bomba de eflujo asociada con tolerancia a fármacos, en el Capítulo 2 se explora más a fondo el papel de la bomba de eflujo Tap en micobacterias utilizando el modelo de granuloma y estudios de RNA-seq. En el modelo de granuloma, el mutante de *Mtb* defectivo en la bomba de eflujo Tap mostró una tasa de replicación ligeramente más baja que la cepa salvaje y desarrolló una menor proporción de bacterias tolerantes a RIF que la cepa salvaje. A través de los estudios de RNA-seq, se detectó un mayor número de genes diferencialmente expresados en fase exponencial en comparación con los detectados en fase estacionaria, lo que sugiere que Tap podría ser más relevante para *Mtb* en estado replicativo. Además, los resultados obtenidos sugieren que la ausencia de Tap podría alterar la composición de la pared celular y, en consecuencia, comprometer la virulencia de *Mtb*, provocando que la bacteria sea más susceptible a diversos fármacos, principalmente a aquellos dirigidos a la pared celular.

INTRODUCTION

INTRODUCTION

Tuberculosis, an old disease

Tuberculosis (TB) has plagued humankind since antiquity. Despite its long history, TB is still the leading cause of mortality worldwide among bacterial infections [1].

TB is an airborne infectious disease caused by organisms from the *Mycobacterium tuberculosis* Complex (MTBC). Although the disease is mainly caused by *Mycobacterium tuberculosis* (*Mtb*), other members of the MTBC, such as *Mycobacterium africanum*, *Mycobacterium bovis* and *Mycobacterium caprae*, can also cause TB in humans. TB disease most often affect the lungs (pulmonary TB), but bacteria can also spread and affect other parts of the body (extrapulmonary TB). Symptoms of active TB are persistent cough, fatigue, weight lost, fever, night sweats and coughing up blood [2].

TB throughout history

TB disease is thought to be among the oldest diseases in human history, and *Mtb* has killed more people than any other microbial pathogen [3].

The earliest evidence of TB in humans and animals were bone deformities found in fossils from the Neolithic period and Egyptian mummies [3,4]. TB was well known in ancient Greece, when Hippocrates (460-370 B.C.) used the term "*phthisis*" to describe the progressive decay of patient's body due to pulmonary TB [3,4].

In the 17th century, TB caused an epidemic in Europe, which persisted for the next 200 years. At that time, TB disease was known as the "Great White Plague" due to the paleness of people suffering from TB. During the industrialization process, bad sanitary and social conditions such as high population density in the cities, poorly ventilated or overcrowded housing, and malnutrition contributed to the spread of the disease in Europe and North America [3,4].

In 1865, the French military surgeon Jean-Antoine Villemin demonstrated the infectious nature of TB. He noticed an enhanced prevalence of TB in crowded urban areas, whereas in other areas, such as Australia or New Zeeland, TB had not been known until the pioneers arrived [4,5]. However, it was not until 1882 when Robert Koch identified, isolated, and cultivated the causative agent of TB, the tubercle bacillus (lately named *Mtb*). He also reproduced the disease by inoculating the bacillus into laboratory animals. Robert Koch presented this extraordinary result to the Society of Physiology in Berlin on 24 March 1882, determining a milestone in the fight against TB [6].

From sanatorium to vaccine and drug treatments

Around the mid-19th century, sanatoriums were introduced as a first approach to treat and cure TB. Hermann Brehmer, a botany student suffering from TB, described for the first time the sanatorium cure in 1854 in his doctoral dissertation "Tuberculosis is a curable disease" and reported his healing after travelling to the Himalayas. The concept of a TB sanatorium was based on the idea of isolating patients from their regular environment and treating them with fresh air and sunlight exposure, along with a regimen of rest, rich diet, supervised exercise and proper sanitation and hygiene. Hermann Brehmer opened the first sanatorium for TB patients, and similar sanatoriums were built in different places in the next decades[4,7].

One of the major progresses to fight TB was the development of the live attenuated BCG vaccine (Bacilli Calmette-Guérin) by Albert Calmette and Camille Guérin. They obtained an attenuated strain of *M. bovis* after 230 serial passages (from 1908 to 1921) and demonstrated that BCG conferred protection against TB in different animal models. BCG was first administered in humans in 1921 and is still the only licensed vaccine for TB [3,4,8]. The original culture of BCG was distributed to different laboratories around the world between 1924 and 1960. Until 1960, when the lyophilized methods appeared, laboratories maintained BCG by passaging on non-synthetic culture media and used it for local vaccine production. This parallel passaging of BCG in different media led to genetically different sub-strains still existing today.

Another milestone in the fight against TB was the discovery of effective anti-TB drugs. In 1943, at the laboratory of Selman Waksman, Albert Schatz discovered streptomycin, the first bactericidal antibiotic effective against *Mtb* [9]. During the following two decades, new anti-TB drugs were discovered, including *p*-aminosalicylic acid (1948), isoniazid (1952), pyrazinamide (1954), cycloserine (1955), ethionamide (1961), kanamycin (1957), capreomycin (1963), ethambutol (1961) and rifampicin (1963) [10]. However, drug resistant TB (DR-TB) strains rapidly appear after the administration of these drugs alone, and it was soon acknowledged that this problem could be overcome by using combination regimens. Accordingly, the focus of TB drug development has always been on combinatorial drug regimens rather than drugs alone, to prevent the development of drug resistance [10,11].

The combination of these two major advances, vaccine and chemotherapy, and the global improvement of public health produced a marked decrease in TB incidence, being regarded as a controlled disease. Owing to this initial success in the fight against TB, public health institutions put aside TB control programs, which combined with an increase in immigrants from TB high prevalence nations to developed ones, the onset of the HIV/AIDS epidemic, variable protection of BCG against pulmonary TB and the appearance of DR-TB, led to the re-emergence of the disease in the late 1980s [9,12]. As a result, TB was declared a global health emergency in 1993 by the World Health Organization (WHO)[13].

Although several TB control strategies aiming to reduce the global TB burden have been created since then, TB is still a major public health threat [1]. To face TB, WHO established a global End TB Strategy in 2014 whose main targets were to reduce TB deaths by 90% and TB incidence rate by 80% between 2015 and 2035, in order to end the global TB epidemic [14]. However, the reduction in TB deaths and TB incidence achieved between 2015 and 2020 fell far short of the 2020 milestone of the strategy[1]. Moreover, the COVID-19 pandemic has worsened the situation, thus making it even more difficult to meet the End TB Strategy targets[1].

BCG is still the only licensed vaccine for TB and just three new anti-TB drugs with novel molecular modes of action (MoA) have been approved for the treatment of DR-TB in the last 40 years: bedaquiline (2012), delamanid (2014) and pretomanid (2019). Therefore, a combined strategy based on the development of new anti-TB drugs, as well as new effective vaccines and diagnostic tools, is crucial to achieve the End TB Strategy objectives.

TB, a disease of today

Despite being curable and preventable, TB is the second deadliest infectious disease worldwide, ranking only after the COVID-19 (although it is estimated that soon will retake the first position) and above HIV/AIDS, and the 13th leading cause of death. According to the WHO, an estimated 10.6 million people developed TB in 2021 and 1.6 million died from the disease worldwide (including 187,000 people co-infected with HIV), which is equivalent to a staggering 4,000 deaths per day [15].

The COVID-19 pandemic has had a devastating impact on the fight against TB, reversing years of progress in providing essential TB services and reducing TB disease burden. The main effect of COVID-19 pandemic on TB is a huge drop in case notifications of people newly diagnosed with TB compared with 2019. Specifically, there was a fall of 18% (from 7.1 million to 5.8 million new TB cases reported) between 2019 and 2020, reaching levels of 2012. Moreover, for the first time since 2012, TB death rates have started to increase globally due to restricted access to TB diagnosis and treatment derived from COVID-19 pandemic, whereas deaths from HIV/AIDS continued to decline between 2019 and 2020 [1]. Other impacts include declines in the number of people provided with treatment for DR-TB. These impacts derived from the COVID-19 are forecast to worsen in the coming years due to several factors: (i) the ongoing COVID-19 surges, (ii) the negative impact of COVID-19 on broader TB determinants, such as income levels and undernutrition, and (iii) the increased TB transmission that is expected after missing a high number of TB cases in the past two years[1,16].

According to the WHO, about a quarter of the global population is latently infected with *Mtb*, meaning that they are asymptomatic and cannot transmit the infection [15]. However, they have a 5-15% lifetime risk of developing active TB disease, being this rate higher in individuals immunocompromised by several factors, including HIV co-infection, diabetes and undernutrition [17]. For this reason, TB incidence is much higher in areas where many of these conditions coincide, such as South-East Asia and Africa (accounting for 68% of new cases) [15].

The estimated TB incidence and mortality worldwide in 2021 is shown in **Figure 1 & Figure 2**, respectively. In 2021, only eight countries (India, Indonesia, China, the Philippines, Pakistan, Nigeria, Bangladesh and the Democratic Republic of the Congo) accounted for more than two thirds of total new TB cases.

Likewise, a similar inequity is observed in mortality distribution, since about 82% of TB deaths among HIV-negative people occurred in Africa and South-East Asia [15].

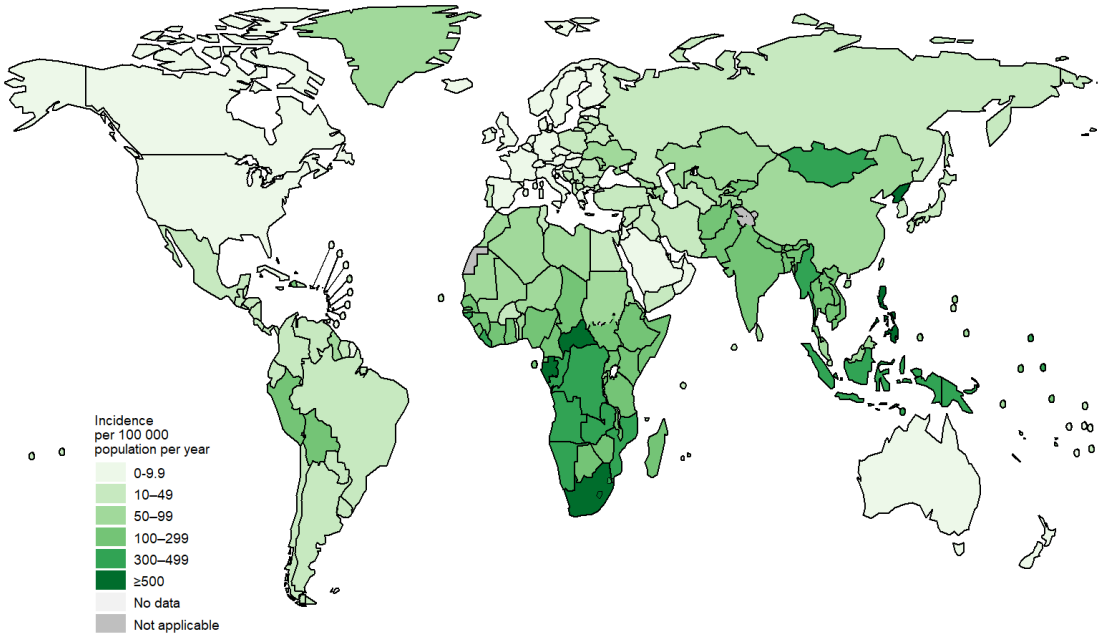

Figure 1. Estimated TB incidence rates in 2021. From [15].

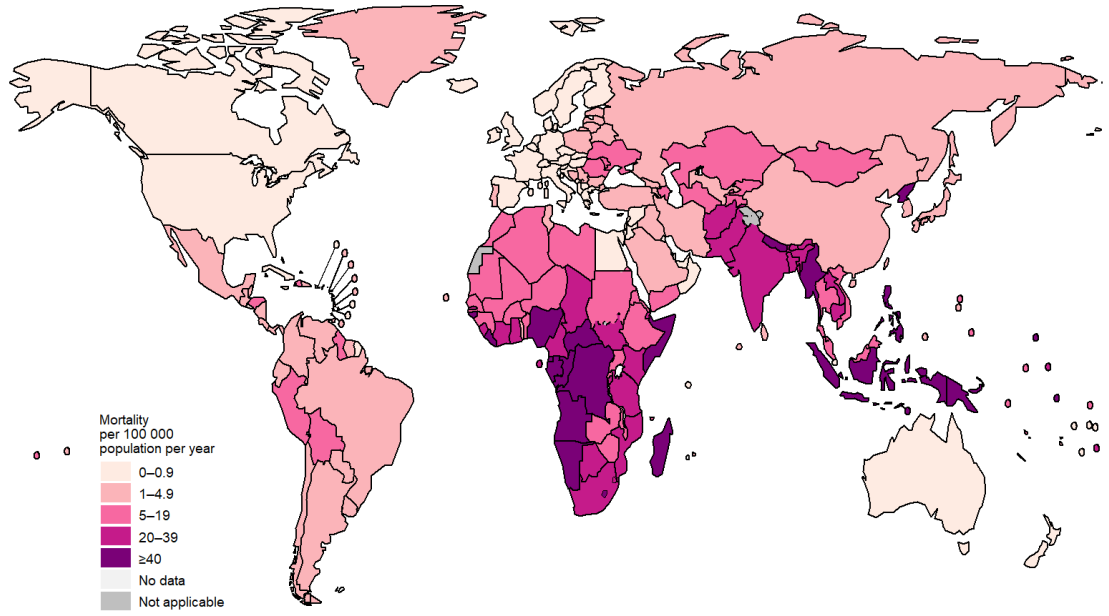

Figure 2. Estimated TB mortality rates in HIV-negative people in 2021. From [15].

The mycobacteria

The mycobacteria are a large group of bacterial species that belong to the family *Mycobacteriaceae*, included into the order *Corynebacteriales*, class *Actinomycetia* and phylum *Actinobacteria*.

The mycobacteria include strict and opportunistic pathogens, as well as non-pathogenic, saprophytic species.

Strictly pathogenic mycobacteria consist of two main groups: (i) the MTBC, comprising *Mtb*, *M. africanum*, *M. bovis*, *Mycobacterium canettii*, *M. caprae*, *Mycobacterium microti*, *Mycobacterium mungi*, *Mycobacterium orygis*, *Mycobacterium pinnipedii* and *Mycobacterium suricattae*), which is responsible for pulmonary and extrapulmonary TB, and (ii) *Mycobacterium leprae*, which causes leprosy (**Table 1**) [18].

Other infections are caused by strict or opportunistic pathogenic mycobacteria from the non-tuberculous mycobacteria (NTM) category. For example, *Mycobacterium marinum* and *Mycobacterium ulcerans* are two strictly pathogenic NTM species, which mostly cause infections of the skin and mucous membranes. Other NTM species are opportunistic pathogens in animals and humans, including species from the *Mycobacterium avium* complex and the *M. abscessus* complex, which can produce infections similar to those caused by *Mtb*. In contrast, other NTM species are saprophytic and non-pathogenic, such as *M. smegmatis* (**Table 1**)[18].

Mycobacteria can be further classified in rapidly and slowly growing mycobacteria, based on their ability to form visible colonies on agar medium in less or more than 7 days, respectively [18]. All strict and most opportunistic pathogens are slow-growing mycobacteria, including *Mtb*, *M. ulcerans* or *M. leprae*, that cause TB, Buruli ulcer or leprosy, respectively. By contrast, rapidly growing mycobacteria are non-pathogenic or opportunistic pathogens (**Table 1**)[18].

Table 1. The mycobacteria. Adapted from [6].

Rapidly growing mycobacteria	Slowly growing mycobacteria		
Non-tuberculous mycobacteria (NTM)		***Mtb* complex (MTBC)**	***M. leprae***
M. abscessus complex	*M. marinum*	*M. tuberculosis*	
M. abscessus subsp. *abscessus*	*M. ulcerans*	*M. africanum*	
M. abscessus subsp. *bolletii*	*M. avium* complex	*M. bovis*	
M. abscessus subsp. *massiliense*	*M. avium*	*M. canettii*	
M. chelonae	*M. intracellulare*	*M. caprae*	
M. fortuitum	*M. chimaera*	*M. microti*	
M. smegmatis	*M. haemophilum*	*M. mungi*	
M. vaccae	*M. xenopi*	*M. orygis*	
	M. kansasii	*M. pinnipedii*	
True pathogens	*M. simiae*	*M. suricattae*	
Opportunistic pathogens	*M. terrae* complex		
Saprophytes	*M. gordonae*		

Phenotypically, mycobacteria are aerobic, acid-fast and non-motile bacilli of 1-10 μm length and 0.2-0.5 μm width. Their colony morphology varies depending on the species from rough to smooth and from pigmented to non-pigmented [19].

One of the most remarkable characteristics of mycobacteria is their cell envelope, which is crucial for their physiology, virulence and host-pathogen interactions, since many relevant cell processes are located in this compartment. From inside to outside, the cell envelope consists of a conventional bacterial plasma membrane, periplasmic space, a cell wall core (including peptidoglycan, arabinogalactan and mycolic acids), some specific lipids non-covalently associated to mycolic acids and the capsule [20].

The mycolic acids of the cell wall core and the non-covalently attached lipids -associated with mycobacterial virulence- are known as “mycomembrane” or outer membrane and form a highly impermeable bilayer that confers to mycobacteria their characteristic drug resistance, although it can be also the target of several antimicrobials [20]. This high content of uncommon lipids is responsible for the distinctive acid-fast / Zielh-Neelsen mycobacteria staining.

Mycobacterium tuberculosis

Pathogenesis and virulence of *Mtb*

Mtb is an obligate intracellular pathogen, and humans are its only known reservoir. *Mtb* infection initiates when the bacilli reach the lungs by inhalation of aerosolized droplets expelled from individuals with active pulmonary TB (*e.g.* by coughing or sneezing). Once in the alveolar space, bacteria are internalized via phagocytosis by alveolar macrophages -the cell type that *Mtb* primarily infects-. The pattern-recognition receptors (PRRs) present on host cells recognize pathogen-associated molecular patterns (PAMPs) found on the surface of the bacilli, inducing the secretion of cytokines and chemokines that leads to the recruitment of additional phagocytic cells (neutrophils, interstitial macrophages and dendritic cells) into the site of infection [21,22].

Within macrophages, *Mtb* initially resides inside phagosomes. Then, interferon-γ (IFN-γ) activation of macrophages promotes the delivery of *Mtb* into mature phagolysosome, a compartment characterized by acidic pH, reactive oxygen and nitrogen intermediates, as well as lytic enzymes. However, *Mtb* has evolved diverse strategies to overcome host defences and establish suitable conditions to survive and proliferate within the macrophage, such as arresting phagosome maturation and reducing phagosome acidification. In addition, *Mtb* can disrupt the phagosome membrane by secreting the 6-kDa early secretory antigenic target, ESAT-6, through the secretion system ESX-1, allowing the bacteria to escape to the cytosol [2]. Meanwhile, infected cells migrate to pulmonary lymph nodes, where they process and present antigens for T cell priming (both $CD4^+$ and $CD8^+$). After 15-18 days of *Mtb* infection, the adaptive immune response produces primed T cells, which migrate to the site of infection guided by the chemokines produced by infected cells[23].

As a result, the pathogen can (i) be eliminated by host immune response, (ii) progress to active disease (mainly in immunocompromised hosts), or (iii) persist in structures called granulomas – the pathological hallmark of TB [2]. The granuloma is a well-organized structure composed of infected macrophages, epithelioid cells, foamy cells and multinucleated giant cells (MGC) surrounded by neutrophils, dendritic cells, natural killer cells, B and T lymphocytes, fibroblasts and other matrix components [24–26].

The main function of the granuloma is to contain the host immune response and mycobacteria in a limited area, preventing bacterial spread to surrounding tissues. In these structures, bacilli are exposed to a variety of stressful conditions such as hypoxia, acidic pH, low iron availability and nutrient deprivation [27]. To overcome these challenging host immune responses, the bacteria have evolved mechanisms to maintain viability with limited or no replication. This state (called dormancy) is characterized by a low metabolic activity and changes in the composition and spatial architecture of the cell wall [28]. Consequently, bacteria show phenotypic drug tolerance to drugs targeting functions required for growth, meaning that they are able to survive drug pressure for a prolonged period in the absence of drug resistance-conferring mutations [29,30].

Therefore, granulomas establish a dynamic balance between host defenses and bacterial dormancy. In 90% of infected individuals, the pathogen is contained within the granuloma and persists in a latent state, known as latent TB infection (LTBI) [31,32]. This asymptomatic and non-transmissible stage can last for years or even for life. During LTBI, solid granulomas prevail, which are typically encircled by a fibrotic wall that separates it from the surrounding tissue [33].

Nevertheless, the containment of the infection can fail due to a dysregulation in the immune response (*e.g.,* HIV, malnutrition and old age). As a result, dormant bacteria can reactivate, leading to the formation of a necrotic zone in the center of granulomas (known as *caseum* because of its milky appearance), which contains extracellular *Mtb* released by necrotized foamy macrophages. Caseous necrosis -a hallmark of pulmonary TB pathology- is associated with reduced vascularization of the lesion (hypoxia) and high lipid content [33,34]. Further loss of granuloma integrity allows the entry of vascular oxygen and nutrients, which promotes the growth of the bacteria. Finally, bacteria are released into the lungs (causing pulmonary TB) and spread to other parts of the body (producing extrapulmonary TB). In this situation, individuals develop the disease, meaning that they are symptomatic and contagious [2,31,35,36].

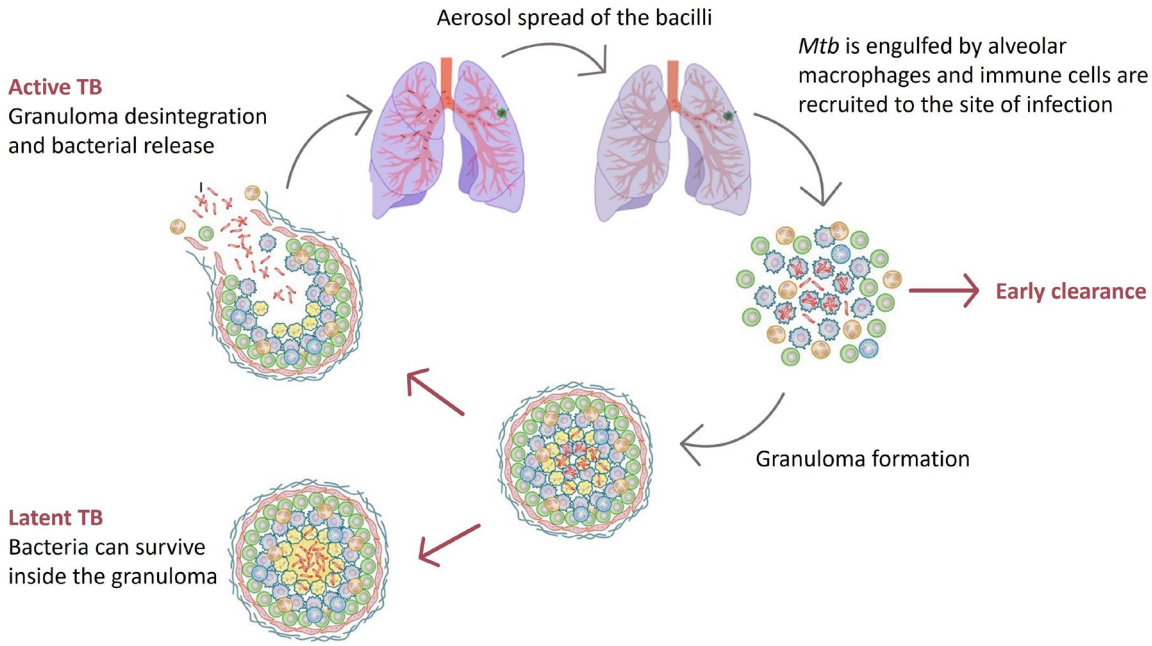

Figure 3. Transmission cycle of *Mtb*. Upon *Mtb* infection, bacteria reach the lungs, triggering a host immune response. This can lead to early clearance or bacterial contention in granulomas (LTBI). However, in 5-15% of infected individuals, the infection can progress to clinical disease (in weeks or decades) and bacteria are released to the lungs and other parts of the body. Adapted from [37].

Vaccines

BCG is the only vaccine licensed to be used for TB. It provides a strong effective protection in children against disseminated forms of the disease. However, it shows variable protective efficacy against pulmonary TB in adults. To overcome this problem, several vaccine candidates against TB are under development [38]. One of them is MTBVAC, a live attenuated vaccine based on the deletion of two genes (*phoP* and *fadD26*) encoding key virulence factors of *Mtb* in a clinical isolate of lineage 4 of *Mtb* [39]. MTBVAC is being developed at the University of Zaragoza (UZ) in collaboration with the industrial partner Biofabri, responsible of industrial and clinical development. In 2022, MTBVAC finished Phase 2 clinical trials with both newborns and adults in South Africa, one of the largest endemic countries, and has recently entered Phase 3 efficacy trials [40].

Diagnosis

There are diverse technologies used to diagnose active TB, including imaging, microscopy, culture-based methods, and molecular tests.

Chest X-ray is an established triage which allows the observation of pulmonary lesions but requires a microbiological test due to the lack of specificity[2].

Sputum smear microscopy is one of the most widely used techniques to detect mycobacteria from clinical specimens. It is based on visualizing the presence of acid-fast bacilli with the microscope after Ziehl-Neelsen or auramine-rhodamine stain. However, it shows low sensitivity in comparison with culture-based methods (described below) and it cannot differentiate between *Mtb* and NTM [41].

Culture-based methods are the gold standard for TB diagnosis and drug-susceptibility testing. Commercially available automated systems, such as BACTEC™ and MGIT™, provide results faster than culture methods that use solid media. However, these methods still have several limitations, including increased risk of culture contamination and the need for complex laboratory infrastructure [41].

The WHO has recommended using rapid molecular techniques, such as Xpert MTB/Rif Ultra (Cepheid) and Abbott RealTime MTB RIF/INH Assay (Abbott), for TB diagnosis due to their higher sensitivity compared to conventional sputum smear microscopy and their capacity to detect drug resistance within two hours [42].

Two immune-based methods are widely used to detect LTBI: the Tuberculin Skin Test (TST) or Mantoux test, and the Interferon Gamma Release Assay (IGRA). The TST is based on an intradermal injection of tuberculin or purified protein derivative (PPD). If an individual has cell-mediated immunity to these antigens, a hypersensitivity reaction is likely to occur after 48-72 hours. The main disadvantage of TST is that BCG vaccination or previous exposure to NTM can interfere with the result [2]. IGRA is an immunological assay that measures IFN-γ production in blood samples after stimulation with *Mtb* antigens encoded in RD1 (region of difference 1). Therefore, in contrast to TST, IGRA test allows differentiation of *Mtb* infected individuals from those vaccinated with BCG or pre-exposed to NTM [2].

Despite recent advances achieved in the field, accurate and rapid diagnostic methods are still needed to administer proper therapies based on the drug resistance profile and prevent TB transmission.

Treatment

Up until recently, the frontline treatment for drug-susceptible TB (DS-TB) included a 2-month initiation phase of isoniazid (INH), rifampicin (RIF), pyrazinamide (PZA) and ethambutol (EMB), followed by a 4-month continuation phase of INH plus RIF [43,44]. This 6-month regimen has been widely adopted for decades and has a global success rate over 85%[1].

Recently, a 4-month, all-oral regimen for DS-TB has been recommended by the WHO, since it is as effective as the standard 6-month regimen but shorter, thus having the potential to improve patients' adherence to the treatment. This regimen consists of a 2-month intensive phase of INH, PZA, rifapentine (RPT) and moxifloxacin (MOX), followed by a 9-week continuation phase of INH, RPT and MOX [45].

The main reason for prescribing a combination of anti-TB drugs with different modes of action is to reduce the emergence of DR-TB. Yet, irregular drug supply, non-compliance to the treatment, patient pharmacogenomics, inappropriate drug regimens and lack of supervision has led to the emergence of resistant strains [46].

Mtb drug-resistant strains are classified into five groups by the WHO: [1,47]

- Isoniazid-resistant TB: *Mtb* strains resistant to INH.
- Rifampicin-resistant TB (RR-TB): *Mtb* strains resistant to RIF.
- Multidrug resistant TB (MDR-TB): *Mtb* strains resistant to INH and RIF, the cornerstone drugs for TB treatment.
- Pre-extensively drug-resistant TB (pre-XDR-TB): *Mtb* strains that fulfil the definition of MDR/RR-TB and are also resistant to any fluoroquinolone (MOX or levofloxacin, LVX), a class of second-line anti-TB drugs.
- Extensively drug-resistant TB (XDR-TB): *Mtb* strains that fulfil the definition of MDR/RR-TB and are also resistant to any fluoroquinolone (MOX or LVX) plus at least one of the drugs bedaquiline (BDQ) or linezolid (LZD).

The standard regimen is not effective for patients with DR-TB, which accounts for roughly half a million cases every year [15]. According to the WHO, the most affected countries by MDR-TB in 2021 were India, the Russian Federation and Pakistan, being responsible for 42% of worldwide cases [15].

Treatment of DR-TB requires the use of second-line drugs, which are less effective, have more severe side effects and need longer treatment periods, thus complicating patients' adherence to the treatment. Moreover, cure rates of DR-TB therapies remains low, since latest data indicate that only 60% of RR/MDR-TB and around 34% of XDR-TB cases have positive outcomes, making DR-TB a threat to global public health [15,48]. Hence, alternative therapies involving new drugs and shorter regimens, along with novel applications for approved drugs, are urgently needed to combat DR-TB.

In the last years, several studies (*e.g.,* TB-PRACTECAL and ZeNix) have been performed to assess the efficacy and safety of novel regimens for DR-TB treatment, leading to significant changes in the therapeutic options for DR-TB. In 2022, the WHO published a rapid communication informing key changes in the treatment of DR-TB, which have been included in the WHO Consolidated Guidelines on DR-TB Treatment (released in December 2022) [49,50]. These recommendations are summarised below.

A new 6-month BPaLM regimen, based on BDQ, pretomanid (PTD), LZD and MOX, may be used in MDR/RR-TB patients without previous exposure to BDQ, PTD and LZD in place of the 9-month regimen (described below) or longer (≥18 months) regimens. This regimen could be also used without MOX in patients with pre-XDR-TB (*i.e. Mtb* resistant to any fluoroquinolone). Hence, both BPaLM and BPaL regimens may be employed in patients with MDR-TB, RR-TB or pre-XDR-TB regardless of their HIV status, since they showed high treatment success rates [49–51].

Moreover, there is a 9-month all-oral regimen consisting of BDQ (used for 6 months), in combination with LVX/MOX, ethionamide (ETH), EMB, INH (high-dose), PZA and clofazimine (CFZ) for 4 months (with the possibility of extending to 6 months if the patient remains sputum smear positive at the end of 4 months); followed by 5 months of treatment with LVX/MOX, CFZ and EMB. Importantly, ETH can be replaced by 2 months of LZD (600 mg) [49,50].

This alternative 9-month all-oral therapy is preferred over longer (≥18 months) regimens in adults and children with MDR/RR-TB without resistance to fluoroquinolones, without previous exposure to second-line drugs and with no extensive pulmonary TB disease or severe extrapulmonary TB [49,50].

In the case of patients with XDR-TB or those who have failed shorter therapies, the WHO recommends individualized longer regimens designed using the priority grouping of drugs indicated in the "WHO consolidated guidelines for DR-TB treatment" from 2020 [52]. Drugs are classified into A, B and C groups based on their class, effectiveness, and safety (**Table 2**). These agents should be chosen based on the resistance profile, patients' known contraindications, drug-drug interaction, clinician preferences or operational considerations, among others [52].

Table 2. Classification of drugs recommended for patients with XDR-TB or those who have failed shorter treatment regimens.

Group A (include all three drugs)	Levofloxacin (LVX) or Moxifloxacin (MOX)
	Bedaquiline (BDQ)
	Linezolid (LZD)
Group B (add one or both drugs)	Clofazimine (CFZ)
	Cycloserine (CS) *or* Terizidone (TRD)
Group C (add to complete the regimen and when drugs from groups A and B cannot be used)	Ethambutol (EMB)
	Delamanid (DLM)
	Pyrazinamide (PZA)
	Imipenem-Cilastatin (IMP-CLN) *or* Meropenem (MER)
	Amikacin (AMK) *or* Streptomycin (STR)
	Ethionamide (ETH) *or* Prothionamide (PTO)
	p-aminosalicylic acid (PAS)

Drug resistance

TB drug resistance can result from both intrinsic and acquired resistance mechanisms.

Overall, mechanisms of drug resistance can fall into several categories: barrier mechanisms (changes in drug uptake or efflux), drug degrading or inactivating enzymes, modification of pathways involved in drug activation, target modification, target overexpression or target replacement [53,54].

One of the main causes of *Mtb* intrinsic resistance is the thick and highly hydrophobic mycobacterial cell wall envelope, which act as an effective permeability barrier to many drugs. It has been observed that changes in cell wall composition can affect drug uptake. For example, inactivation of genes of the antigen 85 (Ag85) complex affects trehalose dimycolate (TDM) content (which is important for cell wall integrity in *Mtb*), thus altering cell envelope permeability and resulting in enhanced susceptibility to several drugs [54].

Moreover, *Mtb* has numerous genes encoding efflux systems which have been described to contribute to intrinsic resistance by expelling drugs out of the bacteria. Mycobacterial drug efflux pumps can be grouped into five different structural families: the major facilitator superfamily (MFS), the small multidrug resistance (SMR) family, the resistance-nodulation-cell division (RND) superfamily, the adenosine triphosphate (ATP)-binding cassette (ABC) superfamily and the multidrug and toxic compound extrusion (MATE) family [53].

While some efflux pumps have narrow substrate specificity (such as TetV pumps), most transporters export a wide range of structurally dissimilar substrates[53]. For example, the Tap efflux pump (encoded by the *rv1258c* gene), which belongs to MFS superfamily, has been reported to export PAS, aminoglycosides and tetracycline (TET), thereby conferring resistance to these drugs[55]. Interestingly, this efflux pump is regulated by WhiB7, a transcriptional regulator that contributes to intrinsic drug resistance in mycobacteria by activating its own expression and many other drug resistance genes, including: (i) *erm37* gene, which encodes a 23S rRNA methyltransferase that alters the drug-binding site of macrolides, thus preventing their binding to 23S rRNA, and (ii) *eis* gene, which encodes an aminoglycoside N-acetyltransferase that acetylates and inactivates several aminoglycosides [56,57].

Since there are no reports of horizontal gene transfer in mycobacteria, acquired drug resistance is caused by spontaneous mutations in chromosomal genes in response to the selection pressure of the drugs[53].

Spontaneous mutations typically occur in genes encoding drug targets to prevent efficient drug binding (*e.g.,* mutations in *rpoB* gene, which encodes the target of RIF, or in *embB* gene, encoding the target of EMB). These drug resistance-conferring mutations can also be found in the promoter of genes encoding drug targets, leading to increased target expression (*e.g.,* mutations in *inhA* promoter confer INH resistance), or in genes encoding drug-activating enzymes, such as *katG*, which is required for INH activation [53].

While in other bacteria efflux pumps are frequent mechanisms of acquired drug resistance that confer high levels of resistance to the drugs transported by the efflux pumps (*e.g.,* AcrAB efflux pump in *E. coli*)[58], most mycobacterial efflux pumps contribute to intrinsic drug resistance by conferring basal levels of resistance. In the last years, it has been observed that mutations in the transcriptional repressor *rv0678* lead to the overexpression of MmpL5-MmpS5 system, thus conferring resistance to BDQ, CFZ and azoles [59–61]. Therefore, drug efflux represents a promising target for designing novel anti-TB drugs.

Non-tuberculous mycobacteria

The incidence of NTM infections is increasing worldwide, thus representing a threat to global public health. NTM mainly cause infections in immunocompromised individuals or people with pre-existing lung diseases, including cystic fibrosis (CF) and bronchiectasis. NTM are thus largely opportunistic and, in contrast to *Mtb*, are acquired from the environment as they are highly abundant in the soil and in natural and drinking water sources [18].

The *M. abscessus* complex, which comprises three subspecies (*M. abscessus* subsp. *abscessus*, *M. abscessus* subsp. *massiliense* and *M. abscessus* subsp. *bolletii*), accounts for the majority of rapidly growing NTM-related infections. In addition to being responsible for a wide range of skin and soft tissue infections, these bacteria are frequent opportunistic pathogens of the lung in patients immunocompromised or with pre-existing lung pathologies, *e.g.,* CF, bronchiectasis or chronic obstructive pulmonary diseases. In CF patients, *M. abscessus* infections are associated with serious airway damage and lung function decrease [18,62].

M. abscessus infectious are extremely difficult to treat owing to intrinsic and acquired multidrug resistance mechanisms to most available antimicrobials and anti-TB drugs, thus requiring long-term treatments with multidrug regimen [49].

To date, there is no official standard treatment for *M. abscessus* pulmonary infections. Guidelines issued by the British Thoracic Society (BTS) and American Thoracic Society and Infectious Diseases Society of America (ATS/IDSA) describe a multidrug therapy for at least 12 months, which consists of an initial phase (including intravenous and oral drugs), followed by a continuation phase (with inhaled and/or oral drugs)[62]. The combination of drugs used for treatment of *M. abscessus* infections depends on the macrolide-sensitive or macrolide-resistant phenotype of the isolates, and includes clarithromycin/azithromycin (macrolides, only in the first case), amikacin (parenteral aminoglycoside), tigecycline (tetracycline), imipenem (β-lactam), clofazimine (phenazine), linezolid (oxazolidinone), minocycline (tetracycline), moxifloxacin (fluoroquinolone) and cotrimoxazole [62]. Such prolonged regimens are difficult to tolerate, and compliance is challenging. Despite these aggressive and lengthy treatments, cure rates are low (33-57%), being comparable to or even worse than those of MDR-TB [62]. Thus, there is an urgent need to develop new drugs, as well as more effective and safer treatments for NTM-related infections.

Drug discovery process

One of the greatest challenges to global public health is antimicrobial resistance, which has been estimated to cause 10 million deaths per year by 2050. Therefore, it is urgently needed to discover and develop new antimicrobials with novel modes of action effective against MDR bacteria.

The drug discovery process starts with the identification of hit compounds, *i.e.,* molecules active *in vitro*, which are modified and optimized along the whole process until a drug candidate is selected to enter preclinical and ultimately clinical trials. The main stages of the drug discovery process are described below.

Hit identification

In the past decades, the first step of the drug discovery process, which consists of identifying hit compounds, has been mostly performed by high throughput screening (HTS) of large compound libraries. Compound libraries used for HTS are usually composed of a large number of molecules (ca. 0.5-2 million) which can come from different sources, such as natural products or combinatorial chemistry [63,64].

Hits can be also identified by *in silico* approaches, including Fragment-Based Drug Discovery (FBDD) or virtual screening. For these approaches, the three-dimensional structure of the target needs to be known in order to dock a ligand or a fragment library [65,66].

Two different approaches have been used for HTS in antimicrobial drug discovery: whole cell and target-based screening.

Whole cell-based screenings test the potency of the compounds against bacterial cultures, allowing the identification of molecules with antimicrobial activity. This type of screening has been very useful in the identification of antimicrobials coming from microbes, such as those from the genus *Streptomyces*. In fact, most drugs discovered between the 1940s and 1970s were identified following this strategy [64]. This approach opens the path to discovery of compounds that inhibit new targets or pathways. However, no information on the MoA is provided, thus being necessary to perform subsequent assays in order to identify the drug target and confirm the MoA [63,64,66].

Target-based screenings consist in searching molecules that directly bind and inhibit a purified protein whose implication in bacterial survival either *in vitro* or *in vivo* has been validated, and its major advantage is that the target is already known, allowing rational drug design. This approach requires large-scale protein production (commonly by heterologous protein expression and subsequent purification) and the development of a robust assay that allows the identification of inhibitors from the chemical library. A limitation of this strategy is that target-based inhibitors might not penetrate the impermeable bacterial cell wall and cannot reach the intracellular target, thus lacking antimicrobial activity. This approach has not yielded clinically useful new antimicrobials due to this limitation, among others [64].

In the last years, with the implementation of novel genetic tools, target-based whole-cell screenings have gained much attention since they combine the advantages of both approaches while eliminating their drawbacks. An example of this strategy is the use of knockout or conditional knockdown strains, which is based on the assumption that a reduction in the target might render the bacteria hypersensitive (in comparison to the wild type strain) to the drugs inhibiting that target. Another option is to employ mutants that overexpress genes conferring resistance phenotypes (*e.g.* efflux pumps), to search for drugs that specifically reverse the resistance phenotype [67].

Several hits are usually identified in screening programs, although not all of them have the potential to become new antimicrobials. Therefore, it is essential to evaluate the compounds before subsequent development into a lead compound. This evaluation usually assesses the physicochemical properties of the hits, the possibility of future drug structural modifications and scale-up synthesis, preliminary activity assays against relevant strains, preliminary safety assays in mammalian cell lines, and assays of spontaneous selection of resistance [64].

Hit to Lead

This stage of the drug discovery process aims to improve the activity and safety profile of the hits selected by means of structure-activity relationship (SAR) investigations around each core compound structure [63].

Moreover, Minimal Inhibitory Concentration (MIC) assays are performed against a panel of relevant pathogens and cytotoxicity assays against eukaryotic cell lines. The most promising compounds are further evaluated against a panel of clinical isolates, including MDR strains. In addition, time kill assays of the hits against the target pathogen allow to distinguish between bactericidal (*i.e.* it kills the bacteria) or bacteriostatic (*i.e.* it blocks bacterial growth) activities [64].

Several assays are also performed to obtain important information regarding absorption, distribution, metabolism and excretion (ADME) properties, as well as pharmacokinetic (PK) and pharmacodynamic (PD) parameters [63].

Subsequent experiments assess hit liabilities, providing information on metabolic stability in human microsomes and potential interferences with human targets that must be avoided during drug development, such as cytochrome P450s and hERG potassium channel inhibition. The mutagenic potential of the hits is determined by the Ames test [63,64].

Finally, resistance studies are performed to measure the rate at which spontaneous mutants emerge and to evaluate their associated fitness cost. It is also necessary to elucidate the MoA of the compounds by different approaches, such as whole genome sequencing (WGS), transcriptomics, or proteomics (**Chapter 1 - 1. Introduction**). Knowing the MoA of the compounds, along with issues related to drug uptake and efflux, is critical for improving the activity and selectivity while reducing their toxicity [64].

At the end of this stage, a lead compound is selected to enter the lead optimisation process.

Lead optimization

In this stage, lead compounds undergo several assays similar to those performed during hit to lead scheme but with stricter criteria, with a view to optimizing their efficacy and selectivity [64].

New experiments are carried out in addition to the aforementioned ones, including PK studies and efficacy assays in rodent models. Finally, the most promising compounds are re-synthesised at large scale prior to entering preclinical trials [64].

Preclinical development and clinical trials

Preclinical studies are aimed at ensuring safety and efficacy of drug candidates before progressing into clinical trials. Data obtained from these assays allow dosage adjustment and determination of the administration route for first time in humans studies (Phase 1). Successful compounds follow a well-defined clinical development process (Phases 1-4) and need approval of regulatory agencies, such as FDA (Food and Drug Administration) and EMA (European Medicines Agency).

As shown in **Figure 4**, the whole drug discovery process can take up to 15-20 years to be completed from hit identification to commercialization.

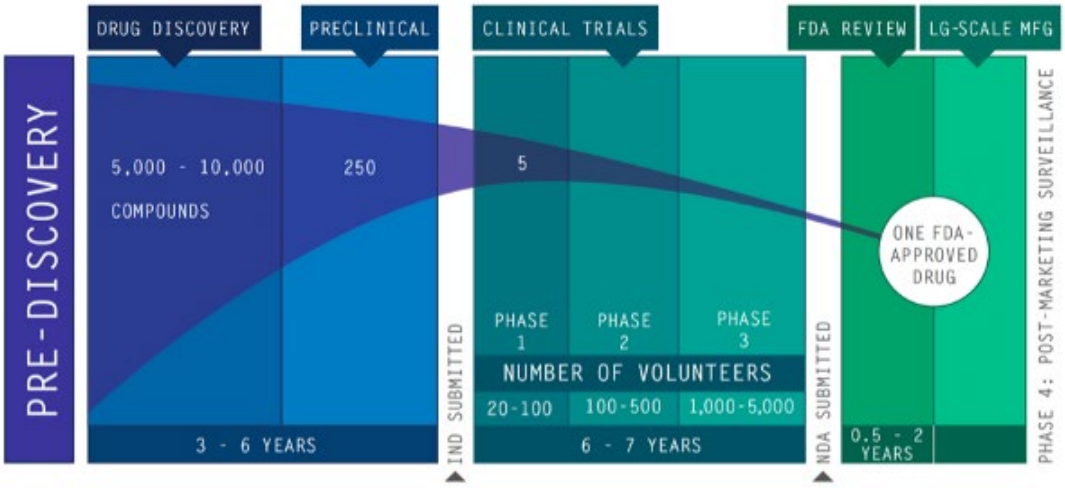

Figure 4. Drug discovery and development timeline. The drug approval pipeline can take approximately 15 years. It is estimated that only one new drug reaches the market from 5,000-10,000 initial compounds. From [68].

Drug repurposing

An alternative to the lengthy and costly process described above is drug repurposing, *i.e.,* the process of finding novel clinical applications for drugs already approved for other indications and with known pharmacological properties [69].

Drug repurposing is gaining traction in both the public and private sector as a strategic approach that bypasses much of the discovery and preclinical stages, since PK, PD and toxicity profiles of the drugs are already known. Furthermore, since there is safety information from previous Phase 1 studies, in some cases repurposed drug candidates can enter clinical trials at Phase 2, as long as the already approved posology is maintained, saving time and money. Drug repurposing can also bypass the scale-up of the manufacturing process [69].

Despite the above-mentioned advantages of drug repurposing over *de novo* drug development, this process also comes with several limitations that must be considered, such as toxicology, dosage and pharmacokinetics. Antimicrobials typically require higher concentrations than other drugs to be active. Hence, repurposed drugs could require higher doses (than those indicated in the original registration) to exert activity against bacteria, which may result in toxicity and side effects. In such cases, drug repurposing might provide new lead chemical scaffolds that would need to undergo the entire development process [69].

TB and *M abscessus* drug pipeline

Drug repurposing has been applied to TB to introduce in the pipeline novel drugs to treat DR-TB. Several drug classes have been added: (i) fluoroquinolones, such as MOX and LVX; (ii) oxazolidinones, including LZD (currently in use against MDR and XDR-TB) and others in Phase 2 of clinical trials (sutezolid, delpazolid); (iii) the broad-spectrum β-lactam MER, which was included in 2020 in the group C of drugs recommended by the WHO to treat XDR-TB; (iv) CFZ, a drug used in multidrug therapy to treat leprosy, is also recommended to treat MDR and XDR-TB [49,52].

As previously mentioned, drug repurposing can also provide interesting lead chemical scaffolds that need to be modified to develop novel molecules with improved antimycobacterial and chemical properties (in comparison to the parent compound), such as better resistance profiles, safety, tolerability or PK/PD properties.

For example, the recently approved DLM and PTD are derivatives of 5-nitroimidazoles -molecules active against anaerobic bacteria (*e.g., Clostridium difficile* and *Helicobacter pylori*)- [70]. Moreover, SQ-109, a molecule currently in Phase 2, arose from a screening focused on EMB analogues. Currently, there are several analogues of BDQ (a diarylquinoline) in clinical development, including TBAJ-587, TBAJ-876 and sudapyridine, which show better safety and PK profiles than BDQ.

Importantly, BDQ (the first anti-TB drug approved in the last 40 years), as well as other drugs which are in Phase 2 (BTZ043, Q203, OPC-167832), were identified by whole cell-based screenings, whereas target-based screenings have not yielded clinically useful anti-TB agents [71,72].

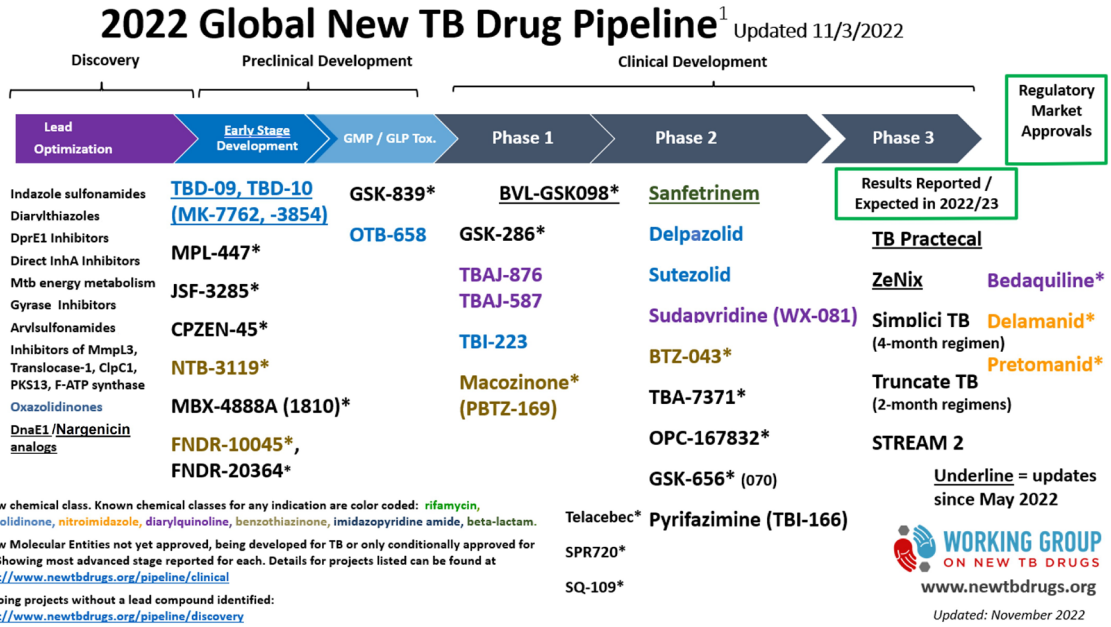

Figure 5. New TB drug pipeline. From [73]. Accessed on 19th Dec 2022.

In recent years, the oxidative phosphorylation (OxPhos) pathway has emerged as an attractive target space for drug development against *Mtb*. The first clinical validation of this pathway as a mycobacterial drug target occurred in 2012 with the approval of BDQ, a drug targeting the mycobacterial F_1F_0 ATP synthase. This was followed by the introduction of several drugs into clinical trials, such as Q203, an imidazopyridine amide that targets the cytochrome bc_1:aa_3 complex (the primary terminal oxidase of *Mtb*), and SQ-109, which reduces ATP synthesis due to its uncoupler activity [74,75].

The length of current TB regimens is based largely on the need to eradicate the slow-growing, dormant populations of *Mtb*[76]. Since a sustained proton motive force (PMF) and ATP replenishment are essential even for the viability of dormant populations of *Mtb*, inhibition of the OxPhos pathway is regarded as an effective strategy to shorten the length of future TB regimens by eradicating non-replicating bacteria [74]. Therefore, there are several projects in the TB drug pipeline aiming to identify drug candidates that target energy metabolism with a view to shortening TB therapy [73].

Interestingly, while most anti-TB drugs are not active against *M. abscessus*, those targeting the OxPhos pathway, such as BDQ and CFZ, are effective [77,78]. Specifically, CFZ is currently one of the most promising drugs in the treatment of *M. abscessus* and *M. avium* infections due to low MIC values, its synergistic interaction with standard-of-care drugs and its ability to prevent regrowth after clarithromycin (CLA) and AMK exposure [62].

Currently, only few molecules are in clinical development for the treatment of *M. abscessus* pulmonary infections compared to TB drug pipeline. Most of the candidates and leads are derived from repurposing and reformulation of existing drugs or cross-testing of a few TB-active compounds, rather than optimized to eradicate the major pathogens *M. avium* and *M. abscessus*. Therefore, new drug candidates are sorely needed to achieve all-oral bactericidal drug regimens effective for *M. abscessus* infectious.

In summary, despite global efforts in the TB drug discovery field in the last two decades have led to substantial progress and new molecules progressing in the clinical pipeline, new antimicrobials as well as new combinations of approved drugs and clinical candidates are needed to achieve shorter, better tolerated and more successful treatments, not only against *Mtb* but also against NTM species.

OBJECTIVES

OBJECTIVES

The aim of this work is to characterize the antimicrobial activity and elucidate the MoA of a new chemical series developed in a medicinal chemistry program previously performed at the University of British Columbia (UBC) and the Centre for Drug Research and Development (CDRD; now AdMare BioInnovations) (**Chapter 1**), and to study the role of the Tap efflux pump in mycobacteria, as well as the activity of two butyrophenones (bromperidol, BPD and domperidone, DPR) with potential Tap inhibitory activity (**Chapter 2**).

In order to achieve this general objective, several objectives were proposed for each chapter:

Chapter 1. Antimicrobial characterization and elucidation of the molecular mode of action of a new chemical series

- To characterize the antimicrobial activity of the chemical series against diverse bacteria.
- To identify mutants with changes in their susceptibility profile to the study compounds.
- To analyse the global transcriptome of *Mtb* after treatment with the compounds.

Chapter 2. Evaluation of the activity of butyrophenones and the role of the Tap efflux pump in mycobacteria

- To evaluate the activity of BPD and DPR in a 3D *in vitro* granuloma model.
- To study the role of the Tap efflux pump by using the granuloma model and RNA-seq studies.

Chapter 1

Antimicrobial characterization and elucidation of the molecular mode of action of a new chemical series

1. Introduction

There is an urgent need to develop drugs with novel MoA that are not affected by pre-existing resistance mechanisms, and to shorten the duration of TB treatments to improve patients' adherence, thereby restricting the emergence of drug resistance.

Since target-based approaches have had little success against bacterial infectious diseases, including TB, current drug discovery programmes focus on whole cell-based screenings, which allow the identification of molecules with antimicrobial activity. However, this approach does not provide information about the MoA or the target of the hits identified [79].

Although not a requisite for FDA approval, understanding the MoA of new molecules accelerates further lead optimization and provides useful information for clinical development. For example, it allows the establishment of SAR to improve the activity and selectivity of the compound, while reducing its toxicity [80]. Therefore, several studies are typically performed in the hit to lead phase of the drug discovery process in order to elucidate the MoA of the compounds.

1.1. Approaches to elucidate the MoA

There are different approaches to identify the MoA of newly discovered molecules. Some of the most widely used strategies are described below.

Isolation of spontaneous resistant mutants

The most straightforward approach to elucidate the MoA is based on the isolation of spontaneous mutants resistant to the compounds and characterization of the chromosomal mutations involved in the resistance phenotype [11,80].

Bacteria are continuously evolving; hence, exposure to antimicrobials will ultimately select for resistant mutants if the number of bacteria screened is large enough to exceed the frequency of mutation conferring resistance to the compound. Once resistant mutants are selected, the mutations underlying the resistance phenotype are identified by WGS. Then, the implication of the mutations identified in the resistance phenotype are usually confirmed by biochemical or genetic studies (*e.g.,* by constructing strains with the gene mutated overexpressed or deleted) [79].

Due to the variety of bacterial resistance mechanisms, resistance-conferring mutations can arise in genes encoding the target, but also in genes unrelated to the direct target, such as those encoding drug resistance mechanisms or drug activating pathways [80]. For example, the target of BDQ, which was identified by resistance selection assays, is the c-ring of ATP synthase (encoded by *atpE*). Therefore, mutations in *atpE* reduce drug binding and result in high level resistance. However, other mechanisms of resistance have also been identified by resistance selection assays, including mutations in the *rv0678 gene* encoding a transcriptional repressor and in the *pepQ* gene encoding a putative peptidase [11]. Mutations in *rv0678* confer low-level resistance to BDQ and other drug classes, including azoles, CFZ and PBTZ-169, through upregulation of MmpL5/MmpS5 system [59–61,81]. Interestingly, only mutations in *rv0678* are clinically relevant. Hence, this approach is a powerful means of target identification when the mutations map to the target itself, but sometimes there is a disconnect between the mechanism of resistance of a hit and its mechanism of action [79].

During the drug discovery process, resistance selection assays are also performed to determine the frequency of mutation to the compounds, and information derived from these studies is then applied to the design of new analogues [11]. Nonetheless, spontaneous resistant mutants cannot always be selected. A common approach to overcome this problem is to increase the frequency of mutation, thereby increasing the variability of the population. This can be achieved by different means, such as the use of bacterial strains defective in DNA repair systems or exposure of bacteria to increasing drug concentrations over time [80,82]. However, these methods might not yield resistant mutants, especially for compounds with multiple drug targets.

Screening of mutant libraries

Mutant libraries are considered an invaluable shortcut to identify the MoA of novel compounds when resistant mutants are not easily selected [80]. Mutant libraries can include knockout, conditional knockdown and/or overexpression mutants. A common approach is to screen these libraries to search for individuals with an increased or decreased susceptibility to the drug in comparison to the wild type strain [79,80]. This approach is based on the idea that depletion of a target would render the bacteria hypersensitive to inhibitors that act on that target or pathway [79], whereas target overexpression would have the opposite effect.

Importantly, this strategy allows rapid identification of the genes responsible for the resistant or susceptible phenotype by finding the location of a foreign sequence in the genome (*e.g.,* in transposon mutant libraries, by sequencing from the transposon sequence).

Furthermore, mutant libraries can also provide insights into mechanisms related to drug uptake or efflux, which need to be considered during the drug discovery process.

Use of omics (transcriptomics, proteomics, and metabolomics)

An alternative approach is the use of omics, such as transcriptomics, proteomics and metabolomics, which allow global profiling of transcriptome, proteome and metabolome, respectively. These techniques are very useful for generating hypothesis about the MoA of novel antimicrobials [83].

While microarrays have been the main technique for transcriptomic profiling for a long time, RNA-seq -which uses next-generation sequencing (NGS)- is now the method of choice in most cases since it enables to study the entire transcriptome without the need of hybridization probes and offer higher specificity and sensitivity than microarrays [83,84].

RNA-seq is a useful technique which can provide new insights for anti-TB drugs currently used, as well as aid to elucidate the MoA of new compounds identified by whole-cell screening assays. These changes in gene expression profiles after drug treatment can provide valuable information about the ability of *Mtb* to escape or counteract the effect of the drug, and allow monitoring of the physiology of the bacteria during treatment [84].

While transcriptomics provides a useful overview of global gene expression, proteomics can be also used as a complementary technique that provides a comprehensive insight into the protein profile, and metabolomics can be employed to find the metabolic pathway affected or as an in-depth analysis of drug effects on bacterial metabolism [84].

1.2. A novel series of anti-TB compounds

In this Chapter, we employed different approaches to elucidate the MoA of a new chemical series developed in collaboration among UBC, CDRD (now AdMare BioInnovations) and UZ.

This new chemical series was developed in a medicinal chemistry program led by UBC and AdMare that generated more than fifty chemical analogues. Then, a collaboration was initiated among UBC, AdMare and UZ to characterise the antimicrobial activity of this chemical series against diverse bacteria, as well as elucidate their MoA.

Eight representative compounds of this chemical series (named compounds C1, C2, C3, C4, C6, C7, C8 and C9) were used at the UZ to characterize their antimicrobial activities. Compounds C1, C2 and C9 were used for MoA studies, with the assumption that analogues coming from the same chemical series should display similar MoA.

2. Objectives

The main objective of Chapter 1 was to characterize the antimicrobial activity and elucidate the MoA of a new chemical series developed in collaboration among UBC, AdMare and UZ.

In order to achieve this general objective, several specific objectives were proposed:

- To characterize the antimicrobial activity of this chemical series against diverse bacteria, including intracellular *Mtb*, and to evaluate their cytotoxicity against the THP-1 cell line.
- To identify mutants with changes in their susceptibility profile to C2 and C9 by standard mutant isolation assays with *Mtb* H37Rv and screening of a *M. bovis* BCG transposition library, respectively.
- To evaluate under different iron conditions the activity of the study compounds against *Mtb* mutants with *mmpL4*/*mmpS4* genes deleted or overexpressed.
- To identify and characterize synergistic partners of C9 and C1 against *Mtb* and *M. abscessus,* respectively.
- To study the potential role of this chemical series as efflux inhibitors (EI).
- To construct *Mtb* mutants with *mmpL5*/*mmpS5* genes deleted or overexpressed to evaluate their susceptibility to the compounds under different iron conditions.
- To study the mechanism of resistance of Gram-negative bacteria to the study compounds, and to isolate and characterize *E. coli* Δ*acrB*-derived mutants resistant to C2.
- To analyse the global transcriptome of *Mtb* after treatment with C9.

3. Results and discussion

3.1. Characterization of the antimicrobial activity

3.1.1. Activity against mycobacteria, Gram-positive and Gram-negative bacteria

The antimicrobial activity of this new chemical series was characterised against mycobacteria, Gram-positive and Gram-negative bacteria by liquid MIC assays.

Compounds were active against mycobacteria (*Mtb*, *M. bovis* BCG, *M. smegmatis*, *M. abscessus*) and Gram-positive bacteria (*Corynebacterium glutamicum*, *Corynebacterium diphtheriae*, *Enterococcus faecalis*, *Staphylococcus aureus* and *Streptococcus agalactiae*), showing MIC values lower than 16 µg/mL (except for *M. abscessus,* with MIC values of 32 µg/mL). However, they were not active against Gram-negative bacteria under the conditions tested (MIC > 64 µg/mL) (**Figure 6**).

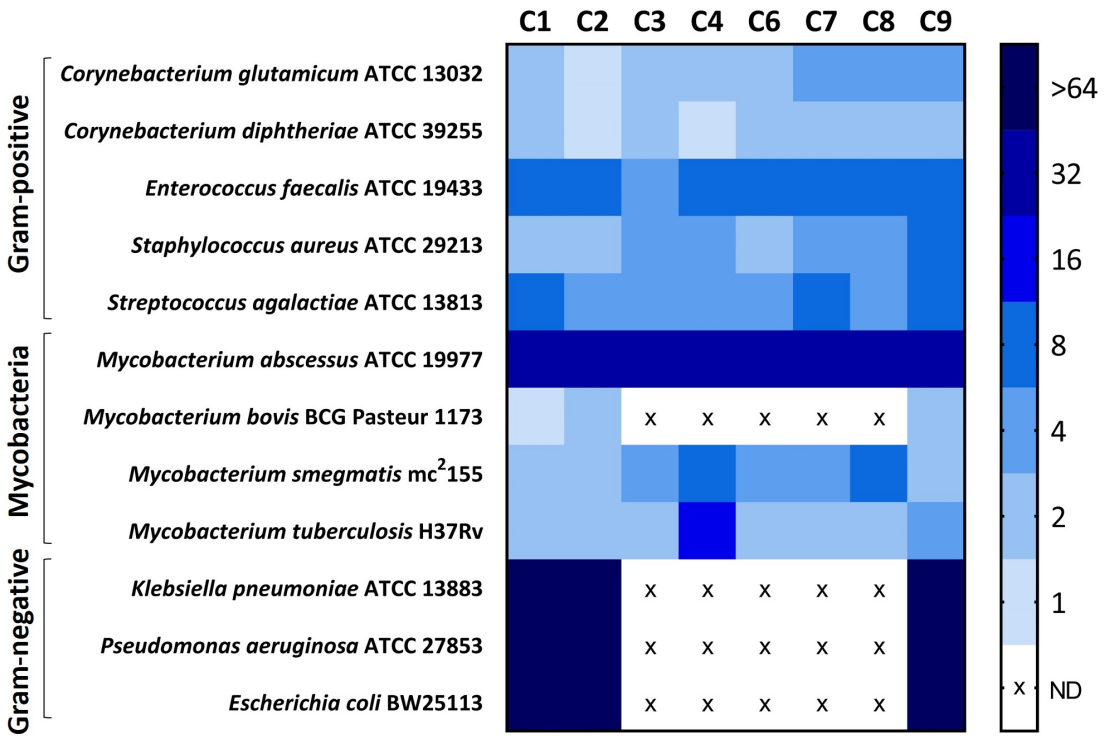

Figure 6. Antimicrobial activity of the study compounds against several bacterial strains. MTT was used as the bacterial growth indicator.

3.1.2. *Mtb* time kill assays under replicating and non-replicating conditions

The potent antimicrobial activity of these compounds against *Mtb* (MIC < 4 µg/mL, except for C4) led us to further study their activity over time by time kill assays to distinguish between a bactericidal or bacteriostatic effect. In these assays, bactericidal activity was defined as greater than 3 log_{10}-fold decrease in CFUs (colony forming units) [85].

Time kill assays against *Mtb* H37Rv under replicating conditions revealed that C9 at 4xMIC (16 µg/mL) had a slow onset of bactericidal activity against *Mtb* (**Figure 7A**). Since new drugs that eradicate the slow-growing, dormant *Mtb* populations are needed to achieve shorter TB therapies, we performed time kill assays under non-replicating conditions by adding the study compounds to late stationary phase cultures [86]. C1, C2 and C9 at 100 µg/mL were able to reduce the bacterial load 2-logs in the first 4 days of treatment and 3-logs within 2-3 weeks, confirming their bactericidal activity against non-replicating bacteria. Moreover, the killing curves indicated that these compounds were more potent than INH (**Figure 7B**).

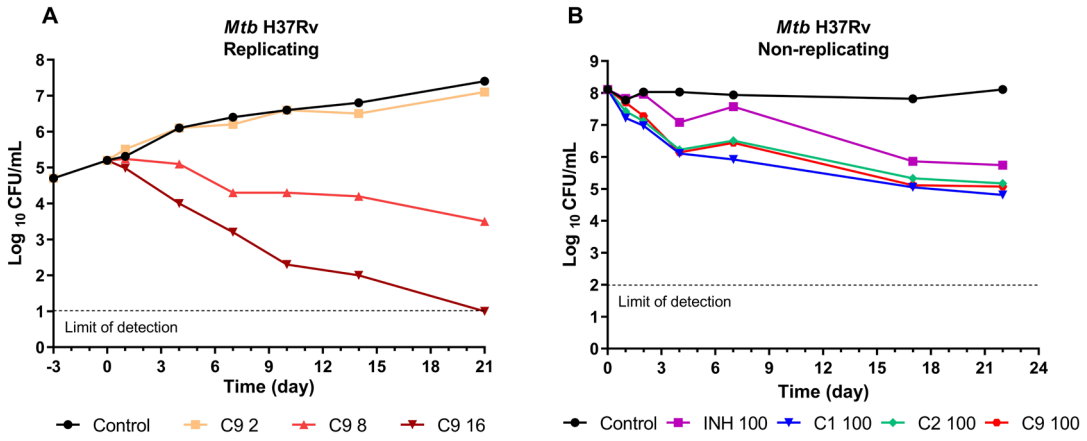

Figure 7. Time kill assays against exponential or stationary phase cultures of *Mtb* H37Rv. (A) Bacteria were inoculated at a cell density of 10^5 CFU/mL and C9 was added at different concentrations after 3 days of incubation at 37ºC. (B) Drugs were added to *Mtb* cultures in stationary phase (6 weeks of incubation at 37ºC). Concentration of drugs are indicated in µg/mL. INH, isoniazid. MIC INH = 0.25 µg/mL; MIC C1 = 2 µg/mL; MIC C2 = 2-4 µg/mL; MIC C9 = 2-4 µg/mL (MIC values are those from replicating conditions).

Taken together, time kill assays revealed that this new chemical series has strong bactericidal activity against *Mtb* both in exponential and stationary phase. Importantly, bacterial growth rebound was not observed after 21 days of treatment with the compounds alone.

3.1.3. Intracellular activity and cytotoxicity assays

The antimicrobial activity of the compounds was also evaluated against THP-1 cells infected with *Mtb* H37Rv-Luc. Moreover, the cytotoxicity of the compounds against THP-1 cell line was assessed to measure cell viability. RIF and INH were included as internal controls.

These compounds were active against *Mtb* inside THP-1 cells, showing MIC values equal or lower than those obtained against extracellular *Mtb*, except for C3 (**Table 3**). Importantly, compounds were not toxic to THP-1 cells at the doses required for activity against *Mtb* (**Table 3 & Figure 8**). The selectivity index (SI), defined as the ratio of the toxic concentration of a drug against its effective concentration, was higher than 8-16 for all compounds (except for C3), which is considered acceptable for this type of assay.

Table 3. Activity of compounds against *Mtb* in extracellular (Extra Activity) and intracellular conditions (Intra Activity), and their toxicity against THP-1 cells (Toxicity). SI (selectivity index) was calculated as the ratio of the toxic concentration (IC50) of the compound over its effective concentration (MIC50). MIC90 and MIC50 are the minimum drug concentrations inhibiting bacterial growth by 90% and 50%, respectively; IC50 is the minimum drug concentration inhibiting cell viability by 50%. Values are in µg/mL. INH, isoniazid; RIF, rifampicin.

Compounds	Extra Activity	Intra Activity		Toxicity	SI
	MIC90	MIC90	MIC50	IC50	(IC50/MIC50)
C1	2	1	0.25	2-4	8-16
C2	2	1	0.125	4	32
C3	2	4	0.5-1	2-4	4-8
C9	2	2	0.5	4-8	8-16
INH	0.25	0.063	0.03	>1	>33.3
RIF	0.125	0.125	0.063	>1	>16

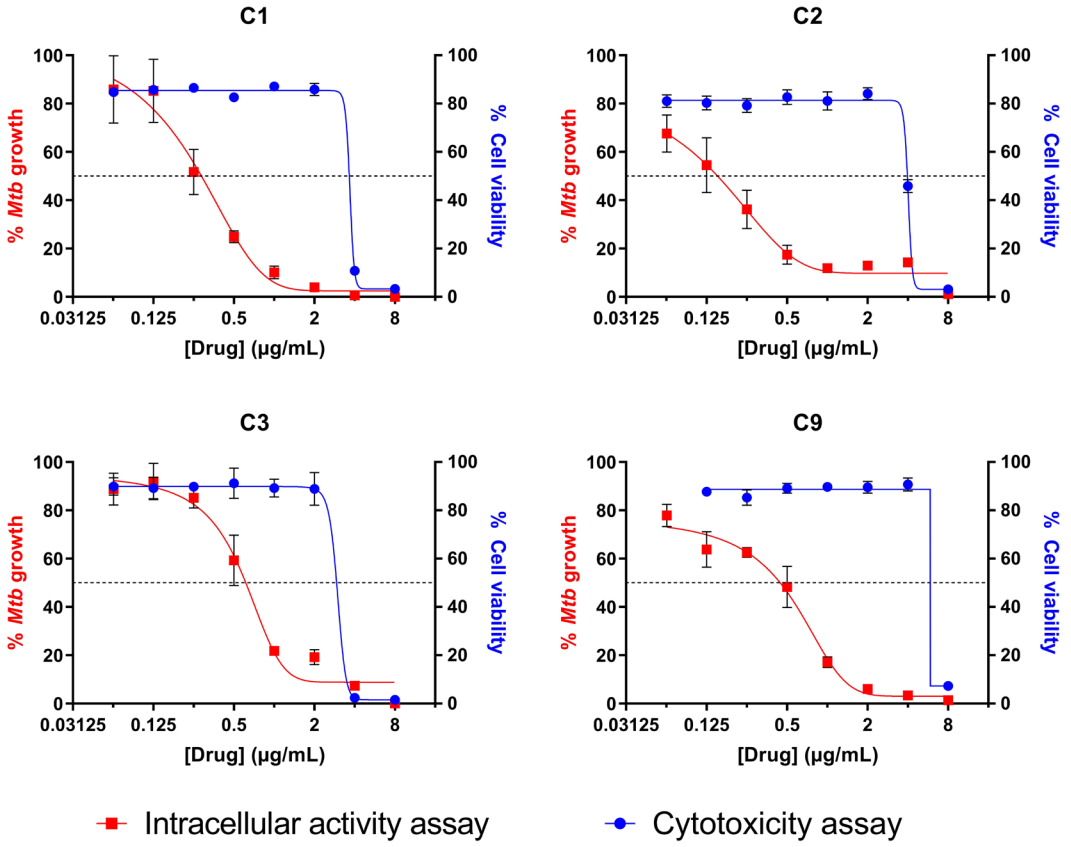

Figure 8. Dose response curves of C1, C2, C3 and C9 compounds against intracellular *Mtb* H37Rv-Luc (red) and THP-1 cell line (blue). Dashed lines indicate MIC50 and IC50. Data represent mean ± SEM (standard error of the mean) from 3 technical replicates.

Therefore, this new chemical series is active not only against extracellular *Mtb*, but also against *Mtb* inside THP-1 cells, and shows little toxicity against THP-1 cells.

3.2. Elucidation of the molecular mode of action

3.2.1. Standard mutant isolation assays

During my Master's thesis [87], two complementary approaches were used to isolate mutants resistant to the compounds: (i) standard mutant isolation assays at inhibitory concentrations using the wild type strain *S. aureus* methicillin-sensitive (MSSA) ATCC 29213; (ii) screening of a transposition library of *M. smegmatis* HS42 mutants. These approaches were not able to isolate resistant mutants, suggesting that the mutation frequency conferring resistance to the compounds is low ($<10^{-8}$) (**Appendix I-Table AI.1**).

In this study, we attempted alternative strategies to isolate resistant mutants by seeding three different inocula (10^7, 10^8 and 10^9 CFU) of *Mtb* H37Rv in 7H10-OADC agar plates containing 2x, 4x or 10x the MIC of C2, taking as reference the solid MIC values previously determined for different bacterial densities of this strain. BDQ was used as internal functionality control. Difference in MICs between low (10^5) and high (10^7) inoculum were of 2-fold, indicating that the activity of the C2 compound was inoculum independent (**Table 4**). It was not possible to isolate mutants resistant to C2; however, mutants resistant to BDQ were isolated with frequencies of mutation similar to those reported by Andries *et al.* [88] (**Table 5**).

Table 4. Solid MIC values of C2 and BDQ in 7H10-OADC agar plates against different inocula of *Mtb* H37Rv. BDQ, bedaquiline.

Inoculum (total CFU)	Solid MIC (µg/mL)	
	C2	BDQ
10^7	16	0.125
10^5	8	0.063

Table 5. Summary of the experimental conditions used for the isolation of *Mtb* H37Rv mutants resistant to C2 and BDQ. Frequencies of mutation were calculated as the ratio of total number of colonies isolated in the presence of the drug over the total CFUs seeded.

Inoculum	Compound concentration (x MIC)	Colonies isolated	Frequency of mutation
10^7-10^9 CFU	C2 32-128 µg/mL(2x-8x)	0	$<10^{-9}$
10^8 CFU	BDQ 0.5 µg/mL (4x)	9	$3{\cdot}10^{-8}$
	BDQ 1 µg/mL (8x)	9	$3{\cdot}10^{-8}$

Attempts to isolate mutants resistant to these compounds were thus unsuccessful, suggesting that this new chemical series may have more than one target.

3.2.2. Screening of the *Mycobacterium bovis* BCG Tn*SPAZ* transposition library

Since standard mutant isolation assays were unsuccessful, we then screened an *M. bovis* BCG Tn*SPAZ* transposition library as an alternative strategy to identify mutants with an increased or decreased susceptibility to these compounds (specifically, C9). The screening assay was set up as described in ***Material and methods***.

Results of the screening and validation assays

For the screen performed in order to select resistant mutants, no mutants were retrieved from the pool plates. Regarding the susceptibility screen, 48 mutants (1.67% of the library) did not grow in the presence of sub-inhibitory concentrations (1/8x and 1/4x MIC) of C9 but did grow in the control plate (without C9). Therefore, these 48 mutants were selected for further validation of their susceptible phenotype.

As a primary validation assay, the MIC of C9 against each potential susceptible mutant was determined in liquid medium (7H9-Gly-ADC) by doing 1.4-fold (instead of 2-fold) serial dilutions of C9 to detect subtle differences in their susceptibility profiles. Since most mutants only showed a one-dilution decrease in their MIC to C9, we selected 19 mutants for secondary validation assays to confirm these variations in drug sensitivity by susceptibility testing on agar plates, which can better detect subtle differences in drug sensitivity. This assay was performed by seeding 5 µL of 10-fold serial dilutions of the candidate mutants in control plates (without C9) and agar plates containing sub-inhibitory concentrations of C9 (1, 2 and 4 µg/mL), taking as reference the solid MIC values previously determined for BCG wild type (**Table 6**). Similar to the C2 compound (**Table 4**), the activity of C9 was inoculum independent (**Table 6**).

Table 6. Solid MIC values of C9 in 7H10-OADC agar plates against three different inocula of BCG wild type.

Inoculum (total CFU)	Solid MIC C9 (µg/mL)
10^7	16
10^5	8-16
10^3	8

As a result, seven mutants (M8, M9, M10, M11, M17, M18 and M19) were more susceptible to C9 than the wild type strain (**Figure 9 & Appendix II-Figure AII.1**). Their susceptible phenotype was observed in agar plates containing 4 µg/mL of C9, since these mutants were not able to grow at this concentration, while the wild type strain grew normally for all four dilutions tested (**Figure 9 & Appendix II-Figure AII.1**).

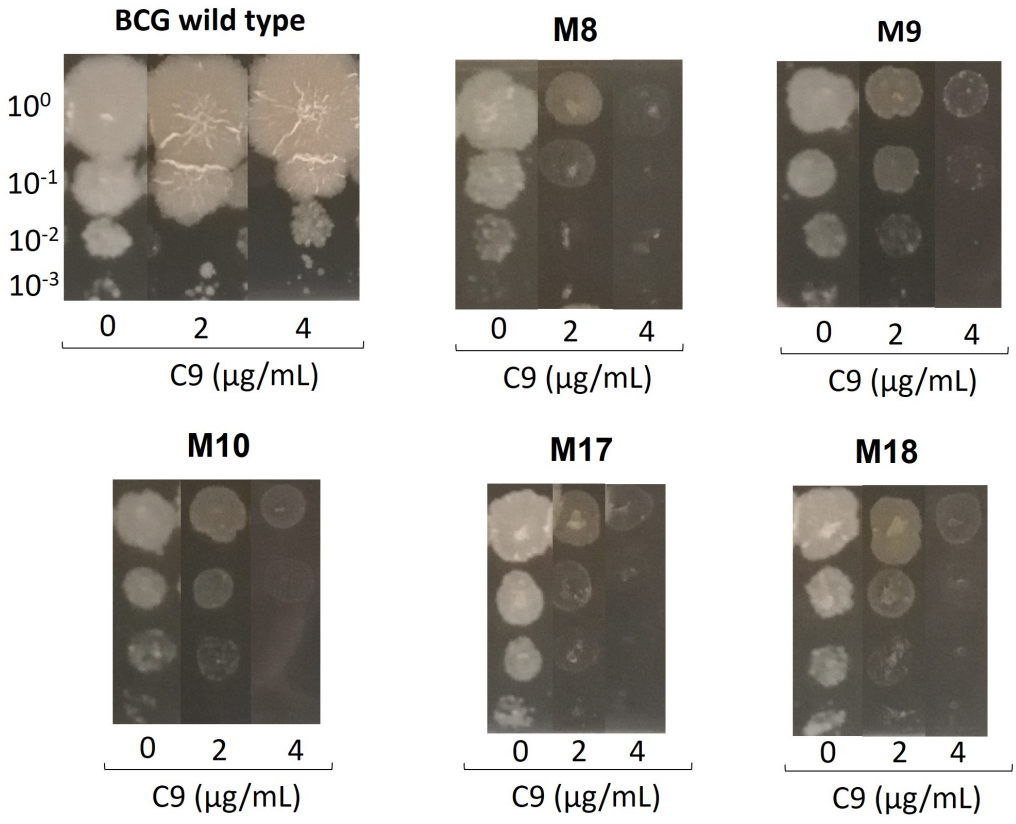

Figure 9. Susceptibility testing in agar plates of five representative *M. bovis* BCG susceptible mutants (M8, M9, M10, M17 and M18) and the wild type strain. 10-fold serial dilutions of 0.12 OD_{600nm} cultures were seeded in agar plates containing none or sub-inhibitory concentrations of C9 (2 and 4 µg/mL). Agar plates were incubated at 37 ºC for 18 days.

As a tertiary validation assay, the susceptibility of M8, M17 and M18 mutants was evaluated by time kill assays using the BacTiter-Glo Microbial Cell Viability Assay (Promega), which measures the number of viable bacteria based on the amount of ATP present. BacTiter-Glo Kit was used as the bacterial readout instead of CFU enumeration since it minimizes both sample handling and waiting time until results are obtained. Before conducting this assay, a relationship between RLU and CFU was established to confirm that the transposon insertion in the genomes of the selected mutants did not alter luminescence production.

The three mutants tested (M8, M17 and M18), which showed very similar killing curves, were more susceptible to C9 than the wild type strain. This increased susceptibility to C9 was evident when bacterial cultures were treated with 4 µg/mL (**Figure 10**).

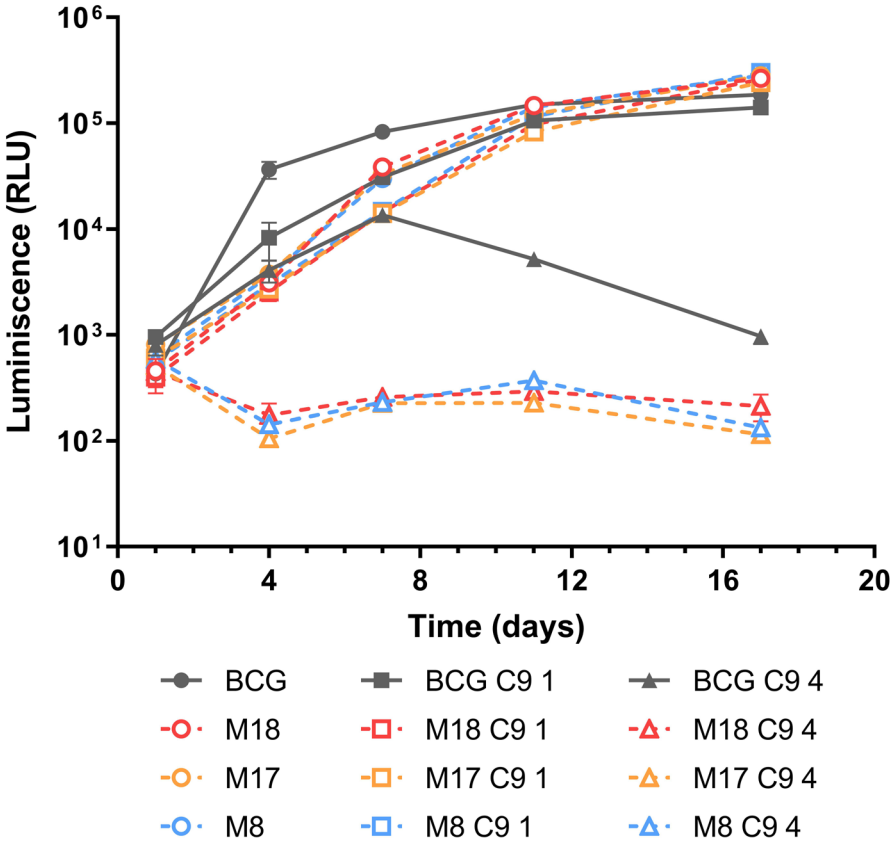

Figure 10. Time kill assays of *M. bovis* BCG wild type (solid lines & symbols) and M8 (blue), M17 (orange) and M18 (red) *M. bovis* BCG mutants (dashed lines, open symbols) exposed to 1 (■) or 4 (▲) µg/mL of C9, plus non-treated cultures (●) in 7H9-0.025%Tyl-10%ADC medium. Bacteria were inoculated at a cell density of 10^5 CFU/mL and C9 was added at the concentrations indicated. BacTiter-Glo Microbial Cell Viability Assay (Promega) was used to measure the number of viable bacteria (on days 1, 4, 7, 11 and 17 after the addition of C9) by mixing equal volumes of bacterial cultures and BacTiter reagent. Data represent mean ± SD (standard deviation) from 2 technical replicates. RLU: relative luminescence units.

It should be noted that untreated mutants produced less luminescence than untreated BCG wild type on day 4 (**Figure 10**). Taking into account that the luminescent signal is proportional to ATP levels, it could be speculated that M8, M17 and M18 mutants have the transposon inserted in a genome site relevant for bacterial metabolism, which might affect ATP production in these mutants. This result will be further discussed along this Chapter.

Taken together, the increased susceptibility of M8, M9, M10, M11, M17, M18 and M19 mutants was confirmed by susceptibility testing in agar plates, as well as by time kill assays in the case of M8, M17 and M18 mutants.

Identification of the transposon insertion site in the genomes of C9-susceptible *M. bovis* BCG mutants

Mutants M7, M17 and M18 were selected to identify the location of the transposon in their genomes. To achieve this goal, they were propagated in 7H9-Tween-ADC and their DNA was isolated to perform LM-PCR (ligation-mediated PCR) and Sanger sequencing of the PCR product.

M8, M17 and M18 mutants had the transposon inserted at nucleotide 571,769, disrupting *mmpL4* gene (BCG_0489c, from nucleotides 569,403 to 572,306) (**Figure 11**). This gene codifies a probable conserved transmembrane transport protein MmpL4 (967 amino acids), which has 100 % identity with MmpL4 of *Mtb* H37Rv, known as siderophore exporter MmpL4. Hence, these mutants only would produce the first 179 amino acids of MmpL4 instead of the full length protein, resulting in a loss of MmpL4 protein function.

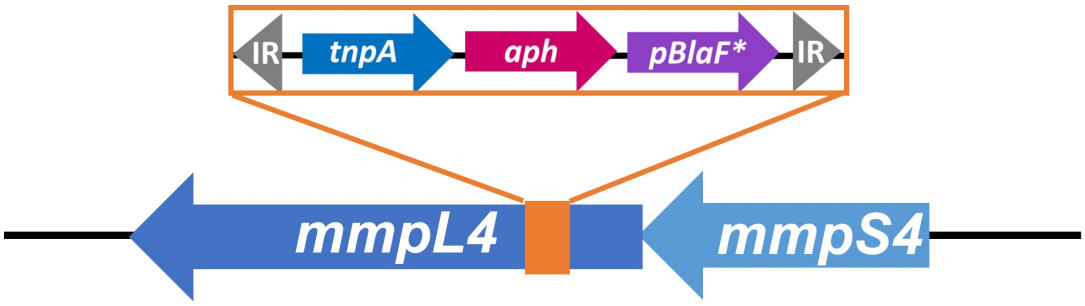

Figure 11. Schematic representation of the location of Tn*SPAZ* transposon in the genomes of M8, M17 and M18 mutants. Tn*SPAZ* transposon is represented by an orange box.

Role of MmpL4 in the increased susceptibility to C9

The genome of *Mtb* H37Rv contains 13 MmpL (mycobacterial membrane protein large) proteins (MmpL1-13), which belong to the RND superfamily of membrane transporters based on their topological organization. MmpL-mediated substrate transport across the cytoplasmic membrane is energetically dependent on the PMF, as for most RND proteins [89]. Not only are MmpL transporters important for the translocation of virulence-associated envelope lipids and siderophores across the plasma membrane, but also responsible for intrinsic drug-resistance in both non-tuberculous and tuberculous mycobacteria by extruding drugs from the cytoplasm. For example, over-expression of *mmpL5/mmpS5* genes due to mutations in its transcriptional repressor *rv0678* has been associated with increased resistance to BDQ, CFZ and azole drugs [59–61,89,90].

Specifically, MmpL4/MmpL5 transporters require their accessory MmpS4/MmpS5 (mycobacterial membrane protein small) proteins to export the two types of siderophores produced by *Mtb* to scavenge iron from the environment: the membrane-bound mycobactins and the water-soluble carboxymycobactins. Siderophores have high affinity for Fe^{3+} and can scavenge it from insoluble hydroxides and iron-binding proteins. Importantly, MmpL4/MmpS4 and MmpL5/MmpS5 mycobactin export systems are essential for siderophore-mediated iron acquisition and have been described to be required for *Mtb* virulence [91]. Hence, these transporters represent promising drug targets.

To confirm that *mmpL4* gene was responsible for the observed C9-susceptible phenotype, we first determined the MIC of C9 against *Mtb*-derived strains deficient in *mmpL4* (L4KO) or *mmpL4/mmpS4* (L4S4KO) genes, as well as their complemented strains (L4c and L4S4c, respectively). A strain overexpressing *mmpL4/mmpS4* was also included (L4S4sb). These strains are described in detail in **Table 31**. Since previous studies have suggested that MmpL4 and MmpL5 are functionally redundant *in vitro* [91], we also evaluated the susceptibility of these strains to several drugs extruded by the MmpL5/MmpS5 system, including BDQ and the azole drugs econazole (ECO) and ketoconazole (KET).

Both L4KO and L4S4KO mutants were slightly more susceptible to C9 and ECO than H37Rv wild type and their respective complemented strains (L4c and L4S4c). In contrast, over-expression of *mmpL4/mmpS4* did not lead to changes in MIC values. All strains tested had the same MIC of BDQ and KET (**Table 7**).

Table 7. Susceptibility of *Mtb*-derived strains to C9, BDQ, ECO and KET in 7H9-Gly-ADC.

Strain	MIC (µg/mL)			
	C9	BDQ	ECO	KET
H37Rv	4	0.063	16	8-16
L4KO	2 **(2)**	0.063	8 **(2)**	8
L4c	4	0.063	16	8-16
L4S4KO	2-4 **(1-2)**	0.063	8 **(2)**	8
L4S4c	4	0.063	16	8
L4S4sb	4	0.063	16	8

C9, compound 9; BDQ, bedaquiline; ECO, econazole; KET, ketoconazole. Values in parentheses indicate fold reduction in MIC values compared to the wild-type.

Since liquid MIC assays are not sensitive enough to detect subtle differences in drug susceptibility profiles, we then evaluated by time kill assays the susceptibility of H37Rv wild type and L4KO mutant to C9, in 7H9-ADC medium supplemented with 0.2% glycerol (**7H9-ADC-Gly**) or 0.025% Tyloxapol (**7H9-ADC-Tyl**). We selected L4KO to confirm these results as both L4KO and L4S4KO mutants showed similar MIC values and mutants identified in the screening (M8, M17 and M18) had the Tn*SPAZ* transposon interrupting only *mmpL4* gene (**Figure 11**).

As a result, L4KO mutant showed no growth defects in comparison with the parental H37Rv strain under standard aerobic growth conditions, in line with previous results [91,92]. Importantly, time kill assays confirmed that L4KO mutant was more susceptible to C9 than H37Rv wild type. This increased susceptibility was higher in medium containing glycerol (**Figure 12A**) rather than tyloxapol (**Figure 12B**).

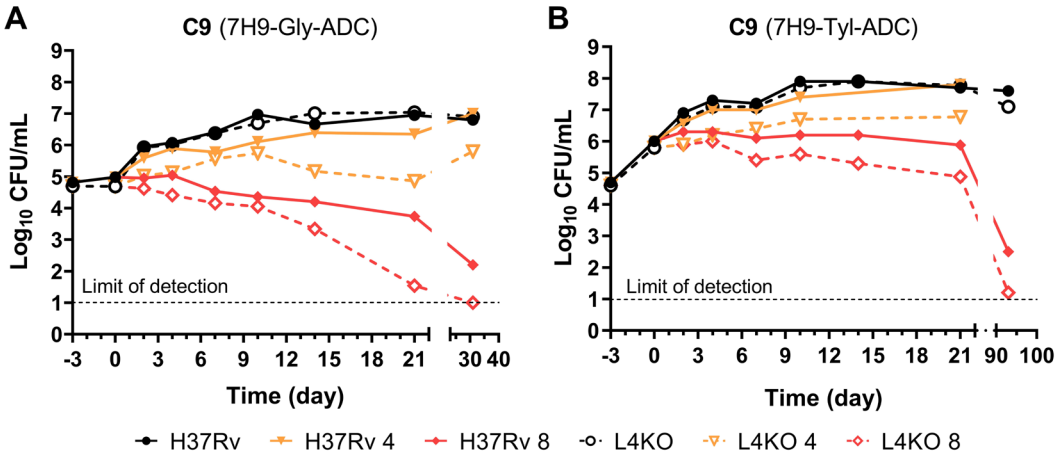

Figure 12. Time kill assays of H37Rv wild type (solid lines) and L4KO mutant (dashed lines) exposed to 4 (orange) or 8 (red) µg/mL of C9, in 7H9-0.2%Gly-10%ADC (A) and 7H9-0.025%Tyl-10%ADC (B) media. Untreated cultures are shown in black lines. Bacteria were inoculated at a cell density of 10^5 CFU/mL and C9 was added at different concentrations after 3 days of incubation at 37 ºC.

In 7H9-Gly-ADC medium (**Figure 12A**), treatment with 4 µg/mL of C9 was bacteriostatic against L4KO mutant, whereas H37Rv wild type was able to grow at this concentration after 21-day incubation. Moreover, 8 µg/mL of C9 was bactericidal (> 3-log reduction) for L4KO, but not against H37Rv after 21 days of treatment.

As previously mentioned, the potency of C9 seemed to decrease in medium with tyloxapol, causing only a 1-log reduction when added to L4KO cultures at 8 µg/mL and showing a bacteriostatic profile against H37Rv after 21 days (**Figure 12B**). These differences could be also due to the dispersion effect of the tyloxapol.

It is worth noting that after 100 days of incubation, the single addition of C9 at 8 µg/mL at time day 0 was able to almost fully sterilize the L4KO culture and caused a 4-logs decrease in the number of viable cells of the H37Rv wild type strain (**Figure 12B**). Given that C9 stability assays have not been performed, we can speculate two scenarios: (i) that the compound could be extraordinarily stable over such prolongated incubation times, and thus it would continue killing *Mtb* upon time, or (ii) that the compound has been degraded but it causes a cellular damage for which bacteria are not able to recover and for which the L4KO mutant is worst equipped than the wild type strain.

To sum up, by time kill assays, we have demonstrated that MmpL4 is involved in the *Mtb*'s increased susceptibility to C9, thus confirming previous results derived from the screening and subsequent validation assays.

3.2.3. Effect of iron levels on the susceptibility to the compounds

MmpL4/MmpS4 proteins, along with MmpL5/MmpS5, are involved in siderophore export, thus being required for siderophore-mediated iron acquisition [91]. Likewise, their expression is induced under iron-limited conditions [93]. Taking into consideration these data and our previous findings that L4KO was more susceptible to C9 than the wild type strain (**Table 7 & Figure 12**), we hypothesized that the MoA of this new chemical series could be related to iron metabolism. Therefore, several assays were performed to determine whether the activity of these compounds varied depending on the iron concentration present in the media.

We first determined the MIC of C1 and C9 against H37Rv wild type, L4KO and L4S4KO in 7H9-Gly-ADC supplemented with 0.2 mM of deferoxamine (DFO), a heterologous siderophore that chelates Fe^{3+} in the medium at a 1:1 molar ratio [94]. BDQ, ECO and KET were also included due to their association with MmpL5/S5 system, as described above.

Both L4KO and L4S4KO strains were more susceptible to C1 and C9 in this iron-restricted medium (**Table 8**) than in iron-complete medium (**Table 7**), showing MIC values 4-8-fold lower than those of H37Rv wild type. In contrast, MIC values of BDQ, ECO and KET against *Mtb* H37Rv, L4KO and L4S4KO did not change in this iron-restricted medium.

Table 8. Susceptibility of H37Rv wild type, and L4KO and L4S4KO mutants to C1, C9, BDQ, ECO and KET in 7H9-Gly-ADC supplemented with 0.2 mM DFO.

Strain	MIC (µg/mL) in 7H9-Gly-ADC supplemented with 0.2 mM DFO				
	C1	C9	BDQ	ECO	KET
H37Rv	2	8	0.063	16	8
L4KO	0.25-0.5 **(4-8)**	1-2 **(4-8)**	0.063	8 **(2)**	8
L4S4KO	0.25-0.5 **(4-8)**	1-2 **(4-8)**	0.063	8 **(2)**	8

BDQ, bedaquiline; ECO, econazole; KET, ketoconazole. Values in parentheses indicate fold reduction in MIC values compared to the wild-type.

Next, we further assayed the antimicrobial activity of these compounds in media with different iron levels. The medium used in this assay was self-made 7H9 (without 40 µg/mL of ferric ammonium citrate) plus 0.2% glycerol and 10% ADC, supplemented with 4 (**Fe 4**) or 40 (**Fe 40**) µg/mL of $FeCl_3$. We also included an additional iron-restricted condition by adding 0.2 mM of DFO to the medium containing 40 µg/mL of $FeCl_3$ (**Fe 40 + DFO**). The total estimated amount of $FeCl_3$ in the different assay conditions was 247 µM (**Fe 40**), 24.7 µM (**Fe 4**) and 47 µM (**Fe 40 + DFO**).

In iron-replete medium (**Fe 40**), L4KO was slightly more susceptible to C9 than H37Rv wild type and the complemented strain, as previously described (**Table 7 & Table 9**). In contrast, in both iron-restricted media (**Fe 4** and **Fe 40 + DFO**), L4KO displayed an 8-fold decrease in the MIC of C9 compared to H37Rv wild type. Importantly, this phenotype was complemented (L4c strain) (**Table 9**).

These results indicated that the susceptibility of L4KO to C9 increased in iron-restricted medium, whereas the susceptibility of H37Rv wild type did not change under different iron conditions when assayed by liquid MIC determination. Since the MIC of BDQ and INH under the conditions tested remained relatively unchanged, we consider that the effects observed are specific to the compounds of study.

Table 9. Susceptibility of H37Rv wild type, L4KO and L4c to C9, INH and BDQ under different iron conditions. Data from two independent experiments are shown.

Condition	Strain	MIC (µg/mL)		
		C9	INH	BDQ
Fe 40	H37Rv	2	0.031	0.031
	L4KO	**1**	0.063	0.031
	L4c	2	0.031-0.063	0.031
Fe 4	H37Rv	2	0.031	0.031
	L4KO	**0.25-0.5**	0.063	0.031
	L4c	2	0.016	0.031
Fe 40 + DFO	H37Rv	2-4	0.125	0.031
	L4KO	**0.25**	0.125	0.031
	L4c	2	0.063-0.125	0.031

The medium used in this assay was self-made 7H9 (without 40 µg/mL of ferric ammonium citrate) plus 0.2% Gly and 10% ADC. This medium was supplemented with 4 or 40 µg/mL of $FeCl_3$ (in the presence or in the absence of 0.2 mM of DFO).

These results indicated that the MoA of this new chemical is related to iron metabolism and interconnected with the function of MmpL proteins.

One alternative approach to elucidate the MoA of a new chemical series is the use of **transcriptomics**, as it is explained in ***Chapter 1, Section 3.2.8***. This strategy requires a high starting inoculum to obtain enough bacterial RNA to be analysed. Since liquid MIC and time kill assays are usually performed at a starting inoculum of 10^5 CFU/mL, these assays were repeated at higher bacterial densities (10^7 CFU/mL) to establish the optimal conditions for RNA extraction and subsequent RNA-seq analysis.

We first determined the MIC of C9 against 10^7 CFU/mL of *Mtb* H37Rv and L4KO, in media with different iron levels (**Fe 40, Fe 4** and **Fe 40 + DFO**). The effect of 0.025% Tyloxapol was also assessed (**Table 10**).

Table 10. MIC of C9 against ca. 10^7 CFU/mL (high inoculum) of *Mtb* H37Rv and L4KO under different iron conditions, and in the presence or in the absence of 0.025% Tyloxapol. Bacteria were inoculated to a cell density of $5 \cdot 10^5$ CFU/mL in each medium and incubated at 37°C for 5 days for bacterial adaptation to the media. Then, bacterial cultures were adjusted to an OD_{600nm} of 0.2 for liquid MIC assay. MTT was added after 7-day incubation at 37°C.

Condition	Strain	-/+ 0.025% Tyl	MIC C9 (µg/mL)
Fe 40	H37Rv	-	8
		+	8
	L4KO	-	8
		+	8
Fe 4	H37Rv	-	8
		+	8
	L4KO	-	8
		+	8
Fe 40 + DFO	H37Rv	-	8
		+	8
	L4KO	-	8
		+	8

The medium used in this assay was self-made 7H9 (without 40 µg/mL of ferric ammonium citrate) plus 0.2% Gly and 10% ADC. This medium was supplemented with 4 or 40 µg/mL of $FeCl_3$ in the presence or in the absence of 0.2 mM of DFO. The effect of 0.025% Tyloxapol was also evaluated.

Table 10 shows that MIC values of C9 did not change under the conditions tested. While L4KO mutant was more susceptible to C9 than *Mtb* H37Rv wild type at a starting inoculum of 10^5 CFU/mL (**Table 9**), this mutant displayed the same susceptibility level to C9 as *Mtb* H37Rv at higher bacterial densities (10^7 CFU/mL) (**Table 10**). Furthermore, bacterial cultures of L4KO at 10^7 CFU/mL did not display an increased susceptibility to C9 in iron-restricted medium (**Table 10**), in contrast to the results obtained at 10^5 CFU/mL (**Table 9**).

These results led us to hypothesize that mutants deficient in MmpL4, a protein required for siderophore-mediated iron acquisition, might have a reduced metabolism in comparison to *Mtb* wild type due to their reduced capacity to uptake iron and the toxic effect exerted by C9. This would explain the increased susceptibility of L4KO (at 10^5 CFU/mL) to C9 when MTT is used as the bacterial growth indicator. However, when the activity of C9 is evaluated against bacterial cultures at 10^7 CFU/mL, this higher bacterial density could better reduce MTT even in MmpL4 mutants, thus explaining that both L4KO mutant and the wild type strain display the same MIC values at higher bacterial densities.

Subsequently, time kill assays at 10^7 CFU/mL were performed to clarify the results obtained by liquid MIC assays. We observed that L4KO was slightly more susceptible to C1 and C9 than H37Rv in both iron-replete and iron-restricted conditions, specially at inhibitory concentrations (32 µg/mL, 4xMIC) (**Figure 13 C D G H**). Regarding the killing curves of C1, a 1-$\log_{10}$ CFU/mL difference was detected between H37Rv and L4KO after 10-14 days of treatment with 32 µg/mL of C1 (**Figure 13 C D)**. This difference was higher (1.7-$\log_{10}$) on day 21. As for C9 at 32 µg/mL, 0.6-$\log_{10}$ CFU/mL differences were obtained between H37Rv and L4KO (**Figure 13 G H)**.

Moreover, iron levels did not have an impact on the killing curves of *Mtb* H37Rv and L4KO treated with C9 or C1 (**Figure 13 A B E F**), in line with liquid MIC results at high inoculum densities (**Table 10**).

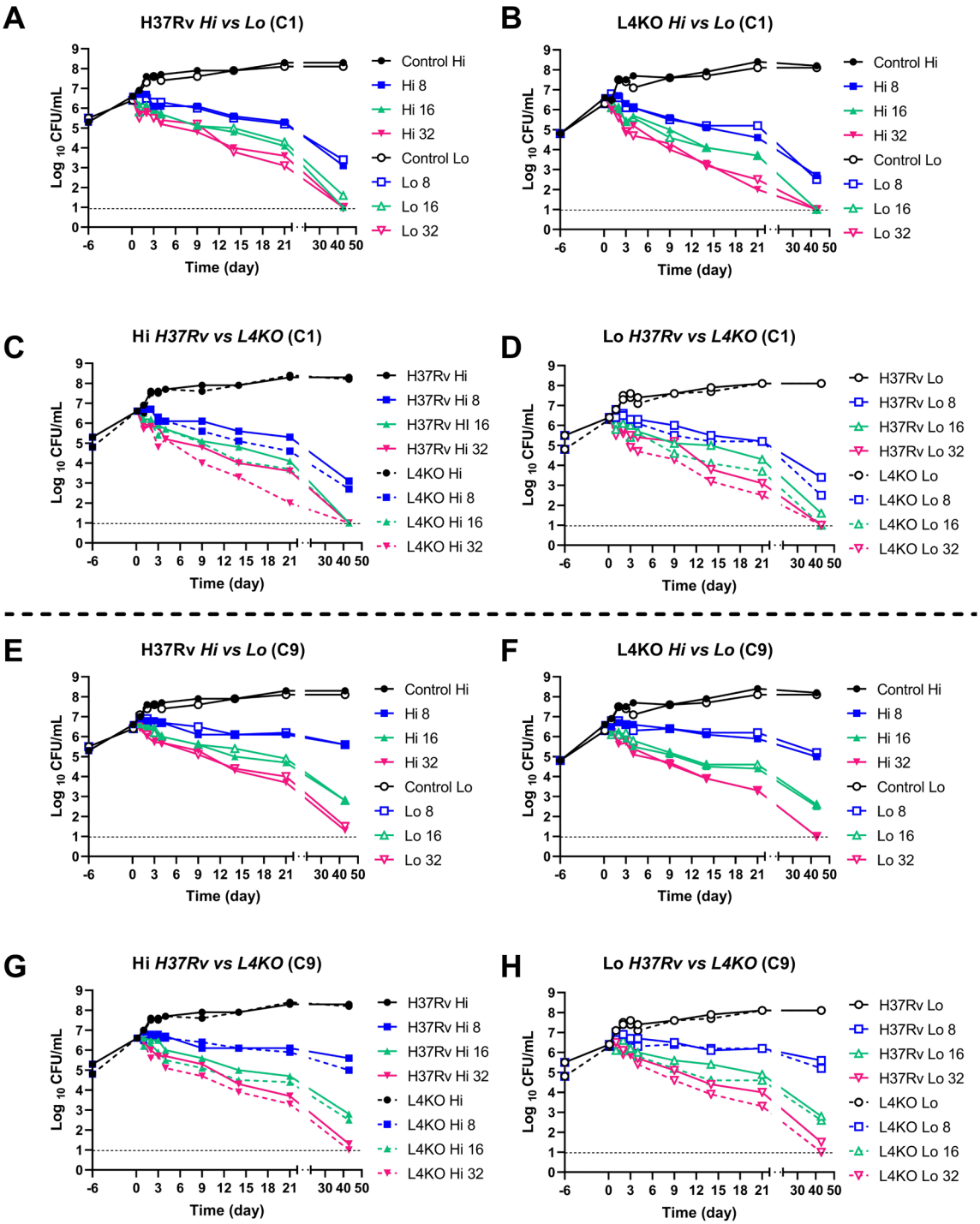

Figure 13. Time kill assays of C1 (A-D) and C9 (E-H) against *Mtb* H37Rv and L4KO under different iron conditions. Bacteria were inoculated to a cell density of 10^5 CFU/mL and incubated at 37 °C for 6 days for bacterial adaptation to each medium. The OD_{600nm} of bacterial cultures was measured before adding the compounds (day 0). The medium used in this assay was self-made 7H9 (without 40 µg/mL of ferric ammonium citrate) plus 0.2% Gly, 0.025% Tyl and 10% ADC. This medium was supplemented with 4 (Lo, low iron) or 40 (Hi, high iron) µg/mL of $FeCl_3$. Compound concentrations are indicated in µg/mL.

The differences observed in the susceptibility of L4KO at high and low bacterial densities (under iron-restricted conditions) could be due to the different iron requirements depending on the bacterial density assayed or the growth phase of the bacteria when the drugs are added. For example, previous results indicated that, whereas *mmpL5* and *mmpS5* expression increases 2-fold in L4KO mutant (compared to wild type) at exponential phase, their expression levels scarcely change in L4KO cultures at stationary phase [92].

It should be noted that in the susceptibility assays performed at a starting inoculum of 10^7 CFU/mL (**Figure 13** & **Table 10),** bacteria were adapted to the different iron conditions for 5-6 days before adding the compounds. By contrast, in the liquid MIC assays performed against low bacterial densities, drugs were added on day 0, without prior bacterial adaptation to the different media (**Table 8** & **Table 9**). If we hypothesize that C9 is affecting (directly or indirectly) an important pathway of iron acquisition for MmpL4 mutant, the addition of C9 to *Mtb* cultures without prior bacterial adaptation to the iron-restricted medium could block the capacity of L4KO to acquire iron, thus explaining the increased susceptibility of L4KO in comparison to *Mtb* wild type under these conditions. However, it could be speculated that, when C9 is added after bacterial adaptation to iron-restricted media, the MmpL4 mutant has been able to acquire iron during the adaptation period before adding C9, thus explaining that the L4KO do not display an increased susceptibility to C9 in iron-restricted medium in those conditions.

3.2.4. Effect of C9 on O_2 consumption and ATP levels

O_2 consumption assays of *Mtb* and L4KO after C9 treatment

To gain insights into *Mtb*'s metabolic response to C9, O_2 consumption assays were performed using BD™ OBS plates, which have a fluorophore quenched by O_2 in a quantitative manner. In these assays, the fluorescence signal is inversely proportional to the amount of O_2 in the sample. Thus, fluorescence increases when bacterial respiration consumes O_2 from the medium [95].

We first compared the O_2 consumption from *Mtb* H37Rv and L4KO after treatment with increasing concentrations of C9. The killing activity of C9 was correlated with its impact on O_2 consumption during the initial days of drug exposure, using a starting inoculum of 10^7 CFU/mL.

Results shown in **Figure 14A** suggested that L4KO might have an impaired O_2 consumption ability, which may reflect a major metabolic impairment, compared to the wild type strain despite no differences were observed in the growth curves of both strains by CFU assessment (**Figure 14B**). This is consistent with the results previously obtained in the time kill assays of M7, M18 and M19 mutants (**Figure 10 & Figure S2**), in which untreated mutants produced less luminescence than the wild type strain after 4 days of culture. Since BacTiter-Glo Kit measures the number of viable bacteria based on the amount of ATP present, these differences in luminiscence could be explained by a reduced ATP production in mutants with *mmpL4* disrupted because of an altered O_2 consumption.

Importantly, treatment with C9 strongly decreased the O_2 consumption rate of L4KO mutant at concentrations that did not reduce CFUs after 48 h of treatment (*e.g.,* at 8 µg/mL) (**Figure 14**). In contrast, only a slight decrease in O_2 consumption was observed when H37Rv was treated with 8 µg/mL of C9 (**Figure 14**).

Therefore, these results indicated that L4KO is more susceptible to C9 than the wild type strain even at a high starting inoculum (10^7 CFU/mL) and that the MoA of this new chemical series could be associated with alterations in the OxPhos.

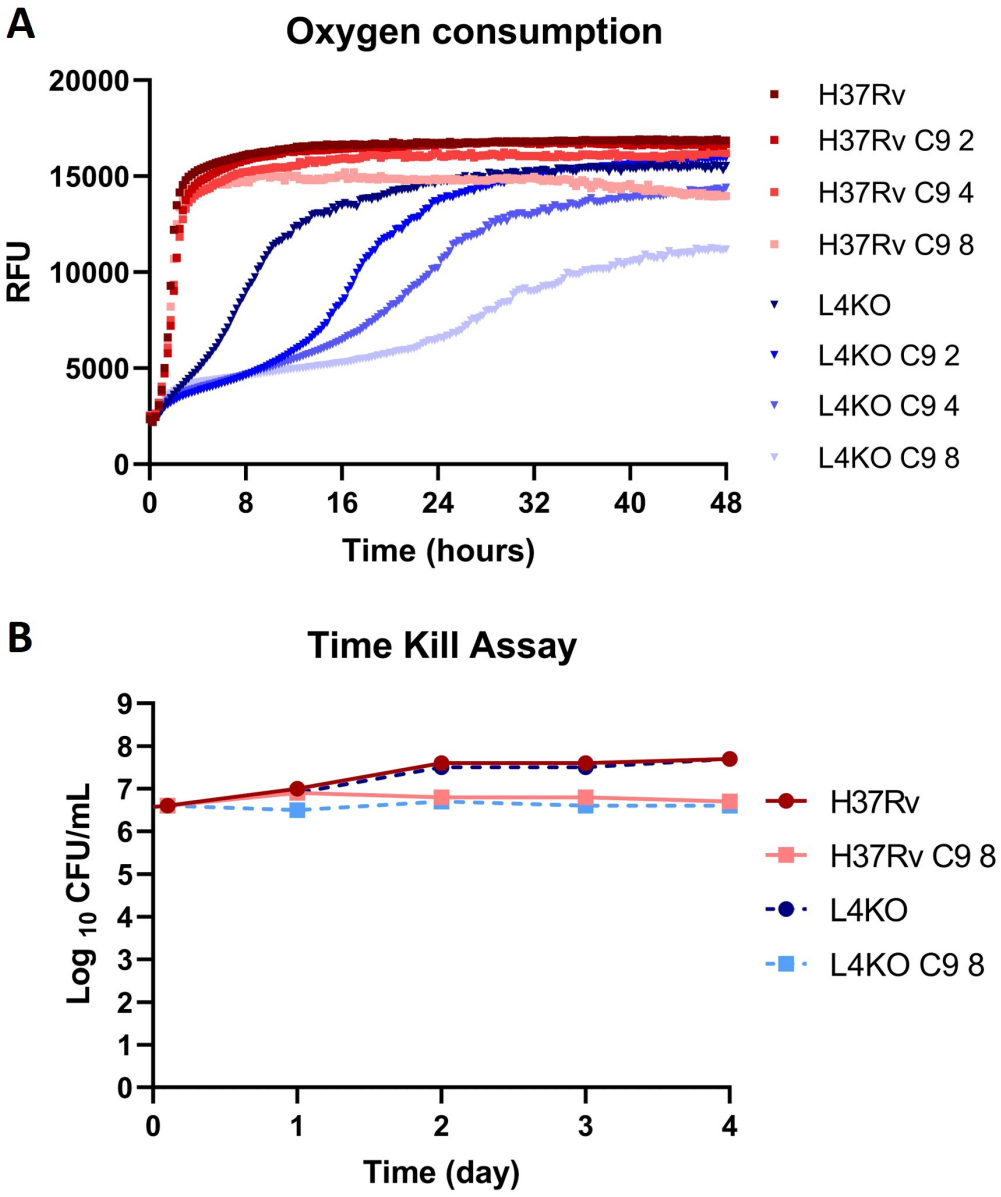

Figure 14. Oxygen consumption profiles and time kill assays of *Mtb* H37Rv and L4KO after treatment with C9. (A) Cultures of *Mtb* H37Rv (red) and L4KO (blue) were adjusted to 10^7 CFU/mL in 7H9-Gly-ADC medium, treated with increasing concentrations of C9 in BD™ OBS plates and data were collected for 48 h using a Synergy Microplate Reader (Biotek). (B) Initial 4 days of killing activity of C9 using a starting inoculum of ca. 10^7 CFU/mL. Concentrations are expressed in µg/mL.

Effect of *Mtb* treatment with several anti-TB drugs on ATP levels

Previous studies have shown that antimicrobial efficacy is linked to bacterial cellular respiration [96–98]. Based on the results described in the previous section, we sought to determine whether C9 could be targeting or affecting the OxPhos by measuring ATP levels at early time points (after 24 and 48 h of treatment). By keeping treatment time short and drug concentrations low, the effects of drug treatment on bacterial viability were minimized. Bacterial cultures of ca. 10^7 CFU/mL were thus treated with 9 different anti-TB drugs with known modes of action (**Figure 15**).

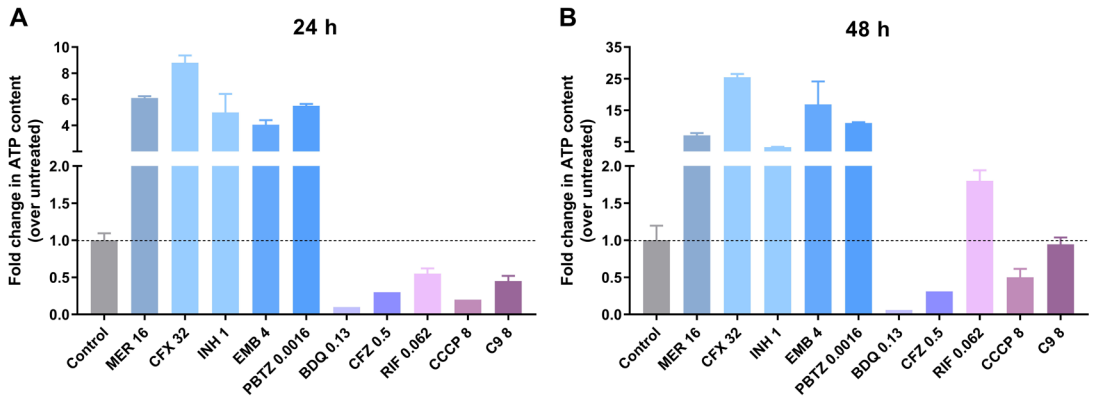

Figure 15. Effect of treatment with several anti-TB drugs on *Mtb* ATP content. Exponentially growing cultures were diluted to ca. 10^7 CFU/mL and treated with several drugs for 24 h (A) or 48 h (B) prior to ATP determination with BacTiter-Glo reagent. The fold change in ATP content of drug-treated cultures compared to that of untreated control cultures is shown on the *y*-axis. Data represent mean±SD from at least 2 technical replicates. Two independent experiments were performed. Drugs were added at 2xMIC and concentrations are expressed in µg/mL. MER, meropenem; CFX, cefadroxil; INH, isoniazid; EMB, ethambutol; BDQ, bedaquiline, CFZ, clofazimine; RIF, rifampicin; CCCP, Carbonyl Cyanide 3-Chlorophenylhydrazone; C9, compound 9.

Cell wall biosynthesis inhibitors, including MER, cefadroxil (CFX), INH, EMB and PBTZ-169, caused a burst in ATP (**Figure 15**) at 24 and 48 h post-treatment, in line with results previously reported by Shetty *et al.* in *M. bovis* BCG [99] , where cell wall inhibitors appear to trigger a common stress response resulting in increased O_2 consumption, which in turn results in increased ATP levels [99]. Importantly, this increase in ATP levels has been associated with the lethal effect of these drugs and is specific to cell wall biosynthesis inhibitors (independently of their target) [98,99].

In contrast, BDQ, CFZ and CCCP (Carbonyl Cyanide 3-Chlorophenylhydrazone, a membrane potential decoupler compound) triggered a drop in ATP levels after 24 and 48 h of treatment due to their role as OxPhos inhibitors, in line with results published by other groups (**Figure 15**) [98,99]. Similarly, RIF led to a decrease in ATP levels after 24 h of treatment (**Figure 15**), which was consistent with previous studies describing that RIF alters *Mtb* metabolism *in vitro* by decreasing ATP levels after 6 and 12 h of treatment [96,97]. However, the molecular mechanism underlying this effect remains unknown [96,97].

The addition of C9 triggered a drop in ATP levels after 24 h of treatment but to a lesser extent than other energy metabolism inhibitors (**Figure 15**). Importantly, this decrease in ATP levels during the initial 24 h of treatment was not due to a reduction in CFU counts (**Figure 14A**). In contrast, C9 did not lead to major changes in ATP levels after 48 h of treatment in comparison to untreated bacteria (**Figure 15**).

Taken together, these results suggested that C9 might interfere with energy metabolism during the initial 24 h of treatment, leading to a decrease in ATP levels and, despite its potential role with the MmpL4 and MmpL5 membrane proteins, having a distinct mode of action compared to cell wall targeting compounds.

3.2.5. *In vitro* antimicrobial drug interactions of the study compounds

A complementary approach that can provide information on the possible MoA of a drug is based on the identification of the interaction profile in combination with other drug partners. In this section, we investigated and validated these interactions with several antimicrobials in three mycobacterial species: *Mtb*, *M. abscessus*, and *M. ulcerans*.

Mycobacterium tuberculosis

Synergy screening and validation of drug interactions

Following the FDA approval of the ATP synthase inhibitor BDQ in 2012 and the progression of the cytochrome bc_1:aa_3 inhibitor Q203 in the clinical pipeline, drugs targeting energy metabolism have gained a lot of attention. Interestingly, it has been reported that the combination of OxPhos inhibitors has the potential for synergistic activity by counteracting *Mtb* respiratory flexibility (*e.g.* CFZ in combination with BDQ or Q203) [100,101].

Taking into consideration the results described in the previous section, which suggest that this new chemical series could somehow disrupt energy metabolism at early time points, we investigated *in vitro* interactions of C9 with other drugs targeting OxPhos with the aim of gaining insights into the MoA of C9. Moreover, the interaction between C9 and first- and second-line antimicrobials was also evaluated since anti-TB drugs are always prescribed as part of combination therapies. This synergy screening was performed against *Mtb* H37Rv and L4KO mutant (owing to its increased susceptibility to C9).

C9 enhanced the potency (at least 4-fold) of BDQ, BTZ043, CFZ, KET and PBTZ-169 against *Mtb* H37Rv (**Table 11**). The synergism observed between C9 and inhibitors of the electron transport chain (ETC), including BDQ, CFZ and KET, could be explained by C9 also impairing energy metabolism. Regarding the interaction with benzothiazinones (BTZ043 and PBTZ-169), which inhibit DprE1, thus blocking the synthesis of an arabinan precursor essential for the mycobacterial cell wall, previous studies have demonstrated that benzothiazinones synergize with drugs affecting the ETC, such as BDQ and CFZ [102].

Concerning ECO, Q203, SQ109 and thioridazine (TDZ), C9 slightly increased their activity (2-fold) (**Table 11**). Interestingly, most of these synergistic combinations had a higher effect in L4KO mutant than in *Mtb* H37Rv (**Table 11**).

Table 11. *In vitro* interaction of C9 (primary compound) with clinically approved or investigational anti-TB drugs with known modes of action (secondary compounds, n=17) against *Mtb* H37Rv and L4KO mutant. MIC values of secondary compounds were determined in the absence or in the presence of sub-inhibitory concentrations of C9 (1/8x and 1/4x MIC). Synergy was defined by at least 4-fold reductions in the MIC of secondary compounds in the presence of C9 at concentrations equal or <1/4xMIC.

Compounds	H37Rv		L4KO
	None *vs* 1/8x MIC	None *vs* 1/4x MIC	None *vs* 1/4x MIC
Bedaquiline			
BTZ043			
Clarithromycin		ND	ND
Clofazimine			
Econazole			
Ethambutol		ND	ND
Isoniazid		ND	ND
Ketoconazole			
PBTZ-169			
Pyrazinoic acid		ND	ND
Q203	ND		
Rifampicin			
Spectinomycin		ND	ND
Streptomycin	ND		
SQ109			
Thioridazine	ND		
Vancomycin		ND	ND

Synergy: ≥4-fold reduction
Slight synergy: 2-fold reduction
No interaction: <4 and >0.25 -fold reduction
Antagonism: ≤0.25-fold reduction
ND: not determined

The potential synergistic interaction of C9 with several drugs, including BDQ, CFZ, KET, Q203, PBTZ-169 and SQ109, was further analysed by time kill assays against *Mtb* H37Rv. We also included the cornerstone TB drugs INH and RIF as control drugs which did not display synergism with C9 by MIC assays (**Figure 16** & **Figure 17; summarised in Table 12**).

Time kill assays of drug combinations were performed using sub-optimal drug concentrations (*i.e.* bacteria grow similar to the control in the presence of the drug), such as 1/2x, 1x and 2xMIC of the drug (**Figure 16A,C,D** & **Figure 17**). In the case of BDQ, we also included higher drug concentrations displaying a bactericidal effect (**Figure 16B**).

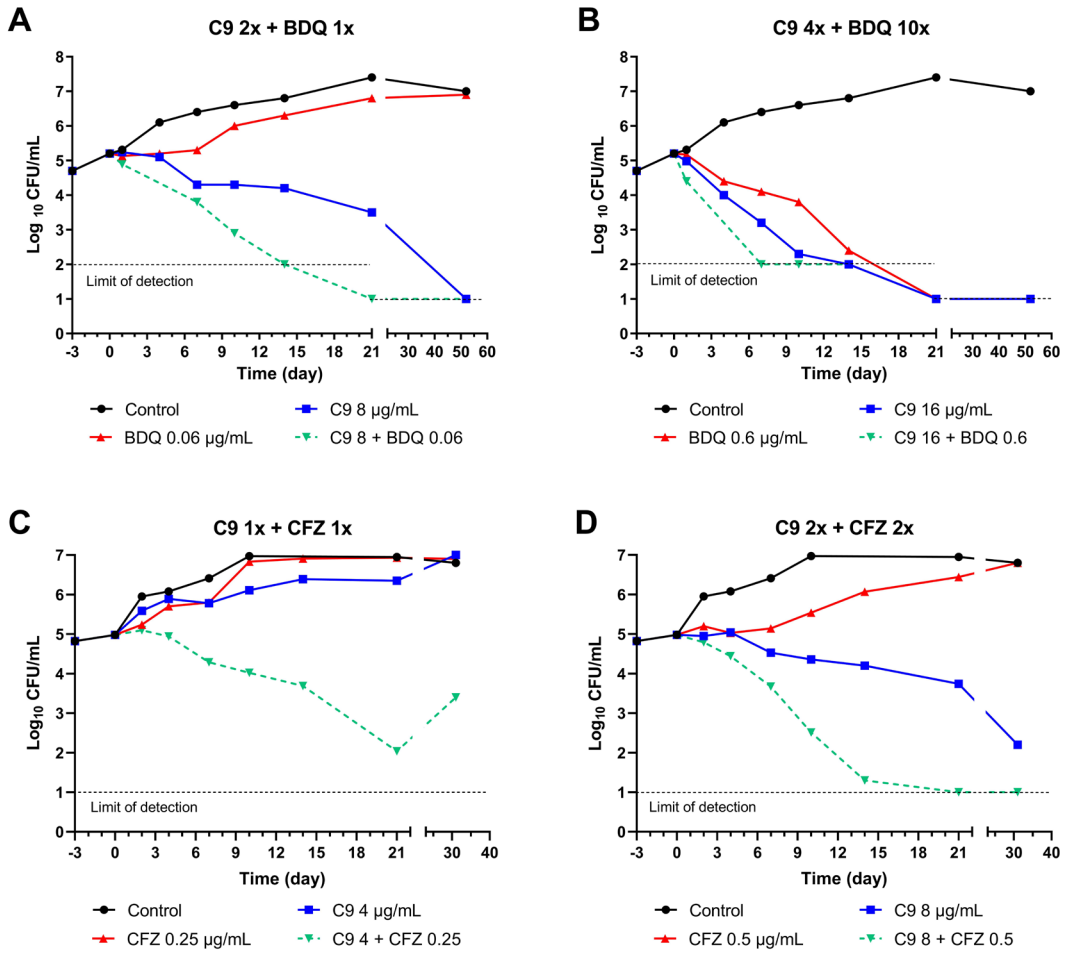

Figure 16. Time kill assays of BDQ and CFZ in combination with C9 against exponential phase cultures of *Mtb*. Bacteria were inoculated to a cell density of 10^5 CFU/mL and incubated at 37°C for three days before adding the drugs. Drug concentrations are indicated in µg/mL in the legend and xMIC in the graph title. MIC C9 = 4 µg/mL; MIC BDQ = 0.06 µg/mL; MIC CFZ = 0.25 µg/mL.

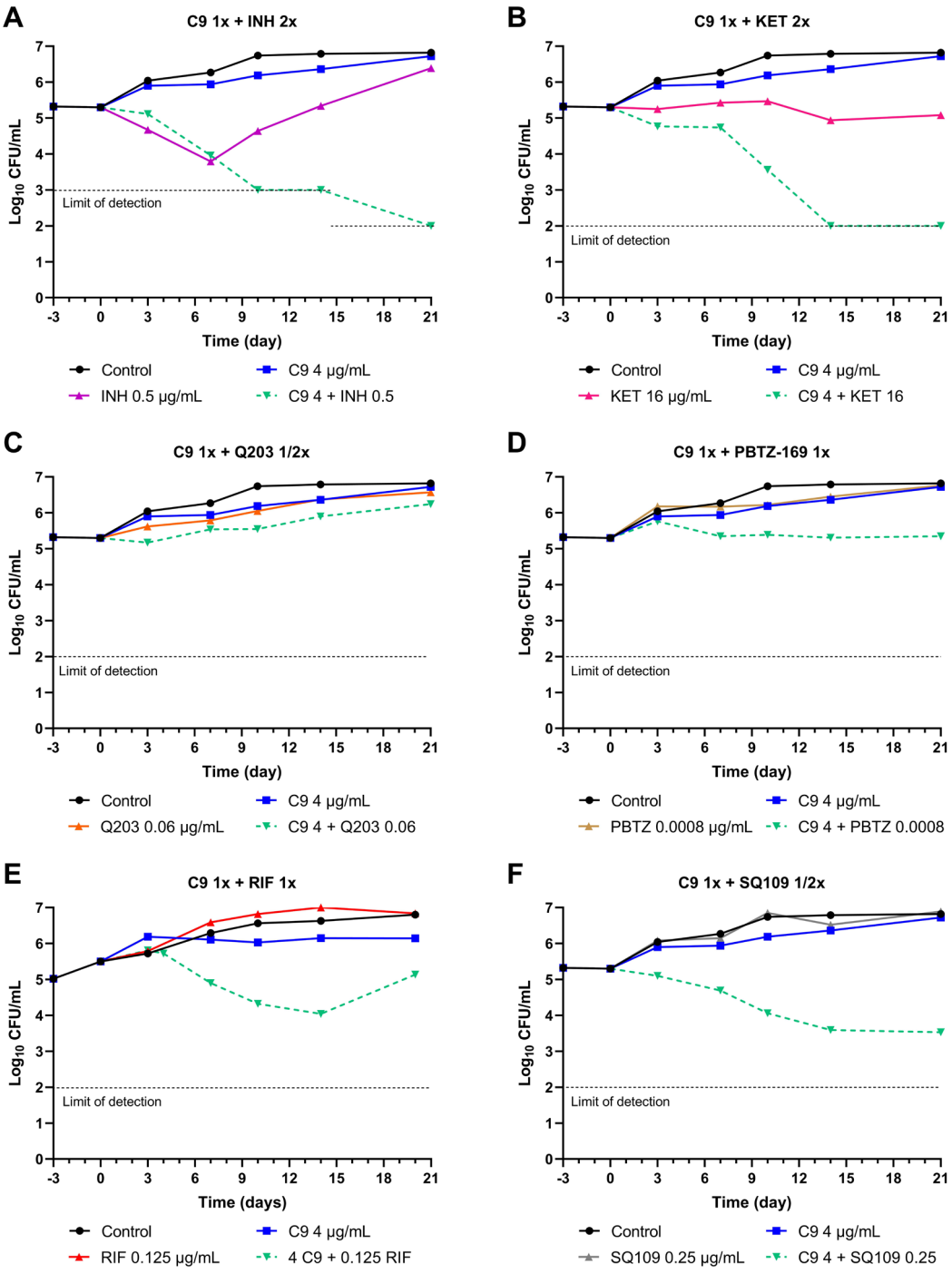

Figure 17. Time kill assays of INH, KET, Q203, PBTZ-169, RIF and SQ109 in combination with C9 against exponential phase cultures of *Mtb*. Bacteria were inoculated to a cell density of 10^5 CFU/mL and incubated at 37°C for three days before adding the compounds. Drug concentrations are indicated in µg/mL in the legend and xMIC in the graph title. MIC C9 = 4 µg/mL; MIC INH = 0.25 µg/mL; MIC KET = 8 µg/mL; MIC Q203 = 0.12 µg/mL; MIC PBTZ-169 = 0.0008 µg/mL; MIC RIF = 0.125 µg/mL; MIC SQ109 = 0.5 µg/mL.

Table 12. Summary of the pair-wise combinations analysed by time kill assays after 10, 14 and 21 days of treatment. Only those time kill assays performed with C9 at 1xMIC are shown (except the combination with BDQ, in which C9 was used at 2xMIC).

C9 at 1x MIC combined with	Δlog$_{10}$ CFU/mL between [2] the combination and the most active antimicrobial alone		
	10 day	14 day	21 day
Bedaquiline (1xMIC) [1]		(*)	(*)
Clofazimine (1xMIC)			
Isoniazid (2xMIC)	(*)	(*)	(*)
Ketoconazole (2xMIC)		(*)	(*)
Q203 (1/2xMIC)			
PBTZ-169 (1xMIC)			
Rifampicin (1xMIC)			
SQ109 (1/2xMIC)			

[1] 2xMIC of C9 instead of 1xMIC was used in the combination.

[2] Synergy is defined as a ≥2 log$_{10}$ reduction

≥3 log$_{10}$ reduction
≥2 log$_{10}$ reduction
<2 log$_{10}$ reduction
≥2 log$_{10}$ increment
(*) Combination reached the limit of detection

As a result, C9 showed favourable interactions with BDQ, CFZ, INH, KET and SQ109 at the concentrations tested. Therefore, we confirmed the synergism previously observed between C9 and inhibitors of energy metabolism, such as BDQ, KET and CFZ. These combinations increased the rate of killing when compared to single drugs alone and, importantly, reached the limit of detection after 14-21 days of incubation (depending on the combination analysed) (**Figure 16, Figure 17B**). In the case of C9 and CFZ at 1xMIC (**Figure 16C**), the 3-log reduction in bacterial burden achieved at day 21 was followed by a rebound of bacterial growth at day 31, Importantly, no CFU were detected on day 31 when both C9 and CFZ were assayed at 2xMIC (**Figure 16D**).

The combination of C9 at 1xMIC with SQ109 at sub-inhibitory concentrations (1/2xMIC) was able to reduce CFUs up to 2-log at day 10 and 3-log at day 21 in comparison to single drugs alone, thus displaying a synergistic interaction under the conditions tested.

The combination of PBTZ-169 with C9 at 1xMIC led to a 1-log reduction in CFU when compared to single drugs alone, which did not display activity against *Mtb*. In this case, it would be necessary to test this pair-wise combination at higher concentrations to define the degree of interaction between C9 and PBTZ-169.

Moreover, C9 in combination with RIF decreased bacterial burden up to 2-logs within 14 days (**Figure 17E**). However, this positive interaction was lost on day 20 at the concentrations tested (1xMIC). Hence, it would be interesting to evaluate whether this outgrowth of bacteria could be prevented by using higher drug concentrations, as observed with the pair-wise combination C9/CFZ at 2xMIC (**Figure 16D).**

C9 also acted synergistically with INH and prevented the emergence of INH-resistant bacteria, as it is detailed in the following section (**Figure 17A**).

It should be mentioned that, whereas RIF and INH were not identified as synergistic partners of C9 in the screening performed by liquid MIC determination, both drugs displayed a positive interaction with C9 by time kill assays (**Figure 17A,E**). Hence, this result reinforced the relevance of characterizing the antimicrobial activity over time by time kill assays.

In summary, C9 showed synergistic interactions with drugs used for TB therapy at concentrations that had little antimicrobial effect alone. Importantly, most of these interactions were bactericidal and reached the limit of detection at the concentrations tested. Nonetheless, several pair-wise combinations, such as RIF/C9 and PBTZ-169/C9, should be tested at different concentrations to fully define the degree of interaction of the combination.

Interaction between C9 and INH

No synergistic interaction was detected when comparing the killing curves of both drugs alone with that of their combination from day 0 to day 7, because the main activity in the combination was dependent on INH during this period of time (**Figure 17A**). This correlated with the results obtained by liquid MIC assays (**Table 11**), in which growth inhibition is measured after 6 days of treatment. However, the combination further decreased bacterial load at longer time points. Therefore, we confirmed by time kill assays that this interaction was synergistic and bactericidal.

Consistent with other reports, INH showed a fast killing rate at shorter times followed by a significant bacterial regrowth mainly due to the emergence of INH-resistant bacteria [103–105]. Interestingly, the combination INH/C9 prevented the emergence of INH-resistant bacteria since none of the residual colonies were INH-resistant (**Figure 18**). In contrast, colonies isolated after 2-3 weeks of INH mono treatment were INH-resistant, as they were able to grow on 7H10-OADC plates containing 4 or 16 µg/mL of INH (8x and 32xMIC, respectively) (**Figure 18**).

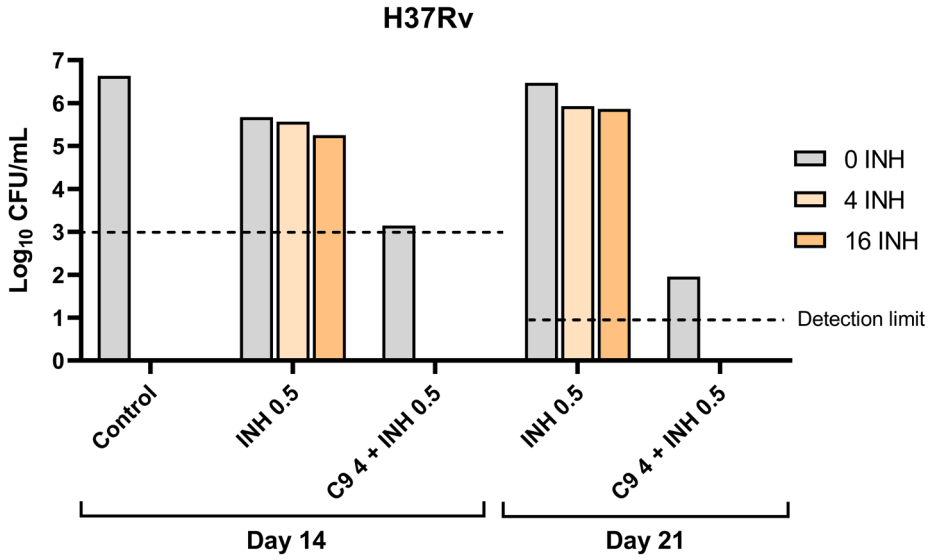

Figure 18. Bacterial viability (CFU/mL) of *Mtb* H37Rv after 14 and 21 days of treatment with 0.5 µg/mL of INH alone or in combination with C9 at 4 µg/mL. These cultures were plated on 7H10-OADC (without INH; grey bars) and 7H10-OADC-INH plates containing 4 (pale orange bars) or 16 (dark orange bars) µg/mL of INH to evaluate whether these bacteria were resistant to INH. In several conditions ("control" and "C9 4 + INH 0.5"), no CFU were detected when the cultures were plated on 7H10-OADC-INH plates (dashed lines indicate the limit of detection for those cases).

An aliquot was taken from *Mtb* cultures treated with 0.5 µg/mL of INH for 21 days to evaluate the susceptibility of this INH-resistant population to C9. Remarkably, this population of INH-resistant bacteria was slightly more susceptible to C9 than *Mtb* H37Rv (confirmed by MIC in liquid media and time kill assays) (**Table 13 & Figure 19**). Moreover, the synergistic interaction between INH and C9 against *Mtb* H37Rv was lost against this INH-resistant population (**Figure 19**).

Table 13. Determination of MICs of C9 and INH in liquid media against *Mtb* H37Rv and INH-resistant bacteria. Values are indicated in µg/mL. C9, compound 9; INH, isoniazid.

Drug	*Mtb* H37Rv	INH-resistant
C9	4	2
INH	0.5	>8

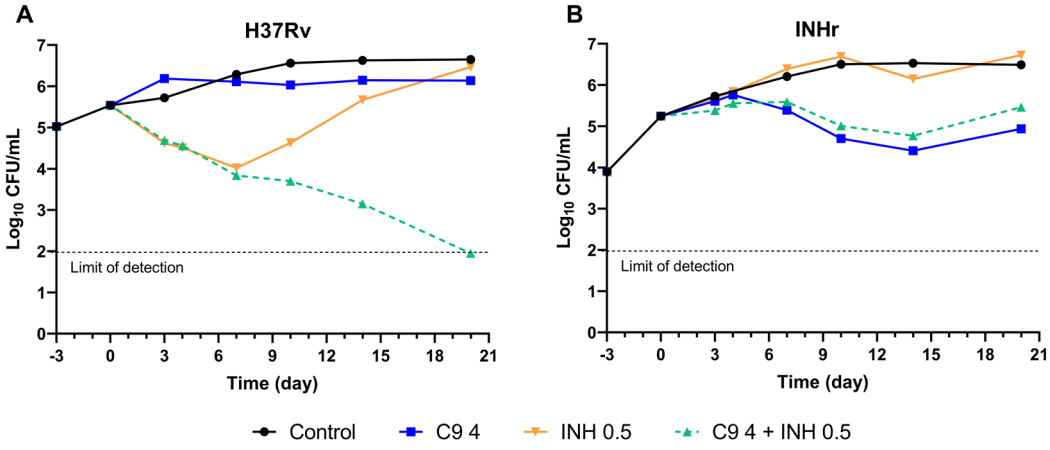

Figure 19. Time kill assays of C9 and INH alone and in combination against *Mtb* H37Rv (A) and INH-resistant bacteria (B). Bacteria were inoculated to a cell density of 10^5 CFU/mL and incubated at 37°C for three days before adding the compounds. Drug concentrations are indicated in µg/mL in the legend.

Resistance to INH is most often a result of mutations in *katG* gene, which encodes a catalase peroxidase that protects *Mtb* from reactive oxygen species (ROS) and activates the pro-drug INH [104]. In order to study whether this population of bacteria was resistant to INH due to mutations in *katG,* this gene was PCR amplified and PCR products sequenced. A missense mutation (Asn35Asp) previously described in INH-resistant isolates [106] was identified after comparing the sequences of *katG* from *Mtb* H37Rv and INH-resistant bacteria, suggesting that an altered KatG enzyme could be involved in the INH-resistant phenotype. Nonetheless, it must be considered that mutations in other genes associated with resistance to INH (*e.g., inhA* promoter) could be also responsible for the INH-resistant phenotype.

To study the possible implication of KatG in the susceptibility to this new chemical series, we evaluated the activity of these compounds against three mutants defective in the three *katG* genes of *M. smegmatis (*MSMEG_3461, MSMEG_3723 or MSMEG_6384). Although *M. smegmatis* contains three *katG* genes (MSMEG_3461, MSMEG_3723 and MSMEG_6384) that codify for three catalase-peroxidase enzymes, they do not have the same relevance in the susceptibility of this strain to INH [107] .

MSMEG_6384 knockout mutant, the most resistant strain to INH owing to the predominant role of MSMEG_6384 in INH activation [107], was slightly more susceptible to the study compounds than *M. smegmatis* mc^{2}155 (**Table 14**) in line with the results obtained in *Mtb* with the population of INH-resistant bacteria (**Table 13 & Figure 19**).

Table 14. MIC values (µg/mL) of INH and compounds of this new chemical series against *M. smegmatis* mc^{2}155 and three *katG* deletion mutants.

Strains	MIC values (µg/mL)				
	C1	C3	C6	C9	INH
***M. smegmatis* mc^{2}155**	2	8	4	2	16-32
KO MSMEG_3729	2	4	4	2	32
KO MSMEG_3461	1-2	8	2-4	2	32-64
KO MSMEG_6384	**1**	**2-4**	**2**	2	**256**

Taken together, we found that *Mtb* INH-resistant bacteria due to mutations in *katG* and *M. smegmatis* mutants defective in *katG* were slightly more susceptible to the compounds, raising the hypothesis that bacteria without a functional catalase peroxidase could be worst equipped to counteract the oxidative stress induced by the study compounds.

Effect of drug treatments on ATP content

OxPhos inhibitors have been described to attenuate the bactericidal activity of cell wall synthesis inhibitors by suppressing the ATP burst triggered by these drugs. For example, this effect has been observed when combining INH with Q203 or BDQ [98,99,108]. Therefore, these studies suggest that drug-induced changes in ATP homeostasis critically drive lethal metabolic alterations [109].

Based on these previous data, the synergistic interaction between INH and C9 was further analysed by measuring ATP content after 10 and 14 days of treatment, and ATP levels were normalized by the number of viable bacteria (ATP/CFU·mL^{-1}).

C9 alone reduced ATP levels in *Mtb* H37Rv at days 10 and 14. By contrast, the combination INH/C9 caused an extraordinary increase in ATP (>30-fold) at days 10 and 14, at the time we observe by time kill assays that the combination is killing the bacteria (**Figure 19A & Figure 20**). This rise in ATP levels could reflect an increase in O_2 consumption, which keeps production of KatG high to fight potential increases in ROS production and hence allows for INH activation and *Mtb* killing.

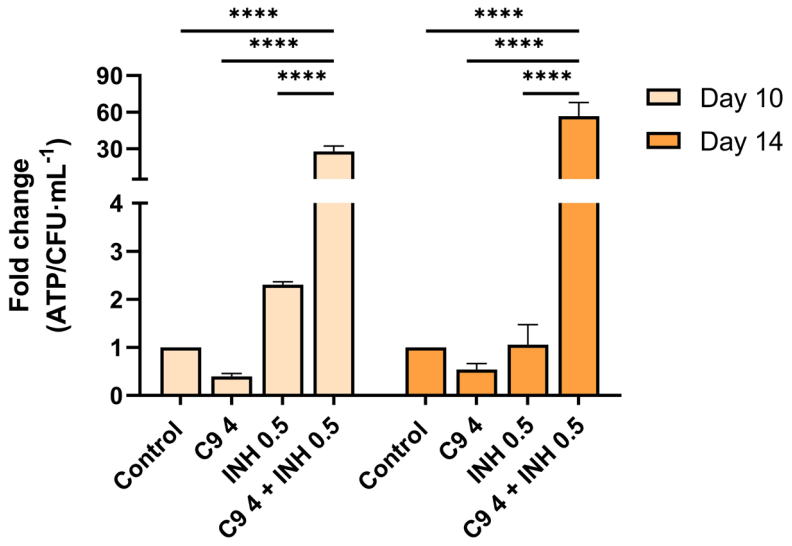

Figure 20. Effect of treatment of *Mtb* H37Rv with C9, INH and C9/INH on bacterial ATP content. ATP content was determined with the BacTiter-Glo reagent after 10 and 14 days of treatment and normalized by viability. Data represent mean±SD from 3 technical replicates. *p<0.05; **p<0.01; ***p<0.001; ****p<0.0001, by two-way ANOVA.

Interaction between C9 and RIF or Q203

ATP levels were also determined in the combinations C9/RIF and C9/Q203 so as to stablish a link between ATP levels and synergistic activities.

The synergistic combination C9/RIF, which reduced CFUs up to 2-logs within 14 days, triggered an 8 to 9-fold increase in ATP levels at days 10 and 14 (**Figure 21B**). However, this rise in ATP levels was lower than in the synergistic combination C9/INH (**Figure 20**).

By contrast, a strong reduction in ATP content was observed in the combination C9/Q203, which showed a slight tendency to no interaction or antagonism by time kill assays in comparison to single drugs alone (**Figure 22**).

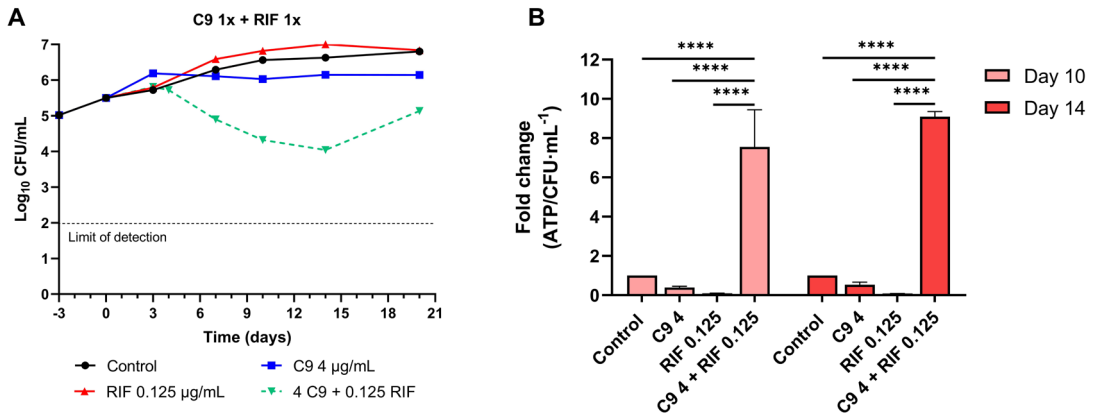

Figure 21. Time kill assays of C9 and RIF alone and in combination against *Mtb* H37Rv (A; same as Figure 17E) and its effect on ATP levels (B). ATP content was determined with the BacTiter-Glo™ assay after 10 and 14 days of treatment and normalized by viability. Data represent mean±SD from 3 technical replicates. ****p<0.0001, by two-way ANOVA.

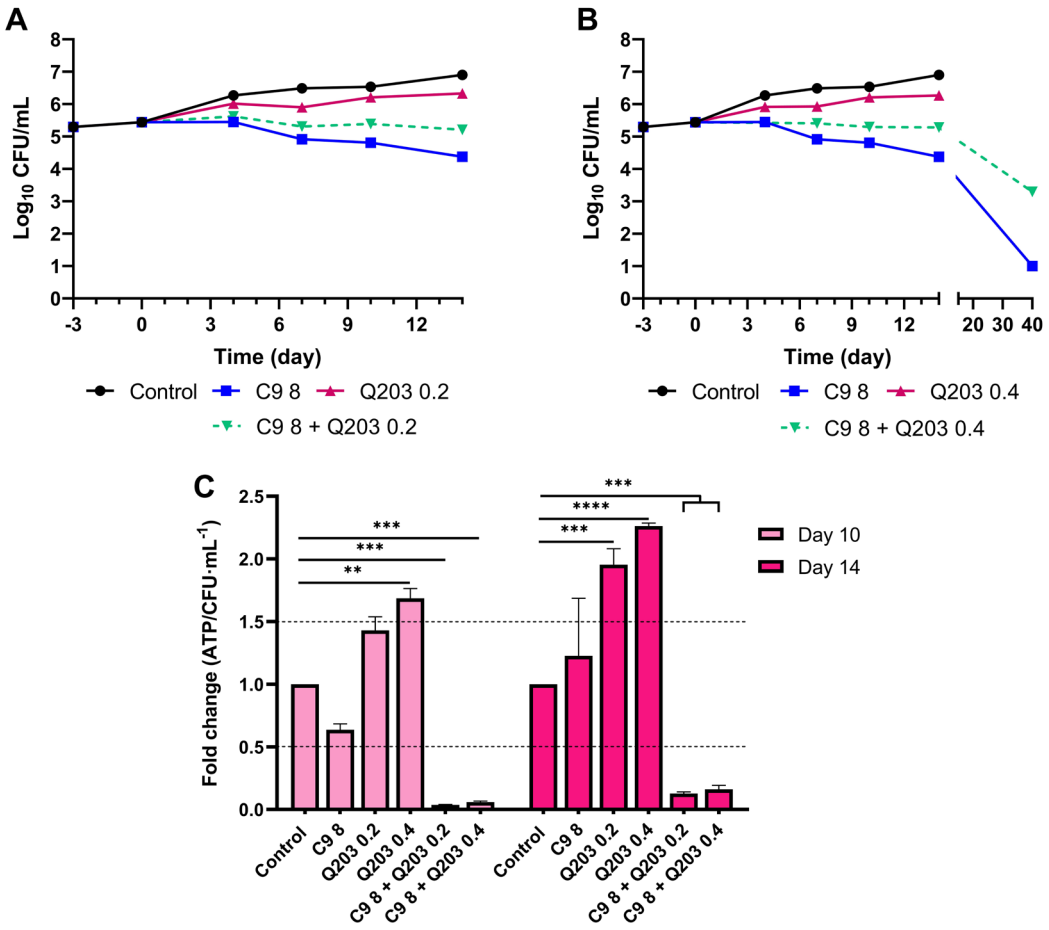

Figure 22. Time kill assays of C9 and Q203 alone and in combination against *Mtb* H37Rv (A, B) and its effect on ATP levels (C). ATP content was determined with the BacTiter-Glo™ assay after 10 and 14 days of treatment and normalized by viability. Data represent mean±SD from 3 technical replicates. **p<0.01; ***p<0.001; ****p<0.0001, by two-way ANOVA.

To sum up, synergistic combinations (such as C9/RIF and C9/INH) caused an increase in ATP production, while the combination C9/Q203, which was not synergistic, led to a strong reduction in ATP levels. These data suggest that C9 in combination with other drugs could trigger a stress response resulting in an enhanced OxPhos (a potential source of ROS), which leads to an increase in ATP levels. Since ATP homeostasis is crucial for the survival of bacteria, this ATP burst might be toxic for *Mtb* and cause dysregulation of many pathways, contributing to the bactericidal effect of the synergistic combinations.

Mycobacterium abscessus

The ATP synthase inhibitor BDQ also displays *in vitro* and *in vivo* activity against *M. abscessus* and is currently being evaluated in clinical trials against *M. abscessus* pulmonary infections [77]. This repositioning strategy is gathering more and more interest in the scientific community. A good example of this is the RespiriNTM project supported by the Innovative Medicines Initiative (IMI), which aims to identify novel drugs that synergize with inhibitors of the respiratory pathway.

Interaction assays of BDQ with the study compounds

In this context, taking into consideration the synergism previously observed between C9 and BDQ in *Mtb*, we aimed to evaluate whether BDQ showed favourable interactions with this new chemical series against *M. abscessus*.

First, the activity of the compounds was evaluated in the absence or in the presence of 1/4xMIC of BDQ in 7H9-Gly-ADC medium. MIC values of the compounds (C1, C2, C6, C7, C8 and C9) were reduced by 4-8-fold in the presence of 1/4xMIC of BDQ (**Table 15**), suggesting that this chemical series acts synergistically with BDQ against *M. abscessus,* in line with previous results obtained in *Mtb*.

Table 15. MIC values (µg/mL) of the compounds in the absence or presence of 1/4xMIC of BDQ against *M. abscessus.* Fold reduction was calculated by dividing the MIC of the compound alone by the MIC of the compound in the presence of 1/4xMIC of BDQ.

Compounds	MIC values (µg/mL)		
	Alone	plus BDQ 0.063 (1/4x MIC)	Fold-reduction
C1	8-16	4	**2-4**
C2	16	4	**4**
C3	32	16	2
C4	>32	32	>1
C6	16	4	**4**
C7	32	4	**8**
C8	32	4	**8**
C9	16	2	**8**

BDQ, bedaquiline. MIC BDQ = 0.25 µg/mL

We also confirmed the synergistic interaction of BDQ with C1 and C2 in both 7H9-Gly-ADC and CaMHB (Cation-adjusted Müller-Hinton broth) media by checkerboard assays (FICI = 0.25-0.375) (**Table 16 & Figure 23**).

Table 16. Synergistic interactions between BDQ and C1 or C2 against *M. abscessus* cultured in 7H9-ADC-Gly and CaMHB. FICI is the Fractional Inhibitory Concentration Index of C1 or C2 in combination with BDQ. The most effective combinations are indicated (MICsyn). Fold reduction: MIC/MICsyn. Synergy (FICI≤0.5), no interaction (0.5<FICI≤4) and antagonism (FICI>4.0).

Media	MIC C1 (µg/mL)	MICsyn C1 (µg/mL)	Fold reduction	MIC BDQ (µg/mL)	MICsyn BDQ (µg/mL)	Fold reduction	FICI
7H9-Gly-ADC	32	8	4	0.25	0.03	8	0.375
	32	4	8	0.25	0.063	4	0.375
CaMHB	8	2	4	0.063	0.008	8	0.375
	8	1	8	0.063	0.016	4	0.375
Media	**MIC C2 (µg/mL)**	**MICsyn C2 (µg/mL)**	**Fold reduction**	**MIC BDQ (µg/mL)**	**MICsyn BDQ (µg/mL)**	**Fold reduction**	**FICI**
7H9-Gly-ADC	32	4	8	0.25	0.063	4	0.375
CaMHB	16	2	8	0.13	0.016	8	0.25

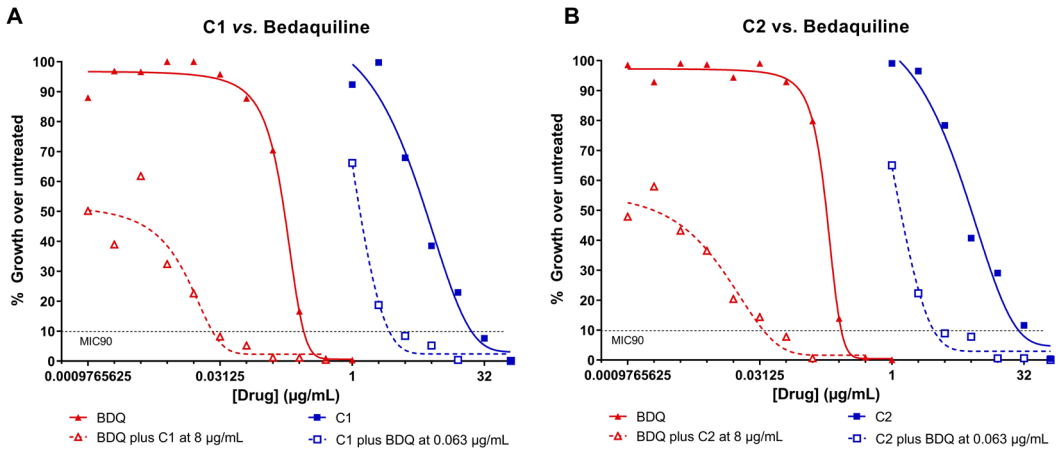

Figure 23. Dose-response interaction curves of C1 (A) and C2 (B) (in blue) with BDQ (in red). Solid lines represent the dose response curve of drugs alone while dashed lines represent the dose response curves in the presence of sub-inhibitory concentrations (1/4xMIC) of the synergistic partner.

Time kill assays were then performed to investigate whether C1 and BDQ alone or in combination exerted bactericidal or bacteriostatic activity against *M. abscessus*. Both 7H9-Gly-ADC and CaMHB media were used (**Figure 24**).

C1 alone displayed dose-dependent bactericidal activity in both media since the rate of killing increased with progressively higher drug concentrations (**Figure 24 A,E**), although it was more active in CaMHB than in 7H9. In contrast, time kill curves of BDQ at concentrations above its MIC showed a bacteriostatic profile regardless of the dose (**Figure 24B,F**) in line with previous studies [110].

For time kill assays of drugs combinations, we selected concentrations that had little antimicrobial effect (*i.e.,* bacteria grow similar to the control in the presence of the drug) (**Figure 24C,G**) or had a bacteriostatic effect (**Figure 24D,H**).

The combination of BDQ/C1 was more active than each of the drugs alone, both in 7H9-Gly-ADC and CaMHB. The combination of C1 at 50 µg/mL and BDQ at 6 µg/mL led to a 3-log reduction in CFUs within 9 days in 7H9-Gly-ADC (**Figure 24D**). This decrease in bacterial burden was followed by a rebound of bacterial growth on day 13. Interestingly, this outgrowth of bacteria was not observed in the killing curves performed in CaMHB (**Figure 24H**), suggesting that this combination is more active in CaMHB than in 7H9; this is consistent with C1 being more active in CaMHB (**Figure 24E**) than in 7H9 (**Figure 24A**). In line with these findings, we previously observed that C1, C2 and BDQ had lower MICs against *M. abscessus* in CaMHB than in 7H9 (**Table 16**). This lower activity of BDQ in 7H9 compared to CaMHB has also been described by Lee *et al.* [111]. Since both media have different pH (CaMHB, 7.4; 7H9, 6.8), these variations in drug activity depending on the media used could be explained by differences in compound stability, as pointed out in previous studies [112,113].

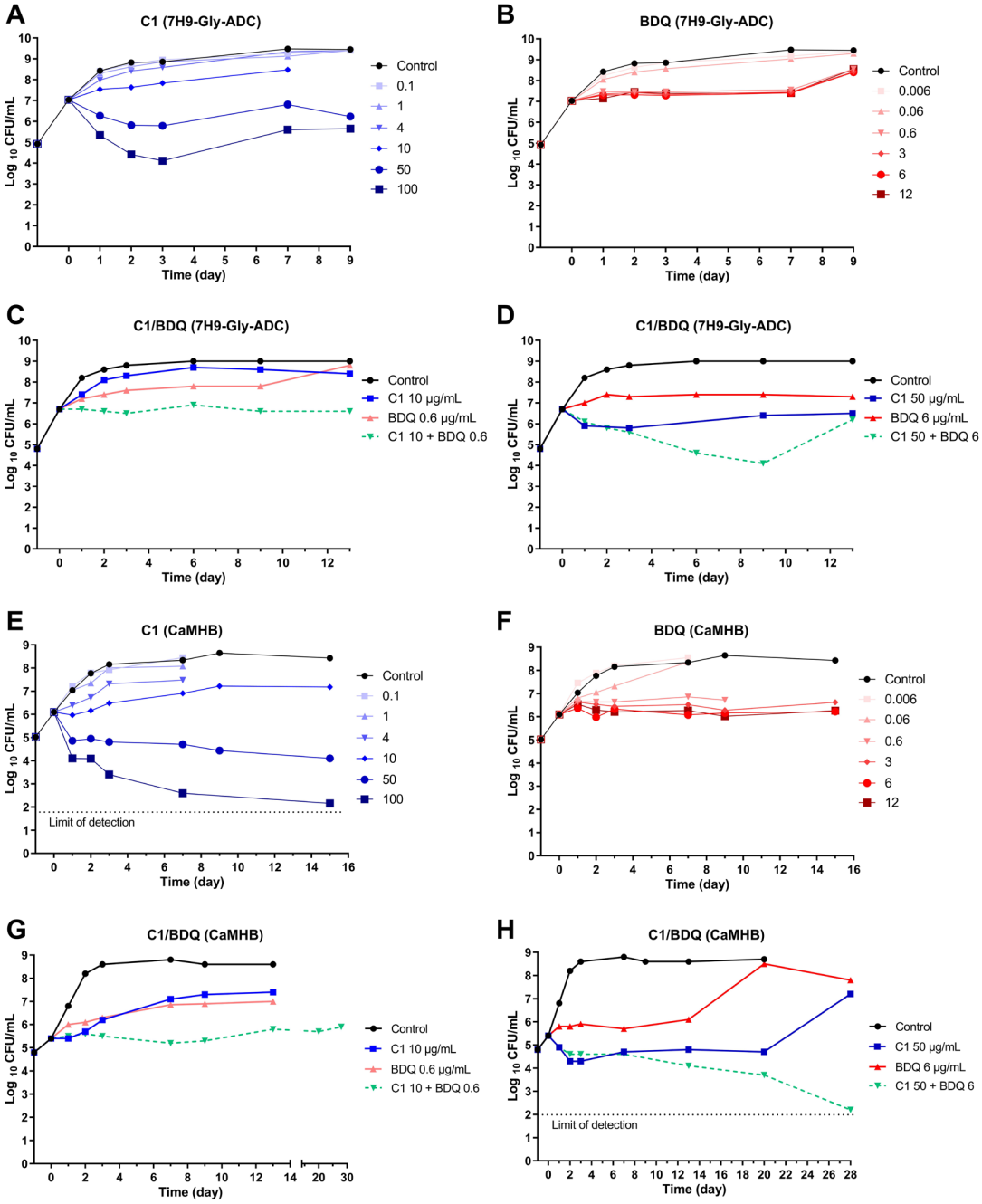

Figure 24. Time kill assays of *M. abscessus* exposed to different concentrations of BDQ and C1 alone or in combination in 7H9-Gly-ADC and CaMHB medium. Exponentially growing bacteria were diluted to 10^5 CFU/mL and incubated for 1 day before the addition of the compounds. In 7H9-Gly-ADC, MIC values of BDQ and C1 were 0.25 and 32 µg/mL, respectively. In CaMHB, MIC values of BDQ and C1 were 0.063 and 16 µg/mL, respectively. Compound concentrations are expressed in µg/mL.

Taken together, these results demonstrated that this new chemical series improves the activity of BDQ against *Mtb* and NTMs, such as *M. abscessus.*

O_2 consumption assays

Based on the synergism observed between the compounds and BDQ, we aimed to determine whether C1 could be also targeting energy metabolism or affecting its activity in *M. abscessus*.

As previously described for *Mtb* (**Figure 14**), *M. abscessus* cultures (seeded at 10^7 cells/mL) were exposed to increasing concentrations of C1, BDQ and CFZ, and O_2 consumption was measured for 17 h (**Figure 25A, C, E**).

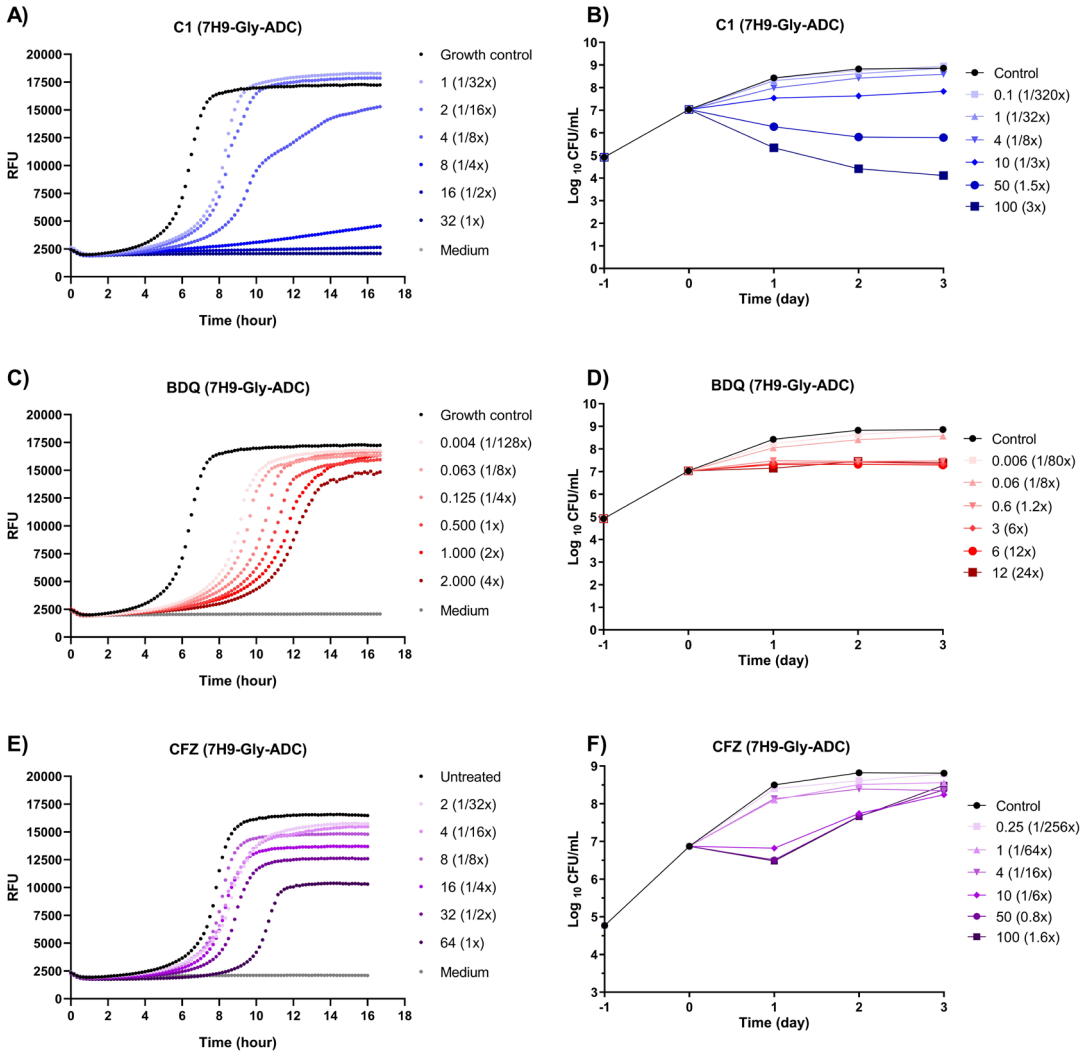

Figure 25. O_2 consumption assay in *M. abscessus* using BD™ OBS plates. O_2 consumption profiles from *M. abscessus* (at 10^7 CFU/mL) treated with increasing concentrations of C1 (A), BDQ (C) and CFZ (E) in 7H9-Gly-ADC and time kill assays of *M. abscessus* exposed to different concentrations of C1 (B), BDQ (D) and CFZ (F) in 7H9-Gly-ADC. Compound concentrations are expressed in µg/mL. RFU: relative fluorescence units.

C1 inhibited O_2 consumption at concentrations that did not reduce CFUs after 24 h of treatment (*e.g.,* at 4 µg/mL) (**Figure 25A,B**). Similarly, BDQ and CFZ, OxPhos inhibitors used as controls [108], also decreased O_2 consumption in a dose-dependent manner but to a much lesser extent than C1. This is especially evidence at sub-optimal concentrations of the individual drugs (*i.e.,* minor effects on cell viability) (**Figure 25C,E**).

Hence, these results suggest that this new chemical series could synergize with BDQ by interfering with energy metabolism.

Mycobacterium ulcerans clinical isolates

The synergism observed between this new chemical series and several inhibitors of energy metabolism in *Mtb* and *M. abscessus* suggests that these compounds could affect energy metabolism. The lack of synergism with Q203 (**Figure 22**), a cytochrome bc_1:aa_3 inhibitor, led us to hypothesize that both C9 and Q203 could share the same target.

Mtb expresses two respiratory terminal oxidases, the cytochrome bc_1:aa_3 and the cytochrome bd oxidase, which couple the oxidation of menaquinol to the reduction of O_2 to form H_2O. While the cytochrome bc_1:aa_3 is the primary terminal oxidase in *Mtb*, the presence of an alternate bd-type terminal oxidase limits the bactericidal and sterilizing potency of Q203 against this bacterium [114].

M. ulcerans strains belonging to the classical lineage from African and Australian origin have lost all alternate terminal electron acceptors and rely exclusively on the cytochrome bc_1:aa_3 to respire. In contrast, the ancestral *M. ulcerans* strains possess two terminal electron acceptors, similar to *Mtb*. As a result, Q203 is bactericidal at low dose against classical *M. ulcerans* strains replicating *in vitro* and in mice [115].

To evaluate whether the absence of an alternate bd-type terminal oxidase in the classical *M. ulcerans* lineage sensitizes the bacterium to this new chemical series, we determined their MIC against classical and ancestral *M. ulcerans* strains.

As expected, MIC values of Q203 against ancestral lineage isolates encoding a functional cytochrome bd oxidase were higher compared to the classical strains, which have only the cytochrome bc_1:aa_3 (**Table 17**). However, classical lineage isolates were not more susceptible to the study compounds than ancestral lineage isolates, indicating that the cytochrome bc_1:aa_3 is not the target of these compounds. In fact, MIC values of the compounds were slightly higher (2-4-fold increase) against classical *M. ulcerans* strains.

Table 17. Susceptibility of *M. ulcerans* clinical isolates to Q203 and compounds of study.

Clinical isolate	Origin	Lineage	MIC (µg/mL)				
			Q203	C1	C9	C3	C6
ITM C05142	Australia	Classical	**0.0001**	**4**	**8**	**8**	**8**
ITM 063846	Benin	Classical	**0.0004**	2-4	**4-8**	4	4
ITM C05143	Mexico	Ancestral	0.002	1	2	ND	ND
ITM C08756	Japan	Ancestral	>0.05	1	1-2	2	2
ITM 070290	China	Ancestral	>0.05	1-2	2-4	2-4	2

ND: not determined.

Therefore, these results confirmed that the cytochrome bc_1:aa_3 is not the target of the compounds.

3.2.6. Efflux pump studies in mycobacteria

In the previous section, it was demonstrated the synergism of C9 with BDQ, CFZ and KET, drugs extruded by the MmpL5/MmpS5 system [59–61]. These results prompted us to hypothesize that this synergism could arise from inhibition of efflux activity mediated by the study compounds.

C9 behaves as an efflux inhibitor

To study whether this new chemical series could modulate efflux, we evaluated the capacity of *M. smegmatis* to accumulate ethidium bromide (EtBr) in the presence of increasing concentrations of C9.

To determine the effect of C9 on EtBr accumulation, C9 was added to *M. smegmatis* cells at inhibitory and sub-inhibitory concentrations together with EtBr at 1 µg/mL. VER, a well-known EI that increases EtBr accumulation, was included as a positive control.

The kinetics of EtBr accumulation in the presence of C9 (observed as an increase in fluorescence due to the binding of EtBr to nucleic acids) was dose-dependent at sub-inhibitory concentrations of C9. EtBr accumulation was maximally achieved at the MIC concentration (2 µg/mL), with no substantial changes at higher concentrations (4 µg/mL). Importantly, at 1 µg/mL of C9 (1/2xMIC), it was similar to that obtained with VER, which produced an increase in fluorescence over time due to its role as an EI (**Figure 26**).

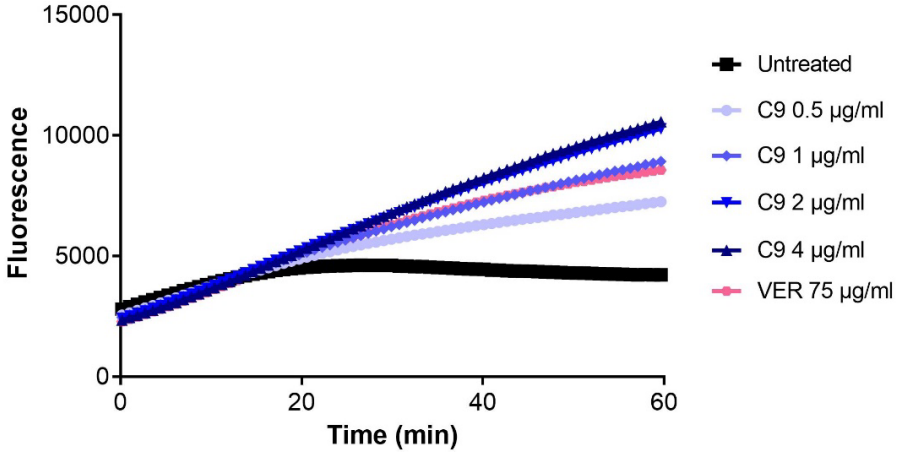

Figure 26. Effect of C9 and VER on the accumulation of EtBr (at 1 µg/mL) in *M. smegmatis*. Data are expressed as arbitrary units of fluorescence; values are averages of three technical replicates. Untreated is a negative control with only the bacterial suspension. Accumulation of EtBr was recorded fluorometrically with a Synergy HT Detection Microplate Reader (Biotek® Instruments), using 530/25nm and 590/20nm as excitation and emission wavelengths, respectively. VER, verapamil. MIC C9 = 2 µg/mL.

Therefore, the enhanced accumulation of EtBr in the presence of C9 suggests its involvement in the inhibition of efflux in *M. smegmatis*.

Implication of MmpL5/MmpS5 system in the susceptibility of *Mtb* to this new chemical series

Taking into consideration the increased susceptibility of MmpL4 mutants to the compounds under low iron conditions (**Table 9**), the strong synergism between C9 and substrates of MmpL5/MmpS5 export system (**Figure 16 & Figure 17**), and the partially redundant function of both MmpL4 and MmpL5 proteins *in vitro* [91], we aimed to study the implication of MmpL5/S5 system in the susceptibility to the study compounds. Thus, we constructed *Mtb* strains deficient in *mmpL5* (L5KO) or *mmpL5/mmpS5* (L5S5KO) genes and an *Mtb* strain overexpressing *mmpL5/mmpS5* operon in the replicative pSUM36 plasmid (named pACM1). The entire process of construction of these strains is detailed in ***Materials and methods*** (**Table 31**).

Once constructed, we characterised their susceptibility profile to several antimicrobials, including the MmpL5/S5 substrates BDQ, KET and CFZ, in iron-replete (7H9-Gly-ADC) and iron-restricted conditions (7H9-Gly-ADC supplemented with 0.2 mM of DFO). The susceptibility of L4KO strain was also evaluated as an internal control (**Table 18**).

Table 18. Susceptibility of *Mtb* wild type, and *mmpL4* and *mmpL5/S5* mutants to several antimicrobials, under iron-replete (7H9-Gly-ADC) and iron-restricted (7H9-Gly-ADC plus 0.2 mM DFO) conditions. INH, isoniazid; BDQ, bedaquiline; KET, ketoconazole; CFZ, clofazimine. *Mtb* pACM1 is an *Mtb* strain overexpressing *mmpL5/S5* operon in the replicative pSUM36 plasmid.

Condition	Strains	MIC (µg/ml)					
		C1	C9	INH	BDQ	KET	CFZ
7H9-Gly-ADC	**H37Rv**	2	4	0.25	0.031	16	0.25
	L4KO	2	2.83-4	0.25	0.031	16	ND
	L5KO	2	4	0.25	**<0.016**	**4-5.7**	**0.125**
	L5S5KO	2	4	0.25	**<0.016**	**4.0**	ND
	pACM1	ND	ND	0.25	**0.5**	**32**	**0.50**
7H9-Gly-ADC + 0.2 mM DFO	**H37Rv**	1.4	2.8-4	0.25	0.022	11.3	ND
	L4KO	**0.5**	**1**	0.25	0.031	8	ND
	L5KO	1.4	2.8	0.25	**<0.016**	**4.0**	ND
	L5S5KO	1.4-2	2.8-4	0.25	**<0.016**	**4.0**	ND

L5KO and L5S5KO were more susceptible to BDQ, KET and CFZ than *Mtb* wild type, whereas MIC values of C1, C9 and INH against these strains remained unchanged. Importantly, *Mtb* pACM1 (overexpressing MmpL5/S5) was less susceptible to BDQ, CFZ and KET than *Mtb* wild type, as previously described [59].

The susceptibility of L5KO and L5S5KO mutants to C1, C9, INH, BDQ and KET did not change under low iron conditions in comparison to iron-replete medium, while L4KO mutant was more susceptible to both C1 and C9 under low iron conditions, as previously shown (**Table 9**).

Hence, these results indicated that MmpL4 but not MmpL5 is involved in the increased susceptibility to both C1 and C9 under low iron conditions. Moreover, while BDQ, KET and CFZ are MmpL5/S5 substrates, the study compounds are not extruded by MmpL5. Further experiments are needed to unravel whether the study compounds synergize with MmpL5/S5 substrates by interfering with the activity of this export system.

3.2.7. Efflux pumps studies in Gram-negative bacteria

Whereas this new chemical series exerted antimicrobial activity against mycobacteria and Gram-positive bacteria, it was not active against the Gram-negative bacteria tested, *i.e., E. coli, P. aeruginosa* and *K. pneumoniae* (MIC>64 µg/mL) (**Figure 6**).

Drug efflux is one of the main mechanisms of intrinsic drug resistance in Gram-negative bacteria, since they express a plethora of efflux pumps that lower the intracellular concentration of antimicrobials, thus allowing bacteria to survive at higher drug concentrations [116].

During my Master's thesis [87], the activity of the study compounds was evaluated in the presence of sub-inhibitory concentrations of several EI against *P. aeruginosa* and *K. pneumoniae*, with the aim of unraveling whether efflux pumps could be involved in the resistance of Gram-negative bacteria to the compounds. Interestingly, only PAβN at sub-inhibitory concentrations enhanced the activity of the compounds against Gram-negative bacteria (**Appendix III-Table AIII.1 & Figure AIII.1**), suggesting that the PAβN-inhibited efflux pumps could contribute to resistance by extruding these compounds out of the bacteria [87].

Taking into consideration that PAβN acts as a competitive inhibitor of RND efflux pumps of Gram-negative bacteria, including Mex pumps of *P. aeruginosa* and AcrB of *E. coli,* the results obtained suggested that RND pumps of Gram-negative bacteria could efflux these compounds, thus conferring resistance [116]. This hypothesis is further supported by our finding that *Mtb* mutants deleted in the MmpL4 transporter (a member of the RND superfamily of efflux pumps) have an increased susceptibility to the study compounds.

Drug susceptibility of *E. coli* strains

To fully demonstrate that RND efflux pumps are involved in the mechanism of resistance of Gram-negative bacteria to the compounds, their MIC were determined in liquid media against several *E. coli* BW25113-derived strains deficient in efflux pumps of different families: AcrB (RND superfamily), MdfA (MFS superfamily) and EmrE (SMR superfamily). MOX, a well-known AcrB substrate, was included as a control.

Only those *E. coli* strains deficient in AcrB were more susceptible (>16-fold MIC reduction) to this new chemical series than *E. coli* wild type. AcrB is an RND-type efflux pump constitutively expressed in *E. coli* and is largely responsible for the intrinsic resistance of *E. coli* to dyes, detergents, and most lipophilic antimicrobials [117]. Thus, these results suggested that AcrB is involved in the resistance of *E. coli* to the study compounds by extruding them out of the bacteria (**Table 19 & Figure 27**).

Table 19. Susceptibility of *E. coli* BW25113-derived strains to C1, C2, C9 and MOX.

***E. coli* strains**	**MIC values (µg/mL)**			
	C1	**C2**	**C9**	**MOX**
BW25113 (wild type)	>64	>64	>64	0.125
ΔacrB	**4**	**4**	**4**	**<0.008**
ΔemrE	>64	>64	>64	0.125
ΔmdfA	64-128	64	>64	0.125
ΔacrB ΔemrE	**4**	**4**	**4**	**<0.008**
ΔemrE ΔmdfA	>64	64	>64	0.125
ΔacrB ΔemrE ΔmdfA	**4**	**4**	**2**	**<0.008**

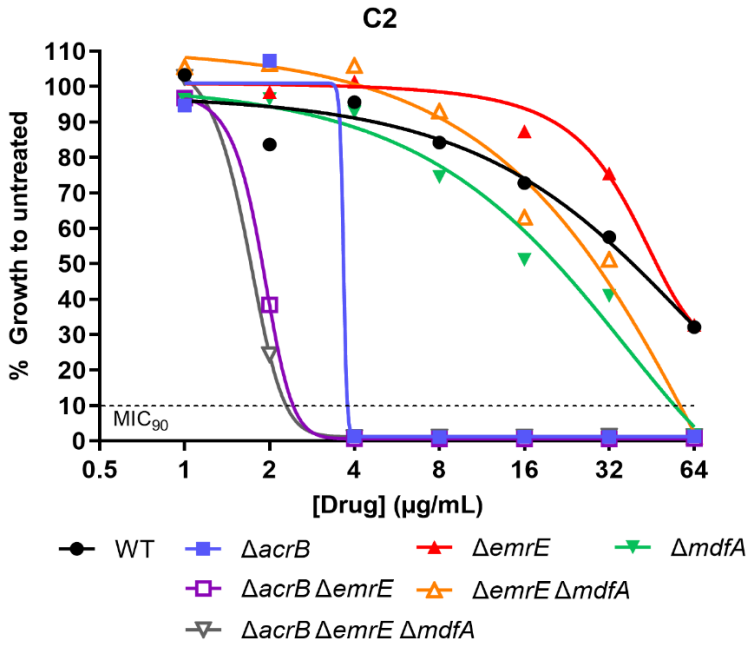

Figure 27. Dose-response curves of C2 against *E. coli* BW25113-derived strains.

Double mutant isolation assays and validation assays

E. coli ΔacrB, a single mutant strain having MICs of C1, C2 and C9 compounds lower than the wild type BW25113 (**Table 19**), could favour intracellular accumulation of the compounds, so it was used in an attempt to isolate spontaneous double mutants resistant to the compounds with a mechanism different from AcrB.

To set up the double mutant isolation assay, the MIC of C2 on solid media was first determined against two different inocula of *E. coli* Δ*acrB* to evaluate whether compound activity varied depending on the total CFU seeded. Difference in MICs between low and high inoculum were of 2-fold (**Table 20**), indicating that the activity of C2 was inoculum independent, as previously observed in *Mtb* H37Rv (**Table 4**).

Table 20. Solid MIC values of C2 in LB agar against different inocula of *E. coli* Δ*acrB*.

Inoculum (total CFU)	Solid MIC (µg/mL)
10^5	16
10^7	32

Then, resistant candidate double mutants were selected by plating 10^8 or 10^9 CFU of *E. coli ΔacrB* on LB agar plates containing C2 at 4x, 10x or 20xMIC, taking as reference an MIC of 16 µg/mL (**Table 21**). Frequencies of mutation were calculated as the ratio of total number of colonies isolated after 24 h of incubation at 37°C on the drug-containing plate over the total number of CFU seeded.

Table 21. Summary of the experimental conditions used for the isolation of mutants resistant to C2 derived from *E. coli* Δ*acrB* single mutant. Frequencies of mutation were calculated as the ratio of total number of colonies isolated in the presence of C2 over the total CFUs seeded.

Inoculum (CFU)	C2 concentration (xMIC)	Colonies isolated	Frequency of mutation
10^8	64 µg/mL (4x)	115	$1.2 \cdot 10^{-6}$
	160 µg/mL (10x)	106	$1.1 \cdot 10^{-6}$
10^9	320 µg/mL (20x)	18	$1.8 \cdot 10^{-8}$

A total of 18 colonies (candidate double mutants) were selected for phenotypic validation assays. Before testing their susceptibility to C2, candidate double mutants were cultured in drug-free medium to reverse any transient phenotypic resistance. As a primary validation, the MIC of C2 was determined against each potential double mutant. All of them displayed an 8-fold increase in their MIC compared to the Δ*acrB* single mutant strain (**Table 22**). This resistance to C2 was maintained (8- to 16-fold) after serial passage of representative candidate double mutants in the absence of drug pressure (**Table 23**), suggesting the involvement of a genetic resistance mechanism. Likewise, these potential double mutants were also resistant to C1 (**Table 23**). However, although MOX and C1, C2 and C9 compounds are all extruded by AcrB efflux pump (**Table 19**), these candidate double mutants did not display high level of resistance against MOX (**Table 23**), hence strongly suggesting that they were true double mutants in a different gene.

Table 22. Susceptibility of *E. coli* wild type, Δ*acrB* single mutant and candidate double mutants to C2.

***E. coli* strains**	**MIC C2 (μg/mL)**
BW25113	>64
Δ*acrB* single mutant	8
Mutants 1-18 (Δ*acrB*-derived strains)	64

Table 23. Susceptibility of *E. coli* candidate double mutants M1 and M2 (after serial passage) to C1, C2 and MOX.

***E. coli* strains**	**MIC (μg/mL)**		
	C1	**C2**	**MOX**
Δ*acrB*	4	4-8	0.008
Δ*acrB* M1 P5	>64	>64	0.015
Δ*acrB* M2 P5	32-64	>64	0.015
Δ*acrB* M2 P3	64	>64	0.015

PX indicates the number of the serial passage.

Subsequently, 10 candidate double mutants (for which the MIC of C2 was 64 µg/mL) were selected to evaluate their susceptibility by time kill assays. All the candidate double mutants tested were able to grow in the presence of inhibitory concentrations of C2 (8 and 32 µg/mL) for the *E. coli ΔacrB* single mutant from which they were selected. However, these candidate double mutants were more susceptible to C2 than the wild type strain BW25113, which grew after treatment with 64 µg/mL of C2 (**Figure 28 & Appendix IV-Figure IV.1**).

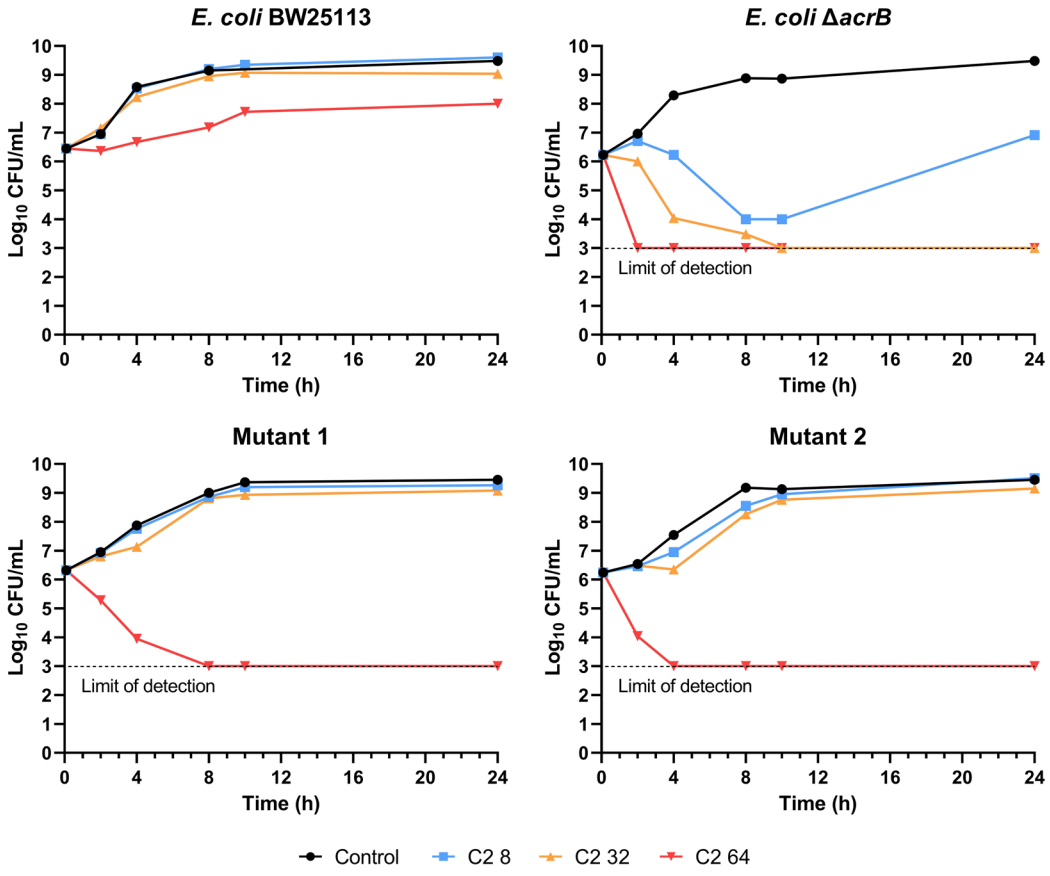

Figure 28. Time kill assays of C2 against *E. coli* BW25113, Δ*acrB* single mutant and two representative Δ*acrB*-derived candidate double mutants (M1 and M2). Overnight *E. coli* cultures were 1/1000 diluted in LB and drugs were added at the indicated concentrations.

Taken together, the results obtained by MIC in liquid media (**Table 22**) and time kill assays (**Figure 28 & Appendix IV-Figure IV.1**) confirmed that the candidate double mutants selected were resistant to C2 and that this resistance phenotype was independent of AcrB efflux system.

Whole Genome Sequencing of candidate double mutants

To identify the genetic mutations causing the resistance to C2, ten confirmed resistant candidate double mutants and *E. coli ΔacrB* single mutant were propagated in LB, and their DNA was isolated for WGS using Illumina technology.

Bioinformatics analysis identified a nonsense SNP (single nucleotide polymorphism) in *hns* gene (g326a leading to W109stop) in both M1 and M8 mutants. Regarding M6 mutant, two frameshift indels (insertion/deletion) were detected in the *hns* gene: c.114_126delCGAACGTCGCGAA and c.140delC leading to p.N38fs and p.A47fs, respectively (**Table 24**). The remainder mutants did not show any SNPs or indels compared to *E. coli* Δ*acrB* genome with frequencies > 0.9 and supported by more than 20x coverage.

Table 24. SNPs and indels with frequencies >0.9 and supported by more than 20x coverage.

Mutants	Locus	Consequence
M1 & M8	*hns* c.326G>A | p.W109*	Nonsense SNP
M6	*hns* c.140delC|p.A47fs	Frameshift indel
	hns c.114_126delCGAACGTCGCGAA|p.N38fs	Frameshift indel

The *hns* gene encodes H-NS, a histone-like nucleoid structuring protein of 137 amino acids, that is one of the most abundant proteins in the *E. coli* nucleoid and is involved in global gene regulation in Gram-negative bacteria. It is composed of two functional domains separated by a flexible linker: a central domain (residues 21-63), implicated in dimerization, and the C-terminal domain (residues 92-137), required for DNA binding. Previous studies have shown that the ability of H-NS to form a dimer is essential to function as a transcriptional repressor [118]. Hence, the frameshift indels identified in M6 double mutant will result in an aberrant protein from amino acid 38 onwards, and the nonsense SNP found in both M1 and M8 mutants would have a functional impact on the DNA-binding activity of the H-NS protein.

H-NS has been described to contribute to multidrug resistance by regulating the expression of multidrug exporter genes. In a previous study, Nishino and Yamaguchi found that H-NS represses the expression of some TolC-dependent multidrug exporter genes and, as a result, deletion of *hns* gene confers multidrug resistance on an *acrAB*-deficient strain due to an increased expression of several TolC-dependent exporter genes, including *acrE*, *mdtE* and *emrK* [117].

Based on these data, we aimed to determine by qRT-PCR which drug exporters were up-regulated in M1, M6 and M8 mutants (with SNPs or indels in *hns* gene) and M2 mutant (without any SNP or indel in the *hns* gene identified by WGS). The expression levels of TolC-dependent drug exporter genes, including *acrD*, *acrE*, *mdtE* and *mdtA* of the RND family and *emrK* of the MFS family, in these mutants (M1, M2, M6 and M8) and in the wild type strain BW25113 were compared with those in *E. coli* Δ*acrB* (**Figure 29**). Both *gapA* and *rrsA* transcripts were use as internal invariant controls.

The results showed that *emrK* gene was over-expressed (>10-fold) in all mutants compared to *E. coli* wild type and Δ*acrB.* The *mdtA* gene was also upregulated (>2-fold) in M1 and M8 mutants, and *acrE* gene was overexpressed in M1 and M6. In contrast, *acrD* was not upregulated in these mutants, in line with the results previously reported by Nishino and Yamaguchi, which showed that deletion of *hns* in *E. coli* W3104 Δ*acrAB* did not increase the expression levels of *acrD* [117].

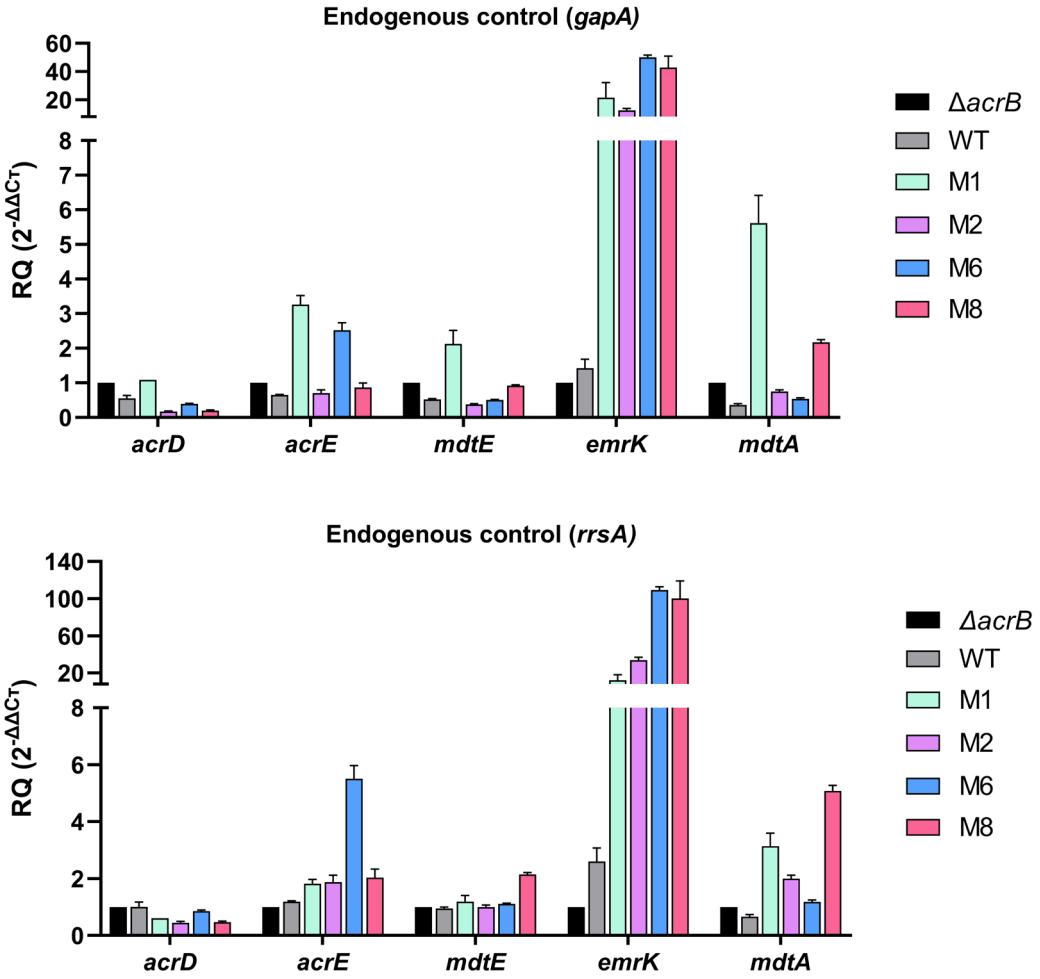

Figure 29. Expression of TolC-dependent efflux pumps in *E. coli* BW25113 wild type, Δ*acrB* single mutant and Δ*acrB*-derived double mutants (M1, M2, M6 and M8). Data are relative to *E. coli* Δ*acrB*. Both *gapA* (upper panel) and *rrsA* (lower panel) were used to normalize gene expression. Data represent mean±SEM from 3 technical replicates.

Hence, our data suggest that *E. coli* Δ*acrB*-derived mutants might be resistant to the study compounds due to the overexpression of other efflux pumps, including AcrE and MdtA from RND family and EmrK from MFS family. Nonetheless, this upregulation of diverse efflux pumps could confer resistance not only to the study compounds but also to other drugs, as previously observed in an *E. coli* strain deleted in *acrAB* and *hns* genes [117]. Hence, we evaluated the susceptibility of *E. coli* wild type, *ΔacrB* single mutant and M1, M2, M6 and M8 mutants to several drugs.

As a result, *E. coli ΔacrB* was more susceptible to several drugs, including MOX, oxacillin (OXA), erythromycin (ERY) and VER, than the wild type strain (**Table 25**), indicating that these drugs are AcrB substrates. In contrast, M1, M2, M6 and M8 mutants were more resistant to these compounds than *E. coli ΔacrB*, in line with the results previously published by Nishino and Yamaguchi using an *E. coli* strain deleted in *acrAB* and *hns* genes [117].

Table 25. Susceptibility of *E. coli* wild type, Δ*acrB* single mutant and several Δ*acrB*-derived mutants to diverse drugs. MOX, moxifloxacin; OXA, oxacillin; ERY, erythromycin; VER, verapamil.

Strains	MOX	OXA	ERY	VER
BW25113	0.125	>128	128	2048
Δ*acrB*	0.008	<2	8	512
M1	0.030	4	128	1024
M2	0.015	8	64	1024
M6	0.030	16-32	64-128	2048
M8	0.030	4-8	128	1024

To sum up, we have demonstrated that RND efflux pumps (*e.g.,* AcrB of *E. coli*) are involved in the mechanism of resistance to these compounds in Gram-negative bacteria. Moreover, our data suggest that *E. coli* Δ*acrB*-derived mutants are resistant to the study compounds and other drugs, such as MOX, OXA, ERY and VER, possibly due to the overexpression of several efflux pumps, including AcrE and MdtA from RND family and EmrK from MFS family.

It should be noted that, while the M2 mutant did not have any SNP or indel in the *hns* gene identified by WGS, this mutant showed the same susceptibility profile as M1, M6 and M8 mutants (with SNPs or indels in *hns*) and similar gene expression patterns of diverse efflux pumps. Hence, it would be necessary to perform Sanger sequencing of the *hns* gene to confirm whether this gene has some SNP which has not been identified by WGS.

3.2.8. Global transcriptional response of *Mtb* to C9 by RNA-seq

Transcriptomic studies of *Mtb* after drug treatment have improved the understanding of many anti-TB drugs currently used, as well as provided insights into the MoA and targets of novel drugs coming from HTS [84]. Therefore, this approach was used to further elucidate the MoA of this new chemical series against *Mtb*.

The experimental design is highly important when performing omic studies. Drug concentration and incubation time need to be carefully defined since drug exposure leads to global effects that are dependent on both drug concentration and duration of exposure [84].

In this work, RNA-seq studies were performed to analyse the impact of C9 on the transcriptome of *Mtb*, focusing on the changes in the gene expression profile during the initial phase of treatment (4 and 24 hours) and after long exposure to C9 at low concentrations (9 days). The conditions for RNA-seq studies (**Table 26**) were selected based on previous time kill assays (**Figure 30**), considering that bacteria need to be collected before phenotypic cell death occurs to detect only the transcriptional changes due to the drug effect. We were interested in analysing the transcriptome of *Mtb* after long exposure to C9 at 1xMIC to study the mechanisms that allow the bacteria to adapt and survive drug treatment. At every time point, untreated cultures were used as controls to identify differentially expressed genes (DEGs) in treated samples.

Table 26. Conditions used to study the global transcriptional response of *Mtb* to C9. Bacterial cultures were treated in triplicate with C9 at the concentrations indicated and RNA was extracted at different time points (4 h, 1 day or 9 days). MIC of C9 against ca. 10^7 CFU/mL was 8 µg/mL.

Time point	Condition
4 hours	Untreated (control)
	C9 at 80 µg/mL (10x MIC)
1 day	Untreated (control)
	C9 at 8 µg/mL (1x MIC)
	C9 at 32 µg/mL (4x MIC)
9 days	Untreated (control)
	C9 at 8 µg/mL (1x MIC)

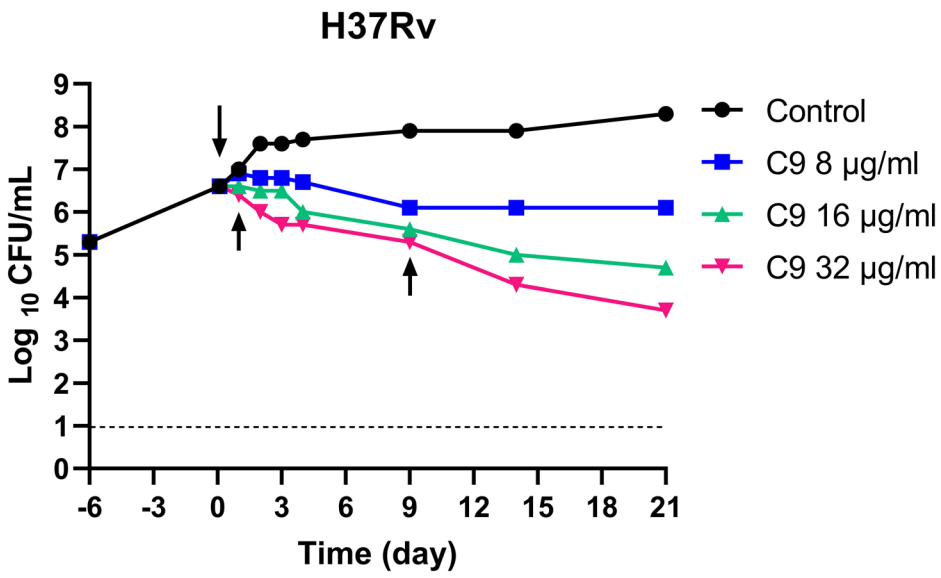

Figure 30. Time kill assays of C9 against *Mtb* H37Rv. Bacteria were inoculated to a cell density of 10^5 CFU/mL and incubated at 37°C for 6 days before adding C9 on day 0 (arrow). RNA was extracted after 1 and 9 days of treatment (arrow).

Principal component analysis (PCA) plots show the first two principal components that explain data variability, reflecting the association between samples at the different time points analysed (**Figure 31**).

Samples treated with C9 were clearly separated from untreated samples, and triplicates clustered together. Regarding the PCA plot at day 1, drug treatment explained 76.2% of variance, whereas drug concentration (8 *vs* 32 µg/mL) was responsible for 16.5% of variance, indicating that the bacterial response to C9 treatment also varied depending on the drug concentration.

These results confirmed that C9 treatment caused relevant transcriptional changes in comparison to untreated samples, and that transcriptomic profiles of triplicates were very similar.

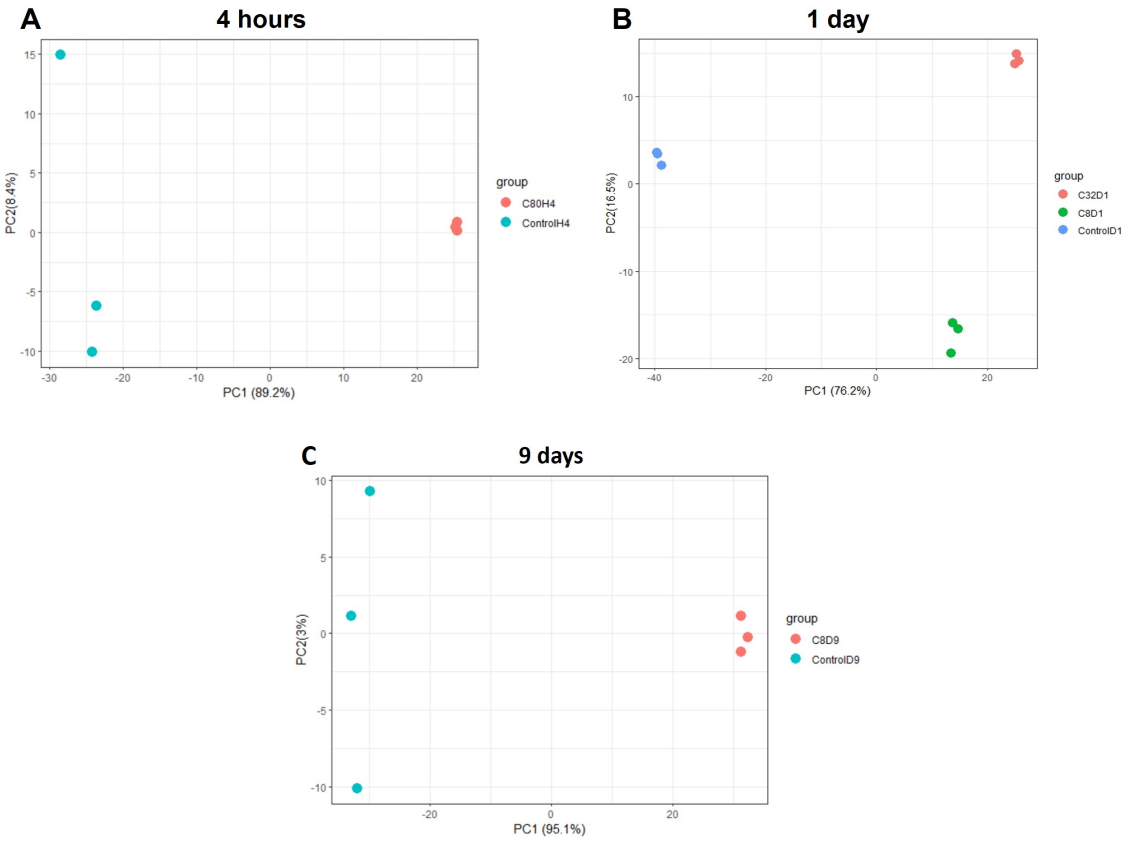

Figure 31. PCA plots showing association between samples at the different time points analysed. Triplicates are indicated in the same colour. A: C80H4 (80 µg/mL, 4 hours), ControlH4 (untreated, 4 hours); B: C8D1 (8 µg/mL, 1 day), C32D1 (32 µg/mL, 1 day), ControlD1 (untreated, 1 day); C: C8D9 (8 µg/mL, 9 days), ControlD9 (untreated, 9 days).

A differential gene expression analysis was performed using RStudio, comparing each drug condition with its respective control (untreated sample). DEGs with statistical significance were selected using a cut-off of adjusted p-values (p-adj) ≤ 0.05, and log_2FoldChange (log_2FC) values ≥ 1.5 (for up-regulated genes) or ≤ -1.5 (for down-regulated genes).

Volcano plots allowed visualization of differential gene expression analysis in each condition (**Figure 32**). The most statistically significant and differentially expressed genes were in the upper corners of the plots.

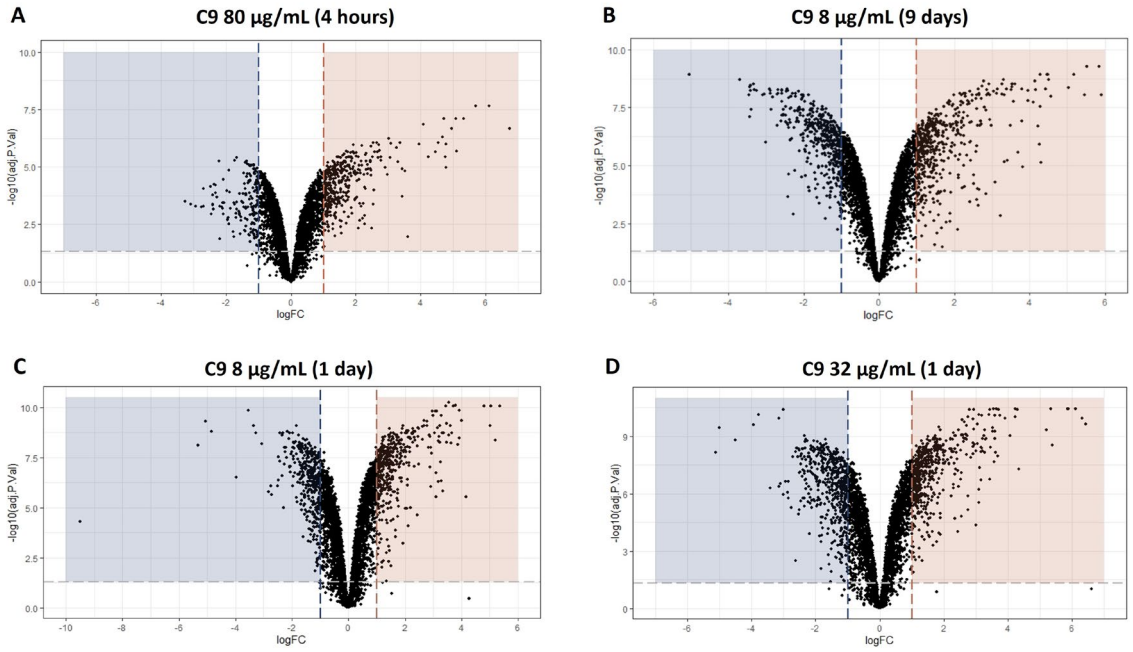

Figure 32. Volcano plots of DEGs. Genes (dots) are plotted based on their log_2FC in gene expression and statistical significance ($-log_{10}$ adjusted p-value) under different treatments. Genes in orange area are those with a $log_2FC \geq 1.5$ and p-adj ≤ 0.05 (up-regulated), whereas genes in grey area are those with a $log_2FC \leq -1.5$ and p-adj ≤ 0.05 (down-regulated).

All conditions analysed showed a higher number of genes upregulated than downregulated (**Table 27**). Regarding the analysis on day 1, although the number of DEGs increased with drug concentration (310 genes with 8 µg/mL of C9 *vs* 463 genes with 32 µg/mL), both conditions shared a common transcriptional response for 219 genes (138 up-regulated and 81 down-regulated) (**Figure 33**). Interestingly, 28 genes out of 138 were also up-regulated after 4 hours and 9 days, while only 3 genes out of 81 were down-regulated in all conditions (**Figure 33**).

Table 27. Number of DEGs with statistical significance under different conditions. Up-regulated ($log_2FC \geq 1.5$ and p-adj ≤ 0.05). Down-regulated ($log_2FC \leq -1.5$ and p-adj ≤ 0.05).

Condition	Time	Up-regulated	Down-regulated	Total
C9 80 *vs* untreated	**4 h**	184	50	***234***
C9 8 *vs* untreated	**1 day**	191	119	***310***
C9 32 *vs* untreated	**1 day**	250	213	***463***
C9 8 *vs* untreated	**9 day**	232	196	***428***

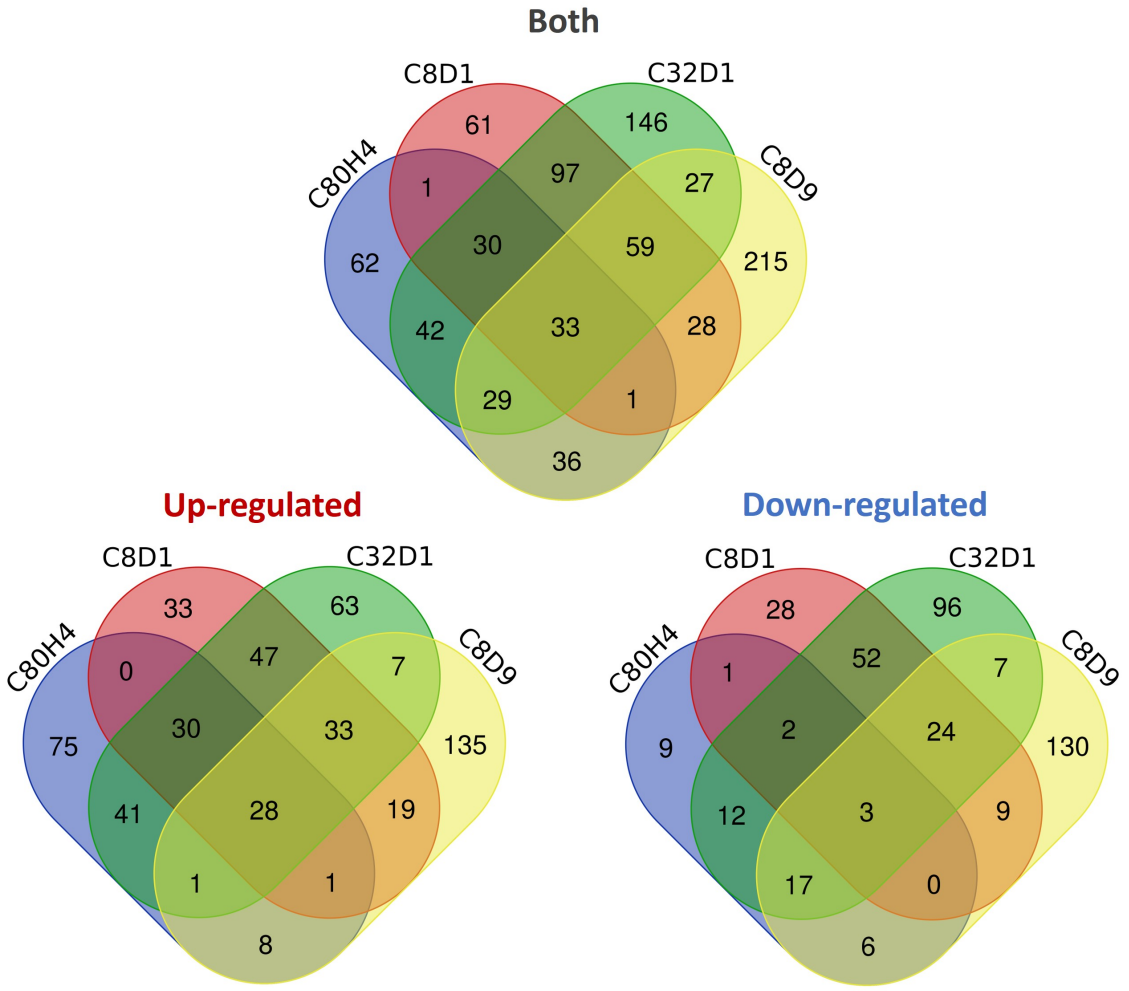

Figure 33. Venn diagrams of up-regulated, down-regulated, and both up-regulated and down-regulated DEGs in the different conditions assayed. C80H4 (80 µg/mL, 4 hours); C8D1 (8 µg/mL, 1 day); C32D1 (32 µg/mL, 1 day); C8D9 (8 µg/mL, 9 days).

Owing to the large number of up-regulated and down-regulated genes, a general transcriptomic analysis focused on cellular processes and biological pathways instead of an individual gene analysis was carried out.

The biological pathway enrichment analysis was performed with the DEGs from each comparison using BiNGO (Biological Networks Gene Ontology) software, a tool that determines which molecular pathways are significantly overrepresented in a set of genes.

One limitation of this analysis is that some genes are not annotated with the corresponding Gene Ontology (GO) term, leading to underrepresentation of the biological pathways in which those selected genes are involved.

Table 28 shows the number of DEGs selected for the analysis per condition and those excluded by BiNGO due to the lack of information.

Table 28. Number of genes per comparison used for BiNGO analysis. "*DEG"* refers to the number of statistical differentially expressed genes (p-adj ≤ 0.05 and log_2FC values ≥1.5 or ≤-1.5) included for the analysis. Those genes that did not have GO information annotated ("*DEG without information"*) were excluded from BiNGO analysis.

Condition	Time	Up-regulated		Down-regulated	
		DEG	DEG without information	DEG	DEG without information
C9 80 *vs* control	**4 h**	184	77	50	15
C9 8 *vs* control	**1 day**	191	69	119	35
C9 32 *vs* control	**1 day**	250	102	213	62
C9 8 *vs* control	**9 day**	232	98	196	57

The analysis of biological pathways overrepresented in up-regulated and down-regulated genes provided some interesting findings that are discussed in detail below.

Iron metabolism

Cellular response to iron starvation and siderophore biosynthesis were overrepresented pathways among upregulated genes in all conditions.

To overcome iron limitation, mycobacteria produce two types of siderophores, the membrane-bound mycobactins and the water-soluble carboxymycobactins [119]. In this study**, *mbt* genes** encoding the proteins required for siderophore biosynthesis were up-regulated (**Figure 34**) [120]. Interestingly, the expression of *mbt* genes increased overtime, reaching up to 5-log_2FC in gene expression after 9 days of treatment with 8 µg/mL of C9.

The non-essential gene ***rv0560c***, which encodes a putative benzoquinone methyltransferase, was also strongly up-regulated in all conditions tested (4.7-log_2FC after 4 h of incubation with 80 µg/mL) (**Figure 34**). It is overexpressed in response to diverse stresses, including salicylate, PAS, menadione, plumbagin and the respiratory inhibitors chlorpromazine (CPZ) and TDZ [121,122]. Specifically, salicylate is known to accumulate as an intermediate in iron-depleted mycobacteria during the biosynthesis of siderophores, accounting for the up-regulation of *rv0560c* during iron depletion[121]. Therefore, these results suggested that *Mtb* could be sensing iron restriction after C9 treatment.

The **iron-regulated ABC transporter IrtAB** was also overexpressed (**Figure 34**). IrtAB couples Fe^{3+}-carboxymycobactin import and iron assimilation from both imported carboxymycobactin and membrane associated mycobactin [123].

Among the overexpressed genes was the ***esx-3* gene cluster** (*rv0282-rv0292*), one of five type VII secretion systems (T7SS) of *Mtb* that is required for siderophore-mediated iron acquisition through secretion of a pair of proteins belonging to the PE-PPE family (PE5-PPE4) and associated with *Mtb* virulence[119,124].

The IdeR-controlled gene ***ppe37***, which is induced under iron limiting conditions and involved in heme acquisition, was strongly up-regulated under all conditions tested (**Figure 34**) and among the top 10 up-regulated genes after 9 days of treatment [93,125].

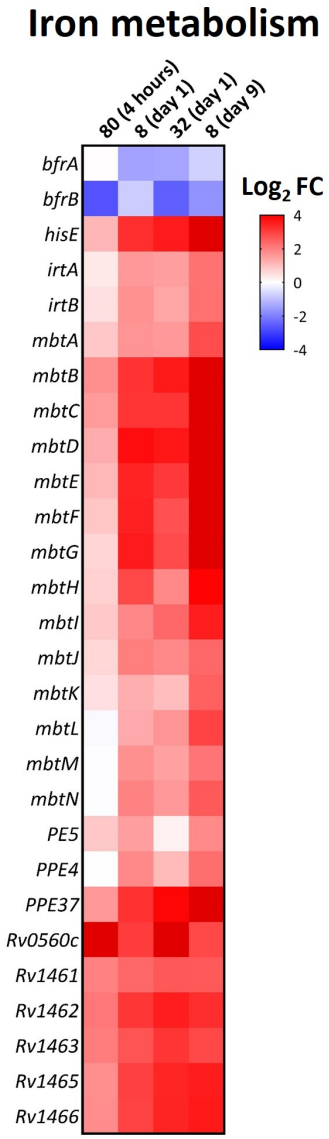

Figure 34. Changes in gene expression of genes associated with iron metabolism after C9 treatment. The concentration of C9 used in each condition is indicated in µg/mL. Colour scale represent log_2FC in gene expression.

Treated bacteria also up-regulated the ***suf* operon** (*rv1460-rv1466*; *sufRBDCSUT*) (**Figure 34**), the only Fe-S cluster biogenesis system present in *Mtb*. Fe-S cluster proteins are involved in numerous cellular processes, including respiration, central metabolism, DNA repair, gene regulation and RNA modification. Hence, *Mtb* expresses the *suf* system to survive under several stress conditions, including iron limitation, and oxidative and nitrosative stress, as inadequate assembly of Fe-S clusters can result in metabolic paralysis and cell death [126].

Interestingly, *Mtb* maintained a high expression of genes involved in iron acquisition at day 9, the last time point examined, indicating that bacteria still try to obtain iron after long exposures to the drug. In contrast, iron storage genes ***bfrA*** and ***bfrB*** were downregulated in all conditions (**Figure 34**). Due to the high toxicity of iron at high concentrations, *bfrA* and *bfrB* genes, which code for the bacterioferritin BfrA and ferritin-like protein BfrB, respectively, are overexpressed in the presence of iron to store the excess as protein-bound iron. However, these genes are downregulated under low-iron conditions [120].

Interestingly, prior to RNA extraction, we observed that pellets of *Mtb* cultures treated with 8 µg/mL of C9 for 9 days showed an orange pigmentation compared to untreated bacteria (**Figure 35**). Similar results have been described with mutants defective in IdeR (the major iron-dependent regulatory protein), Esx-3 region, or IrtA/IrtB [93,124,127], which developed an orange pigmentation when cultured in iron-replete medium. These mutants experience iron deprivation in iron-replete medium and respond by up-regulating siderophore biosynthesis. Consequently, these studies maintain that accumulation of iron-bound siderophores on the surface of bacteria is likely the cause of the orange pigmentation in these mutants [93,124,127]. We propose that a similar phenomenon could be happening after C9 treatment.

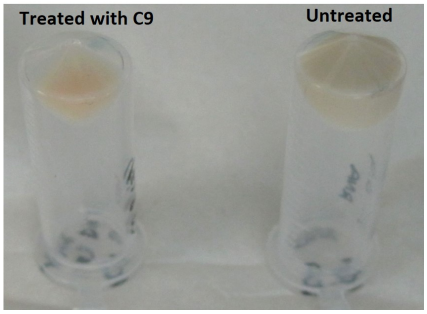

Figure 35. Pellets of *Mtb* cultures untreated (right) or treated (left) with 8 µg/mL of C9 for 9 days, prior to RNA extraction for RNA-seq.

Altogether, the differential expression of genes involved in iron acquisition, transport and storage, similar to that reported in several studies under low-iron conditions, indicated that C9 could induce a state of iron-starvation. These results agree with our hypothesis that the MoA of this new chemical series is linked to iron metabolism.

Metabolic changes

Proton transmembrane transport and ATP metabolic process were overrepresented pathways among down-regulated genes. These results led us to study in detail the gene expression of key components of the ETC after C9 treatment.

Mtb has three membrane-bound NADH dehydrogenase complexes (**Figure 36**) that are capable of oxidizing the cofactor NADH into NAD+, leading to the reduction of the menaquinone pool (MK/MKH_2). These include a proton-translocating type I NADH dehydrogenase (NDH-1), which is not essential for growth or persistence, and two non-proton-translocating type II NADH dehydrogenases (NDH-2) encoded by *ndh* and *ndhA*. We observed that the ***nuo* operon** (*nuoA-nuoN*), which encodes the NDH-1, was downregulated in all conditions. In contrast, ***ndh*** was upregulated (mainly after 1 day of treatment) while ***ndhA*** did not display significant changes (**Figure 37**).

Moreover, *Mtb* has two succinate dehydrogenases (SDH; **SDH-1** and **SDH-2**), which couple the oxidation of succinate to fumarate with the reduction of menaquinone (**Figure 36**), and one **fumarate reductase** which can catalyse the reaction in both directions and is responsible for maintaining the PMF under anaerobic conditions [75]. Whereas genes encoding SDH-2 (*sdhA-sdhD*) and SDH-1 (*rv0249c-rv0247c*) were downregulated in all conditions, those coding the fumarate reductase (*frdA-frdD*) were upregulated after 4 h of treatment with 80 µg/mL but did not show major changes at latter time points analysed (**Figure 37**).

Mtb has a **cytochrome bc_1:aa_3 supercomplex** which transfers electrons from menaquinol to O_2, a process linked to H^+ translocation across the membrane (**Figure 36**). We found that the genes encoding this supercomplex (*qcrA-C* and *ctaB-E*) were downregulated. The cytochrome bd (*cydA-B* and *cydD-C* genes), an alternative terminal oxidase used by *Mtb* when the cytochrome c pathway is inhibited, was also strongly downregulated in all conditions tested except after 4 h of treatment, which was slightly upregulated (less than 0.95-log_2FC) (**Figure 37**).

During electron transport along the respiratory chain, protons are pumped across the membrane, leading to a PMF that can be used for ATP synthesis. The entire *atpBEFHAGDC* operon (encoding the F_1F_0 ATP synthase; **Figure 36**) was downregulated in all conditions analysed (**Figure 37**), indicating reduced respiration-associated ATP synthesis after C9 treatment.

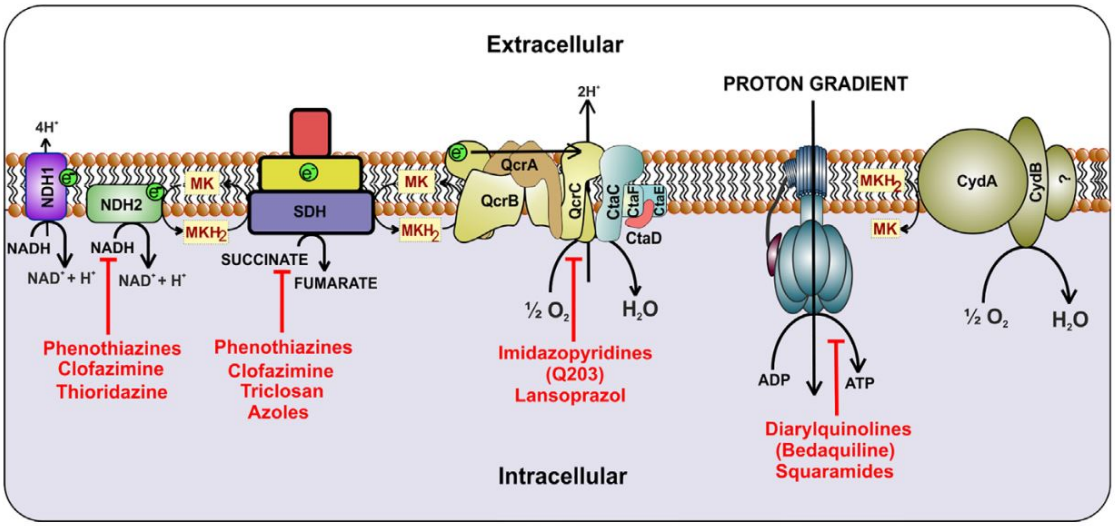

Figure 36. ETC of *Mtb* and drug inhibitors of each complex. From [128].

Moreover, genes encoding enzymes of **TCA cycle**, including *citA*, *icd1*, *fum*, *mdh*, *sucC* and *sucD*, were mostly downregulated (**Figure 37**).

This downregulation of genes encoding enzymes of OxPhos and TCA cycle could be explained by the high number of Fe-S/heme proteins implicated in these pathways and the apparent iron deprivation encountered by *Mtb* after C9 treatment.

A significant downregulation of genes encoding **30S and 50S ribosomal proteins** was also observed upon C9 treatment, suggesting that *Mtb* could inhibit protein synthesis, an ATP consuming process, to evade shortage of energy (**Figure 37**).

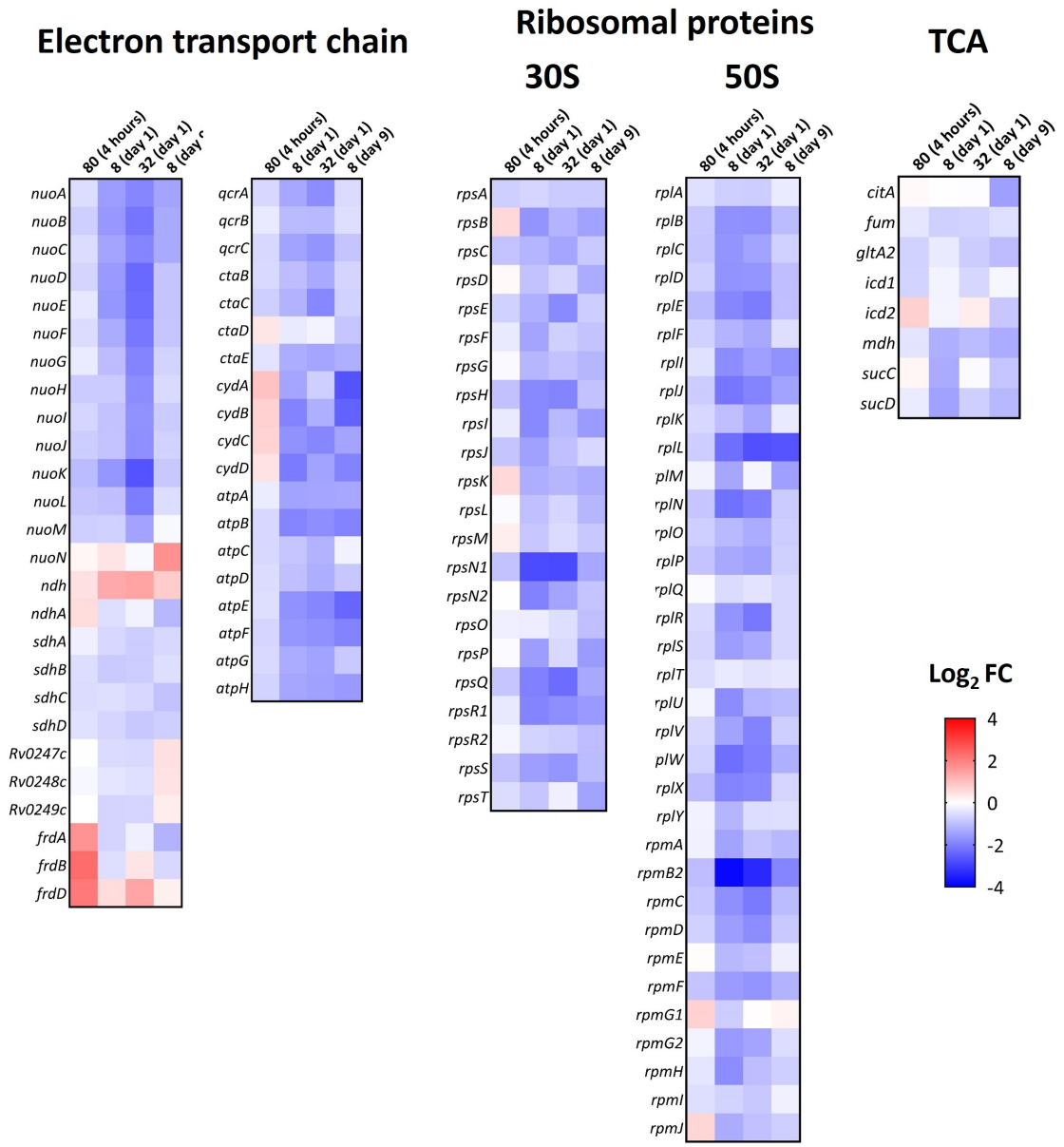

Figure 37. Changes in gene expression of genes encoding enzymes of the ETC and TCA, and 30S and 50S ribosomal proteins, after C9 treatment. The concentration of C9 used in each condition is indicated in µg/mL. Colour scale represent log_2FC in gene expression. TCA, tricarboxylic acid cycle

Regulators of gene expression

RNA-seq analysis showed that the expression of many transcriptional regulators was altered after C9 treatment.

ClgR, a transcriptional regulator that activates the expression of genes encoding protease systems (ClpP1 and ClpP2) and chaperones (Hsp) [129], was up-regulated in all conditions except after 9 days of treatment with C9 at 80 µg/mL (**Figure 38**). The two-component system *mprAB* and the sigma factors *sigE* and *sigB*, overexpressed in response to cell envelope stress and iron restriction [130,131], were also strongly up-regulated after C9 treatment (**Figure 38**). Hence, these results indicated that C9 triggers a stress response related to iron starvation and *Mtb*'s cell wall damage.

Furthermore, many transcriptional regulators involved in metal homeostasis, such as *ideR*, *cmtR*, *zur*, *smtB* and *phoY2*, and genes encoding transmembrane transporters of metal ions, including *rv2025c*, *ctpC*, *ctpG* and *ctpH*, increased their expression after C9 exposure (**Figure 38**). It has been described that the *esx-3* operon (previously mentioned for its association with iron acquisition) is negatively regulated by high concentrations of iron and/or zinc through several transcription factors, including IdeR, Zur and CmtR, to maintain intracellular metal homeostasis [93,132,133].

The Fe-S-dependent regulator WhiB6 was also highly upregulated, particularly after 9 days of treatment (**Figure 38**). Previous studies have shown that *whiB6* is strongly responsive to a wide variety of stress conditions (mainly oxidative stress), indicating that this regulator plays a key role in generalized stress responses in *Mtb* [57].

Hence, these transcriptional changes indicate that *Mtb* strongly upregulates diverse transcriptional regulators involved in protecting *Mtb* against oxidative stress and antioxidant adaptation, in order to counteract the toxic effect of C9.

In contrast, the dormancy regulon, comprised of two sensor kinases (DevS and DosT) and a transcriptional regulator (DevR), was downregulated after C9 treatment (**Figure 38**). This three-component regulatory system is upregulated under O_2 limitation and exposure to nitric oxide or carbon monoxide, but not during Fe starvation [131,134], supporting our hypothesis of C9 inducing a state of iron deprivation.

The strong downregulation of the nitrate transporter NarK2 and the nitrate reductase NarX (**Figure 38**) belonging to the dormancy regulon led us to analyse changes in gene expression of some genes linked to nitrogen metabolism. After nitrate import by NarK2, the nitrate reductase NarGHJI reduces nitrate to nitrite, and nitrites are then reduced to ammonium by the nitrite reductase NirBD, a cytosolic NADH-dependent enzyme[135]. Interestingly, not only were *narK2* and *narX* downregulated, but also *nirB* and *nirD* genes. Moreover, the regulators of nitrogen metabolism *glnB* and *glnD* were upregulated after 1 day of treatment. In contrast, the major *Mtb* glutamine synthetase (encoded by *glnA1)* was downregulated. GlnA1 is strictly regulated by *glnB* and *glnD* genes (among others) as it requires ATP to produce glutamine from glutamate and ammonia. Previous studies have shown that *glnB* and *glnD* are overexpressed in low-ammonia conditions, whereas *glnA1* is upregulated in high-ammonia medium [135,136]. Therefore, the transcriptional changes observed suggest that C9 could be affecting central nitrogen metabolism.

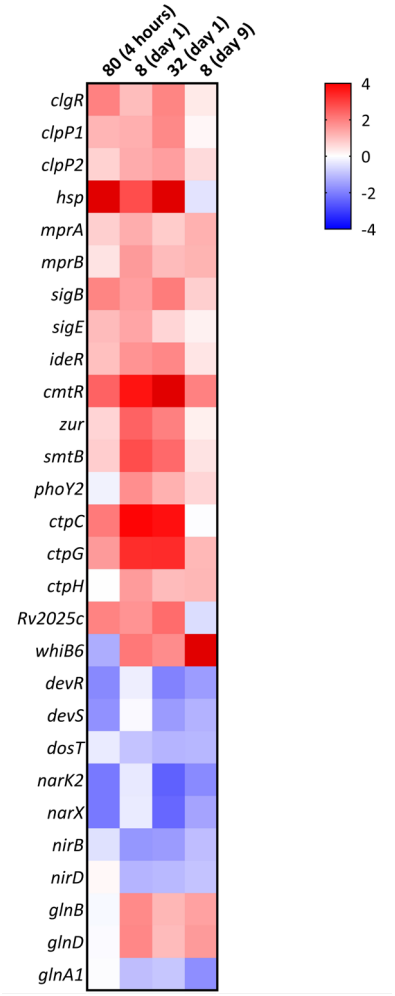

Figure 38. Changes in gene expression of diverse transcriptional regulators after C9 treatment. The concentration of C9 used in each condition is indicated in µg/mL. The colour scales represent log_2FC in gene expression.

Other relevant transcriptional changes

Bacteria that survived after 9 days of C9 treatment showed some specific changes in gene expression that are described below.

Several genes encoding the Mce1 complex (*e.g., mce1A*, *mce1D*, *fadD5*, *yrbE1A* and *yrbE1B*), which participates in fatty acids import, were downregulated in all conditions (**Figure 39**). While genes involved in cholesterol breakdown showed slight or no increase of expression at previous time points, a strong down-regulation of genes required for β-oxidation of the cholesterol side chain (*cyp125*, *fadD19*, *Rv3572* and *fadA5*) and degradation of rings A/B (*kshA*, *kshB*, *hsaA*, *hsaF* and *hsaG)*[137] was observed at day 9 (**Figure 39**). Fatty acids uptake and initiation of cholesterol side chain breakdown are ATP-dependent processes, and many enzymes require iron; since both ATP and iron are likely scarce after C9 treatment as shown by the transcriptional changes previously described, bacteria could inhibit these processes to survive C9 treatment.

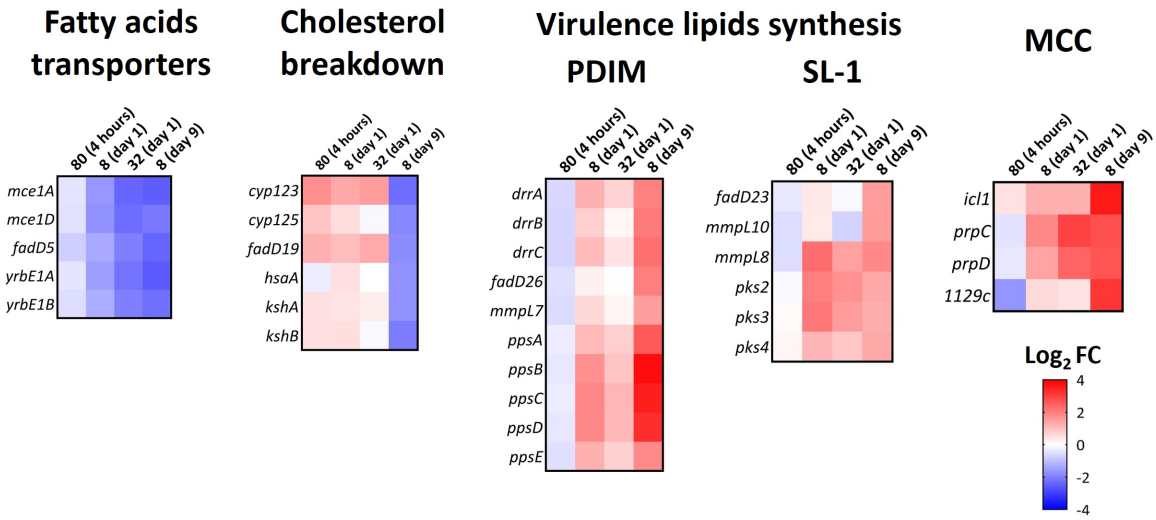

Figure 39. Changes in gene expression of genes encoding proteins involved in fatty acids transport, cholesterol breakdown, synthesis of virulence lipids and MCC, after C9 treatment. The concentration of C9 used in each condition is indicated in µg/mL. The colour scales represent log_2FC in gene expression. MCC, methylcitrate cycle; PDIM, phthiocerol dimycocerosates; SL-1, sulfolipid-1. The colour scales represent log_2FC in gene expression.

Genes implicated in the methylcitrate cycle (MCC), including *prpC*, *prpD*, *icl1* and the regulator *rv1129c*, were strongly overexpressed on day 9 in comparison to day 1 (**Figure 39**). The MCC plays a key role in metabolising the toxic cholesterol breakdown product propionyl-CoA, and *prpD* has been described to be positively regulated by propionyl-CoA accumulation [138,139]. Thus, *prpD* up-regulation after C9 treatment could reflect propionyl-CoA accumulation.

Interestingly, methyl-branched lipids biosynthesis was the most overrepresented pathway among upregulated genes on day 9 (**Figure 39**). We found a strong upregulation of genes required for the synthesis of both sulfolipid-1 (SL-1; *fadD23*, *mmpL8*, *mmpL10* and *pks2-4* genes) and phthiocerol dimycocerosates (PDIM; *drrA-C*, *fadD26*, *mmpL7* and *ppsA-E* genes). These *Mtb* lipids are synthesized from acetyl-CoA and propionyl-CoA, and have been described to act as an effective “sink” to limit propiony—CoA toxicity [137].

Considering that cholesterol degradation is the major source of propionyl-CoA, *Mtb* could down-regulate genes required for cholesterol metabolism to avoid propionyl-CoA accumulation and up-regulate genes involved in both MCC and methyl-branched lipids biosynthesis to eliminate propionyl-CoA toxic metabolites.

4. General discussion and future perspectives

With the increasing incidence of MDR and XDR *Mtb* strains, it has become increasingly important to identify new compounds highly active and with novel modes of action.

Whereas target-based approaches have the main advantage that they allow rational drug design since the MoA and the target are known, they have proven to be ineffective in the discovery of antimicrobials with novel MoA. Phenotypic screenings remain the unique strategy that has identified molecules with novel modes of action. Nevertheless, this approach does not provide any information on how such molecules inhibit bacterial growth. Hence, elucidation of the MoA is key for the development of new antimicrobials identified in phenotypic screenings in order to rationally develop the subsequent steps of the process.

In this study, different approaches were used to elucidate the MoA of a new chemical series found in a screening campaign performed to identify new molecules active against *Mtb*.

One of the standard steps in MoA studies is the isolation of spontaneous resistant mutants. However, attempts to isolate resistant mutants were unsuccessful, suggesting that this chemical series might not have a single specific genetic target and that the mutation frequency to the compounds is low, which is highly desirable for its eventual introduction into clinical practice but complicates target identification.

Then, the identification of mutants susceptible to C9 in the screening performed with the *M. bovis* BCG transposition library aided us to gain insights into the MoA of the compounds. Three mutants (M8, M17 and M18) had the transposon inserted in *mmpL4* gene, which codes for the transmembrane transport protein MmpL4 required for siderophore export. We observed that *mmpL4* inactivation conferred increased susceptibility to the compounds in *M. bovis* BCG and *Mtb*. Remarkably, this increased susceptibility of *Mtb mmpL4* mutants was higher under low iron conditions, suggesting that the MoA of this new chemical series could be related to iron metabolism and interconnected with the function of MmpL proteins.

Proof of this is that C9 treatment strongly increased the expression of genes involved in iron acquisition and transport (*mbt* genes, *irtA, irtB*…), whereas down-regulated genes needed for iron storage (*bfrA* and *bfrB*). These transcriptional changes resembled those reported under iron-limiting conditions [131], indicating that C9 could induce a state of iron-starvation by blocking *Mtb*'s capacity to acquire or utilize iron.

Another finding that further supported that the MoA of these compounds is linked to iron metabolism is the orange pigmentation of pellets of *Mtb* cultures after treatment with 8 µg/mL of C9 for 9 days. Mutants deficient in the iron-sensing transcription factor IdeR or in siderophore-acquisition proteins, such as IrtA and IrtB, develop a similar orange pigmentation in iron-replete medium [93,124,127]. It is reported that these mutants experience iron deprivation in iron-replete medium and respond by up-regulating siderophore biosynthesis, as we observed by RNA-seq analysis after C9 treatment. Accumulation of iron-bound siderophores on the surface of *Mtb* might be the cause of the orange pigmentation in these mutants [93,124,127]. Further experiments would be needed to disentangle whether the accumulation of iron-bound siderophores (extra- or intracellularly) explains the orange pigmentation observed after long exposure to C9 (*e.g.,* by thin layer chromatography and UPLC-MS analysis of lipids, or the chrome azurol S (CAS) assay) [140].

Moreover, identification of synergistic partners of a drug can also provide information on its possible MoA. In the synergy screening performed against *Mtb*, C9 acted synergistically with OxPhos inhibitors, including CFZ (NDH-2 inhibitor), BDQ (ATP synthase inhibitor) and SQ109 (a drug that collapse the PMF). Interestingly, this chemical series also displayed synergism with BDQ against *M. abscessus*. The finding that C9 reduced ATP levels after 24 h of treatment, as described for inhibitors of energy metabolism, along with the general notion that drugs interfering with OxPhos commonly synergize, led us to hypothesize that this new chemical series could be affecting energy metabolism.

The lack of synergism with Q203, a cytochrome bc_1:aa_3 inhibitor, prompted us to study whether C9 and Q203 could share the same target. We found that *M. ulcerans* strains from classical lineage, which rely exclusively on cytochrome bc_1:aa_3 to respire since they lack cytochrome bd, were more susceptible to Q203 but not to C9 than *M. ulcerans* strains belonging to ancestral lineage.

These results indicated that cytochrome bc_1:aa_3 was not the target of these compounds. Were C9 to be a cytochrome bc_1:aa_3 inhibitor, *cydA* and *cydB* genes (encoding the cytochrome bd) should be overexpressed after C9 treatment, as described for Q203 and phenoxyalkylbenzimidazoles [100,101]. By contrast, both *cydA* and *cydB* genes were down-regulated, supporting that cytochrome bc_1:aa_3 is not the target.

The upregulation of the *ndh* gene, while the vast majority of genes involved in OxPhos were downregulated, could reflect an *Mtb*'s compensatory mechanism to survive C9 treatment. During this work, an *Mtb* strain with the *ndh* gene disrupted has been constructed by BAC-recombineering. This mutant will be useful to further study the role of *ndh* in the *Mtb* response to C9 treatment.

It should be noted that C9 showed a characteristic delayed kill observed with other energy metabolism inhibitors (such as BDQ and CFZ) [141] and, importantly, the rate of killing increased when C9 was combined with BDQ or CFZ.

It has been described that compounds blocking OxPhos may indirectly interfere with drug efflux, since efflux pumps require sufficient ATP levels (*e.g.,* ABC efflux pumps) or PMF (*e.g.*, RND efflux pumps) for drug extrusion [75]. In this study, we observed that treatment of *M. smegmatis* with C9 enhanced the intracellular levels of EtBr, indicating that these compounds block efflux activity. Interestingly, similar results have been reported for several inhibitors of OxPhos (CPZ, TDZ and BDQ) [75].

Based on these data, two concomitant MoA could be proposed for this new chemical series (**Figure 40**):

(i) The study compounds might directly interfere with the electron flow in the respiratory chain, lowering PMF generation and ATP production. This reduction in PMF generation might indirectly affect the activity of RND transporters (MmpL5 and MmpL4), thus explaining the strong synergism observed between C9 and drugs extruded by MmpL5 (BDQ, CFZ and azoles). Therefore, C9 would favour the intracellular accumulation of drugs exported by MmpL5, enhancing their activity. Furthermore, a reduced activity of MmpL4 and MmpL5 transporters due to low PMF generation would lead to restriction of iron uptake, in line with the transcriptional changes previously described.

It should be mentioned that MmpL5 is the unique protein capable of exporting siderophores in *mmpL4* mutants. Thus, a *mmpL4* mutant might be worst equipped to uptake iron than the wild type strain in presence of C9, a drug that could be reducing the activity of these transporters.

(ii) The study compounds could directly interfere with MmpL4 and MmpL5 transport proteins, thus interfering with the *Mtb*'s capacity to acquire iron. This iron deprivation would have a drastic effect on the ETC due to the high number of Fe-S/heme proteins implicated in this pathway, in line with the transcriptional changes detected. Moreover, the inhibition of MmpL5 would explain the strong synergism observed between C9 and drugs extruded by MmpL5 (BDQ, CFZ and azoles).

Future experiments beyond this PhD thesis will be performed with the MmpL5 mutants constructed in this work to assess whether this new chemical series synergize with BDQ, CFZ and KET through inhibition of MmpL5/MmpS5 export system (*e.g.,* by checkerboard assays and time kill assays).

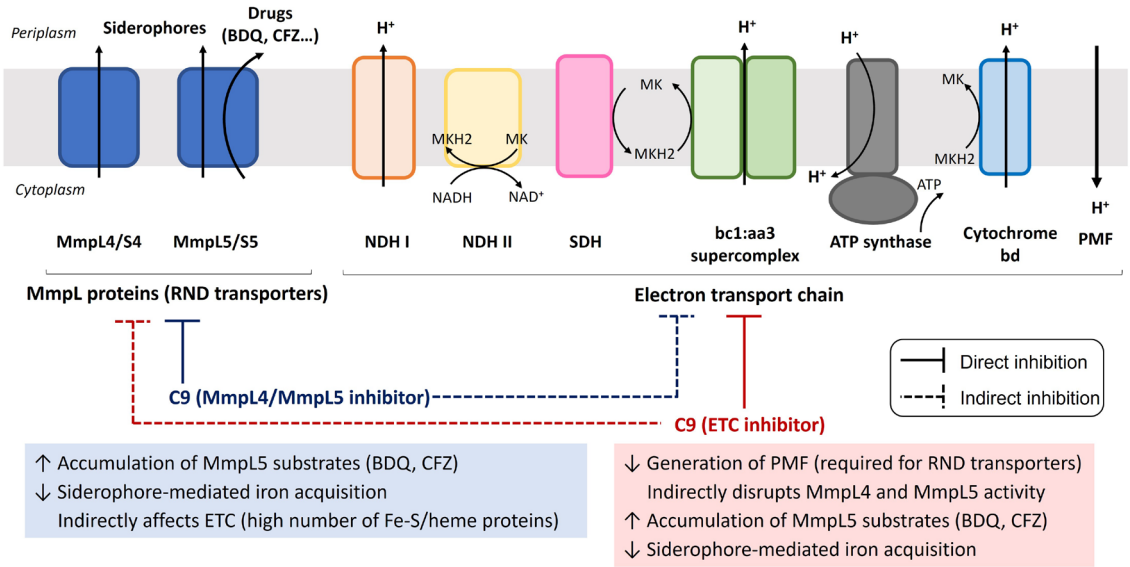

Figure 40. Proposed MoA of this new chemical series. Two concomitant MoA could be proposed for this new chemical series: i) the study compounds affect directly the ETC (C9 ETC inhibitor; red font, lines and box), reducing the generation of PMF, which indirectly affects the activity of RND transporters (MmpL5 and MmpL4) and thus the capacity of *Mtb* to acquire iron; ii) the study compounds block MmpL4 and/or MmpL5 (C9 MmpL4/MmpL5 inhibitor; blue font, lines and box), thus affecting *Mtb*'s capacity to acquire iron, and this iron deprivation has a drastic effect on the ETC due to the high number of Fe-S/heme proteins implicated in this pathway.

Taken together, this new chemical series induces a stress response, as observed with the strong up-regulation of transcriptional regulators required for antioxidant adaptation. Moreover, we found that *Mtb* INH-resistant bacteria due to mutations in *katG* and *M. smegmatis* mutants defective in *katG* were more susceptible to the compounds, raising the hypothesis that bacteria without a functional catalase peroxidase could be worst equipped to counteract the oxidative stress induced by the drugs.

Importantly, this new chemical series was active against *Mtb* in THP-1 cells, exceeding the drug's activity against extracellular *Mtb*. This effect has also been observed with other small-molecule inhibitors targeting the OxPhos pathway [142]. This increased potency of energy metabolism inhibitors against *Mtb* in intracellular conditions is likely due to the bacterial use of host-derived cholesterol and fatty acids instead of fermentable energy sources (such as glycerol or glucose). Therefore, bacteria cannot utilize the glycolytic pathway, and ATP production is restricted to OxPhos[75]. Based on these data, it would be interesting to evaluate whether the susceptibility of *Mtb* to this new chemical series increases in medium containing fatty acids and/or cholesterol in comparison to standard growth medium (with glycerol). Moreover, although these compounds were active against intracellular *Mtb*, the antimicrobial activity of this new chemical series should be confirmed using *in vivo* models of infection (*e.g.,* mouse model).

To sum up, the different approaches used in this study have aided to gain insights into the MoA of this new chemical series against *Mtb*, and to elucidate that efflux pumps are involved in the mechanism of resistance of Gram-negative bacteria to these compounds.

5. Conclusions

- This new chemical series is active against Gram-positive bacteria and mycobacteria, both in extracellular and intracellular conditions.

- RND efflux pumps are involved in the mechanism of resistance of Gram-negative bacteria to the compounds, being AcrB the major contributor to resistance in *E. coli.* In mutants lacking AcrB, mutations (indels or SNPs) in the gene encoding the transcriptional regulator H-NS resulted in the overexpression of other efflux pumps as a secondary mechanism of resistance.

- Attempts to isolate *Mtb* mutants resistant to these compounds were unsuccessful, suggesting that these compounds may have more than one target and that the frequency of mutation is low. This could be an important feature for future preclinical development.

- In iron-replete medium, L4KO was slightly more susceptible to C9 than *Mtb* wild type in MIC assays. The susceptibility of L4KO increased under iron-restricted conditions, suggesting that the MoA of these compounds is related to iron metabolism and interconnected with the function of MmpL proteins.

- C9 treatment increased the expression of genes involved in iron acquisition and transport (*mbt* genes, *irtA, irtB*), whereas down-regulated genes needed for iron storage (*bfrA* and *bfrB*), indicating that C9 could induce a state of iron-starvation by blocking *Mtb*'s capacity to acquire or utilize iron.

- These compounds enhanced the activity of the cornerstone TB drugs INH and RIF, and inhibitors of OxPhos, including BDQ, CFZ and azoles, indicating a potential role in combination therapy against *Mtb*. They also displayed synergism with BDQ against *M. abscessus*.

- C9 treatment reduced ATP levels and disrupted O_2 consumption at early time points, as well as downregulated most genes involved in OxPhos, indicating that these compounds might interfere with this pathway. Studies with *M. ulcerans* indicated that the cytochrome bc_1:aa_3 is not the target of these compounds.

- EtBr accumulation assays indicated that these compounds act as efflux inhibitors in *M. smegmatis*. These compounds might directly inhibit efflux pumps and/or indirectly affect the activity of efflux pumps through inhibition of OxPhos.

Conclusiones

- Los compuestos presentan actividad frente a diversas bacterias Gram-positivas y micobacterias, tanto en condiciones extracelulares como intracelulares.

- Las bombas de eflujo de la familia RND están implicadas en el mecanismo de resistencia de las bacterias Gram-negativas a los compuestos, siendo el transportador AcrB el principal responsable de la resistencia a estos compuestos en *E. coli*. Los mutantes de *E. coli* deficientes en AcrB y con mutaciones (polimorfismos de nucleótido único o inserciones/deleciones) en el gen que codifica para el regulador transcripcional H-NS, sobreexpresan otras bombas de eflujo como mecanismo de resistencia secundario.

- No se ha logrado seleccionar mutantes resistentes a los compuestos, lo que sugiere que estos compuestos podrían tener más de una diana. Se estima que la frecuencia de aparición de mutantes resistentes a los compuestos es baja, lo cual es una característica importante para su posible futuro desarrollo preclínico.

- Los ensayos de CIM realizados en medio repleto de hierro indican que el mutante L4KO es más susceptible al compuesto C9 que la cepa silvestre. La susceptibilidad del mutante L4KO al compuesto C9 aumenta en condiciones restrictivas de hierro, lo que sugiere que el mecanismo de acción molecular de esta nueva serie química está relacionado con el metabolismo del hierro e interconectado con la función de las proteínas MmpL.

- Tras el tratamiento de *Mtb* con el compuesto C9, aumenta la expresión de genes implicados en la adquisición y el transporte de hierro (genes *mbt*, *irtA*, *irtB*), mientras que disminuye la expresión genes necesarios para el almacenamiento de hierro (*bfrA* y *bfrB*), lo que indica que el compuesto C9 podría actuar bloqueando la capacidad de *Mtb* para adquirir o utilizar hierro.

- Los compuestos presentan un efecto sinérgico en combinación con INH y RIF (principales fármacos utilizados para el tratamiento de la TB) y con inhibidores de la fosforilación oxidativa (BDQ, CFZ y azoles). Además, muestran sinergia frente a *M. abscessus* en combinación con BDQ.

- El tratamiento con C9 causa una reducción en los niveles de ATP e interfiere con el consumo de O_2, además de disminuir la expresión de la mayoría de los genes involucrados en la fosforilación oxidativa, lo que indica que estos compuestos podrían interferir con esta vía. Los estudios realizados con *M. ulcerans* indican que el citocromo bc_1:aa_3 no es la diana de estos compuestos.

- Los ensayos de acumulación de bromuro de etidio indican que estos compuestos actúan como inhibidores de eflujo en *M. smegmatis*. Estos compuestos podrían inhibir directamente las bombas de eflujo y/o afectar indirectamente la actividad de las bombas de eflujo como consecuencia de la inhibición de la fosforilación oxidativa.

Chapter 2

Evaluation of the activity of butyrophenones and the role of the Tap efflux pump in mycobacteria

1. Introduction

1.1. Persistence and drug tolerance

The pathological hallmark of TB, the granuloma, limits drug penetration and provides several microenvironments in which bacteria reside in replicating and non-replicating conditions, with different drug susceptibilities [143]. While most cells are quickly eradicated by bactericidal antimicrobials during drug treatment, a small group of phenotypic variants (termed persisters) remain viable in the host with limited or no replication, and show drug tolerance, *i.e.,* they survive antimicrobial treatment without acquiring genetic mutations and maintain susceptibility unchanged [29,30]. When drug pressure is removed, persisters resume growth, leading to recurrent infections [29,30,144]. Hence, the length of current TB regimens is based largely on the need to eradicate this subpopulation of *Mtb* bacilli tolerant to anti-TB drugs, which may serve as reservoirs for TB reactivation and emergence of drug resistance [86].

The ability of *Mtb* to develop persistence is gathering attention as a potential factor contributing to the selection of drug resistance [145]. Thus, understanding the mechanisms underlying persister formation is critical to find new drugs that shorten TB treatment and prevent the emergence of DR-TB strains.

The characteristics of the persister bacilli have been linked to a lower activity of their ribosomes due to Toxin/Antitoxin (TA) systems and efflux pumps, among others [146]. Efflux pumps are energy-dependent membrane proteins capable of exporting a wide variety of compounds from the cytoplasm, including lipids, toxic metabolites, drugs, and virulence factors. Such a heterogeneous substrate profile allows bacterial efflux pumps to play diverse roles in bacterial physiology, drug resistance, and virulence [147]. In *Mtb*, the Tap efflux pump has been described to contribute to drug resistance and to modulate the growth of *M. bovis* BCG [55,148,149].

Importantly, up-regulation of efflux pumps in response to various cues, including antimicrobial treatment and macrophage infection, has been associated with drug tolerance in *Mtb*. For example, Adams *et al.* showed that *Mtb* becomes tolerant to RIF upon intracellular residence through the induction of the Tap efflux pump, since two *Mtb* strains with different transposon insertions in the *tap* gene lost RIF tolerance [150,151].

Moreover, this RIF tolerance induced after macrophage infection was reduced in the presence of VER (an EI) suggesting that efflux pumps could be involved in macrophage-induced drug tolerance [150,151].

1.2. *In vitro* models to study *Mtb* persistence and drug tolerance

Persisters are strongly associated with bacteria in slow- or non-replicating states. Hence, several *in vitro* assays that mimic microenvironments of TB infection have been developed to evaluate drug activity against non-replicating bacteria [86,145]. Models for non-replicating state include nutrient starvation, the Wayne model of hypoxia, lipid-rich environment, and low pH (pH 4.5-5.5) [86,143]. Another approach is the use of the conditionally replicating streptomycin-starved/dependent 18b (ss18b) *Mtb* strain, which only grow in the presence of streptomycin (STR) but enter into a non-replicating state when STR is removed from the medium [152]. Alternative approaches are based on culturing *Mtb* under intracellular conditions using different cell lines, such as THP-1 (human cell line) and J774 (murine cells), or primary cells, *e.g.*, Peripheral Blood Mononuclear Cells (PBMCs) [86].

However, these approaches do not consider that granulomas pose an additional hurdle in drug development, since drug activity depends on its ability to penetrate them and reach bacteria in both intracellular and extracellular niches. Therefore, over the last decade, several independent laboratories have described *in vitro* granuloma models which mimic the organization of human nascent granulomas and the immune environmental conditions leading *Mtb* to enter a dormant-like state [153–155]. Hence, these models constitute a valuable tool to study both the efficacy of drug candidates and the mechanisms underlying drug tolerance within the granuloma's environment.

1.3. Background: the antipsychotic butyrophenones are inhibitors of the Tap efflux pump in mycobacteria

New drugs targeting drug-tolerant bacterial populations and persisters are needed to achieve shorter anti-TB therapies [86]. Ideally, such anti-tolerance or anti-persistence drugs should be targeting those molecular mechanisms underlying tolerance and persistence, such as efflux pumps or TA systems. Drug repurposing -the process of finding new uses for existing drugs- is gaining traction as a strategic approach that can provide new molecules with lower costs and faster drug development timelines than *de novo* drug development (described in **Chapter 1**) [69].

In a previous study [156], a high throughput synergy screen (HTSS) of chemical libraries containing drugs with known pharmacological properties (including clinically approved drugs) was performed to identify compounds that enhanced the activity of spectinomycin (SPT) -an antibiotic that is not clinically effective in treating TB on its own and a substrate of the mycobacterial Tap efflux pump-. As a result, several butyrophenones were found to improve the activity of SPT against *M. smegmatis* and *Mtb*.

Butyrophenones are a chemical family of compounds used to treat several psychiatric disorders due to their high affinity for dopamine D2 receptors [157]. They have similar pharmacological effects to phenothiazines, a class of neuroleptics whose antimycobacterial activity have long been known [158,159]. By contrast, this was the first study to describe the antibacterial activity of butyrophenones [156]. Interestingly, this study showed that bromperidol (BPD), a representative butyrophenone drug, greatly improves the activity of diverse anti-TB drugs against *Mtb in vitro* and in a macrophage model [156].

Taking into account that BPD displayed a strong synergism with SPT, an antibiotic substrate of the mycobacterial Tap efflux pump, several assays were performed prior to this work to study whether this synergism could arise from BPD-mediated inhibition of Tap efflux activity. These studies revealed that all butyrophenones tested but melperone displayed strong synergism with two Tap substrates (STR and TET) against *M. smegmatis* strains overexpressing Tap. However, these combinations had no interaction against the wild type strain (**Appendix V-Figure AV.1 & Table AV.1**) (*Santiago Ramón-García & Jose A. Aínsa, unpublished*).

The interaction between BPD and SPT was further analysed against *Mtb* H37Rv wild type, a *tap* knockout mutant (KOTap) and its complemented derivative (KOTAPc) by checkerboard assays. As a result, the synergistic interaction observed between BPD and SPT against *Mtb* wild type (FICI=0.25) was eliminated in the KOTap mutant (FICI=0.75) but restored in the complemented strain, which displayed the same FICI as *Mtb* wild type (FICI=0.25) (**Appendix V-Figure AV.1 & Table AV.1**) (*Santiago Ramón-García & Jose A. Aínsa, unpublished*). Hence, these results indicated that the synergism between butyrophenones and Tap substrates is Tap efflux pump specific in mycobacteria.

Taken together, these studies indicated that butyrophenones inhibit Tap efflux activity in both *M. smegmatis* and *Mtb*, thus enhancing the activity of diverse Tap substrates.

2. Objectives

Taking into consideration the previous association of the Tap efflux pump with drug tolerance and the Tap inhibitory activity of the butyrophenones in mycobacteria, the main objective of Chapter 2 was to further study the role of Tap and the activity of two butyrophenones (BPD and DPR) in mycobacteria.

In order to achieve this general objective, several specific objectives were proposed:

- To characterize the antimicrobial activity of BPD and DPR against *Mtb* *in vitro* and *ex vivo*, and to evaluate their cytotoxicity against THP-1 cells and PBMCs.
- To evaluate the activity of BPD and DPR against dormant mycobacteria and their ability to reduce RIF tolerance in a 3D *in vitro* granuloma model.
- To study the role of Tap in dormancy in the *in vitro* granuloma model.
- To evaluate the transcriptional changes upon *tap* deletion in *Mtb* under exponential and stationary phase by RNA-seq, and to confirm the changes in gene expression by qRT-PCR.

3. Results and discussion

3.1. Antimicrobial activity of butyrophenones

We first evaluated the antimicrobial activity of two butyrophenones, BPD and DPR, against *Mtb* in extracellular and intracellular (THP-1 cell line) conditions, as well as their cytotoxicity against THP-1 cells (**Figure 41 & Table 29**). DPR, a butyrophenone analogue used to promote lactation and to treat nausea, was included in this work since it displays an improved safety profile over BPD due to its inability to cross the blood brain barrier [160–162]. BPD was included to confirm results previously published [156].

Both butyrophenones were active against *Mtb* inside THP-1 cells, displaying MIC values 4-8-fold lower than those obtained against *Mtb* in extracellular conditions (**Table 29**), as previously described for BPD [156]. Importantly, the SI was 16-32 for both compounds (**Figure 41**).

Table 29. Activity of BPD and DPR against *Mtb* in extracellular (Extra Activity) and intracellular conditions (Intra Activity), and their toxicity against THP-1 cells (Toxicity). SI (selectivity index) was calculated as the ratio of the toxic concentration (IC50) of the compound over its effective concentration (MIC50). MIC90 and MIC50 are the minimum drug concentrations inhibiting bacterial growth by 90% and 50%, respectively; IC50 is the minimum drug concentration inhibiting cell viability by 50%. Values are in µg/mL. BPD, bromperidol; DPR, domperidone; INH, isoniazid; RIF, rifampicin.

Compounds	Extra Activity	Intra Activity		Toxicity	SI
	MIC90	MIC90	MIC50	IC50	(IC50/MIC50)
BPD	32-64	16	2	32-64	16-32
DPR	64	8-16	1-2	16-32	16-32
INH	0.25	0.063	0.03	>1	>33.3
RIF	0.125	0.125	0.063	>1	>16

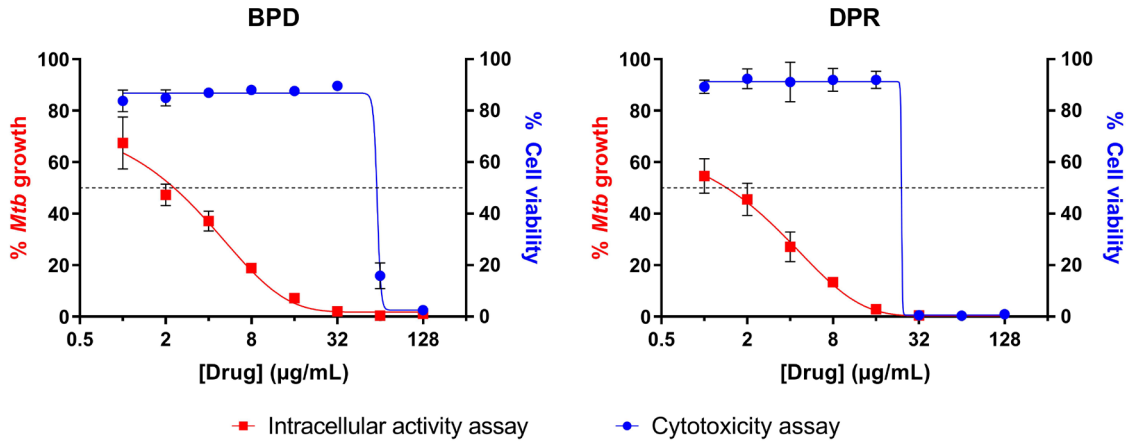

Figure 41. Dose response curves of BPD and DPR against intracellular *Mtb* H37Rv-Luc (red) and THP-1 cell line (blue). Dashed lines indicate MIC50 and IC50. Data represent mean ± SEM from 3 technical replicates.

Taken together, both butyrophenones displayed more activity *ex vivo* (*Mtb*-infected THP-1 cells) than *in vitro*.

3.2. Characterization of *Mtb* KOTap mutant

We further characterised the role of the Tap efflux pump in *Mtb* by different approaches due to its previous association with bacterial physiology, intrinsic drug resistance and drug tolerance [55,150].

3.2.1. Growth kinetics in liquid medium

Previous studies showed that *M. bovis* BCG KOTap cells had a progressive growth defect after cycles of sub-cultivation in liquid medium [55]. Thus, we aimed to evaluate whether the *Mtb*-derived KOTap mutant also arrests growth after three serial passages in 7H9-Tween-ADC medium.

In contrast to the results obtained with *M. bovis* BCG [55], the *Mtb* KOTap mutant did not display a progressive growth defect in comparison to the wild type strain (**Figure 42**), suggesting that the Tap efflux pump could have different roles in *Mtb* and *M. bovis* BCG.

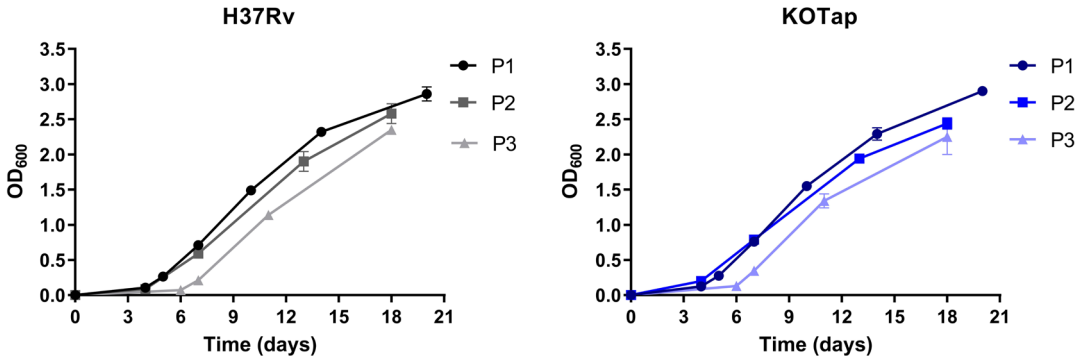

Figure 42. Growth kinetics of *Mtb* H37Rv and KOTap mutant. Frozen stocks of both strains were inoculated in 7H9-Tween-ADC to a cell density of 10^5 cells/mL. After 1 week, strains were sub-cultivated in fresh media. Bacteria were subcultured on a weekly basis, *i.e.,* the second subculture (P2) was inoculated from the first (P1), and the third subculture (P3) from the second (P2). Data represent mean ± SEM from duplicates.

3.2.2. Intracellular replication in THP-1 cell line

Since the *Mtb* Tap efflux pump has been described to be transcriptionally induced upon macrophage infection [134,163], we aimed to evaluate whether Tap disruption had an effect on the intracellular replication of *Mtb* in the THP-1 cell line.

We observed that the KOTap mutant displayed a compromised intracellular replication on day 4 post-infection in comparison to *Mtb* wild type (**Figure 43, Appendix VI-Table VI.1**). These results were in agreement with a previous study describing that *Mtb* CDC1551 transposon mutants of Tap display reduced viability after 96 h of THP-1 cells infection [150].

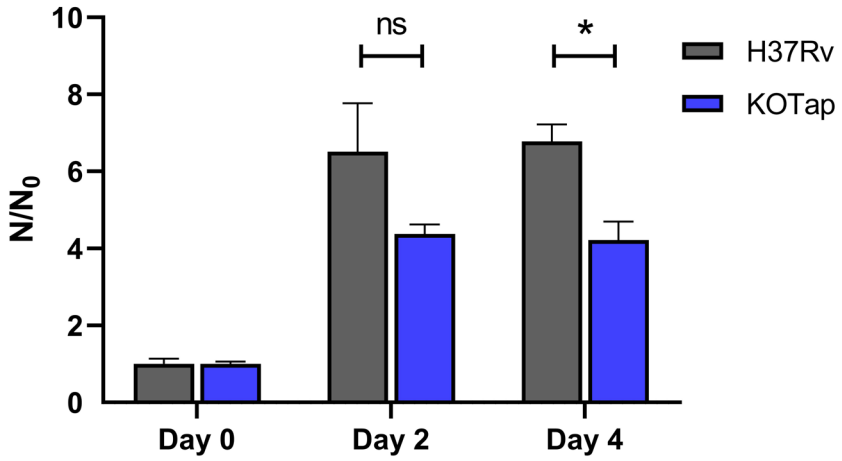

Figure 43. Replication rates of *Mtb* H37Rv and KOTap mutant in THP-1 cell line referred to 4 h post-infection. N: number of viable bacteria on day 0, 2 and 4 post-infection; N_0: number of viable bacteria after 4 h of infection. Data represent mean ± SEM from three independent wells. Statistical analysis was performed using two-way repeated measures ANOVA and Sidak's multiple comparisons test. ns, non-significant; *, $p<0.05$.

Hence, the Tap efflux pump not only confers drug resistance by extruding diverse drugs [55], but also plays a role in *Mtb* intracellular survival, thus representing a promising drug target for developing anti-persistence drugs.

3.3. Development of a 3D *in vitro* granuloma model

Human *in vitro* granuloma models mimic the environment encountered by the bacilli during human infection, thus constituting a key tool to study the role of diverse genetic factors in drug tolerance, and to test the efficacy of drug candidates against replicating and non-replicating mycobacteria [143,153].

Based on our previous results, we used the human 3D *in vitro* granuloma model developed by Arbués *et al.* [155] to evaluate the role of the mycobacterial efflux pump Tap in dormancy and to test the activity of BPD and DPR against dormant mycobacteria, since this model has been described to display features of *Mtb* associated with dormancy, such as the loss of acid-fastness, accumulation of lipid bodies and an increase in drug tolerance [155].

The in vitro granuloma studies included in this Chapter were performed in the research stay done at the SwissTPH (Basel, Switzerland) using M. bovis BCG Pasteur, a slow growing, non-pathogenic mycobacteria that can be handled in a BSL-2 laboratory and commonly used as a surrogate of the pathogenic Mtb. This in vitro granuloma model was then implemented at the University of Zaragoza to confirm in Mtb some results obtained with M. bovis BCG.

3.3.1. Study of Tap in the *in vitro* granuloma model

Mycobacterium bovis BCG

We first determined the optimal MOI to generate the *in vitro* granuloma model with *M. bovis* BCG. To do so, PBMCs from three independent donors were infected with *M. bovis* BCG at five different MOI (bacteria:PBMC), including 1:5, 1:10, 1:25, 1:50 and 1:100, and granuloma formation was monitored for 8 days. Uninfected PBMCs were included as a control for spontaneous aggregation [155].

PBMC infection with *M. bovis* BCG at MOIs of 1:25 and 1:50 induced the formation of granulomas, and no extracellular bacilli were detected (**Figure 44**). In contrast, PBMCs infected with *M. bovis* BCG at higher MOIs (1:5 and 1:10) were not able to contain the infection in the granulomas, and thus, extracellular bacterial growth was observed on day 8 post-infection (**Figure 44**).

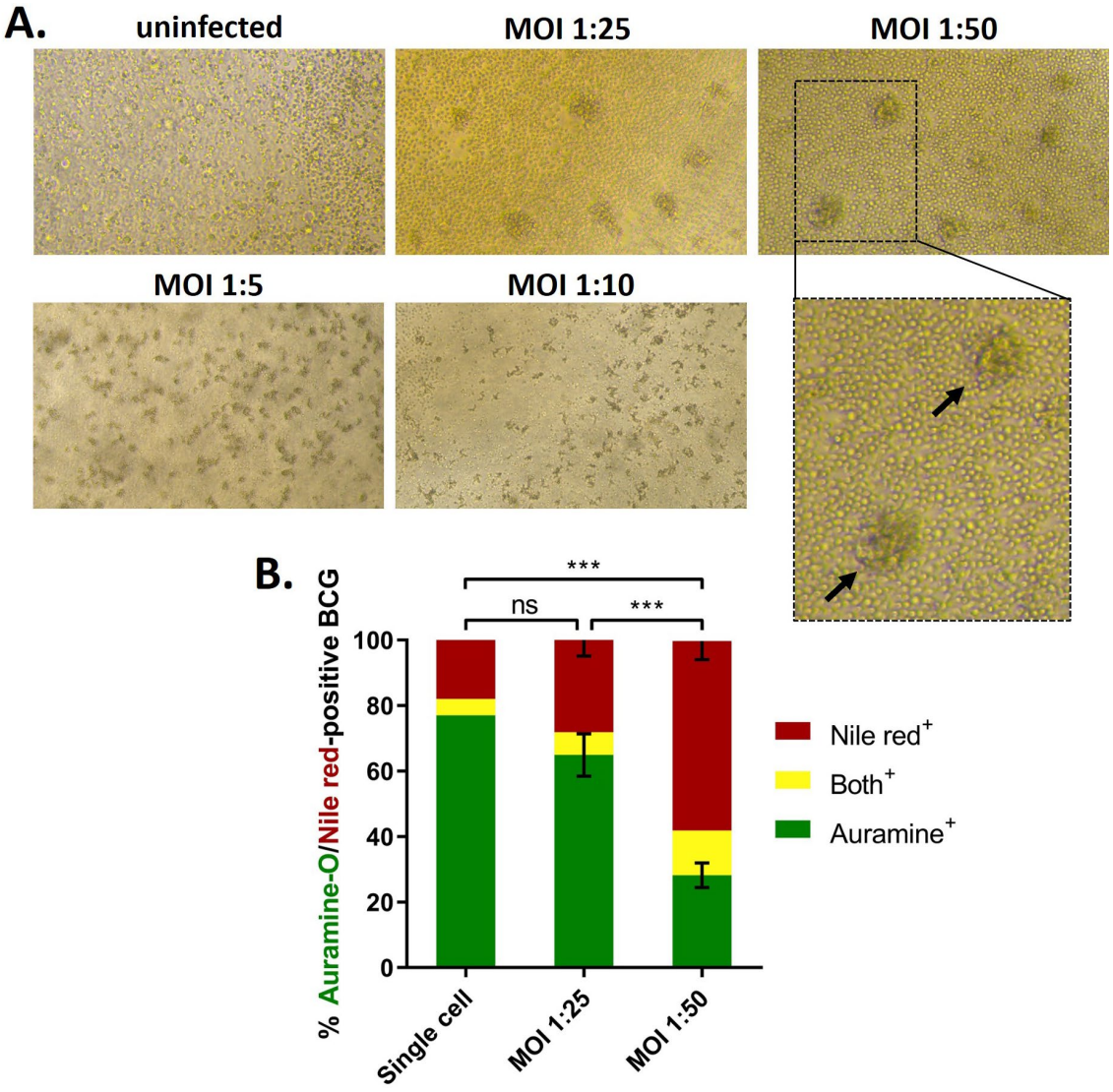

Figure 44. Human, *in vitro* granulomas upon infection with *M. bovis* BCG. A) Representative bright-field microscopy images of *in vitro* granulomas formed after 8 days of infection with *M. bovis* BCG at different MOIs (1:5, 1:10, 1:25 and 1:50) compared to uninfected PBMCs from a representative donor. Close-up of granulomas formed upon infection with *M. bovis* BCG at an MOI of 1:50 (granulomas indicated by arrows). B) Percentages of auramine-O- (green), Nile red- (red) and both stains-positive (yellow) bacteria quantified by fluorescence microscopy (mean ± SEM from three independent donors) after granuloma formation (8 days post-infection). An *M. bovis* BCG single cell suspension was included as an internal control. Statistical analysis was performed using two-way repeated measures ANOVA and Sidak's multiple comparisons test. ns, non-significant; ***, $p<0.001$.

To confirm that the *in vitro* granulomas observed at MOIs of 1:25 and 1:50 triggered a switch of mycobacterial metabolism into dormancy in *M. bovis* BCG, bacteria were recovered from the granulomas on day 8 post-infection and subjected to a dual auramine-O/Nile red staining to simultaneously evaluate bacterial acid-fastness (auramine-O) and lipid body accumulation (Nile red). This dual staining was used as a proxy of the metabolically-active (auramine-O positive) or dormant-like (Nile red positive) status of the recovered bacilli.

The *M. bovis* BCG single cell suspension used for PBMC infection, which came from an exponentially growing *M. bovis* BCG culture *(**Material and methods**),* was included as a control of metabolically active *M. bovis* BCG.

The proportion of lipid-rich (Nile red-positive) bacteria after 8 days post-PBMC infection increased compared to *M. bovis* BCG single cell suspension (**Figure 44B**). Importantly, while PBMC infection with *M. bovis* BCG at both MOIs 1:25 and 1:50 induced granuloma formation (**Figure 44A**), the proportion of Nile red-positive bacteria was higher at an MOI of 1:50 in comparison to an MOI of 1:25 (**Figure 44B**), indicating that PBMCs are more capable of controlling the infection at lower MOIs.

Based on these results, the experiments were performed infecting PBMCs with *M. bovis* BCG at an MOI of 1:50, since it induced granuloma formation and recovered bacilli exhibited dormancy characteristics, including accumulation of lipid inclusions and loss of acid-fastness, as reported previously by Arbués *et al.* [153] in *Mtb*.

Then, *M. bovis* BCG wild type and an *M. bovis* BCG-derived strain with the *tap* gene disrupted (KOTap) were used to study the role of the Tap efflux pump in dormancy in the *in vitro* granuloma model.

As shown in **Figure 45A,** the disruption of *tap* did not lead to differences in terms of granuloma formation in comparison to *M. bovis* BCG wild type. However, granulomas differed in number and size across donors (**Figure 45A**), as previously described with *Mtb* [153].

The replication rates of both strains were then assessed in the granuloma model. We observed that the *M. bovis* BCG KOTap mutant showed a lower replication rate than the wild type strain on day 8 post-infection (**Figure 45B, Appendix VI-Table VI.2**), in agreement with which was observed for the equivalent *Mtb* strains in the THP-1 cell line (**Figure 43**). However, in this set of experiments, differences in replication rates for the *M. bovis* BCG strains in the *in vitro* granulomas were not statistically significant in comparison with that observed for the *Mtb* strains when infecting THP-1 cells.

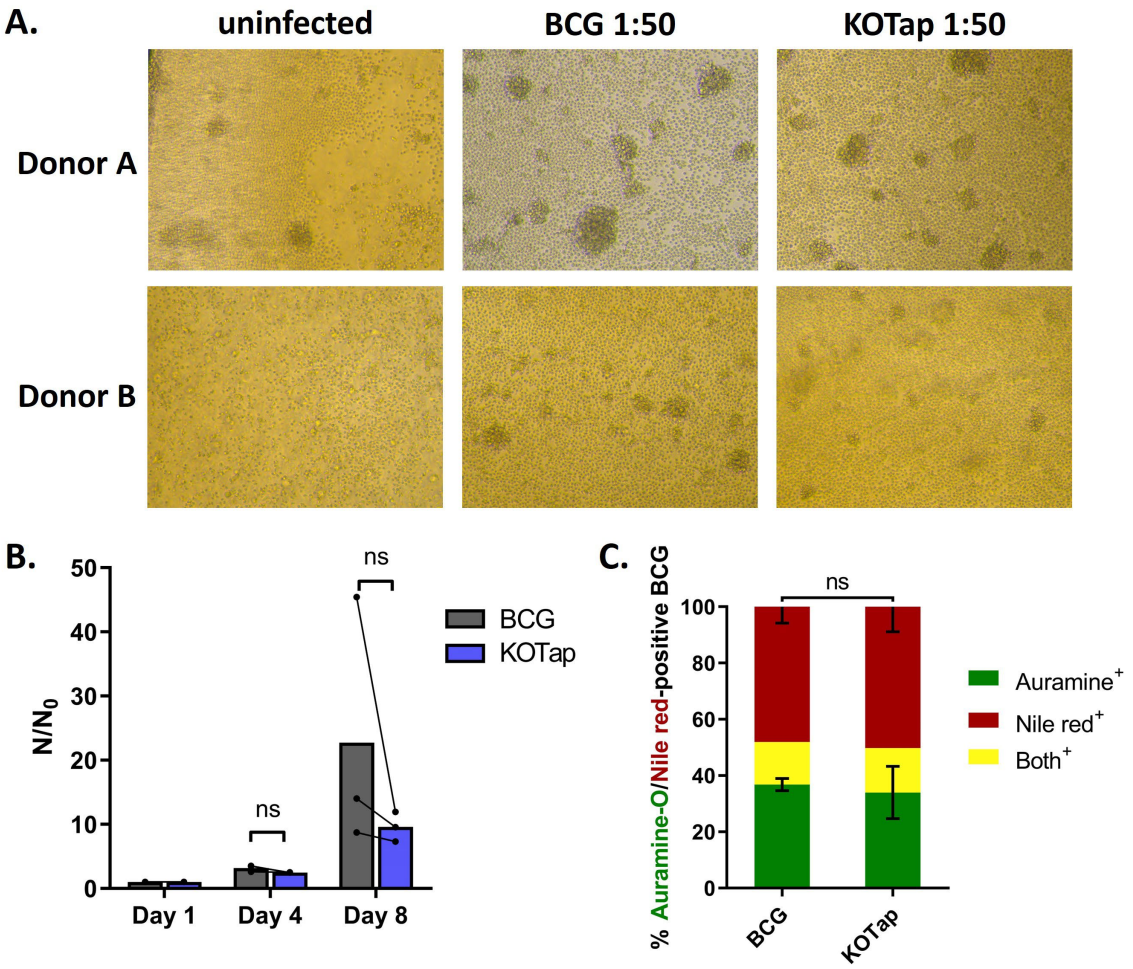

Figure 45. Human, *in vitro* granulomas upon infection with *M. bovis* BCG wild type and the KOTap mutant. A) Representative bright-field microscopy images of *in vitro* granulomas formed after 8 days of infection with *M. bovis* BCG wild type and KOTap mutant (MOI 1:50) compared to uninfected PBMCs from two independent donors (A and B). B) Replication rates of *M. bovis* BCG wild type and KOTap mutant referred to day 1 post-infection. Bars indicate mean values from 3 independent donors, circles represent the value for each individual donor and lines connect results from the same donor. N: number of viable bacteria on day 1, 4 and 8 post-infection; N_0: number of viable bacteria on day 1 post-infection. C) Percentages of auramine-O- (green), Nile red- (red) and both stains-positive (yellow) *M. bovis* BCG quantified by fluorescence microscopy (mean ± SEM from 2 independent donors) after granuloma formation (8 days post-infection). Statistical analysis was performed using two-way repeated measures ANOVA and Sidak's multiple comparisons test. ns, non-significant.

Afterwards, several features characteristic of *in vivo* dormancy were evaluated to study the capacity of Tap mutants to enter a dormant state, including bacterial acid-fastness, lipid body accumulation and RIF tolerance.

The formation of *in vitro* granulomas promoted a significant accumulation of bacteria harbouring a dormant-like phenotype (Nile Red-positive) on day 8 post-infection (**Figure 45C**). We observed that Tap disruption did not alter significantly the profile of dual staining in comparison to *M. bovis* BCG wild type on day 8 (**Figure 45C**), indicating that KOTap bacteria exhibit loss of acid-fastness and accumulate lipid bodies when they go into dormancy, as *M. bovis* BCG wild type.

As shown in **Figure 46**, the proportion of RIF-tolerant *M. bovis* BCG wild type bacteria increased 13.1-fold on day 8 in comparison to day 1, confirming that *M. bovis* BCG displays dormant-like characteristics in the granuloma model, as previously described with *Mtb* [17]. In contrast, the *M. bovis* BCG KOTap mutant only showed a 3.7-fold increase in the percentage of RIF-tolerant bacteria (**Appendix VI-Table VI.3**).

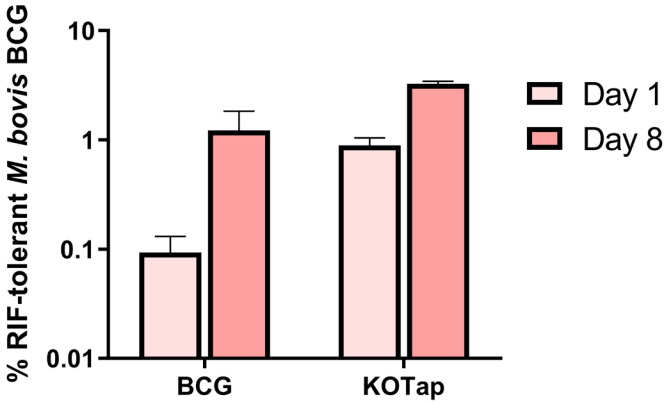

Strain	Day 8 / Day 1
BCG	13.1
KOTap	3.7

Figure 46. Percentage of RIF-tolerant *M. bovis* BCG bacteria. On days 1 and 8 post-infection, infected PBMCs were left untreated or treated with RIF at 0.1 µg/mL and incubated for 3 days prior to retrieval of mycobacteria for CFU assessment. Data represent mean ± SEM from three technical replicates of a single donor. The percentage of RIF-tolerant bacteria was calculated by using the formula: % RIF-tolerant bacteria = CFU (RIF-treated) / CFU (untreated) x 100. Day 8 / Day 1 was calculated by dividing the % RIF-tolerant bacteria on day 8 *vs* day 1.

It should be noted that in this experiment performed with a single donor, the proportion of RIF-tolerant bacteria on day 1 post-infection was higher in the KOTap mutant than in the *M. bovis* wild type strain (**Figure 46**). Further experiments should be performed with more donors to confirm these results.

Mycobacterium tuberculosis

This *in vitro* granuloma model was then developed using *Mtb* H37Rv and the *Mtb*-derived KOTap mutant in order to confirm in *Mtb* the results obtained with *M. bovis* BCG related to replication rates and induction of RIF tolerance.

First, the optimal MOI to generate the *in vitro* granuloma model with *Mtb* was determined by infecting PBMCs from two independent donors with *Mtb* H37Rv at five different MOI (bacteria:PBMC), including 1:50, 1:100, 1:200, 1:400 and 1:600, and granuloma formation was monitored for 8 days as described above for *M. bovis* BCG.

PBMCs infected with *Mtb* H37Rv at the highest MOIs tested (1:50 and 1:100) were not able to contain the infection in the granulomas, and hence, extracellular bacilli were observed on day 8 post-infection. In contrast, PBMC infection with *Mtb* H37Rv at an MOI of 1:200 induced the formation of granulomas, and no extracellular bacterial growth was detected. Based on these results and taking into consideration the MOI used by Arbués *et al.* for generating the *in vitro* granuloma model with *Mtb* [153,155], the experiments were performed infecting PBMCs with *Mtb* at an MOI of 1:200.

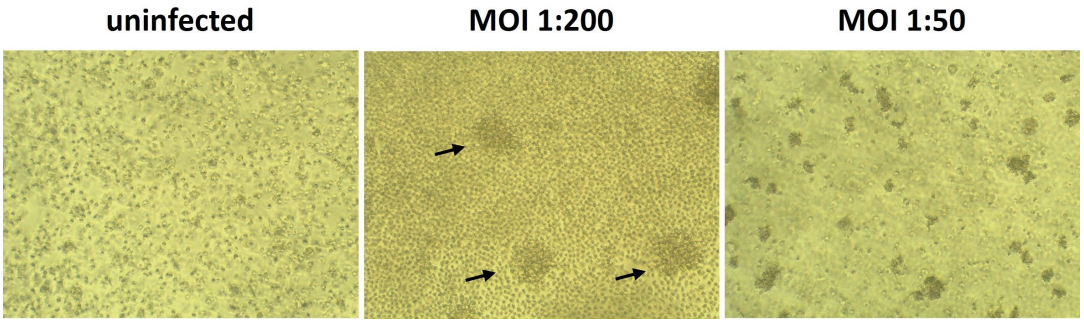

Figure 47. Human, *in vitro* granulomas upon infection with *Mtb* H37Rv. Representative bright-field microscopy images of *in vitro* granulomas formed after 8 days of infection with *Mtb* H37Rv at different MOIs (1:50 and 1:200) compared to uninfected PBMCs from a representative donor. Some representative granulomas are indicated by arrows.

As shown in **Figure 48**, no differences were detected in terms of granuloma formation after PBMC infection with *Mtb* wild type and KOTap, in line with the results obtained using *M. bovis* BCG (**Figure 45A**).

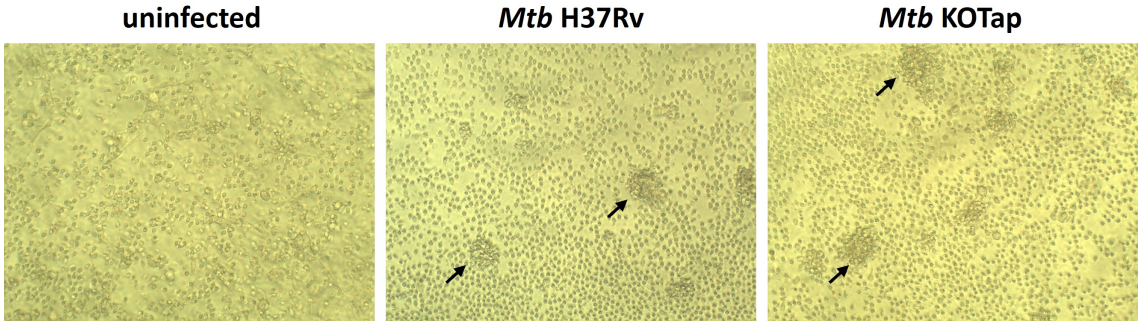

Figure 48. *In vitro* granuloma model with *Mtb.* Representative bright-field microscopy images of *in vitro* granulomas formed after 8 days of infection with *Mtb* H37Rv and KOTap (MOI 1:200) compared to uninfected PBMCs from a representative donor. Some representative granulomas are indicated by arrows.

Moreover, we observed that the *Mtb* KOTap mutant showed a slight lower replication rate than *Mtb* wild type which seemed to be more evident at latter time points (**Figure 49**, **Appendix VI-Table VI.4**), as previously observed with the equivalent *M. bovis* BCG strains in the granuloma model (**Figure 45B**) and with *Mtb* in the THP-1 cell line (**Figure 43**). However, in this set of experiments, differences in replication rates for *M. bovis* BCG and *Mtb* strains in the *in vitro* granulomas were not statistically significant in comparison with the results obtained with the *Mtb* strains when infecting THP-1 cells.

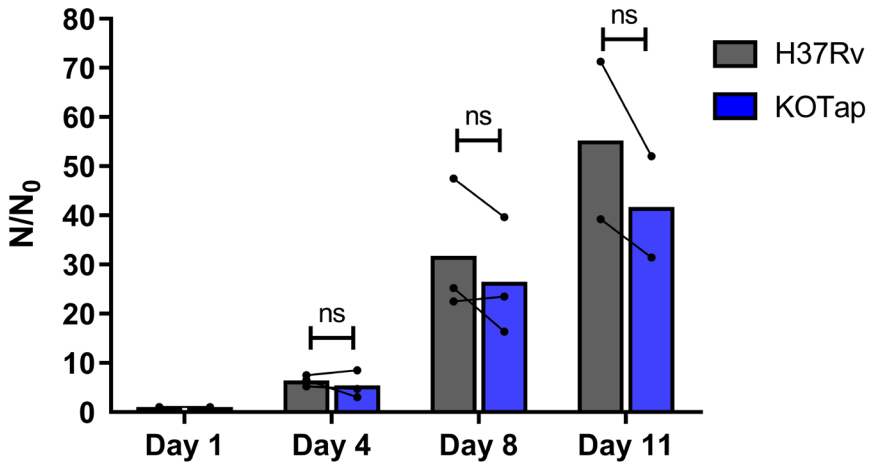

Figure 49. Replication rates of *Mtb* H37Rv and KOTap referred to day 1 post-infection. Bars indicate mean values of 3 independent donors (except for day 11), circles represent the value for each individual donor and lines connect results from the same donor. N: number of viable bacteria on day 1, 4, 8 and 11 post-infection; N_0: number of viable bacteria on day 1 post-infection. Statistical analysis was performed using two-way repeated measures ANOVA and Sidak's multiple comparisons test. ns, non-significant.

In line with data previously published[153], *Mtb* dormancy induced by the *in vitro* granuloma model led to a 3.5-fold increase in the percentage of RIF-tolerant bacilli (**Figure 50**). By contrast, the KOTap mutant had a lower increase (2.5-fold) in the proportion of RIF-tolerant bacteria, in accordance with the results obtained with *M. bovis* BCG (**Figure 46**).

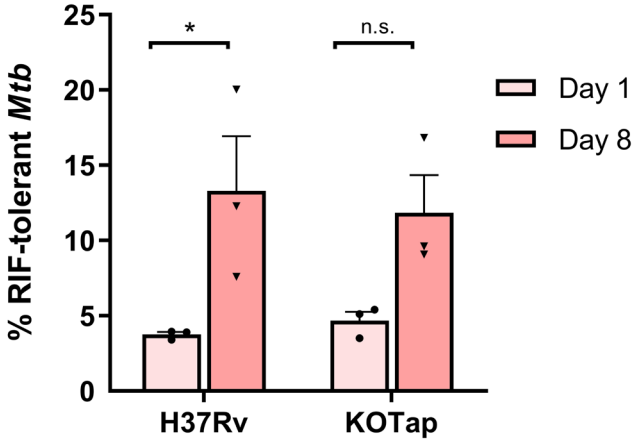

Strain	Day 8 / Day 1
H37Rv	3.5
KOTap	2.5

Figure 50. Percentage of RIF-tolerant *Mtb*. On days 1 and 8 post-infection, infected PBMCs were left untreated or treated with RIF at 1 µg/mL and incubated for 3 days prior to retrieval of mycobacteria for CFU assessment. Bars represent mean ± SEM from three independent donors. Circles and triangles represent the value for each individual donor. The percentage of RIF-tolerant bacteria was calculated as described in Figure 46. Statistical analysis was performed using two-way repeated measures ANOVA and Sidak's multiple comparisons test. ns, non-significant; *, $p<0.05$.

Taken together, we found that *M. bovis* BCG- and *Mtb*-derived KOTap mutants developed RIF-tolerant bacteria (day 8 *vs* day 1) at a lower rate than their respective parental strains in the granuloma model (**Figure 46 & Figure 50**). Further experiments will be performed with the *Mtb* KOTap complemented strain or an *Mtb*-derived strain overexpressing *tap* to fully confirm that this reduction in the proportion of RIF-tolerant bacteria (day 8 *vs* day 1) is due to Tap disruption.

3.3.2. Activity of BPD and DPR in the *in vitro* granuloma model using *M. bovis* BCG

The *in vitro* granuloma model was used to evaluate whether BPD and DPR were able to penetrate into the granuloma and display activity against dormant bacteria, and to assess their ability to reduce the proportion of RIF-tolerant bacteria within this model.

First, we evaluated the potential cytotoxicity of BPD and DPR on PBMC when treated for three days, the same exposure time used in the *in vitro* granuloma model. Cytotoxicity was estimated by quantification of the lactate dehydrogenase (LDH) released, a cytosolic enzyme that is released into the extracellular space upon damage to the cellular membrane.

As shown in **Figure 50**, >70% cell viability was observed at concentrations of DPR ≤16 µg/mL, which is considered noncytotoxic according to standard international protocols [164]. In contrast, in this set of experiments performed with PBMCs coming from three different donors, BPD at 16 µg/mL was slightly more cytotoxic than DPR at 16 µg/mL since the mean value of cell viability was 67%. RIF at 0.1 µg/mL did not show any cytotoxic effect on PBMCs.

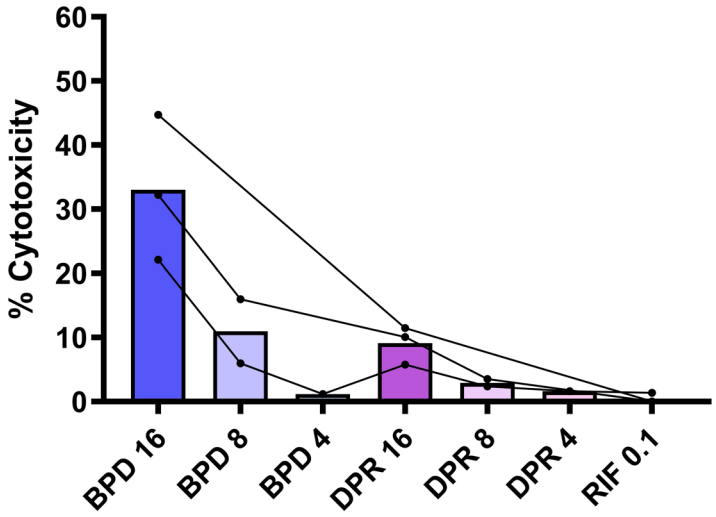

Figure 51. Cytotoxicity of BPD, DPR and RIF on PBMC**.** PBMCs were treated for 3 days with different concentrations of BPD, DPR or RIF. Cytotoxicity was estimated by LDH release quantification. Bars indicate mean values of 2 or 3 independent donors, circles represent the value for each individual donor and lines connect results from the same donor. RIF was included as an internal control. Concentrations are indicated in µg/mL.

Both BPD and DPR were then tested at 16 µg/mL alone or in combination with RIF at 0.01 µg/mL on day 8 post-infection, when the bacilli show characteristics of dormant bacteria in the granuloma model. Importantly, both butyrophenones at 16 µg/mL reduced bacterial viability (**Figure 51**), indicating that the study compounds are capable of penetrating into the granulomas and kill *M. bovis* BCG in a dormant state. Although these compounds did not reduce the proportion of RIF-tolerant bacteria (10.6%) under the conditions tested, the activity of both butyrophenones improved when assayed in combination with RIF.

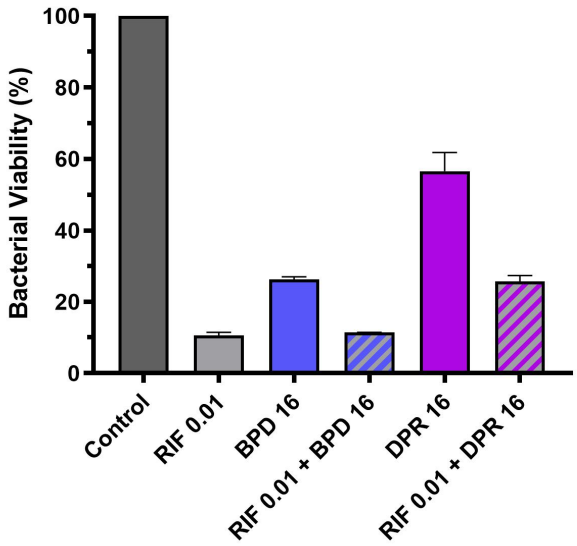

Figure 52. Effect of BPD, DPR and RIF on bacterial viability in the granuloma model. On day 8 post-infection, PBMCs infected with *M. bovis* BCG were left untreated or treated with the drugs and incubated for 3 days prior to retrieval of mycobacteria for CFU determination. Data represent mean ± SEM from two independent biological replicates and one donor. Bacterial viability was calculated by dividing the bacteria that survived drug treatment by bacteria from untreated control. Concentrations are indicated in µg/mL.

Taken together, the results obtained in the granuloma model indicate that butyrophenones are active not only against *Mtb in vitro* and *ex vivo*, but also against dormant bacteria located inside granulomas, thus suggesting that these compounds are able to disrupt and penetrate granulomas to exert their antimicrobial activity. Further experiments will be needed to better study whether butyrophenones are able to reduce the proportion of RIF-tolerant bacteria in this granuloma model, *e.g.,* by testing the activity of butyrophenones in combination with RIF at concentrations that have little antimicrobial effect (>80% bacterial viability).

3.3.3. Gene expression analysis

It has been described that *Mtb* cells in this *in vitro* granuloma model exhibit gene expression profiles characteristic of dormant bacteria, which lead to a slowdown of metabolic activity and an increase of drug tolerance [153,154].

To study whether efflux pumps could contribute to the drug tolerance induced in dormant bacteria, we measured the gene expression of *tap*, as well as *mmpL4* and *mmpL5* (two transmembrane proteins whose implication in iron acquisition and drug resistance has been described in **Chapter 1**) on day 4 and 8 post-infection. We also included *icl1* and *ctaD* genes as internal controls of the dormant state of the bacilli on day 8, since their gene expression profiles have been deeply characterised in dormant *Mtb* [153,154]. The *icl1* gene codifies for the isocitrate lyase, an important enzyme for dormant *Mtb* due to its involvement in both glyoxylate and methylcitrate cycles, which are required for the utilization of fatty acids as a carbon source inside granulomas. In contrast, genes linked to aerobic respiration, such as the *ctaD* gene encoding the cytochrome c oxidase polypeptide I, have been described to be downregulated in lipid-rich persister-like bacilli found in clinical tuberculous sputum [165].

Mycobacterium bovis BCG

We first measured the gene expression profiles of *M. bovis* BCG. The upregulation of *icl1* and downregulation of *ctaD* on day 8 post-infection (**Figure 53B**) was in line with results previously published in dormant *Mtb* [153,154], further supporting the enter of *M. bovis* BCG cells into a dormancy state in the *in vitro* granuloma model.

While *mmpL5* was up-regulated on day 8 post-infection, both *tap* and *mmpL4* genes were slightly down-regulated (**Figure 53A**). Interestingly, all of them were up-regulated on day 4 post-infection. Nonetheless, it must be considered that the expression of *tap* and *mmpL4* genes was measured from *M. bovis* BCG bacteria in granulomas from a unique donor on day 4 post-infection due to the low number of bacteria recovered at that time point from the two other donors and thus poor RNA yield.

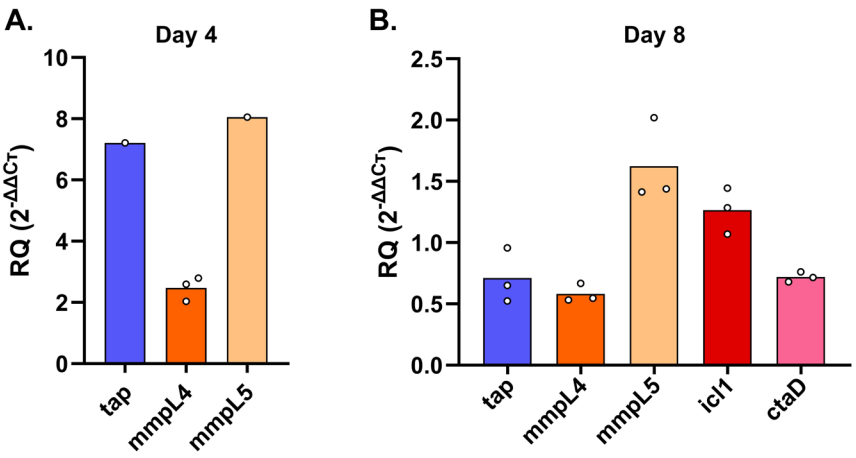

Figure 53. Relative quantification of gene expression of *M. bovis* BCG from *in vitro* granulomas on (A) day 4 and (B) day 8 post-infection, determined by qRT-PCR. Bars picture the mean values obtained from 3 independent donors (except for *tap* and *mmpL4* on day 4 post-infection), circles represent the value for each individual donor. Results are expressed as fold change relative to an aerobically-grown, mid-log *M. bovis* BCG culture, using *sigA* as the endogenous control.

Hence, the results obtained pointed to a higher expression of *tap*, *mmpL4* and *mmpL5* genes on day 4 in comparison to day 8 post-infection, suggesting that these proteins associated with drug resistance and iron acquisition could be more relevant before induction of bacterial dormancy and drug tolerance.

Mycobacterium tuberculosis

Then, we aimed to confirm the gene expression profile of *tap* in *Mtb* H37Rv on day 4 and 8 post-infection, including *icl1* as an internal control of *Mtb* dormancy on day 8. As a result, we observed that *tap* was up-regulated at both time points, being this expression higher on day 4 post-infection (**Figure 54**). Importantly, *icl1* was up-regulated on day 8 post-infection, providing evidence for the dormant state of *Mtb* (**Figure 54**).

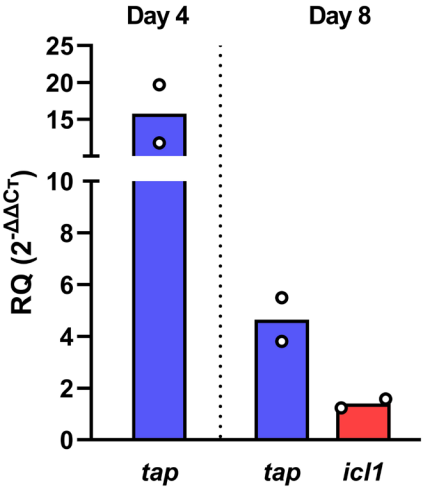

Figure 54. Relative quantification of gene expression of *Mtb* H37Rv from *in vitro* granulomas on day 4 and 8 post-infection, determined by qRT-PCR. Bars picture the mean values obtained from 2 independent donors (circles represent the value for each individual donor). Results are expressed as fold change relative to an aerobically-grown, mid-log *Mtb* H37Rv culture, using *sigA* as the endogenous control.

The higher expression of *tap* on day 4 in comparison to day 8 agrees with the results obtained in *M. bovis* BCG (**Figure 53**) and suggests that the Tap efflux pump could have a more important role before *Mtb* displays features characteristic of dormant bacteria.

3.4. Evaluation of the role of Tap by RNA-seq

In order to gain more insights into the molecular role of the Tap efflux pump in *Mtb,* we performed RNA-seq studies using *Mtb* wild type and the KOTap mutant under exponential (replicative) and stationary (non-replicative) phase. The latter was used as a model for the persistent state of *Mtb*, since it has been described that cultures in stationary phase display characteristics of persistent *Mtb*, such as reduced metabolic activity and phenotypic tolerance [86,143].

RNA-seq was performed from triplicate RNA extractions of each strain under exponential and stationary phase. For RNA-seq data analysis, DEGs with statistical significance were selected using a p-adj ≤ 0.05 and log_2FC values ≥ 1 (for up-regulated genes) or ≤ -1 (for down-regulated genes). Using these parameters, a total of 104 genes were differentially expressed in KOTap in comparison to *Mtb* wild type during exponential growth (6 days; OD_{600nm} = 0.2-0.3) (**Table 30**). Among these genes, 70 were up-regulated and 34 down-regulated. In contrast, only 10 DEGs were detected in stationary phase (6 weeks; OD_{600nm}=2.5-3), 9 of them down-regulated and 1 gene up-regulated (**Table 30**). The number of down-regulated genes under stationary phase increased from 9 to 39 when a less strict cut-off (log_2FC ≤ -0.6 and p-adj ≤ 0.05) was used for data analysis, while only one gene was up-regulated.

Table 30. Number of DEGs in KOTap compared to the wild type strain, using a p-adj ≤ 0.05 and log_2FC values ≥ 1 for up-regulated genes, and log_2FC ≤ -1 for down-regulated genes.

Growth phase	Number of differentially expressed genes	
	Up-regulated	Down-regulated
Exponential	70	34
Stationary	1	9

The PCA plots indicated that KOTap samples clearly separated from H37Rv samples in exponential phase (76.6% of variance) (**Figure 55A**). In contrast, *tap* disruption was only responsible for 43.3% of variance in stationary phase and some triplicates did not cluster together (**Figure 55B**).

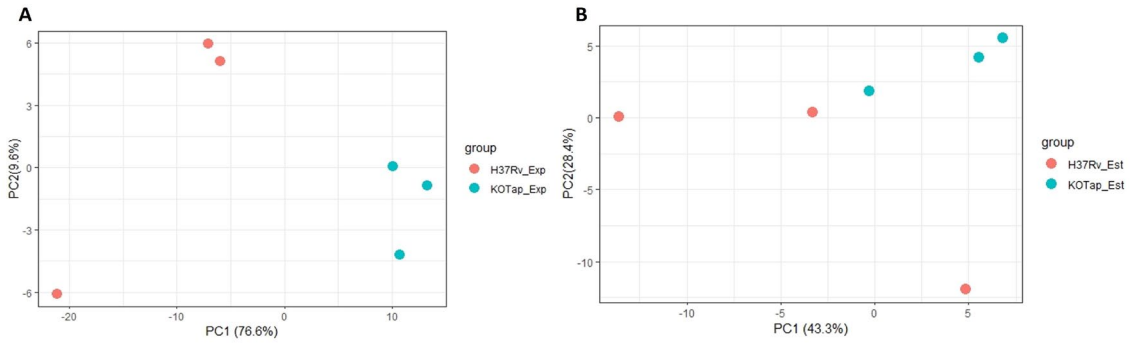

Figure 55. PCA plot showing association between samples analysed in exponential (A) and stationary (B) phase. Triplicates are indicated in red for H37Rv and green for KOTap.

The higher number of genes differentially expressed in exponential phase in comparison to stationary phase (104 *vs* 10) and the distribution of the samples in the PCA plot suggested that Tap could be more relevant for actively replicating *Mtb* than for non-replicating bacteria. Hence, we focused our analysis on the transcriptional changes detected in exponential phase.

A functional category analysis was performed with DEGs in exponential phase, using the functional categories described in Mycobrowser (https://mycobrowser.epfl.ch). Taking into account the functional category size, *i.e.*, the total number of genes included in each category over the total number of genes in *Mtb* genome (indicated in grey in **Figure 56**), we observed an overrepresentation of up-regulated and down-regulated genes belonging to lipid metabolism, and virulence, detoxification and adaptation categories. This analysis also revealed a significant down-regulation of genes belonging to PE/PPE category in the KOTap mutant.

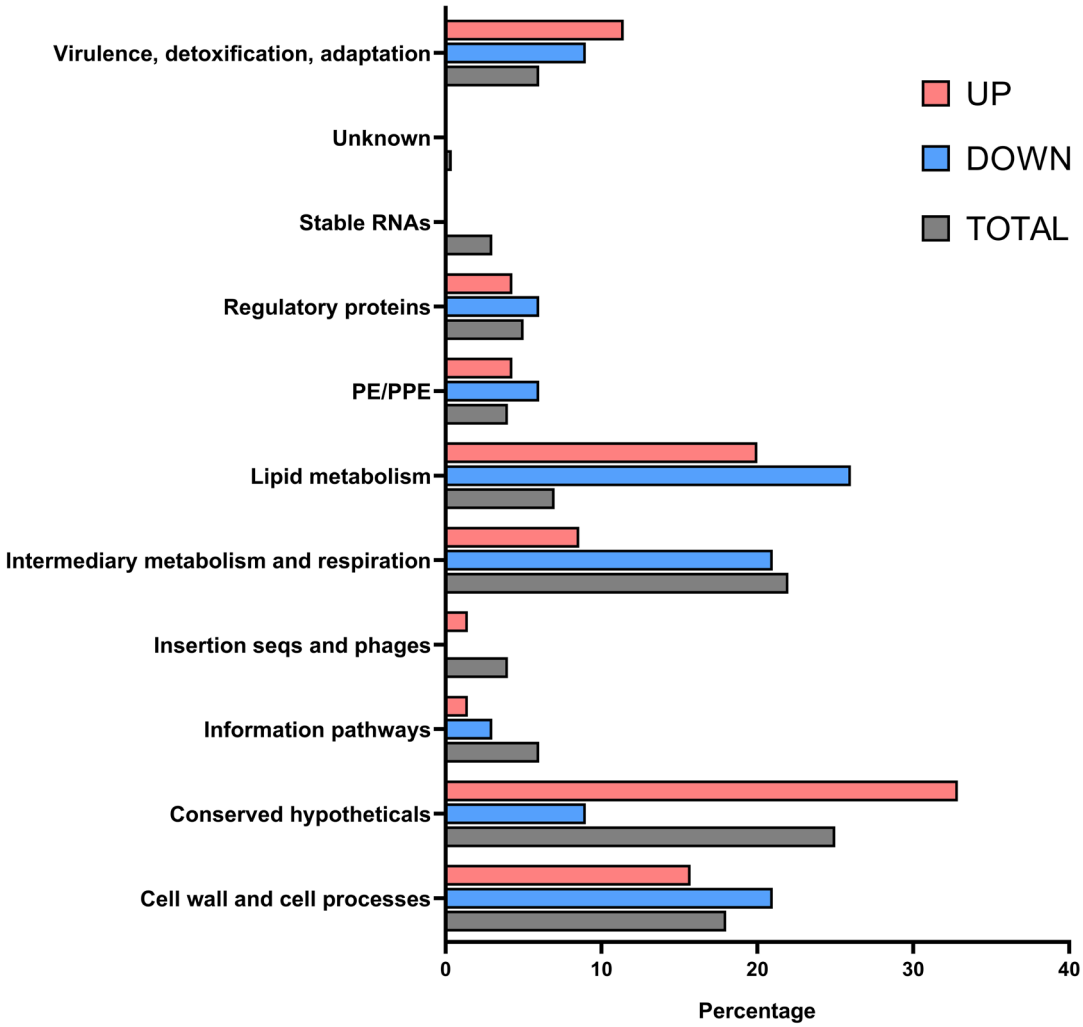

Figure 56. Functional category analysis of DEGs (p-adj ≤ 0.05 and log_2 FC values ≥ 1 or ≤ -1) in KOTap mutant compared to *Mtb* wild type in exponential phase. The percentage of genes up-regulated (UP, red) or down-regulated (DOWN, blue) in each category over the total number of genes up-regulated (70) or down-regulated (34), respectively, is shown. The percentage of total number of genes belonging to each functional category according to Mycobrowser over the total number of genes in the genome of *Mtb* (4187) is depicted in grey (TOTAL).

The analysis of DEGs in the KOTap mutant under exponential phase provided some interesting findings that are discussed in detail below.

Genes upregulated in exponential phase upon *tap* disruption

The most upregulated gene in exponential phase upon *tap* disruption was *rv1954A*, which encodes a protein of unknown function and forms an operon with *higB, higA* and *rv1957* [166]. All these three genes were also upregulated in the KOTap mutant, although to a lesser extent than *rv1954A* (log_2FC between 0.5 and 0.7) (**Figure 57A**).

The genes *higB* and *higA* code for the HigB toxin and HigA antitoxin, respectively. TA systems are stress-responsive elements generally composed of a stable toxin that forms an inactive complex with its cognate antitoxin. In response to specific stress conditions, the antitoxin is degraded by specific proteases and the free active toxin targets important cellular processes (*e.g.,* DNA replication or protein synthesis) [166,167].

Since the HigA antitoxin represses *rv1954A* expression [166], the strong upregulation of *rv1954A* in the KOTap mutant suggests that the HigA antitoxin does not repress *rv1954A* in the absence of Tap. Based on these results, it could be speculated that *tap* disruption triggers a stress response leading to degradation of HigA antitoxin which, in turn, might result in the de-repression of *rv1954A* transcription, thus establishing a link between Tap and TA systems, which have been associated with mycobacterial persistence and drug tolerance [166,167].

Most of the up-regulated genes from the lipid metabolism category were related to iron acquisition pathways. We found a strong upregulation of IdeR-regulated genes in the KOTap mutant, including *mbtA-N*, *ppe37*, *irtA/irtB, hisE, rv1519* and *rv3402c* (**Figure 57B**). These genes have been described to be upregulated under iron-limiting conditions due to their role in iron acquisition [93]. Interestingly, previous studies have also associated the HigBA TA system described above with regulation of iron and zinc homeostasis not only in mycobacteria, but also in other bacteria, such as *Acinetobacter baumannii* [166,168] .

Therefore, the up-regulation of genes involved in iron acquisition suggests that *tap* disruption could directly restrict iron availability or might have a downstream regulatory consequence leading to reduced intracellular levels of iron.

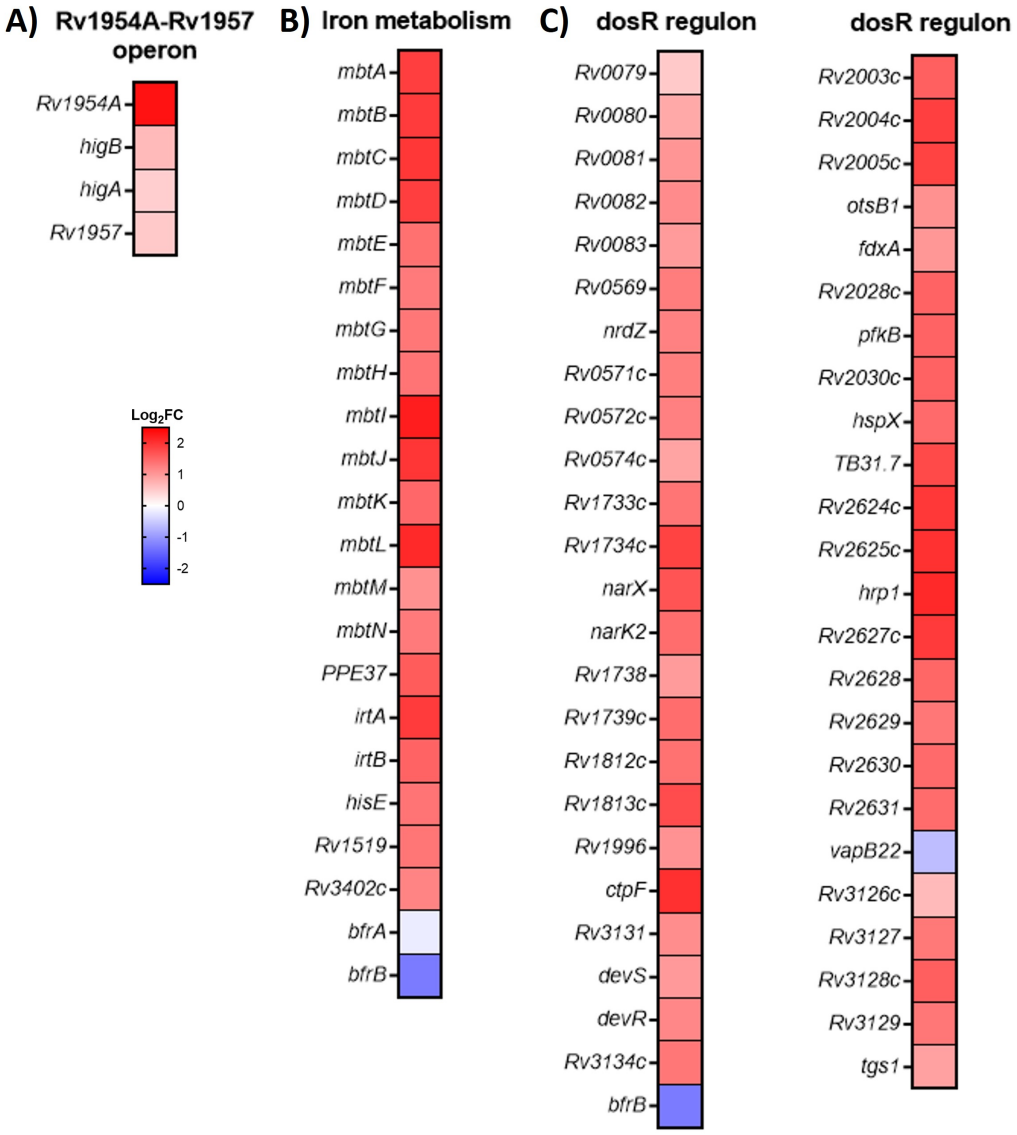

Figure 57. Genes up-regulated in KOTap mutant compared to *Mtb* wild type in exponential phase. The colour scales represent log_2FC in gene expression.

Interestingly, most of the upregulated genes detected upon *tap* disruption belonged to the dormancy regulon (**Figure 56C**), which comprises roughly 50 genes [33]. This three-component regulatory system (DevR/DevS/DosT) has been shown to be upregulated in response to several environmental stresses, including hypoxia, nitric oxide, carbon monoxide, SDS, and low pH [33,169]. Importantly, Ramón-García *et al.* [55] previously reported that four genes belonging to the dormancy regulon (*rv0569, rv1813c, rv3127* and *acg*) were also upregulated in a *M. bovis* BCG KOTap mutant in exponential phase, in line with our data.

Hence, these results might indicate that the dormancy regulon is upregulated in the KOTap mutant in order to survive the stress triggered by *tap* disruption.

Genes downregulated in exponential phase upon tap disruption

The most downregulated genes in the KOTap mutant in exponential phase were *pe8, ppe15* and *esxJ* (**Figure 58A**). Interestingly, both *esxJ* and *pe8* genes were also significantly downregulated in stationary phase.

These genes, along with *esxI*, are located within the ESX-5a region, which has been described to be important for secretion of some PE/PPE proteins, as well as alanine L-dehydrogenase (ALD) and superoxide dismutase A (SodA) enzymes [170,171]. The three replicate ESAT-6 regions of ESX-5, named ESX-5a, ESX-5b and ESX-5c, are relevant for protein secretion and virulence of mycobacteria [170]. These results are in line with those previously obtained by Ramón-García *et al*. in *M. bovis* BCG [55], which showed that genes contained in ESX-5 are down-regulated in *M. bovis* BCG KOTap, suggesting a link between the Tap efflux pump and virulence.

As previously mentioned, most down-regulated genes belonged to lipid metabolism category. Among them, we found several genes of the KstR2 regulon, including *fadD3*, *fadE30*, *fadE31* and *fadE32*, which encode enzymes required for degrading the C and D rings of cholesterol (**Figure 58B**).

Moreover, the genes of the Kas/FAS II operon, which encode five proteins (FabD, AcpM, KasA, KasB and AccD6) required for the extension of mycolic acids, were also downregulated (**Figure 58C**). The biosynthesis of mycolic acids (the major component of the outer lipid envelope of mycobacteria) is an energy-intensive biosynthetic pathway. Hence, this operon has been reported to be transiently down-regulated in response to acidic conditions which mimic the environmental stress signal encountered by intracellular bacteria [172,173]. Similarly, it could be speculated that *Mtb* slows down the mycolic acid biosynthesis as an adaptive response to the stress triggered by *tap* disruption.

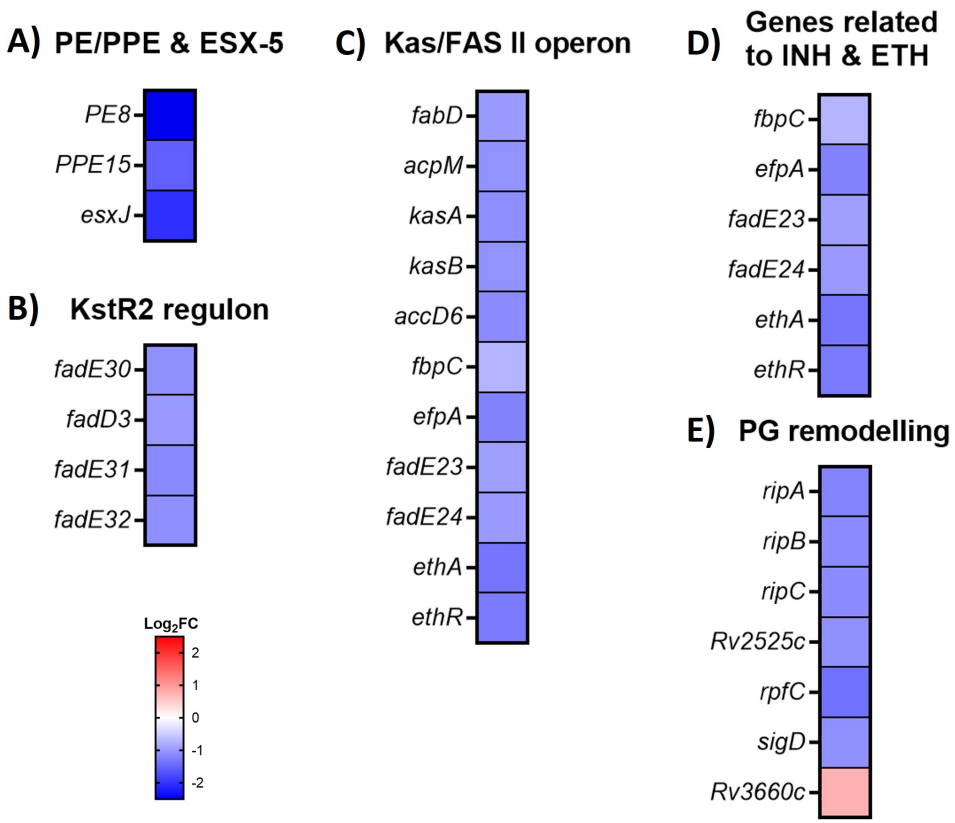

Figure 58. Genes downregulated in KOTap mutant compared to *Mtb* wild type in exponential phase. The colour scales represent log_2FC in gene expression.

Interestingly, while the Kas/FAS II operon was downregulated in the KOTap mutant, this operon has been described to be up-regulated after INH or ETH treatment along with other genes that were down-regulated in KOTap, including *fbpC*, *efpA*, *fadE23* and *fadE24* (**Figure 58D**) [172]. Both INH and ETH are pro-drugs that block the synthesis of mycolic acids by targeting InhA, an NADH-dependent enoyl acyl carrier protein reductase from the fatty acid synthase type II (FASII) cycle, which is involved in the elongation of mycolic acids [172]. Consequently, INH or ETH treatment induces the expression of the genes stated above [172].

Moreover, ETH (a structural analogue of INH) is a prodrug activated by EthA, a mono-oxygenase whose gene expression is repressed by the transcriptional regulator EthR[174]. Importantly, both the transcriptional repressor *ethR* and the ETH activator *ethA* were downregulated in the KOTap mutant (**Figure 58D**).

Taking into consideration that *tap* disruption led to a downregulation of several genes described to be upregulated after INH or ETH treatment, as well as previous reports indicating that *ethR* inactivation leads to ETH hypersensitivity [175], we hypothesized that the KOTap mutant could be more susceptible to these drugs than the wild type strain. Hence, we evaluated their susceptibility to ETH in 7H9-Tween-ADC (the medium employed in the RNA-seq) by CFU assessment.

No differences were observed in the susceptibility to ETH after 6 days of treatment (**Figure 59**), the time point at which we detected the transcriptional changes described above by RNA-seq. In contrast, the KOTap mutant was slightly more susceptible to ETH than *Mtb* wild type after 16 days of treatment with ETH at 8 and 20 µg/mL (**Figure 58**). Further time kill assays will be needed to assess whether the KOTap mutant is able to regrow in the presence of ETH at 20 µg/mL at longer time points, and to stablish a link between the transcriptional changes detected in genes involved in the synthesis of mycolic acids and ETH activation upon Tap disruption and the potential increased susceptibility of KOTap to ETH.

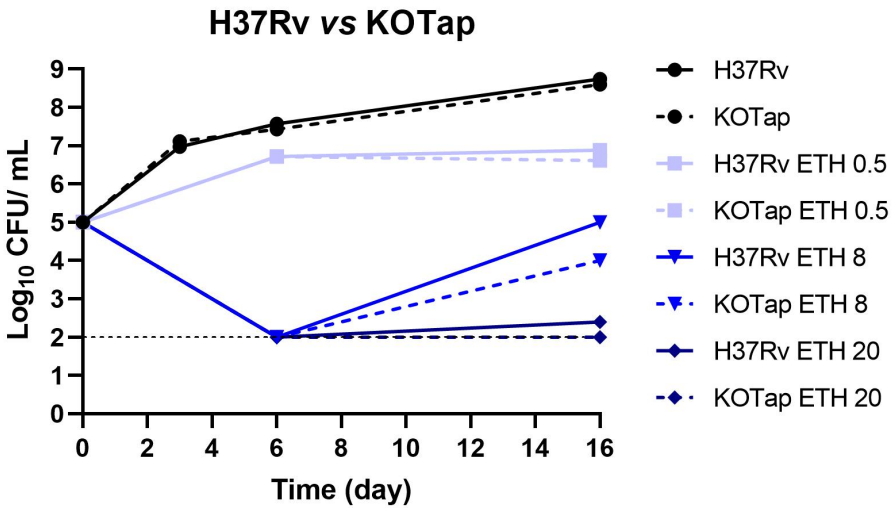

Figure 59. Susceptibility of *Mtb* H37Rv and KOTap to ETH evaluated by CFU assessment after 6 and 16 days of treatment. ETH was added at different concentrations to bacteria inoculated at a cell density of 10^5 CFU/mL in 7H9-Tween-ADC. Concentration of ETH is indicated in µg/mL. ETH, ethionamide.

Moreover, many genes encoding enzymes that act on the peptidoglycan (PG) were downregulated in KOTap, including *ripA*, *ripB* (*rv1478*), *ripD* (*rv1566*), Rv2525c and *rpfC* genes (**Figure 58E**). Similarly, Ramón-García *et al.* reported that that Tap inactivation in *M. bovis* BCG leads to a repression of genes involved in the formation of the PG [55].

The PG, a rigid polysaccharide layer that lies between the outer mycomembrane and the plasma membrane, is composed of multiple strands of a glycan backbone that comprises repeating disaccharide units of *N*-acetylglucosamine (NAG) and *N*-glycolylmuramic acid (NGM) cross-linked by short peptide stems [176]. The synthesis and cleavage of the PG is a carefully coordinated and essential process for the growth and division of bacteria [176]. Several enzymes (named PG hydrolases) are capable of cleaving the PG before incorporating new precursors into the pre-existing cell wall: lytic transglycosylases, DL-endopeptidases and amidases [176].

Both RipA and RipB are DL-endopeptidases that cleave the bond between D-glutamate and meso-diaminopimelate in the peptide stem. RipA is a key enzyme to cleave the mycobacterial septum which is synthesized after chromosome segregation, thus being required for efficient cell division[177]. Moreover, *ripA* deletion sensitizes *Mtb* to RIF and to several cell wall-targeting drugs [176].

The resuscitation-promoting factor C (RpfC) has been associated with lytic transglycosylase activity, responsible for cleaving the bond between NAG and NGM disaccharides of the glycan backbone. Importantly, previous studies have reported that the PG fragments released by RpfC lead to the resuscitation of dormant mycobacteria, thus stablishing a link between cell division and resuscitation from the dormant state [177]. Interestingly, we found that not only *rpfC* was downregulated in KOTap, but also the sigma factor *sigD* involved the regulation of *rpfC* expression [178].

Moreover, *rv2525c* has also been linked to transglycosylase activity, and mutants defective in *rv2525c* were found to be more permeable to β-lactams[179].

Considering that the septa (initially shared between daughter cells) must be degraded by PG hydrolases to complete the division process [177], the downregulation of genes encoding these enzymes could impair cell division in the KOTap mutant, thus resulting in an altered cell morphology. In line with this idea, Ramón-García *et al.* previously showed that *tap* disruption in *M. bovis* BCG leads to an elongated morphology [55]. Importantly, we found that the septum site determining protein (Ssd), encoded by *rv3660c*, was upregulated in the KOTap mutant in exponential phase (**Figure 58E**). A prior study showed that an increased expression of *ssd* in *Mtb* results in elongated cells devoid of septa [180], thus, it could be interesting to confirm in future experiments whether *Mtb* KOTap mutant displays alterations in cell morphology as previously observed in *M. bovis* BCG[55].

Finally, the changes in gene expression detected for several genes by RNA-seq analysis were validated by qRT-PCR (**Figure 60**). Importantly, qRT-PCR assays confirmed the upregulation of genes related to iron acquisition (*mbtI* and *irtA*) and genes from the *dosR* regulon (*rv2005, rv2627, acg, rv2628 rv1737c* and *rv3128c*) in the KOTap mutant in comparison to the wild type strain. Moreover, we also confirmed the strong downregulation of *pe8*. Hence, these results correlated with the transcriptional changes from our RNA-seq study.

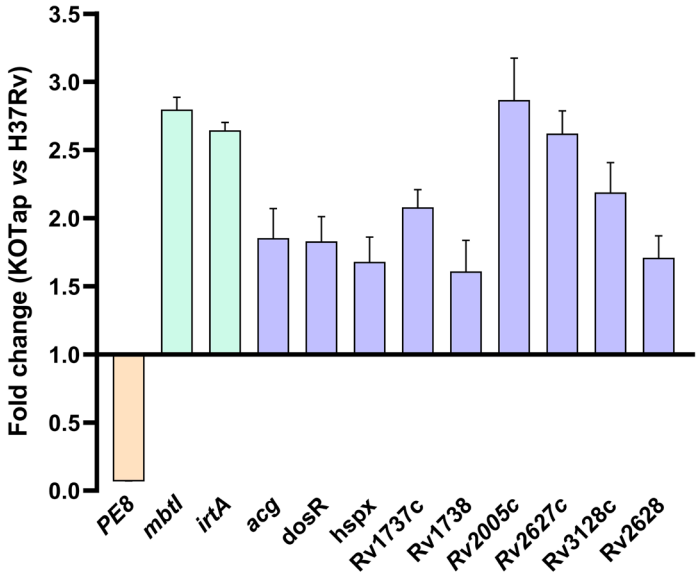

Figure 60. Gene expression of KOTap compared to *Mtb* wild type in exponential phase, determined by qRT-PCR. Expression was normalized using *sigA* gene as housekeeping. Data represent mean ± SEM from two independent biological replicates.

Taken together, these results suggested that the stress conditions caused by *tap* disruption led to the slowdown of cell wall-related processes, such as the biosynthesis of mycolic acids and PG remodelling. Hence, it could be speculated that the absence of Tap in *Mtb* might result in an altered cell wall composition that may compromise its cell wall-associated virulence and render the bacterium more vulnerable to diverse drugs, mainly cell-wall targeting drugs.

4. General discussion and future perspectives

The butyrophenones and their interplay with the Tap efflux pump

Drug repurposing is a strategy gathering momentum in both the public and private sector driven by the high costs of *de novo* drug development [69]. Diverse screening approaches can be employed to identify promising candidates for drug repurposing. Among them, screening for approved drugs that restore or enhance the action of a known antimicrobial is becoming widely used [69]. For example, some screenings aim to identify drugs with the ability to inhibit resistance mechanisms, such as efflux pumps, to restore the activity of clinically approved drugs. Following this approach, in a previous study, Ramón-García *et al.* identified the chemical family of butyrophenones as potent synergistic partners of SPT, an aminocyclitol antibiotic that lacks significant anti-TB activity on its own because it is extruded by the Tap efflux pump [156,181].

Subsequent studies demonstrated that the synergism observed between SPT and BPD against *Mtb* wild type is eliminated in the KOTap mutant but restored to wild type levels in the complemented strain, indicating that the synergism between Tap substrates and butyrophenones is Tap efflux pump specific in mycobacteria (Santiago Ramón-García & José A. Aínsa, unpublished). Recently, Omollo *et al.* followed a similar approach to demonstrate that chlorpromazine (CPZ), a phenothiazine drug, potentiates SPT activity by inhibiting Tap-mediated efflux [182]. Hence, both phenothiazines and butyrophenones are anti-dopaminergic antipsychotics drugs that probably have a similar MoA against mycobacteria, according to the results obtained.

Although the activity of haloperidol (a butyrophenone analogue) was previously investigated as an EI against *Mtb* [183], these findings contribute to shed light on the specific MoA of butyrophenones by both genetic inactivation and chemical inhibition assays, and provide a rationale for the observed synergistic interactions between butyrophenones and Tap substrates. Future work could focus on conducting structural studies of the Tap efflux pump to unravel how butyrophenones might interfere with the activity of this protein.

Elucidating the role of Tap pump from phenotypic analysis

The Tap efflux pump has been previously associated with drug resistance and drug tolerance in *Mtb* [55,148–151]. Considering that the long treatment required to cure TB is, in part, rationalized by the need to eradicate drug tolerant forms of *Mtb*, in this work, we further characterized the role of Tap in mycobacteria and its contribution to drug tolerance by different approaches.

First, we observed that the *Mtb* KOTap mutant exhibited the same growth rate as the wild type strain in nutrient-rich media (7H9-Tween-ADC), by using either optical density (**Figure 42**) or CFU assessment (**Figure 59**) as the readout method. However, potential differences in the growth kinetics of both strains could be masked by the nutrient-rich media employed in these assays. In the event that the Tap efflux pump might be responsible for transporting any molecule relevant for the fitness of the bacteria, these differences would be only detected in minimal media. It should be noted that several genes of the KstR2 regulon, which encode enzymes required for degrading the C and D rings of cholesterol, were down-regulated in the KOTap mutant, suggesting that the Tap mutant could display growth defects depending on the carbon source used in the culture medium. Hence, future studies could focus on evaluating the growth kinetics of Tap mutants in media with different carbon sources, such as cholesterol, propionate, glycerol, acetate, pyruvate, and glucose, which might provide insights into the role of Tap in *Mtb.*

Then, we found that the *Mtb* KOTap mutant showed a growth defect in the THP-1 cell line compared to the wild type strain, in accordance with a previous study describing that *Mtb* CDC1551 transposon mutants of Tap display reduced viability after 96 h of THP-1 cells infection [150]. Hence, these results indicated that Tap plays a role in *Mtb* intracellular survival. Interestingly, both *M. bovis* BCG and *Mtb*-derived KOTap mutants showed a slight lower replication rate than their respective wild type strains in the *in vitro* granuloma model, which better mimic the conditions encountered by the bacilli in a human infection since it comprises B and T cells, apart from monocytes/macrophages [153,154]. It should be noted that the differences in the replication rates for *M. bovis* BCG and *Mtb* strains in the *in vitro* granulomas seemed to be more evident at latter time points (on days 8 and 11 post-infection), suggesting that PBMCs are more capable of controlling the infection when mycobacteria do not express *tap.* Nonetheless, these differences observed within the granuloma model were not statistically significant.

One possible explanation is that the replication rates of both *M. bovis* BCG and *Mtb* strains varied depending on the donor employed for developing the granuloma model, thus reinforcing the necessity for testing several donors when this model is used.

Lessons learnt from the *in vitro* granuloma model

The *in vitro* granuloma model utilized in this work has been described to display features of *Mtb* associated with dormancy, such as loss of acid-fastness, accumulation of lipid bodies and increased RIF tolerance [155]. Hence, we used this model to study the role of Tap in dormancy and, specifically, in the development of tolerance to RIF.

We found that *M. bovis* BCG- and *Mtb*-derived KOTap mutants developed RIF-tolerant bacteria (day 8 *vs* day 1) at a lower rate than their respective parental strains in the granuloma model, suggesting that Tap could contribute to the induction of RIF tolerance within dormant *Mtb*. It has been described that *Mtb* upregulates diverse efflux pumps, including Tap, after exposure to RIF in a THP-1 macrophage model [184]. Hence, it could be possible that diverse efflux pumps along with Tap (such as Rv1410c efflux pump, which has been described to contribute to intrinsic resistance to RIF)[185] might be involved in the induction of RIF tolerance. Therefore, further experiments will be performed with the *Mtb* KOTap complemented strain or an *Mtb* strain overexpressing *tap* to confirm that this reduction in the proportion of RIF-tolerant bacteria (day 8 *vs* day 1) is due to Tap disruption.

Moreover, we observed that Tap deletion did not alter the profile of dual staining in comparison to *M. bovis* BCG wild type on day 8 post-infection, indicating that KOTap bacteria exhibit loss of acid-fastness and accumulate lipid bodies when they go into dormancy, as *M. bovis* BCG wild type.

Interestingly, the gene expression analysis performed in the *in vitro* granuloma model with *M. bovis* BCG and *Mtb* pointed toward a higher expression of *tap* on day 4 compared to day 8 post-infection, suggesting that the Tap efflux pump could have a more important role at early time points and before the mycobacteria display dormant-like features, such as drug tolerance.

In line with these findings, the data obtained from the RNA-seq analysis indicated that Tap disruption triggers more transcriptional changes in actively replicating bacteria (exponential growth phase) than in non-replicating bacteria (stationary growth phase), thus indicating that Tap could be more relevant for replicating bacteria.

Taking into consideration these data and the transcriptional changes detected in genes linked to cell wall formation and lipid metabolism by RNAseq, it could be interesting to evaluate the profile of dual auramine-O/Nile red staining of Tap mutants at early time points, when Tap seems to be more relevant for the bacteria.

In this study, the *in vitro* granuloma model has also been used to evaluate the activity of both BPD and DPR against dormant bacteria and to assess their ability to reduce the proportion of RIF-tolerant bacteria within this model.

Interestingly, we found that both butyrophenones reduced bacterial viability of dormant *M. bovis* BCG at concentrations that did not exert cytotoxic effects on PBMCs, thus indicating that these compounds are able to penetrate into granulomas and display activity against non-replicating bacteria.

However, in this set of experiments, butyrophenones did not reduce the proportion of RIF-tolerant bacteria. Further experiments will be needed to study whether butyrophenones display synergism with RIF against dormant bacteria, *e.g.,* by testing the activity of butyrophenones in combination with RIF at concentrations that have little antimicrobial effect in this granuloma model.

Transcriptomics: a molecular insight into Tap function

Finally, the RNA-seq analysis performed to study the role of Tap in exponential and stationary phase cultures of *Mtb* showed that this efflux pump seems to play a major role in replicating *Mtb*.

We observed that Tap disruption triggers a downregulation of genes involved in cell wall remodelling, specifically, in the biosynthesis of mycolic acids (Kas/FAS II operon) and in the formation of the PG (PG hydrolases). These results suggests that the KOTap mutant could be more susceptible to cell wall-targeting drugs, such as ETH, a prodrug that blocks the synthesis of mycolic acids.

Hence, future work could be focused on testing the susceptibility of KOTap to several cell wall-targeting drugs at different concentrations by time kill assays and in the *in vitro* granuloma model, which mimic diverse environments encountered by the bacilli *in vivo* and allows to study drug penetration.

Furthermore, the strong upregulation of genes involved in iron acquisition suggests that *tap* disruption could directly or indirectly result in reduced intracellular levels of iron. Future work will study the relationship between Tap efflux pump and iron metabolism, for example, by assessing the growth of KOTap in the presence of iron-chelators or in iron-restricted media, as described in **Chapter 1.**

The downregulation of genes encoding Rpfs in the KOTap mutant, which have been linked to the resuscitation of dormant bacteria, led us to hypothesize that Tap disruption might render *Mtb* less able to resuscitate from dormancy. This hypothesis could be tested in the *in vitro* granuloma model since it allows to study both bacterial dormancy and resuscitation [153]. Although in this work we have focused on evaluating the role of Tap in bacteria transition into dormancy, it is also highly important to study the processes triggering resuscitation in order to develop new drugs that target this process. In fact, a recent study has described that resuscitation from dormancy after O_2 starvation is *Mtb* lineage-dependent, since only strains belonging to the Euro-American (L4) lineage recovered from O_2 starvation [186]. Thus, this *in vitro* granuloma model would be a useful tool to study the genetic factors responsible for these differences.

Taken together, the stress conditions caused by *tap* disruption could trigger a stress response that result in the slowdown of cell wall-related processes, including mycolic acids biosynthesis, PG remodelling and iron acquisition. Therefore, disruption of Tap in *Mtb* might result in an altered cell wall composition that may compromise its cell wall-associated virulence and render the bacterium more vulnerable to diverse drugs.

5. Conclusions

- Both BPD and DPR are active not only against *Mtb in vitro* and *ex vivo*, but also against dormant bacteria located inside granulomas.

- Although both *Mtb* and KOTap showed the same growth kinetics in 7H9-Tween-ADC medium, KOTap displayed a compromised growth in THP-1 cells compared to *Mtb*, suggesting that Tap plays a role in intracellular survival.

- Both *Mtb* and *M. bovis* BCG-derived KOTap mutants showed a slight lower replication rate than their respective wild type strains in the granuloma model. However, these differences were not statistically significant, in contrast to the results obtained in the THP-1 cell line.

- *M. bovis* BCG- and *Mtb*-derived KOTap mutants developed RIF-tolerant bacteria (day 8 *vs* day 1) at a lower rate than their respective parental strains.

- The higher expression of *tap* on day 4 compared day 8 post-infection in the granuloma model suggests that the Tap efflux pump could have a more important role before *Mtb* displays features characteristic of dormant bacteria.

- Similarly, a higher number of DGEs was detected by RNA-seq in exponential phase compared to stationary phase, suggesting that Tap could be more relevant for actively replicating *Mtb* than for non-replicating bacteria.

- Tap disruption led to the downregulation of genes involved in the biosynthesis of mycolic acids and PG remodelling, and upregulation of genes from the dormancy regulon and related to iron acquisition pathways, suggesting that the absence of Tap in *Mtb* might result in an altered cell wall composition that may compromise its cell wall-associated virulence and render the bacterium more vulnerable to diverse drugs, mainly cell-wall targeting drugs.

Conclusiones

- Tanto BPD como DPR presentan actividad frente a *Mtb in vitro* y *ex vivo*, así como frente a bacterias latentes ubicadas en el interior de los granulomas.

- No se detectan diferencias en las curvas de crecimiento de la cepa silvestre de *Mtb* y del mutante de *Mtb* defectivo en la bomba de eflujo Tap en medio 7H9-Tween-ADC. Sin embargo, el mutante de Tap presenta una menor tasa de crecimiento en la línea celular THP-1 en comparación con la cepa salvaje, sugiriendo que Tap está implicada en la supervivencia intracelular de *Mtb*.

- En el modelo de granuloma, los mutantes de *Mtb* y de *M. bovis* BCG defectivos en Tap muestran una tasa de replicación ligeramente más baja que sus respectivas cepas de tipo salvaje. Sin embargo, estas diferencias no son significativas, a diferencia de los resultados obtenidos en la línea celular THP-1.

- Los mutantes de *Mtb* y de *M. bovis* BCG defectivos en la bomba de eflujo Tap desarrollan una menor proporción de bacterias tolerantes a RIF que sus respectivas cepas parentales cuando comparamos el porcentaje de bacterias tolerantes a RIF a día 8 frente a día 1.

- Tanto *M. bovis* BCG como *Mtb* muestran mayores niveles de expresión de Tap a día 4 que a día 8 en el modelo de granuloma. Estos resultados sugieren que la bomba de eflujo Tap podría tener un papel más relevante antes de que estas bacterias muestren las principales características asociadas con latencia.

- De manera similar, a través de los estudios de RNA-seq se ha detectado un mayor número de genes diferencialmente expresados en fase exponencial en comparación con los detectados en fase estacionaria, lo que sugiere que Tap podría ser más relevante para *Mtb* en estado replicativo.

- El mutante de *Mtb* defectivo en Tap disminuye la expresión de genes implicados en la biosíntesis de ácidos micólicos y en la remodelación del peptidoglicano, mientras que aumenta la expresión de genes del regulón de latencia y asociados con el metabolismo del hierro. Estos resultados sugieren que la ausencia de Tap podría alterar la composición de la pared celular y, en consecuencia, comprometer la virulencia de *Mtb* y provocar que la bacteria sea más susceptible a diversos fármacos, principalmente aquellos dirigidos a la pared celular.

MATERIAL AND METHODS

MATERIALS AND METHODS

Bacterial strains, media and culture conditions

Bacterial strains used and obtained in this work are listed in **Table 31.**

Escherichia coli strains

E. coli strains were grown in Luria-Bertani (LB) broth or on LB agar plates at 37ºC. When required, medium was supplemented with ampicillin (Amp, 100 µg/mL), kanamycin (Km, 20 µg/mL), or chloramphenicol (Cm, 12.5 µg/mL); 0.15% arabinose (w/v) was used for induction of genes contained in pKD46[187]. IPTG (isopropyl-β-D-thiogalactopyranoside, 0.5 mM) and X-Gal (5-bromo-4-chloro-3-indolyl-β-d-galactopyranoside, 50 µg/mL) were added to LB agar plates when it was required to check *lacZ* phenotype.

E. coli DH10B containing a bacterial artificial chromosome (BAC) library of H37Rv chromosome cloned in pBeloBAC11 were grown at 30°C, when needed, to maintain the thermosensitive pKD46 plasmid [188].

Mycobacterial strains

M. smegmatis, M. bovis BCG and *Mtb* strains were routinely cultured at 37°C in Middlebrook 7H9 broth (Difco™) liquid medium supplemented with 10% ADC (0.5% bovine serum albumin, 0.2% dextrose, 0.085% NaCl and 0.0003% beef catalase) (Difco) and 0.05% Tween 80 (**"7H9-Tween-ADC"**). For drug susceptibility assays, 0.2% glycerol or/and 0.025% Tyloxapol were used instead of 0.05% Tween 80. Middlebrook 7H10 agar (Difco™) supplemented with 10% OADC (0.05% oleic acid, 0.5% bovine serum albumin, 0.2% dextrose, 0.085% NaCl, 0.0003% beef catalase) (Difco) was used for cultures in solid media (**"7H10-OADC"**). Kanamycin (Km, 20 µg/mL) or hygromycin (Hyg, 20 µg/mL) were added to the media when required. 0.2% acetamide was used to induce the expression of *gp60/61* genes in the pJV53H plasmid.

Moreover, for drug susceptibility assays under different iron conditions, the following media were included:

- Iron-replete medium: 7H9 (without 40 µg/mL of ferric ammonium citrate) supplemented with 0.2% Gly, 10% ADC and 40 µg/mL of $FeCl_3$ (**"Fe 40"**).
- Iron-replete medium plus chelator: 7H9 (without 40 µg/mL of ferric ammonium citrate) supplemented with 0.2% Gly, 10% ADC, 40 µg/mL of $FeCl_3$ and 0.2 mM of DFO (an iron chelator) (**"Fe 40 + DFO"**).
- Iron-restricted medium: 7H9 (without 40 µg/mL of ferric ammonium citrate) supplemented with 0.2% Gly, 10% ADC and 4 µg/mL of $FeCl_3$ (**"Fe 4"**).

The total estimated amount of iron in the different conditions was 0.247 mM (**Fe 40**), 0.0247 mM (**Fe 4**) and 0.047 mM (**Fe40 + DFO**) (taking into consideration that DFO binds iron at a 1:1 molar ratio) [94].

M. abscessus was cultivated at 37°C in 7H9 broth supplemented with 0.2% glycerol and 10% ADC (**"7H9-Gly-ADC"**), or in Müller-Hinton broth (Panreac AppliChem) supplemented with 22 mg/L Ca^{2+} and 12 mg/L Mg^{2+} (referred to as **CaMHB**), since this is the Clinical & Laboratory Standards Institute (CLSI)-recommended medium for antimicrobial testing assays against NTM. LB agar was used for CFU assessment.

M. ulcerans clinical isolates were grown at 30°C in 7H9 broth supplemented with 0.2% glycerol, 10% OADC and 0.05% Tyloxapol. For drug susceptibility assays, the medium was not supplemented with Tyloxapol.

Manipulation of *E. coli* and mycobacterial strains was performed in a biosafety level 1 laboratory (BSL1), biosafety level 2 laboratory (BSL2) or biosafety level 3 laboratory (BSL3), according to **Table 31**, with facilities notification A/ES/10/I-05, A/ES/06/I-02 and A/ES/04/I-05, respectively.

Table 31. Bacterial strains used and obtained in this work, and biosafety level.

Strain	Description	Reference
***Mycobacterium tuberculosis* (BSL3)**		
H37Rv (ATCC 25618)	Wild type	Laboratory collection
H37Rv-Luc	Derivative of H37Rv expressing the firefly luciferase *luc* gene from *Photinus pyralis* cloned into pMV306hsp integrative vector; Km^R (Km resistant)	189
H37Rv pJV53H	Derivative of H37Rv carrying pJV53H plasmid; Hyg^R (Hyg resistant)	190
L4KO	Derivative of H37Rv with *mmpL4* gene disrupted; *mmpL4*::Ω*hyg.* Single mutant of *mmpL4*	92
L4S4KO	Derivative of H37Rv with *mmpL4 and mmpS4* genes disrupted; *mmpL4/S4*::Ω*hyg.* Double mutant of *mmpL4* and *mmpS4*	92
L4c	Derivative of L4KO expressing *mmpS4/mmpL4* operon under its own promoter in the integrative vector pMV361; Km^R. Complemented strain of L4KO	92
L4S4c	Derivative of L4S4KO expressing *mmpS4/mmpL4* operon under its own promoter in the integrative vector pMV361; Km^R. Complemented strain of L4S4KO	92
L4S4sb	Derivative of H37Rv expressing *mmpS4/mmpL4* operon under its own promoter in the multicopy pSUM36 plasmid; Km^R	92
L5KO	Derivative of H37Rv with *mmpL5* gene disrupted; *mmpL5*::Ω*km.* Single mutant of *mmpL5*	This study
L5S5KO	Derivative of H37Rv with *mmpL5 and mmpS5* genes disrupted; *mmpL5/S5*::Ω*km.* Double mutant of *mmpL5 and mmpS5*	This study
pACM1	Derivative of H37Rv expressing *mmpS5/mmpL5* operon under its own promoter in the multicopy pSUM36 plasmid; Km^R	This study
ndhKO	Derivative of H37Rv with *ndh* gene disrupted; *ndh*::Ω*km*	This study
KOTAP	Derivative of H37Rv with Rv1258c (*tap*) gene disrupted; Rv1258c::Ω*hyg*	185
KOTAPc	Derivative of KOTAP expressing Rv1258c (*tap*) gene under control of its own promoter in the integrative plasmid pMV361	185

***Mycobacterium bovis* BCG (BSL2)**		
Pasteur 1173	Vaccine against TB, *M. bovis* attenuated strain	Laboratory collection
BCG KOTAP	Derivative of BCG with *tap* gene disrupted; *tap*::*Ωhyg*	[55]
***Mycobacterium smegmatis* (BSL1)**		
mc^2155	Wild type	Laboratory collection
KO MSMEG_3729	Derivative of *M. smegmatis* with the MSMEG_3729 gene disrupted; MSMEG_3729::*Ωhyg*	[191]
KO MSMEG_3461	Derivative of *M. smegmatis* with the MSMEG_3461 gene disrupted; MSMEG_3461::*Ωhyg*	[191]
KO MSMEG_6384	Derivative of *M. smegmatis* with the MSMEG_6384 gene disrupted; MSMEG_6384::*Ωhyg*	[191]
PAC48	Derivative of *M. smegmatis* expressing *tap* gene from *Mycolicibacterium fortuitum* under its own promoter in the multicopy pSUM36 plasmid; Km^R	[149]
***Mycobacterium abscessus* (BSL2)**		
ATCC 19977	Wild type	Laboratory collection
***Mycobacterium ulcerans* clinical isolates (BSL3)**		
ITM C05142	Classical lineage (geographical origin: Australia)	BCCM
ITM C05143	Ancestral lineage (geographical origin: Mexico)	BCCM
ITM 063846	Classical lineage (geographical origin: Benin)	BCCM
ITM C08756	Ancestral lineage (geographical origin: Japan)	BCCM
ITM 070290	Ancestral lineage (geographical origin: China)	BCCM
***Escherichia coli* (BSL1)**		
DH10B BAC Rv339	Used for the construction of L5KO and L5S5KO *Mtb* strains by BAC-recombineering	[188]
DH10B BAC Rv281	Used for the construction of ndhKO by BAC-recombineering	[188]
Stellar	Used for the construction of pACM1 plasmid	Takara Biotech
BW25113	Wild type strain	[192]
Δ*acrB*	BW25113 Δ*acrB*	[192]
Δ*emrE*	BW25113 Δ*emrE*	[192]
Δ*mdfA*	BW25113 Δ*mdfA::km*	[192]
Δ*acrB* Δ*emrE*	BW25113 Δ*acrB* Δ*emrE*	[192]
Δ*emrE* Δ*mdfA*	BW25113 Δ*emrE* Δ*mdfA::km*	[192]
Δ*acrB* Δ*emrE* Δ*mdfA*	BW25113 Δ*acrB* Δ*emrE* Δ*mdA::km*	[192]
Mutants 1-18	Δ*acrB*-derived strains resistant to C2	This study

BCCM, Belgian Co-ordinated Collection of Microorganisms.

Antimicrobial susceptibility testing

Broth microdilution susceptibility testing (liquid MIC)

The MIC of antimicrobials was determined in technical duplicates in clear flat-bottom 96-well plates (TPP™). Antimicrobial stocks at twice the maximal test concentration were prepared in the appropriate liquid medium depending on the strain employed (described in ***Bacterial strains, media and culture conditions*** section). From these stocks, 2-fold or 1.4-fold serial dilutions were performed in 75 µL of medium. Afterwards, 75 µL of bacterial suspensions at 2 x 10^5 CFU/mL were added to each well to obtain a final bacterial density of 10^5 CFU/mL (10^6 CFU/mL for *M. ulcerans*). The correlations between OD_{600nm} and CFU/mL as indicated in **Table 32** were used for bacterial density calculations. Internal growth controls were included in each plate, *i.e.* no drug as 100% growth control and no bacteria as 0% growth control.

Plates were incubated at 37°C for 16-20 h (*E. coli*), 3 days (*M. smegmatis* and *M. abscessus*) and 6 days (*M. bovis* BCG and *Mtb* strains), or at 30ºC for 6 days (*M. ulcerans* clinical isolates) (**Table 32**). Then, 30 µL of 5 mg/mL MTT [3-(4,5-dimethylthiazol-2-yl)-2,5-diphenyltetrazolium bromide] (Sigma-Aldrich) with 20% (v/v) Tween 80 were added to each well.

MTT is a redox reporter of metabolic activity used as a bacterial growth indicator since only metabolically active bacteria are able to reduce MTT (yellow) to formazan product (purple). Therefore, the formation of the formazan precipitate indicates bacterial growth [193].

Table 32. Correlation between OD_{600nm} and CFU/mL, and incubation conditions for each strain.

Strain	OD_{600nm}	CFU/mL	Temperature of incubation	Incubation time of plates	Incubation time with MTT
E. coli	2	10^9	37°C	16-20 h	30 min
M. smegmatis	0.125	10^7	37°C	3 days	3 h
M. abscessus	0.8	4.2 x 10^8	37°C	3 days	3 h
M. bovis* BCG, *Mtb	0.125	10^7	37°C	6 days	24 h
M. ulcerans	0.125	10^7	30°C	6 days	24 h

Following MTT addition, plates were further incubated at 37°C for 30 min (*E. coli*), 3 hours (*M. smegmatis* and *M. abscessus*) or overnight (*M. bovis* BCG, *Mtb* and *M. ulcerans*) before measuring the OD_{580nm} in a Synergy HT microplate reader (BioTek). Absorbance (Abs_{Sample}) was normalized to the percentage of growth (% $Growth_{Sample}$) using the absorbance of positive and negative growth controls ($Abs_{100\%\ Growth\ control}$ and $Abs_{0\%\ Growth\ control}$, respectively) and the following formula:

$$\%\ Growth_{\ Sample} = \frac{Abs_{\ Sample} - Abs_{\ 0\%\ Growth\ control}}{Abs_{\ 100\%\ Growth\ control} - Abs_{\ 0\%\ Growth\ control}} x\ 100$$

The lowest drug concentration that inhibited 90% of MTT conversion to formazan was used to define the MIC_{90} of each compound.

Susceptibility testing on agar plates (solid MIC)

Susceptibility assays in solid medium were performed to evaluate whether compound activity varied depending on the total CFU seeded.

First, duplicate two-fold serial dilutions of compounds were prepared in 7H10-OADC for *Mtb* or in LB agar for *E. coli,* in a 24-well plate format. Importantly, solid media must be melted but tempered to around 55°C to avoid thermal decomposition of antimicrobials. Plates were then stored at 4°C for 24 h to favour drug diffusion in the agar. Subsequently, 10 µL of bacterial suspensions at 10^7 and 10^9 CFU/mL were seeded in the agar surface of the wells, which corresponds to 10^5 and 10^7 CFU per well, respectively. Plates were incubated at 37°C for 24 hours (*E. coli*) or 2-3 weeks (*Mtb*). Solid MIC was defined as the lowest concentration of compound that inhibited bacterial growth.

In parallel, 10-fold serial dilutions of the bacterial suspensions were seeded in agar quad plates to determine the actual number of bacteria per well.

Time Kill Assays

Exponentially growing cultures were diluted in the corresponding medium depending on the bacterial strain tested to obtain a cell density of ca. 10^5 CFU/mL. Except for *E. coli*, cultures were incubated at 37°C for 24 hours (*M. abscessus*) or 3 days (*Mtb*) to allow **exponential growth**. These cultures were then distributed (10 mL) in 25 cm^2 tissue culture flasks and drugs were added at the selected concentrations and combinations.

Growth controls were included to assess bacterial growth without drugs. Cultures were incubated at 37°C and aliquots were taken at different time points to evaluate bacterial density by CFU counting.

At every time point, cultures were shaken vigorously and samples of 100 µL were 10-fold serially diluted in PBS (phosphate buffered saline) with 0.1% tyloxapol to break clumps. Then, 100 µL of the dilutions were plated in duplicate on LB (*E. coli* and *M. abscessus*) or 7H10-OADC (*Mtb*) agar quad plates. Colonies were enumerated after 24 h (*E. coli*), 5 days (*M. abscessus*) or 2 weeks (*Mtb*) of incubation at 37°C. In the case of *Mtb* assays, plates were checked after 3 and 4 weeks of incubation to account for late growers. Cell density was reported as $\log_{10}$ CFU/mL.

Time kill assays were also performed at **high-density inoculum** (10^7 CFU/mL) of *Mtb*. For this, exponentially growing bacteria were inoculated to a bacterial density of 10^5 CFU/mL and incubated at 37°C for 6 days before adding the compounds. For time kill assays against *Mtb* under **non-replicating conditions**, drugs were added to *Mtb* cultures in stationary phase (6 weeks of incubation at 37ºC). Next steps of the protocol were the same as described above.

Drug interaction studies

Synergy screen

This assay was performed to identify *in vitro* synergistic interactions of C9 (*primary compound*) with clinically approved or investigational TB drugs with known modes of action (*secondary compounds)* against *Mtb* H37Rv and L4KO strains.

MIC values of secondary compounds were determined in the absence or in the presence of C9 at 1/8x, 1/4x and 1/2xMIC in clear flat-bottom 96-well plates. This sub-inhibitory concentrations of C9 were added at 2x to the bacterial suspensions (ca. 2 x 10^5 CFU/mL) prior to the addition of 75 µL to wells containing 2-fold serial dilutions of secondary compounds (in 75 µL). MTT was used as the bacterial growth indicator, as previously described. Synergy was defined by at least 4-fold reductions in the MIC of secondary compounds in the presence of C9 at concentrations equal or <1/4xMIC.

Checkerboard assay

Checkerboard assays were performed to define the degree of pair-wise drug interactions. Briefly, each compound was prepared at 4-fold the highest concentration to be tested in the corresponding medium depending on the bacterial strain used. Then, drugs were assayed in pair-wise combinations titrated in two-fold serial dilutions along the X and Y axes of the 96-well plate, and bacteria were added to a final density of 10^5 CFU/mL. MICs of compounds alone were determined in column 1 and row H (**Figure 61**). MTT was used as the bacterial growth indicator, as previously described. The optimal MIC of the combination was calculated as the minimum drug concentration of both drugs inhibiting bacterial growth by 90%.

To quantify the degree of drug interaction, wells with no bacterial growth but that were adjacent to a well where bacteria had grown were selected, and the Fractional Inhibitory Concentration (FIC) of each compound was calculated with the following formula:

$$FIC_A = \text{MIC of A in the presence of B / MIC of A alone}$$

$$FIC_B = \text{MIC of B in the presence of A / MIC of B alone}$$

The Fractional Inhibitory Concentration Index (FICI), the reference parameter to classify drug interactions, was calculated as:

$$FICI = FIC_A + FIC_B$$

The FICI is used as an indicator of synergy (FICI ≤0.5), antagonism (FICI>4) or no interaction (0.5< FICI ≤4) [194]. Moreover, FIC values of every drug can be plotted as isobolograms to allow visual inspection of drug interactions. As shown in **Figure 61**, curves closer to the axis origins indicate a synergistic profile while a straight line indicates a non-interaction profile.

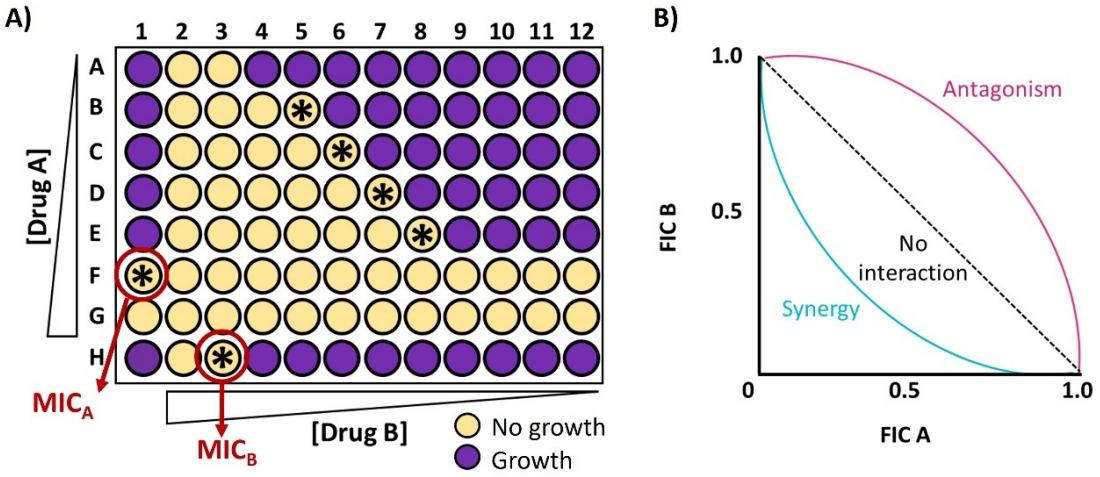

Figure 61. Schematic representation of checkerboard assays. (A) Example of a hypothetical result of synergy; asterisks (*) mark selected wells where the FICI was calculated (B5, C6, D7, E8), or those wells showing MIC of individual drugs (F1 for drug A and H3 for drug B). (B) Isobologram representation of the possible interactions between two drugs in a checkerboard assay.

Time Kill Assays

Time kill assays were also performed as described above to confirm the synergism of some drug combinations. For these assays, we selected drug concentrations that had little antimicrobial effect (*i.e.,* bacteria grow similar to the control in the presence of the drug) or bacteriostatic effect.

Cell biology protocols

THP-1 cells and culture conditions

Frozen stocks of human monocytic THP-1 cells (ECACC 88081201) were thawed in RPMI-1640 medium with HEPES modification (Gibco) supplemented with 1% GlutaMAX (Gibco), 10% heat-inactivated Fetal Bovine Serum (FBS; Gibco) and 1 mM sodium pyruvate (Sigma) (**"cell culture medium"**). Cells were maintained in cell culture medium with 1% penicillin-streptomycin (Sigma) between 2-10 x 10^5 cells/mL at 37°C (5% CO_2).

Intracellular MIC assays

An *Mtb* H37Rv strain constitutively expressing the firefly luciferase *luc* gene from *Photinus pyralis* was used for intracellular MIC assays. *Mtb* H37Rv-Luc cultures grown in 7H9-Tween-ADC-Km to mid-exponential phase (OD_{600nm} = 0.4-0.8) were pelleted, dispersed by using glass beads and resuspended in cell culture medium. Then, the supernatant was collected and centrifuged at 750 rpm for 5 min to discard the remaining clumps. The upper part of the supernatant, containing mostly single bacteria, was recovered and the OD_{600nm} measured prior to THP-1 infection.

THP-1 cells were counted by trypan blue (Sigma-Aldrich) exclusion method and the concentration was adjusted to 2 x 10^5 cells/mL in cell culture medium. Cells were simultaneously differentiated with 20 nM phorbol 12-myristate 13-acetate (PMA) (P1585-1MG, Sigma) and infected at a multiplicity of infection (MOI) of 1:1 with the single bacterial suspension previously prepared. After 4 hours of incubation with stirring, infected cells were washed five times to remove extracellular bacilli and resuspended in cell culture medium at 4 x 10^5 cells/mL. Infected cells (50 µL) were seeded at a concentration of 20,000 cells per well in white flat-bottom 96-well plates containing serial dilutions of the drugs (50 µL). Plates were incubated for 5 days at 37°C (5% CO_2) before the addition of the bacterial growth indicator D-Luciferin (122799, Perking Elmer) at a final concentration of 1.25 mg/mL. Viable *Mtb* H37Rv-Luc bacteria catalyse the oxidation of D-Luciferin (an ATP-dependent reaction) resulting in the production of light (**Figure 62**). Luminescence was measured in a Synergy HT microplate reader (BioTek) 10 min after the addition of D-Luciferin. Internal control wells containing drug-free medium with and without infected THP-1 cells established maximum and minimal light production, respectively.

A 90% reduction in light production was considered growth inhibition. Every compound was assayed in triplicate in at least two independent experiments.

Resazurin-based cytotoxicity assay

THP-1 cells were processed as described above, but not infected, and seeded in clear flat-bottom 96-well plates containing serial dilutions of the compounds. Cells were incubated in the presence of the drugs for 5 days before the addition of 20 µL of 0.1 mg/mL resazurin (Sigma-Aldrich) per well. After 4-5 h of incubation, fluorescence was measured at 530- and 590-nm excitation and emission wavelengths, respectively, to determine the viability of treated macrophages in comparison to that of untreated controls (**Figure 62**) [156]. Every compound was assayed in triplicate in at least two independent experiments.

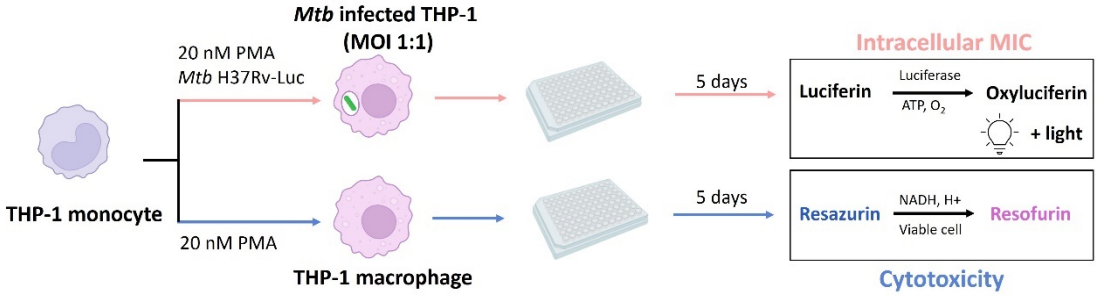

Figure 62. Schematic representation of the procedure for intracellular MIC determination and cytotoxicity assays. Drugs being tested were added to the 96-well plate, prior to the 5 days incubation. Created with Biorender.

Intracellular CFU-based replication assays of *Mtb* strains

THP-1 cells were prepared at a concentration of ca. 6 x 10^5 cells/mL in cell culture medium containing 10 ng/mL of PMA, and 500 µL of this suspension were seeded in flat-bottom 24-well plates to obtain ca. 3 x 10^5 cells per well. After 24-48 h of incubation at 37°C (5% CO_2), differentiated cells were infected with *Mtb* H37Rv wild type or KOTAP mutant at an MOI of 1:1 for 4 h. Bacterial single cells suspensions used for the infection were prepared as described above. Afterwards, media was removed to stop infection and cells were washed three times with 1 mL PBS. Finally, 2 mL of cell culture medium were added to each well to allow intracellular replication and plates were further incubated at 37°C (5% CO_2).

To determine the number of intracellular bacteria at various times post-infection, medium was removed, and infected cells were lysed with 500 µL of 0.1% Triton X-100. Serial dilutions of this suspension were plated on 7H10-OADC quad agar plates and viable bacteria counted after 2-3 weeks of incubation at 37ºC.

Isolation of Peripheral Blood Mononuclear Cells (PBMCs)

PBMCs used in this work were isolated by the group of Dr. Damien Portevin (Tuberculosis Immunology Group, SwissTPH) or were provided by the Biobank of Aragon Health System (PT20/00112), integrated in the Spanish National Biobanks Network and they were processed following standard operating procedures with the appropriate approval of the Ethics and Scientific Committees. All donors provided informed consent, which includes information on the use of blood products for research purposes, as stated in the application SA22-04, and the procedure was previously approved by CEICA (Comité Ético de Investigación Clínica de Aragón, procedure PI22/81).

Briefly, PBMCs were isolated by Ficoll-Paque density-gradient centrifugation of buffy coats from healthy blood donors (as per written informed consent) and stored in liquid nitrogen until use. When needed, PBMCs were thawed and washed twice in RPMI containing 10% FBS and 12.5 U/mL benzonase (BioVision). PBMCs were then rested in RPMI supplemented with 10% FBS (**"RPMI-FBS"**) for at least 6 hours at 37°C (5% CO_2). After resting, cells were adjusted to 10^7 PBMCs/mL in RPMI-FBS.

Cytotoxicity assays (LDH release assay)

Rested PBMCs were distributed in a 96-well plate at 5×10^5 cells per well and incubated at 37°C (5% CO_2) for 1 day before the addition of the drugs (RIF, BPD or DPR). After 3 days of treatment, supernatants were collected and analysed using Cytotoxicity Detection kit^{PLUS} (LDH; Roche) according to manufacturer's instructions.

Human in vitro granuloma model

PBMC infection and granuloma formation

Rested PBMCs were infected with single cell suspensions of mycobacteria at an MOI of 1:50 (BCG:PBMC) or 1:200 (*Mtb*:PBMC) and distributed in 96-, 48- or 24-well plates at 5×10^5, 1.25×10^6 or 2.5×10^6 PBMCs per well, respectively. Mycobacterial single cells suspensions were prepared as described for ***Intracellular MIC assays*** and cryopreserved by adding 50% glycerol (final concentration of 5% glycerol) and storing at -80ºC. Bacterial concentration of frozen stocks was quantified by CFU assessment.

Subsequently, infected PBMCs suspensions were embedded within an extracellular matrix (ECM) by adding the following mixture (in a 1:1 ratio) composed of 950 μL of 3 mg/mL PureCol collagen solution (Advanced BioMatrix), 50 μL of 10x PBS (SAFC Biosciences), 4 μL of 1 mg/mL fibronectin (Sigma) and 10 μL of 1N NaOH (Sigma) per mL of ECM required.

The ECM was left to set for 45 min at 37°C (5% CO_2) before topping up the wells with RPMI-FBS, and plates were incubated at 37°C (5% CO_2). Granuloma formation was monitored using a Leica DM IL LED inverted microscope and a Leica MC170 HD camera.

Retrieval of mycobacteria

At different time-points, supernatant was removed and the ECM was digested with 1 mg/mL collagenase (Sigma) for 40 min at 37°C (5% CO_2). PBMCs were lysed by adding 0.4% Triton X-100 and incubating for 20 min at 37°C (5% CO_2). Volumes of collagenase and Triton X-100 were 50, 125 or 250 μL for 96-, 48- and 24-well plates, respectively. Released bacilli were used for dual auramine-O/Nile red staining or bacterial quantification by CFU assessment.

Dual auramine-O and Nile red staining

Bacilli retrieved as described above were pelleted by centrifugation at 6000×g for 5 min before being inactivated with 1x CellFIX (BD) for 20 min at room temperature (RT). Fixed samples were spotted on glass slides, air dried and heat fixed. Fluorescent acid-fast staining using TB Fluorescent Stain Kit M (BD) was performed in combination with neutral lipid-staining dye Nile red (Sigma) [153]. Stained slides were examined using a Leica DM5000 B fluorescence microscope. For quantitative analysis, at least 200 bacteria per sample were counted.

RIF tolerance and drug activity assays

On days 1 and 8 post-infection, infected PBMCs were either left untreated (control) or treated with the drugs to be studied (RIF, BPD or DPR). Plates were then incubated for three additional days at 37ºC (5% CO_2) prior to retrieval of mycobacteria for CFU assessment. To determine the number of CFU, 10-fold serial dilutions were prepared in triplicate and plated on 7H11-OADC or 7H10-OADC. The percentage of RIF-tolerant bacteria was calculated by using the following formula:

% RIF-tolerant bacteria = CFU (RIF-treated) / CFU (untreated) x 100

RNA extraction and qRT-PCR

On days 4 and 8 post-infection, infected PBMCs were recovered from *in vitro* granulomas after collagenase treatment. The pellet was then resuspended in TRI-reagent (Zymo Research) and stored at -80ºC until RNA extraction. The TRI-reagent suspension was transferred into screw tubes containing glass beads (MP Biomedicals) and bead-beaten using a FastPrep. After removing the cellular debris by centrifugation, total RNA was extracted using Direct-zol RNA MiniPrep (Zymo Research) according to the manufacturer's instructions. Expression of several genes was quantified by qRT-PCR.

Selection of resistant or susceptible genetic mutants

Mutant isolation assays in agar plates and validation of the resistant phenotype

Different inocula (10^7, 10^8 or 10^9 total CFU) of *E. coli ΔacrB* and *Mtb* H37Rv were plated on LB and 7H10-OADC agar plates (respectively) containing 2x, 4x or 10x the MIC of C2 compound, taking as reference solid MIC values previously determined for different bacterial densities of these strains. Plates were incubated at 37ºC for 24 h (*E. coli*) and 3-4 weeks (*Mtb* H37Rv). In parallel, 10-fold serial dilutions of the inoculum were seeded in LB or 7H10-OADC agar plates to determine the actual number of bacteria plated. Frequencies of mutation were calculated as the ratio of total CFU isolated after incubation at 37°C on the drug-containing plate over the total number of CFU seeded.

As a primary validation assay, the resistant phenotype of selected mutants was evaluated by MIC determination. Then, time kill assays were performed to confirm their resistant phenotype. Confirmed *E. coli ΔacrB*-derived resistant mutants and *E. coli ΔacrB* were propagated in LB and their DNA isolated for WGS.

Screening of the *Mycobacterium bovis* BCG TnSPAZ transposition library

The *M. bovis* BCG Tn*SPAZ* transposition library

The *M. bovis* BCG Tn*SPAZ* library was previously constructed and analysed in our laboratory[191]. This library contains 2,880 mutants kept individually in thirty 96-well plates or pooled in three plates. Mutants have the Tn*SPAZ* transposon randomly inserted in their chromosome, which consists of the following elements (**Figure 63**): the transposase gene (*tnpA*) and the inverted repetitions (IR) from the natural IS*1096* transposon of *M. smegmatis*, a Km resistance cassette (*aph*) from Tn903, and a strong and constitutive promoter derived from the *M. fortuitum* β-lactamase gene (*pBlaF**). Therefore, this strategy allows the selection of resistant and susceptible mutants due to target gene inactivation or overexpression of genes situated downstream of Tn*SPAZ* transposon.

Figure 63. Schematic representation of the Tn*SPAZ* transposon.

Screening strategy

The thirty plates of the transposition library were screened to identify mutants with an increased susceptibility to C9, whereas pooled plates were used to screen the library for mutants resistant to C9.

Mutants were transferred from glycerol stock plates (15% glycerol (v/v), stored at -80 ˚C) to fresh 7H9-Gly-ADC (200 µL/well) and incubated at 37˚C until growth was observed (8-10 days). Cultures were then 10-fold diluted and a 96-pin replicator (transferring ca. 3 µL) was used to transfer bacteria to control plates (without drugs) and test plates containing sub-inhibitory (1/4xMIC and 1/16xMIC) or inhibitory concentrations (4xMIC and 16xMIC) of C9 (depending on whether we were searching for susceptible or resistant mutants, respectively).

Test and control plates were incubated for 6 days before adding 30 µL of 0.1 mg/mL resazurin as the bacterial growth indicator. After 48 h of incubation, colour changes from blue (no growth) to pink (growth) were visually evaluated. Susceptible mutants should not grow in the presence of sub-inhibitory concentrations of C9 (test plate) but should grow in the control plate (without C9), from where they were selected for validation of the susceptible phenotype. Resistant mutants should grow in the presence of inhibitory concentrations of C9.

Validation of the susceptible phenotype

As a primary validation assay, the MIC of C9 against potential susceptible mutants was determined doing 1.4-fold instead of 2-fold serial dilutions in order to detect subtle differences in their susceptibility profiles.

Decreases in drug sensitivity were also validated by growth testing in agar plates containing drugs. This assay was carried out by seeding 5 µL spots of 10-fold serial dilutions of the mutants (starting from adjusted suspensions of ca. 10^7 CFU/mL) in 7H10-OADC control plates (without drugs) and in agar plates containing sub-inhibitory concentrations of C9.

The growth of each potential susceptible mutant in the presence of C9 was assessed visually after 2-3 weeks of incubation at 37ºC. Confirmed susceptible mutants were propagated in 7H9-Tween-ADC and their DNA was isolated for LM-PCR and Sanger sequencing of the PCR product.

LM-PCR and Sanger sequencing of the PCR product

The LM PCR was performed to identify the insertion site of Tn*SPAZ* in the selected mutants [191]. Briefly, total DNA extracted from selected mutants was digested with *Sal*I endonuclease (10 U/µL, ThermoFisher) in a final volume of 20 µL, for 1 h at 37°C. Subsequently, the linker fragment *salpt* (generated by hybridization of oligos salPT and salGD shown in (**Table 33**) was ligated by adding 1 µL of *salpt* (25 µM), 1.5 units of T4 DNA Ligase (Invitrogen), ligase buffer (5x) and water. The solution was incubated for 60 min at 24°C, plus 10 min at 60°C. Then, a second digestion with *Sal*I for 15 min at 37°C was performed to eliminate self-ligated fragments. Using this processed DNA as a template, the flanking region of the transposon was PCR amplified using PrimeSTAR HS DNA Polymerase (Takara) and salGD/pBlaF4 primer pair (35 cycles of 98ºC 10 s and 68ºC 2 min) (**Figure 64**).

The PCR fragments were gel-purified (1% TAE) using SpeedTools PCR Clean-up kit (Biotools) according to the manufacturer instructions and sequenced to map the transposon insertion sites.

Table 33. Primers used in LM-PCR.

Primer	Sequence 5'-3'	Description
salPT	TCGAGCTCGTGC	To generate the linker fragment salpt
salGD	TAGCTTATTCCTCAAGGCACGAGC	To generate the linker fragment salpt and LM PCR
pBlaF4	GACCATCGACCACACGCTG	LM PCR. To sequence the PCR fragment and map the transposon insertion site

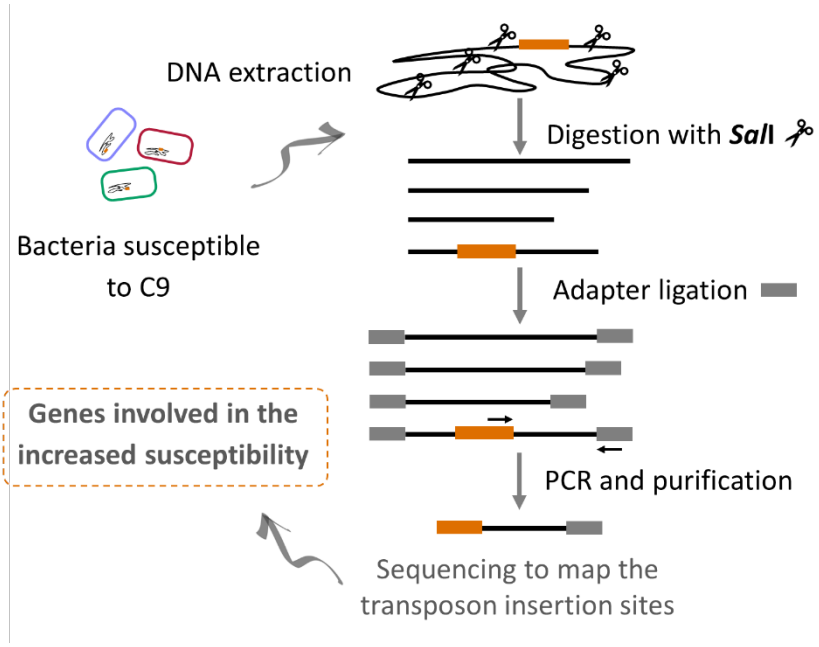

Figure 64. Schematic representation of LM-PCR. Total DNA is restriction digested with *Sal*I. Adapters are ligated and transposon junctions are PCR amplified with pBlaF4 and salGD primer pair. Tn*SPAZ* transposon is represented by an orange box.

Metabolic and physiological protocols

Oxygen consumption assays

Oxygen consumption assays were performed using BD™ Oxygen Biosensor System 96-well plates (BD Biosciences), which have a silicone base embedded with a fluorophore that is quenched by O_2 in a quantitative manner. When bacterial cell respiration consumes O_2 from the medium, the fluorescence emitted at 630 nm increases (after excitation at 485 nm). Thus, the amount of fluorescence signal is inversely proportional to the amount of O_2 in the sample [95].

First, it was necessary to set up the conditions of the assay, such as the bacterial density required to observe O_2 consumption. Three different inocula (10^5, 10^6 and 10^7 CFU/mL) of *M. abscessus* and *Mtb* were assayed in 7H9-Gly-ADC, in a final volume of 200 µL. These experiments indicated that a bacterial density of 10^7 CFU/mL of both *M. abscessus* and *Mtb* strains was needed to obtain the optimal signal-to-noise ratio.

Then, *M. abscessus* and *Mtb* cultures (at 10^7 cells/mL) were exposed to increasing concentrations of different antimicrobials in 200 µL of 7H9-Gly-ADC and data were collected for 16 h and 48 h, respectively, using a Synergy HT Microplate Reader (Biotek). Positive (bacteria without drugs) and negative (only medium) controls were also included.

ATP determination

Bacterial ATP was quantified using the BacTiter-Glo Microbial Cell Viability Assay (Promega). *Mtb* H37Rv cultures were grown at 37ºC in 7H9-Tween-ADC to mid-exponential phase, diluted to ca. 10^7 CFU/mL in 7H9-Gly-ADC and treated with several drugs in 96-well plates (Vf = 100 µL). After 24 and 48 h of incubation at 37ºC, 25 µL of samples were mixed with an equal volume of freshly prepared BacTiter-Glo reagent in white flat-bottomed 96-well plates (Corning) and lysis was carried out for 10 min in the dark at RT. Luminescence was measured using a Synergy HT Microplate Reader (Biotek). Control wells containing medium without bacteria were included to obtain a value for background luminescence.

The ATP content was also determined for certain drugs in parallel to time kill assays. In these experiments, samples were taken for both ATP determination and CFU enumeration, and the amount of ATP measured (expressed in relative light units, RLU) was normalized to bacterial viability ($RLU/CFU \cdot mL^{-1}$).

Ethidium bromide accumulation assays

The capacity of *M. smegmatis* to accumulate EtBr in the presence of C9 was evaluated in order to study whether this compound could be a potential efflux inhibitor. EtBr is a common efflux pump substrate which emits weak fluorescence in aqueous solution (out of the cell) and becomes strongly fluorescent when enters the bacteria due to its binding to nucleic acids.

M. smegmatis cultures were grown at 37ºC in 7H9-Tween-ADC until an OD_{600nm} of 0.6-0.8. Bacterial cultures were centrifuged (3500 g for 10 min) and pellets were washed in PBS. Then, the OD_{600nm} of the culture was adjusted to 0.8 in PBS supplemented with 0.4% glucose. Antimicrobial stocks were prepared in PBS supplemented with 2x EtBr (2 µg/mL) and 0.4% glucose. Before starting the kinetic assay, 100 µL of the bacterial suspension were transferred to wells containing 100 µL of antimicrobial stocks. VER, a well-known efflux inhibitor that increases EtBr accumulation, was included as a positive control. Untreated bacteria were also included as a negative control. Accumulation of EtBr was recorded fluorometrically with a Synergy HT Detection Microplate Reader (Biotek® Instruments), using 530/25nm and 590/20nm as excitation and detection wavelengths, respectively [159].

Nucleic acid and genetic engineering techniques

DNA extraction from *M. smegmatis* and *E. coli*

Genomic DNA was isolated using CTAB method [195]. Briefly, bacterial cultures were centrifuged. The pellets were resuspended in 400 µL of TE (100 mM Tris/HCl, 10 mM EDTA, pH = 8.0) and heat inactivated at 85°C for 15 min. Then, samples were slightly cooled at RT before adding 50 µL of 10 mg/mL lysozyme and incubated at 37°C for at least 1 h (but normally overnight). Subsequently, 75 µL of a solution containing 72.5 µL of 10 % SDS and 2.5 µL of proteinase K (20 mg/mL) were added and mixed by inversion, and the suspension warmed at 65°C for 10 min.

Afterwards, 100 µL of 5 M NaCl and 100 µL of CTAB/NaCl (10 % CTAB in 0.7 M NaCl) pre-warmed at 65°C for 10 min were added and samples incubated for further 10 min at 65°C. Then, genomic DNA was extracted by adding 750 µL of chloroform:isoamyl alcohol (24:1). Samples were mixed by inversion before centrifugation (12,000 rpm for 5 min). The upper aqueous phase was transferred to a new tube containing 420 µL of isopropanol and kept at -20°C for at least 30 minutes for DNA precipitation. Precipitated DNA was pelleted by centrifugation (12,000 rpm for 10 min) and the pellets were washed with 70 % ethanol. After centrifugation (12,000 rpm for 5 min), pellets were vacuum dried and resuspended in 50 µL of nuclease-free water.

DNA was quantified by absorbance readings at 260 nm (Abs_{260nm}) using a ND-1000 spectrophotometer (NanoDrop Technologies).

Plasmid and BAC extraction (Mini-prep) from *E. coli*

Purification of plasmid and BAC DNA was performed using High Pure Plasmid Purification Kit (Roche) or QuickClean II Plasmid Miniprep Kit (GeneScript) according to the manufacturer's instructions. Plasmid and BAC DNA were kept at - 20ºC.

Polymerase chain reaction (PCR)

PCR amplifications for genomic analyses were performed in a final volume of 10 µL or 50 µL with 0.38 and 1.87 U of Mytaq DNA polymerase (Bioline) respectively, 25 µM of each primer and MyTaq Reaction Buffer 5x. The PCR program consisted of an initial denaturation step at 95°C for 1 min, followed by 35 cycles (95°C 15 s, 58°C 15 s and 72°C 1 min/kb) and a final step of 7 min at 72°C. For colony PCR, the initial step was 95°C for 10 min. PCR amplification products were analysed in 0.8-1% agarose gel electrophoresis. DNA Molecular Weight 100 bp (base pairs) or λ *Pst*I were used for molecular weight comparison.

DNA fragments for cloning purposes were PCR amplified using the PrimeSTAR HS DNA polymerase (Takara Bio), which provides high fidelity amplification. PCR products were purified with SpeedTools PCR Clean-Up kit (Biotools) prior to their use in subsequent cloning steps.

Preparation of calcium chloride competent *E. coli* and heat-shock transformation

Calcium chloride protocol and heat-shock transformation was used to introduce foreign DNA into *E.* coli.

E. coli cultures of 200 mL were grown at 37°C until OD_{600nm} reached 0.4. Cultures were then centrifuged (4000 rpm for 10 min at 4°C) and pellets resuspended in 40 mL of ice-cold 100 mM $CaCl_2$ (Sigma-Aldrich), 70 mM $MgCl_2$ (Sigma-Aldrich) and 40 mM sodium acetate (Sigma-Aldrich) solution. Suspensions were centrifuged (4000 rpm for 10 min at 4°C) and pellets resuspended in 2 mL of ice-cold 100 mM $CaCl_2$ and 15% glycerol solution. Aliquots of 100 µL were stored at -80ºC.

When needed, competent bacteria were thawed on ice and 5 µL of ligation reaction (performed with T4 DNA ligase from Invitrogen) were added to the cells. Suspensions were kept on ice for 30 min before heating the mixture at 42ºC for 45 s. Following the heat shock step, tubes were placed on ice for 2 min. Bacteria were recovered in 1 mL of LB and incubated at 37°C for 1 h to allow the expression of antibiotic resistance genes. Finally, serial dilutions were plated onto LB agar plates containing the antibiotic required. Colonies appeared after overnight incubation at 37ºC.

Preparation of *E. coli* electrocompetent cells

Electroporation was used to introduce foreign DNA into *E. coli* DH10B.

A 100 mL bacterial culture was grown at 37°C until an OD_{600nm} of 0.4-0.6. In case of *E. coli* DH10B containing pKD46 plasmid, bacteria were grown at 30°C and induced with 0.15% arabinose at an OD_{600nm} of 0.1. When the optimal OD_{600nm} was reached, cultures were kept on ice for 30 min. After two washes with chilled water and one with cold 10% glycerol, bacteria were resuspended in 1 mL of chilled 10% glycerol. Aliquots of 50 µL were stored at -80ºC for further use.

When needed, competent cells were electroporated with 500 ng of purified PCR amplification product previously purified with SpeedTools PCR Clean-up kit (Biotools) or 250-500 ng of plasmid DNA in 0.2 cm cuvettes (Bio-Rad) with a single pulse (2500 V, 25 µF, 200 Ω) in a GenePulser XcellTM (Bio-Rad). Bacteria were recovered in 1 mL of LB and incubated at 37°C for 1 h before plating serial dilutions onto LB agar plates containing the antibiotic required. Colonies appeared after overnight incubation at 37ºC. Transformations of the thermosensitive pKD46 plasmid were incubated at 30ºC.

Preparation of electrocompetent cells of *Mtb*

Mtb H37Rv electrocompetent cells were prepared as described by Wards *et al*.[196]. Bacterial cultures of 200 mL of were grown to an OD_{600nm} of 0.6-0.8. Then, 20 mL of 2 M glycine were added, and cultures were incubated overnight at 37°C before preparing the electrocompetent cells. All the process was performed at RT. After two washes with water-0.05% Tween-80 and one with 10% glycerol-0.05% Tween-80, bacteria were resuspended in 2 mL of 10% glycerol-0.05% Tween-80. Aliquots of 200-400 µL were stored at -80ºC for further use.

Aliquots of 200-400 µL were electroporated with 250-500 ng of purified plasmid DNA in 0.2 cm cuvettes (Bio-Rad) with a single pulse (2500 V, 25 µF, 1000 Ω) in a GenePulser XcellTM (Bio-Rad). Bacteria were recovered in 1 mL of 7H9-ADC-0.05% Tween 80 and incubated overnight at 37°C to allow the expression of antibiotic resistance genes. Serial dilutions were plated onto 7H10-ADC agar plates containing the antibiotic required for selection. Colonies typically appeared after 3-4 weeks of incubation at 37°C.

Preparation of *Mtb* electrocompetent cells for recombineering and transformation

For the recombineering method, 200 mL cultures of *Mtb* H37Rv containing the pJV53H plasmid were grown until an OD_{600nm} of 0.6-0.8. Then, 0.2% acetamide (w/v) was added and the culture incubated at 37°C overnight. After four washes with 10% glycerol, bacteria were resuspended in 2 mL of 10% glycerol. Aliquots of 200-400 µL were transformed with ~500 ng of purified PCR amplification product in 0.2 cm cuvettes (Bio-Rad) with a single pulse (2500 V, 25 µF, 1000 Ω) in a GenePulser XcellTM (Bio-Rad). Bacteria were recovered in 1 mL of 7H9-ADC-0.05% Tween 80, incubated overnight at 37°C and plated onto 7H10-ADC with the required antibiotic. Colonies typically appeared in 3-4 weeks.

Construction of L5KO and L5S5KO *Mtb* mutants by BAC-recombineering

L5KO and L5S5KO *Mtb* mutants were constructed by BAC-recombineering. This technique uses an *Mtb* H37Rv genomic library constructed in the pBeloBAC11 BAC vector and introduced into *E. coli* DH10B [188]. The entire process of L5KO construction is summarized in **Figure 65**. Primers used for construction and verification of both stains are included in **Table 34**.

The first step was to obtain the allelic exchange substrates (AES) to be used in *Mtb* for gene deletion. Both *mmpL5* and *mmpL5/S5* AES were obtained using the λ Red recombinase system that allows homologous recombination in BACs containing the region with the targeted gene.

Steps performed in *E. coli*

E. coli DH10B containing the BAC Rv339, which has a large fragment of *Mtb* H37Rv genome (from nucleotides 742460 to 811258) including *mmpL5* and *mmpS5* genes, was transformed with pKD46. pKD46 is a thermosensitive plasmid that contains the λ Red recombinase system under the control of the inducible arabinose operon (**Figure 66**). The λ Red recombinase system consists of three genes (γ, β and *exo*) that code for Gam, Bet and Exo proteins, responsible for inhibiting host exonucleases and promoting recombination[187]. The transformation mix was plated onto LB-Amp-Cm and incubated overnight at 30°C. The presence of pKD46 was confirmed by PCR using pKD46-gam-fw and pKD46-bet-rv primers.

Then, a culture of *E. coli* DH10B BAC Rv339 pKD46 was induced with 0.15% arabinose for 3 h to trigger expression of the λ Red recombinase, and electrocompetent cells were prepared as described above. This strain was transformed, separately, with two fragments of DNA, in which the Km^R cassette from pKD4 plasmid[188] had been amplified so that each resulting PCR product was flanked by ~40 pb-arms identical to:

i) two regions in *mmpL5* gene; this PCR product would disrupt the *mmpL5* gene only when inserted into the Rv339 BAC in *E. coli.*

ii) a region in *mmpL5* gene and another region in *mmpS5* gene; this PCR product would disrupt the complete *mmpL5/S5* operon when inserted into the Rv339 BAC in *E. coli.*

Primers are shown in **Table 34**, and their sequences were designed according to the indications given in [187].

The transformation was incubated for 1 h at 37°C to allow expression of the Km^R cassette and to cure pKD46 plasmid. Subsequently, serial dilutions were plated onto LB-Km at 37°C. Recombination of the Km^R cassette at the correct location in the Rv339 BAC (*i.e.* deleting *mmpL5*, or mmpL5/S5 genes) was confirmed by PCR, using one primer outside from the ~40 bp of identity and the other inside the Km^R cassette.

Both *E. coli* DH10B BAC Rv339 Δ*mmpL5::km* and DH10B BAC Rv339 Δ*mmpS5L5::km* strains were grown overnight at 37°C in LB-Km. BACs Rv339 Δ*mmpL5::km* and Δ*mmpS5L5::km* were purified and used as templates to obtain *mmpL5* and *mmpS5/L5* AES, respectively, by PCR. AES products consisted of Km^R cassette flanked with approximately 1000 bp of identity arms for site specific recombination.

Steps performed in *Mtb*

Once the *Mtb* H37Rv pJV53H strain was grown until mid-log phase in 7H9-Tween-ADC, 0.2% acetamide was added to induce the expression of Che9c gp60 and gp61 proteins, responsible for increasing the recombination frequencies (**Figure 66**)[190]. Competent bacteria were prepared as previously described, electroporated separately with both AES and plated onto 7H10-ADC-Km.

Recombination was confirmed by PCR amplification with primers designed to hybridize outside of the genomic region amplified in the AES and primers inside the Km^R cassette.

Finally, *Mtb* H37Rv pJV53H Δ*mmpL5::km* (L5KO) and Δ*mmpS5L5::km* (L5S5KO) strains were grown in 7H9-Tween-ADC-Km without selection for Hyg resistance. Several passages were performed in this medium to cure the recombineering expression plasmid pJV53H.

Table 34. Primers used in the construction and verification of L5KO and L5S5KO strains.

Primer	Sequence 5' - 3'	Description
mmpL5-**P1**-Fw	tgaaatccgcatgatcgtgcaaaggacagctgcg ccgacggtgtaggctggagctgcttc	*mmpL5* identity arm. PCR amplification in pKD4.
mmpS5L5-**P1**-Fw	tgaacttcatgcggcagaggcggagggcgatgat tggaacgtgtaggctggagctgcttc	*mmpS5* identity arm. PCR amplification in pKD4.
mmpL5-**P2**-Rv	accagaaccactttccgaggagggccgcgatcga cggtgtcatgacatatgaatatcctccttagt	*mmpL5* identity arm. PCR amplification in pKD4.
KO-mmpL5-Fw	gtcggagacgacgttctcca	To confirm homologous recombination in BAC and to obtain *mmpL5* AES.
KO-mmpS5L5-Fw	accaccacgacagcgacga	To confirm homologous recombination in BAC and to obtain *mmpS5L5* AES.
KO-mmpL5-Rv	cgtaccacgacttcgccact	To confirm homologous recombination in BAC, and to obtain both *mmpL5* and *mmpS5L5* AES
conf-mmpL5-Fw	agtgaccacaggccaatcgc	To confirm L5KO in *Mtb*
conf-mmpS5L5-Fw	ttggcgacctttgctctggc	To confirm L5S5KO in *Mtb*
conf-mmpL5-Rv	cacctgctcaccgatccgat	To confirm L5KO and L5S5KO in *Mtb*
P1-inv	gaagcagctccagcctacac	Inside the Km^R cassette
P2-inv-long	cttcggaataggaactaaggaggatattcatatg	Inside the Km^R cassette
pKD46-gam-fw	cctgttttcctaatcagcccggc	pKD46 verification
pKD46-gam-rv	aaatgccgtctggcgaagagtg	pKD46 verification

In primers mmpL5-P1-Fw, mmpS5L5-P1-Fw, and mmpL5-P2-Rv, nucleotides identical to *mmpL5* and *mmpS5* genes are shown in green, and nucleotides identical to Km^R cassette in pKD4 plasmid are in blue.

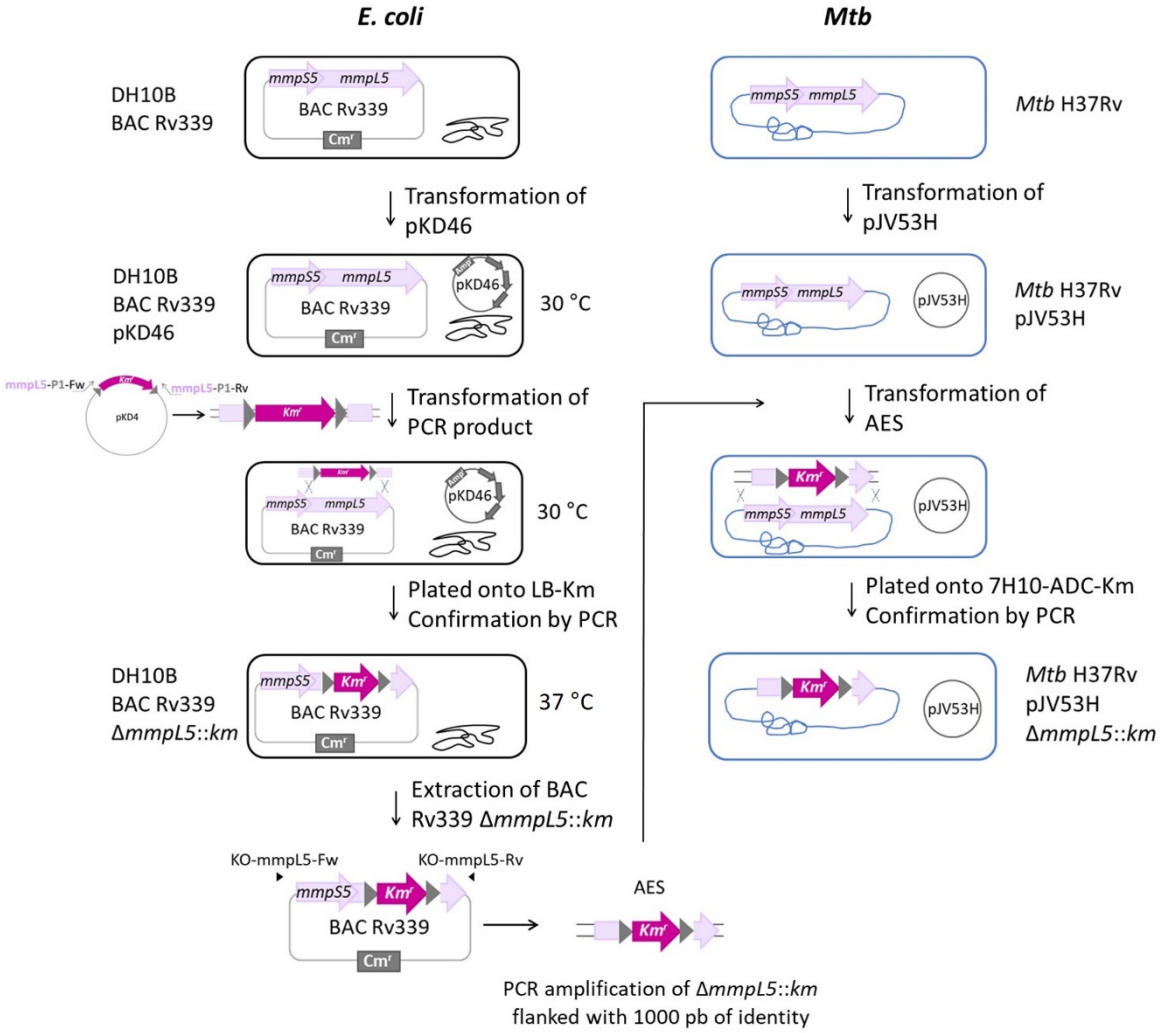

Figure 65. Schematic representation of *Mtb* L5KO construction by BAC-recombineering. Left column represents the steps performed in *E. coli* (grey) to obtain AES for transformation in *Mtb* (right column, bacteria represented in blue). *Mtb* L5S5KO construction followed a similar process.

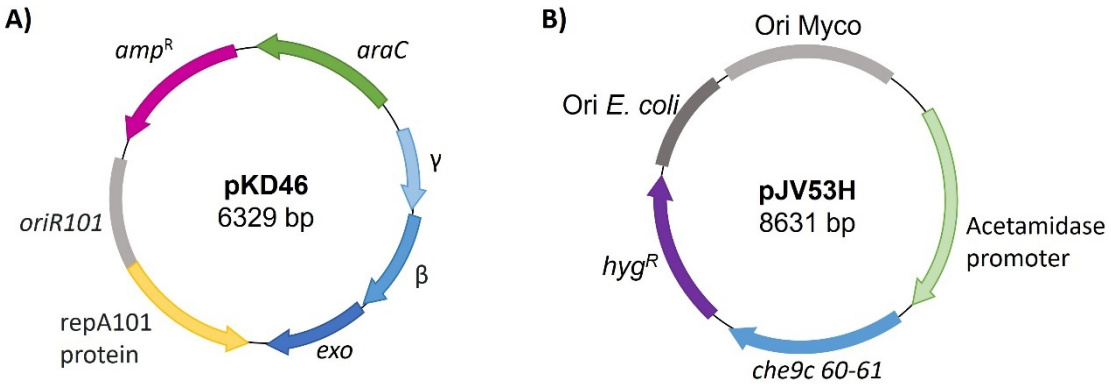

Figure 66. Components of pKD46 and pJV53H plasmids. (A) The replicative plasmid pKD46 contains the λ Red system (γ, β and exo genes) preceded by the arabinose-inducible promoter, RepA101 thermosensitive origin of *E. coli* and Amp resistance cassette. (B) pJV53H is a replicative plasmid that contains replication origins for *E. coli* and mycobacteria, a Hyg resistance cassette and mycobacteriophage Che9c gene products gp60 and gp61 expressed under the control of the acetamide-inducible promoter.

Construction of the replicative plasmid pACM1

A 3,905 bp DNA fragment containing the *mmpS5-mmpL5* operon from *Mtb* H37Rv was PCR amplified using the PrimeSTAR HS DNA polymerase (Takara Bio) with mmpS5L5-Fw/mmpS5L5-Rv primer pair and using the BAC Rv339 as template (**Table 35**). The PCR amplification product was gel-purified using SpeedTools PCR Clean-up kit (Biotools), digested with the restriction enzyme *Hin*dIII and inserted into pSUM36 replicative vector previously digested with *Hin*dIII and 5'-dephosphorylated with alkaline phosphatase (Roche). Ligations were performed with T4 DNA ligase (Invitrogen) according to the manufacturer's instructions. Then, *E. coli* Stellar™ competent cells (prepared as previously described) were transformed with the ligation reaction and plated onto LB-Km-IPTG-X-Gal agar plates to check *lacZ* phenotype. After overnight incubation at 37ºC, recombinant colonies (which appeared in white colour due to the lack of α-complementation) were cultured in LB-Km and plasmid DNA was purified as described above.

The orientation of *mmpS5*/*L5* operon in pSUM36 was confirmed using pSUR1-Fw/ACM4-Rv and pSUR1-Rv/ACM4-Rv primer pairs (see **Figure 67B** for insert orientation). Moreover, when the resulting plasmid pACM1 was digested with *Hin*dIII, two fragments of ~5000 bp and ~4000 bp (corresponding to pSUM36 and mmpS5/L5 operon, respectively) were obtained.

The replicative plasmid pACM1 was transformed in *Mtb* H37Rv competent cells and its presence was confirmed by PCR using pSUR1-Fw and ACM4-Rv primer pair.

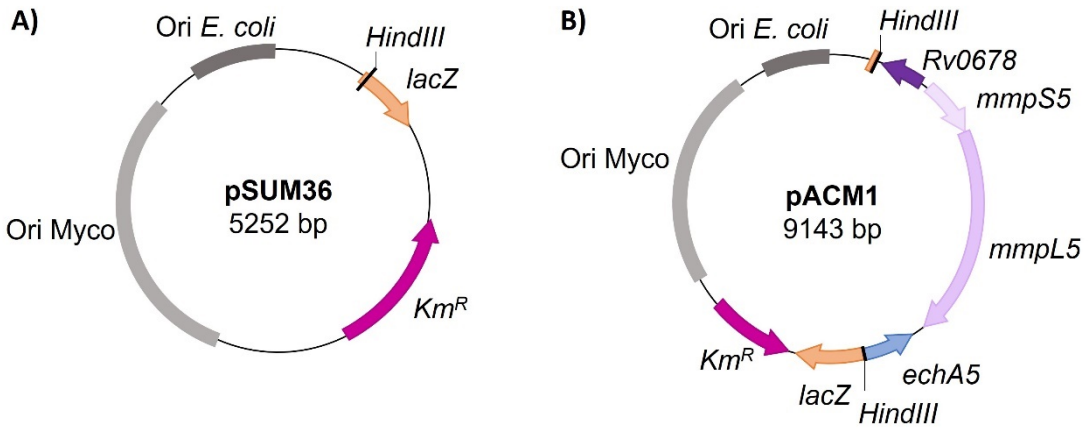

Figure 67. Replicative plasmid pSUM36 and its derivative pACM1. (A) pSUM36 contains replication origins of *E. coli* and mycobacteria, Km resistance cassette and *lacZ* gene. (B) pACM1 carries *Mtb* H37Rv *mmpS5*/*mmpL5* operon.

The DNA fragment amplified and inserted into pSUM36 included the natural promoter of the operon. Consequently, the overexpression of *mmpS5* and *mmpL5* genes is due to the presence of multiple copies of this plasmid.

Table 35. Primers used to amplify the region containing the *mmpS5-mmpL5* operon from *Mtb* H37Rv. Sequence in upper-case were artificially added for cloning purposes.

Primer	Sequence 5'- 3'	Description
mmpS5L5-Fw	TTTTAAGCTTtcgggatcacacaccag	*Hin*dIII site underlined. To amplify *mmpS5/L5* operon.
mmpS5L5-Rv	TTTTAAGCTTatgatcctcactggccgt	*Hin*dIII site underlined. To amplify *mmpS5/L5* operon.
pSUR1-Fw	gcacttcactgacaccctca	To confirm insert orientation in pSUM36 and presence of pACM1 in *Mtb*.
pSUR1-Rv	gactctggggttcgaaatga	To confirm insert orientation in pSUM36.
ACM-4 Rv	tcatcgagatcatcgacggt	To confirm *mmpS5/L5* orientation and presence of pACM1 in *Mtb*.

RNA extraction

RNA extraction from mycobacteria

For mode of action studies of C9, *Mtb* H37Rv cultures were grown in 7H9-ADC supplemented with 0.2% glycerol and 0.025% tyloxapol until an OD_{600nm} of 0.2-0.3 was reached. Cultures were then distributed in 75 cm^2 tissue culture flasks and exposed to C9 at the selected concentrations (***Chapter 1,* Table 26**) for 4 h, 1 day and 9 days before RNA extraction.

For efflux pump Tap studies, three independent cultures of *Mtb* H37Rv wild type and KOTap mutant were grown in 7H9-Tween-ADC at 37ºC to mid-logarithmic phase (6 days; OD_{600nm}=0.2-0.3) or to stationary phase (6 weeks; OD_{600nm}=2.5-3).

In both cases, once grown, bacteria were centrifuged at 3500 rpm for 10 min and pellets were resuspended in 500 µL of wash buffer (0.137 M NaCl and 0.5 % Tween-80 in H_2O DEPC) and 1 mL of RNA protect reagent (Qiagen) to minimize RNA degradation. Bacterial suspensions were centrifuged at 14000 rpm for 5 min after 5-minute incubation at RT and supernatants were discarded. At this point, pellets were stored at -80°C until all samples were collected.

Next steps of the protocol were performed on ice. Pellets were resuspended in 400 µL of fresh lysis buffer (20 mM sodium acetate, 0.5 % SDS and 0.1 mM EDTA) and 1 mL of acid-phenol:chloroform (5:1, pH = 4.5). Bacterial suspensions were transferred to screw tubes containing glass beads (MP Biomedicals) and lysed by mechanical disruption (Fast-Prep) in two cycles (45 s at 6.5 m/s each cycle). Samples were kept on ice for 5 min between pulses.

Then, tubes were centrifuged at 14000 rpm for 5 min at 4°C and the upper aqueous phases were transferred to tubes containing 900 µL of chilled chloroform:isoamylic alcohol (24:1). After centrifugation at 14,000 rpm for 5 min at 4°C, the upper phases were transferred to fresh tubes containing 900 µL of isopropanol and 90 µL of 3 M sodium acetate pH = 5.5 (Invitrogen). Samples were incubated overnight at -20°C for RNA precipitation. All these steps were carried out in the BSL3 laboratory. Hereinafter, subsequent steps were performed in BSL1 facilities.

Precipitated nucleic acids were collected by centrifugation (14,000 rpm for 30 min at 4°C). Supernatants were discarded and pellets were washed with 1 mL of 70 % ethanol. After centrifugation at 14,000 rpm for 5 min at 4°C, pellets were air-dried until ethanol was evaporated and resuspended in RNase-free water (Ambion).

DNA was removed from RNA samples by three consecutive incubations (1h at 37°C) with 1 µL of Turbo DNase (Invitrogen). Then, 0.1 volumes of DNase inactivation reagent were added for removal of Turbo DNase from the samples. After 5 minutes of incubation at RT, samples were centrifuged at 10000 g for 1.5 minutes and supernatants were carefully transferred to fresh tubes.

RNA extraction from *E. coli*

E. coli cultures incubated overnight at 37ºC with shaking were diluted ~1/100 in LB broth about 2 h prior to RNA extraction. When *E. coli* cultures reached an OD_{600nm} of 0.5-0.6, 500 µL of bacterial suspensions were transferred to new tubes and 1 mL of RNA protect reagent (Qiagen) was added. Suspensions were mixed by vortexing for 5 s and incubated for 5 min at RT before centrifugation at 5000 g for 10 min. Then, supernatants were discarded, and pellets were stored at -80°C.

Afterwards, *E. coli* pellets were defrosted, resuspended in 100 µL of TE buffer (30 mM Tris/HCl, 1 mM EDTA, pH 8.5) containing 3 mg/mL of lysozyme and incubated at RT for 5 min. Subsequent RNA purification steps were performed using the RNeasy Mini Kit (Qiagen) according to manufacturer instructions. Briefly, 350 µL of RLT buffer containing β-mercaptoethanol and 350 µL of absolute ethanol were added to the samples. Lysates were transferred to RNeasy mini spin columns placed in 2 mL collection tubes and centrifuged for 15 s at 8000 g. Then, 700 µL of buffer RW1 were added to spin columns before centrifugation at 8000 g for 15s. Once the flowthroughs were discarded, 500 µL of buffer RPE were added to spin columns and centrifuged at 8000 g for 15s (this step was performed twice). Finally, RNA was eluted by adding 30 µL of RNase-free water directly to the spin column membrane and centrifuging for 1 min at 8000 g. DNA was removed from RNA samples using Turbo DNA-free kit (Invitrogen) according to manufacturer instructions.

For mycobacteria and *E. coli* RNA samples, RNA concentration was estimated by reading of Abs_{260nm}/Abs_{280nm} using a ND-1000 spectrophotometer (NanoDrop). RNA integrity was assessed by agarose gel electrophoresis and absence of DNA was confirmed by lack of amplification products after 30 PCR cycles using BCG2A/BCG2B or 16S-F/16S-R primer pairs for mycobacteria and *E. coli* samples, respectively (**Table 36**). RNA samples were stored at -80°C.

Table 36. Primers used to confirm lack of DNA in RNA samples.

Primers	Sequence 5' - 3'	Description
BCG2A	gccgtccatcccgggcatc	Used for *Mtb*
BCG2B	ccatgttcaaaccggtgtc	Used for *Mtb*
16S-F	aggattagataccctggtagtcca	Used for *E. coli*
16S-R	aggcccgggaacgtattcac	Used for *E. coli*

Whole Genome Sequencing (WGS)

Library preparation and Illumina sequencing of genomic DNA extracted from *E. coli ΔacrB* wild type and ten mutants resistant to C2 was performed by the Sequencing and Bioinformatics Service of FISABIO (*Fundación para el Fomento de la Investigación Sanitaria y Biomédica de la Comunidad Valenciana*).

For the computational analysis of the WGS data, reads quality was first assessed using FastQC, a quality control tool for high throughput sequence data[197]. Then, quality-controlled sequencing reads (fastq files) were aligned to the reference genome of *E. coli* BW25113 (available at https://www.ncbi.nlm.nih.gov/refseq/) using the Burrows-Wheeler Aligner (BWA) software package with the bwa-mem option [198]. BWA uses a Burrow-Wheeler Transform to efficiently align sequencing reads to reference genomes allowing for gaps and mismatches. The output of BWA is the sequence alignment map format (known as SAM).

Afterwards, the SAMtools software package [199] was used to convert sam files to bam format and to sort the aligned reads. Duplicate reads were eliminated using the MarkDuplicates tool of PicardTools [200]. These bam files (sorted and without duplicates) were indexed using SAMtools and alignments were visualized on Tablet visor[201]. SNP calling was done using VarScan (variant detection in massively parallel sequencing data)[202], a tool that requires the pileup files generated with SAMtools from bam files (sorted and without duplicates). These SNPs were annotated using SnpEff, a variant annotation and effect prediction tool[203]. Indel calling was done using the tool HaplotypeCaller of GATK (Genome Analysis ToolKit) [204].

Transcriptomics

Library preparation of total RNA extracted from mycobacteria (in triplicates) and Illumina sequencing was performed by the Sequencing Unit of CNAG (*Centro Nacional de Análisis Genómico*). Libraries were sequenced on the Illumina NovaSeq 6000 System using 2 x 150 bp paired-end reads.

Read alignment and differential gene-expression analysis

For the computational analysis of RNA-seq data, reads quality was first assessed using FastQC, and low quality and adaptor sequences were trimmed from fastq files using Trim Galore[205]. Kallisto program[206] was then used to map the trimmed fastq files to the reference genome of *Mtb* H37Rv (Mycobacterium_tuberculosis_H37Rv_genes_v4), a fasta file that was downloaded from Mycobrowser (https://mycobrowser.epfl.ch/). Subsequently, *tximport* R package was used to import kallisto transcript abundances, estimated counts and transcript lengths into RStudio [207].

Afterwards, *edgeR* R package was employed to get counts per million (cpm), and to filter and normalize the data (using the TMM method)[208]. Genes were only retained if they were expressed at a cpm above 1 in at least 3 samples. Filtered and normalized cpm generated with *edgeR* were used for Principal Component Analysis (PCA), a statistical procedure often used to obtain an overview of large data tables and to visualize the relationships among samples.

Limma R package was used for differential gene expression analysis. Specifically, VOOM function from *limma* was applied to model the mean-variance relationship, and then a lineal model was fitted to the data [209]. The differential expression analysis was performed making the comparisons indicated in **Table 37**.

Table 37. Comparisons made for differential gene expression analysis.

RNA-seq project	Condition	Comparison
C9 mode of action studies	4 h of treatment	C9 80 µg/mL *vs* untreated control
	1 day of treatment	C9 8 µg/mL *vs* untreated control
	1 day of treatment	C9 32 µg/mL *vs* untreated control
	9 days of treatment	C9 8 µg/mL *vs* untreated control
Tap efflux pump studies	Exponential phase	KOTap *vs* H37Rv
	Stationary phase	KOTap *vs* H37Rv

As a result, log_2FC and p-adj were generated for each gene and condition compared.

Then, decideTests function from *limma* was used to select DEGs with statistical significance. The filtered gene list was made using a cut-off of p-adj ≤ 0.05 and log_2FC values ≥ 1 (for overexpressed genes) or ≤1 (for downregulated genes). Volcano plots, which were built by plotting -log_{10}P-adj *vs* log_2FC of each gene, allow visualization of statistical DEGs.

Functional category analysis

A functional category analysis was performed with the statistical DEGs from the abovementioned comparisons, using the functional categories described in Mycobrowser (https://mycobrowser.epfl.ch/). *Mtb* H37Rv genome was divided into the following categories: (1) cell wall and cell processes, (2) conserved hypotheticals, (3) information pathways, (4) insertion sequences and phages, (5) intermediary metabolism and respiration, (6) lipid metabolism, (7) PE/PPE, (8) regulatory proteins, (9) stable RNAs, (10) virulence, detoxification and adaptation, and (11) unknown.

Biological pathways analysis

The biological pathways analysis was performed with the statistical DEGs from each comparison using BiNGO, a tool that determines which GO terms are significantly overrepresented in a set of genes [210]. BiNGO requires a gene annotation file of the organism (in this case, *Mtb* H37Rv), which contains the genes of the organism associated with the corresponding GO terms, and a gene ontology file, which links the GO terms with their biological functions.

Quantitative Real Time PCR (qRT-PCR)

Reverse transcription was performed using 500 ng of RNA, 2 µL of Prime Script RT Master Mix (Takara) and RNase-free dH_2O (Takara) until a total volume of 10 µL per reaction. cDNA was obtained after 15 min at 37ºC and 15 s at 85ºC for enzyme inactivation.

TB Green Premix Ex Taq™ (Tli RNase H Plus) (Takara) was used for qRT-PCR reaction. Specific primers were used at a final concentration of 0.25 µM and 1 µL of 1/10 diluted cDNA was added to the reaction mixture. Each reaction was performed in triplicate in the StepOne Plus Real Time PCR System (Applied Biosystems). The PCR amplification program was 95ºC for 10 min followed by 40 cycles of 95ºC for 15 s and 60ºC for 1 min.

Melting curves were performed for each pair of primers to verify that the fluorescence levels were due to the amplification of a specific product. Primers used for qRT-PCR were designed using the PrimerQuest Tool from Integrated DNA Technologies website and are included in **Table 38**. Gene expression was normalized to the expression levels of the housekeeping genes *gapA* and *rrsA* (for *E. coli* samples) or *sigA* (for *Mtb* samples).

Table 38. Primers used for gene expression analysis by qRT-PCR.

Gene	Forward 5'- 3'	Reverse 5' - 3'
Escherichia coli		
rrsA	TCGGAATTACTGGGCGTAAAG	GACTCAAGCTTGCCAGTATCA
gapA	ACTTACGAGCAGATCAAAGC	AGTTTCACGAAGTTGTCGTT
acrB	CATCCTCGTGTTCCTGGTTATG	GCAAAGGTCCCGAGCAATA
acrE	GCTCGCATCAATCTTGCTTATAC	GTTCAGTCGTTTGCCCATTAG
acrD	CTACCGATGGTTCGATGGATAAA	CAGCCAGATACGCATGGAATA
mdtA	CCAGACGCATCCTATCGATTTA	CTTCTACCACCAGCGGTTT
mdtE	CTACGTTAGCCGTCAGGATTAC	AGATTGATCGTCGCCTGTTC
emrK	CGCTGGAGCATACCAAAGATA	CTTGTGGCTGACGGTTTAATG
***Mycobacterium tuberculosis or Mycobacterium bovis* BCG**		
PE8	GCGTACGGCACCTTCTACCA	TTCCCAGAGTGTTGACAAACATG
mbtI	GCCCTGGAAGCCCTTTTTC	CCAGCTGCTTTCGGGATTC
Rv2627c	ACGTCCGGTCAGCAATCATC	AAATCCGCTAGGCTTCTCCA
irtA	GGCCACCGCGTTTGC	CCGGTTAAGCGCCTGTTG
Rv2005c	CGATGCGGCGATGAGGAACA	CCTCGTCCTCCTGCCAAACC
Rv2032 (*acg*)	TTTACGCGACCGACCACTCC	CGCCAGATGCAAAGGATCGT
Rv1738	CGACATATCGATCGACGAAC	GCCAACACCCACCAATTCCT
Rv2628	GATGTGGTCGGATAGGCAGGT	CCTGATAGATGGTGGCGGATTG
Rv2031c (*hspX*)	ATGGCCACCACCCTTCCCGTT	TGTCGAAGGTGGGCCGGAGT
Rv1737c (*narK2*)	CGTGTTCGGTATGGGCATGG	GATGGCGTGGGTGGTGAACAG
Rv3128c	GTGTGTTGGAGTTTGGGCGTGA	TCTTTGGCCTTCGCGGTCTT
Rv3133c (*dosR*/*devR*)	CCGACCGAATGTTCCTAGCC	TCAACTCCGTCGCGAATACC
sigA	CCGATGACGACGAGGAGATC	CGGAGGCCTTGTCCTTTTC
mmpL4	CGCCCTGCCTGGATACAA	GGGTATGAAGTCCGGTAGGTAGTC
mmpL5	TGCCACGTTCTGTCTGAGCTT	GGCACACCGAGGGTCTGA
tap	GGGTATGCCGTGTTGGCTAT	ATGCCAAACCCAGGGTAAGAA
icl1	CCAGAACCAGATGAGCGCGTAT	GGCCCTCTTCGGTGGAAC
ctaD	GCGTCGCGTGCATAAGCTTTT	GCCGTGCATGGTGAACAACTG

APPENDICES

Appendix I. Standard mutant isolation assays

During my Master Thesis [87], two complementary approaches were used to try to isolate mutants resistant to the compounds:

- 10^5, 10^6, 10^7 and 10^8 CFU of *S. aureus* wild type strain were plated onto Cation-adjusted Müller-Hinton (CaMH) agar plates supplemented with C1 at two inhibitory concentrations (4x and 10xMIC) or plates containing gradient concentrations of C1 (from 0 to 10xMIC), thus exposing the bacteria to a complete range of inhibitory concentrations.
- A transposon library of *M. smegmatis* HS42 mutants were plated onto CaMH agar plates supplemented with C9 at inhibitory concentrations (20 and 50 µg/mL) at different inoculum levels (10^5, 10^6, 10^7 and 10^8 CFU).

Table AI.1. Summary of the experimental conditions used for the isolation of *S. aureus* and *M. smegmatis* mutants resistant to C1, C9, RIF and INH. Frequencies of mutation were calculated as the ratio of total number of colonies isolated in the presence of the drug over the total CFUs seeded. Results from [87].

Strain	Inoculum	Compound concentration (x MIC)	Colonies isolated	Frequency of mutation
S. aureus	10^5-10^8 CFU	C1 16-40 µg/mL (4x-10x)	0	$<10^{-8}$
	10^7 CFU	RIF 0.032 µg/mL (4x)	28	$3.4 \cdot 10^{-6}$
		RIF 0.08 µg/mL (10x)	14	$1.7 \cdot 10^{-6}$
M. smegmatis	10^5-10^8 CFU	C9 20-50 µg/mL	0	$<10^{-8}$
	10^6 CFU	INH 160 µg/mL (10x)	18	$1.8 \cdot 10^{-5}$

In summary, no *S. aureus* nor *M. smegmatis* colonies resistant to these compounds could be isolated by these approaches, while mutants resistant to RIF and INH were identified (antimicrobials used as functionality controls).

Appendix II. Validation of *M. bovis* BCG mutants potentially susceptible to C9

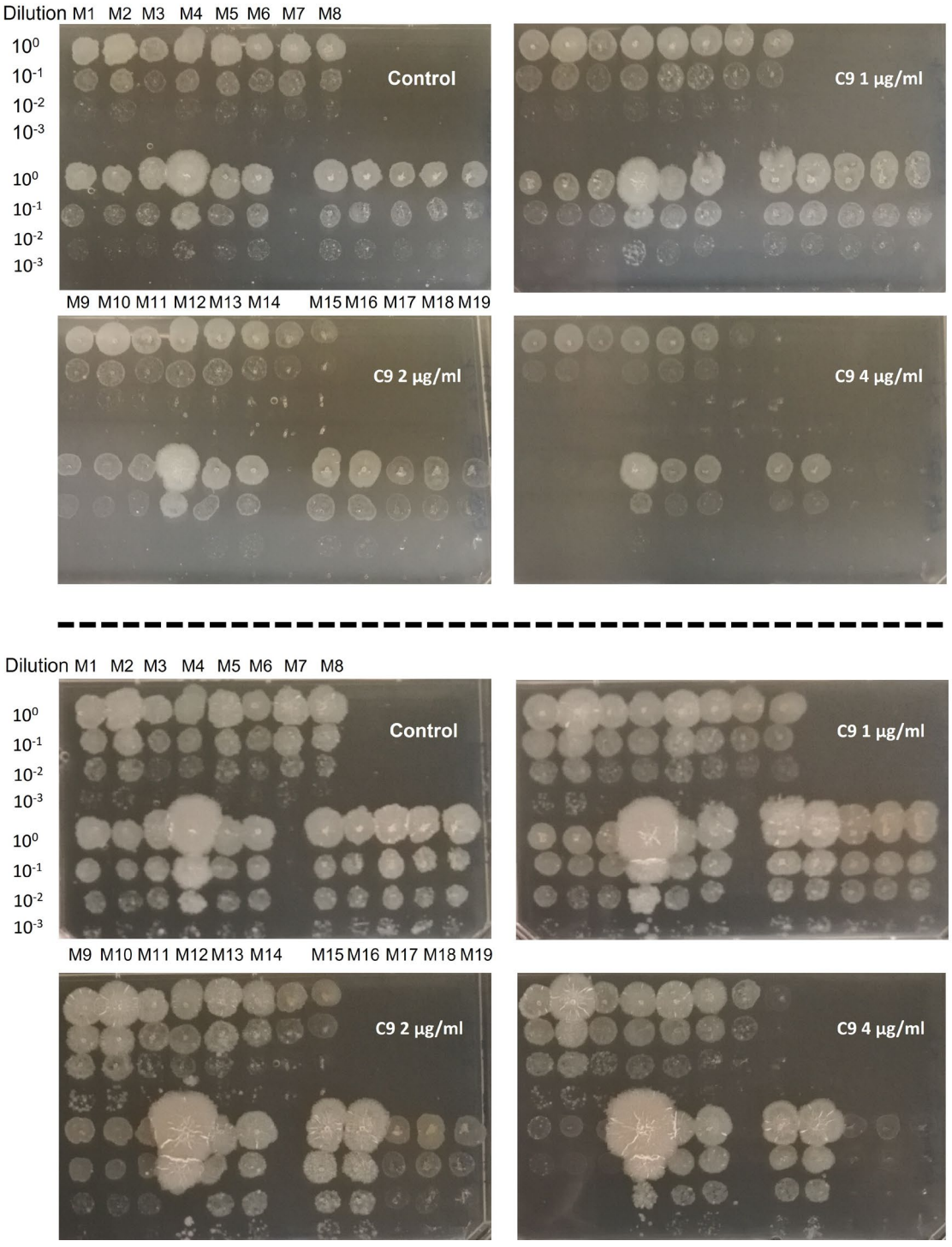

Figure AII.1. Susceptibility testing in agar plates of 19 *M. bovis* BCG candidate mutants. 10-fold serial dilutions of a 0.12 OD_{600nm} suspension were seeded on agar plates containing none (control) or sub-inhibitory concentrations of C9 (1, 2 or 4 µg/mL). Agar plates were incubated at 37 ºC, and pictures were taken after 10 (upper panel) and 18 days (lower panel).

Appendix III. Characterization of the activity of the compounds against Gram-negative bacteria

During my Master Thesis[87], the activity of the this chemical series was characterized against *P. aeruginosa* and *K. pneumoniae*.

Table AIII.1. Susceptibility of *P. aeruginosa* and *K. pneumoniae* to the compounds in the presence or in the absence of several EI (CCCP, REP, VER or PAβN) at sub-inhibitory concentrations. Results from [87].

Strain	Condition	MIC values (µg/ml)		
		C1	C2	C9
P. aeruginosa	w/o EI	>64	>64	>64
	PAβN 32 µg/mL	8	4	16
	CCCP 4 µg/mL	>64	>64	>64
	REP 32 µg/mL	>64	>64	>64
K. pneumoniae	w/o EI	>64	>64	>64
	PAβN 32 µg/mL	32	8	32
	CCCP 0.25 µg/mL	>64	>64	>64
	REP 32 µg/mL	>64	>64	>64
	VER 32 µg/mL	>64	>64	>64

EI: efflux inhibitor; PAβN: phenylalanine-arginine β-naphthylamide; CCCP: carbonyl cyanide 3-chlorophenylhydrazone; REP: reserpine; VER: verapamil.

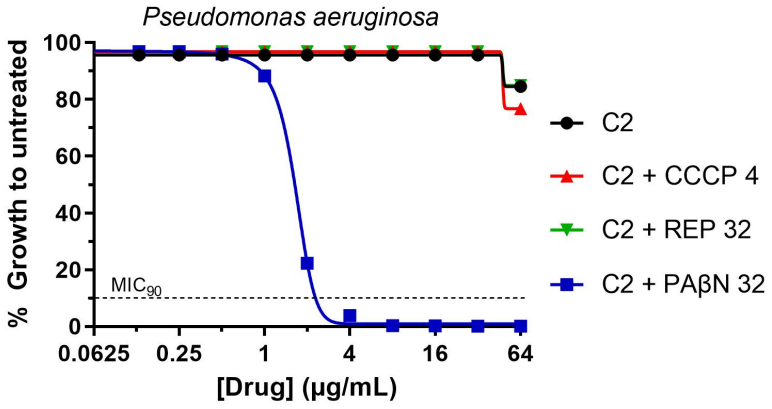

Figure AIII.1. Dose response characterization of C2 alone or in combination with CCCP, REP or PAβN at sub-inhibitory concentrations against *P. aeruginosa*. Results from [87].

Appendix IV. Characterization of *E. coli* Δ*acrB*-derived candidate double mutants

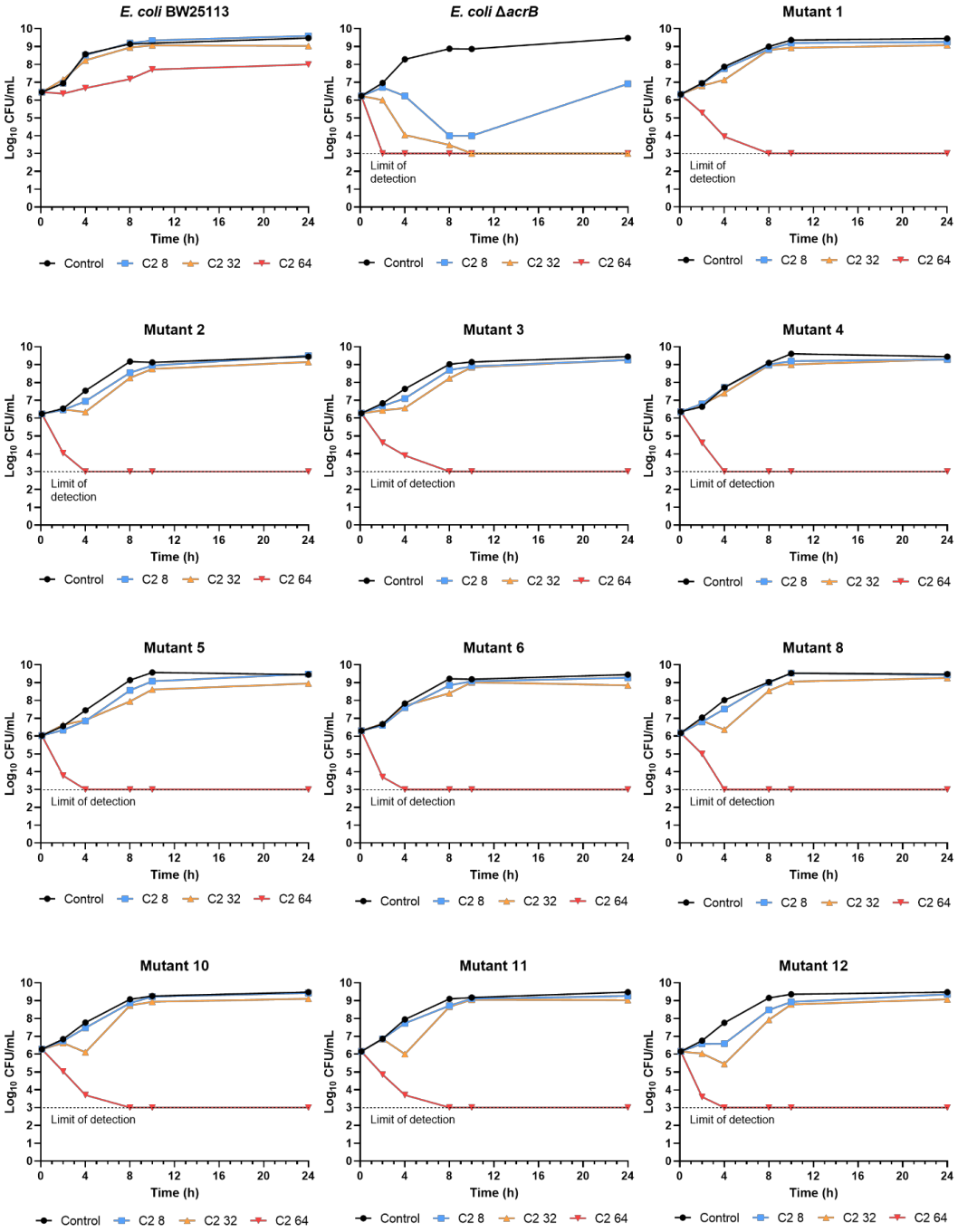

Figure IV.1. Time kill assays of C2 against *E. coli* BW25113, Δ*acrB* single mutant and ten Δ*acrB*-derived candidate double mutants. Overnight *E. coli* cultures were 1/1000 diluted in LB and drugs were added at the indicated concentrations.

Appendix V. Synergism between butyrophenones and Tap substrates in *M. smegmatis* and *Mtb*

Prior to this work, the synergistic interaction between butyrophenones and Tap substrates was evaluated in different bacterial strains (*Santiago Ramón-García & José A. Aínsa, unpublished*).

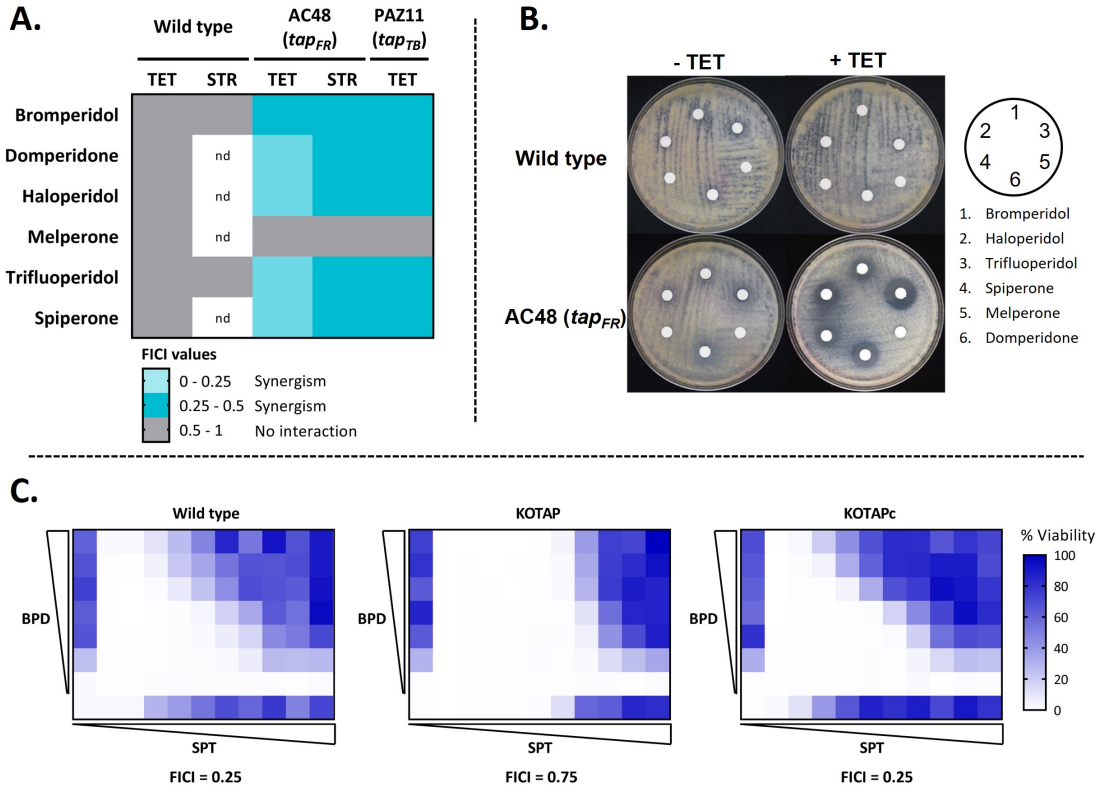

Figure AV.1. Butyrophenone-Tap specificity in mycobacteria (*Santiago Ramón García & José A. Aínsa, unpublished*).

A) Several butyrophenones (bromperidol, domperidone, haloperidol, melperone, trifluoperidol and spiperone) were tested for synergistic activities with TET and STR in *M. smegmatis* wild type, *M. smegmatis* AC48 (overexpressing *tap* from *Mycobacterium fortuitum*, tap_{FR}) and *M. smegmatis* PAZ11 (overexpressing *tap* from *Mtb*, tap_{TB}) by checkerboard assays. Butyrophenone MICs for all three strains were 64-128 µg/mL. Overexpression of tap_{FR} resulted in a 16-fold increase in the MICs of TET and STR compared to the wild type strain. Overexpression of tap_{TB} conferred a low increase (2-fold) in the MIC of STR and a 4-8-fold increase in the MIC of TET; thus, only TET was employed with the tap_{TB} overexpression strain.

B) Several butyrophenones were tested for synergistic activities with TET against *M. smegmatis* wild type and *M. smegmatis* AC48 by disc diffusion assays. Exponential-phase cultures of *M. smegmatis* were spread on NE agar[156] control plates (left side) and agar plates supplemented with 0.25xMIC of TET (right side). Discs containing several butyrophenones (50 µg/disc) were placed onto the lawn as indicated. Visible growth was scored after 72 h of incubation at 37°C.

C) Interaction profiles of BPD and SPT against *Mtb* H37Rv wild type, KOTAP and KOTAPc. Drugs were assayed in a checkerboard format using 2-fold serial dilutions. SPT was assayed in the x-axis while BPD was assayed in the y-axis. Gradient colour from white to blue indicate the percentage of growth over untreated controls

Table AV.1. Synergistic interactions between butyrophenones and different families of compounds against diverse bacterial strains.

Strain	CMPD_A	CMPD_B	[1]MIC_A	[1]MIC_B	FICI
M. smegmatis					
Wild type	Bromperidol	TET	64-128	0.06	1
Wild type	Domperidone	TET	64-128	0.06	1
Wild type	Haloperidol	TET	64-128	0.06	1
Wild type	Melperone	TET	64-128	0.06	1
Wild type	Trifluperidol	TET	64-128	0.06	1
Wild type	Spiperone	TET	64-128	0.06	1
Wild type	Bromperidol	STR	64-128	0.03	1
Wild type	Trifluperidol	STR	64-128	0.03	1
AC48 (*tap*$_{FR}$)	Bromperidol	TET	64-128	1	0.24-0.31
AC48 (*tap*$_{FR}$)	Domperidone	TET	64-128	1	0.19-0.31
AC48 (*tap*$_{FR}$)	Haloperidol	TET	64-128	1	0.18
AC48 (*tap*$_{FR}$)	Melperone	TET	64-128	1	0.75
AC48 (*tap*$_{FR}$)	Trifluperidol	TET	64-128	1	0.18
AC48 (*tap*$_{FR}$)	Spiperone	TET	64-128	1	0.18
AC48 (*tap*$_{FR}$)	Bromperidol	STR	64-128	0.5	0.37
AC48 (*tap*$_{FR}$)	Domperidone	STR	64-128	0.5	0.37
AC48 (*tap*$_{FR}$)	Haloperidol	STR	64-128	0.5	0.31-0.37
AC48 (*tap*$_{FR}$)	Melperone	STR	64-128	0.5	1
AC48 (*tap*$_{FR}$)	Trifluperidol	STR	64-128	0.5	0.37
AC48 (*tap*$_{FR}$)	Spiperone	STR	64-128	0.5	0.37
PAZ11(*tap*$_{TB}$)	Bromperidol	TET	64-128	0.5-1	0.31-0.37
PAZ11(*tap*$_{TB}$)	Domperidone	TET	64-128	0.5-1	0.5
PAZ11(*tap*$_{TB}$)	Haloperidol	TET	64-128	0.5-1	0.37
PAZ11(*tap*$_{TB}$)	Melperone	TET	64-128	0.5-1	0.62
PAZ11(*tap*$_{TB}$)	Trifluperidol	TET	64-128	0.5-1	0.37
PAZ11(*tap*$_{TB}$)	Spiperone	TET	64-128	0.5-1	0.31-0.37
M. tuberculosis					
H37Rv	BPD	SPT	64	64	0.25
KOTAP	BPD	SPT	64	2	0.75
KOTAPc	BPD	SPT	64	64	0.25

[1]MIC values are in µg/mL. FICI is the Fractional Inhibitory Concentration Index. An FICI≤0.5 indicates synergy; an FICI > 0.5 indicates no interaction. BPD, bromperidol; SPT, spectinomycin.

Appendix VI. Chapter 2 results summary tables

Data for analysis done in sections 3.2.2 and 3.3.1. of Chapter 2.

Table VI.1. CFU/mL values used to calculate the replication rates of *Mtb* H37Rv and KOTap mutant in THP-1 cell line (Figure 43).

Time (day)	H37Rv			KOTap		
0	4.95E+05	3.75E+05	-	3.30E+05	4.13E+05	3.65E+05
2	2.10E+06	2.50E+06	3.90E+06	1.75E+06	1.45E+06	1.65E+06
4	3.00E+06	2.60E+06	3.25E+06	1.90E+06	1.45E+06	1.32E+06

Table VI.2. CFU/mL values used to calculate the replication rates of *M. bovis* BCG and the KOTap mutant in the *in vitro* granuloma model (Figure 45).

Donors	Time (day)	BCG			KOTap		
Donor 25	**1**	9.20E+03	7.80E+03	6.20E+03	9.00E+03	1.16E+04	1.18E+04
	4	2.82E+04	2.70E+04	2.52E+04	2.60E+04	2.24E+04	3.200E+04
	8	9.20E+04	1.06E+05	1.26E+05	1.20E+05	1.08E+05	8.200E+04
Donor 30	**1**	7.00E+03	6.20E+03	6.60E+03	1.02E+04	1.14E+04	5.80E+03
	4	2.18E+04	2.28E+04	2.52E+04	2.66E+04	2.42E+04	2.40E+04
	8	2.00E+04	4.00E+04	2.00E+04	9.00E+04	6.00E+04	7.40E+04
Donor 27	**1**	2.48E+04	2.54E+04	3.16E+04	2.12E+04	2.24E+04	2.24E+04
	4	7.60E+04	6.20E+04	7.60E+04	4.20E+04	7.00E+04	5.40E+04
	8	-	1.30E+06	1.18E+06	2.46E+05	2.52E+05	2.90E+05

Table VI.3. CFU/mL values used to calculate the percentage of RIF-tolerant *M. bovis* BCG bacteria (Figure 46).

Time (day)	Control						RIF 0.1					
	BCG	BCG	BCG	KOTap	KOTap	KOTap	BCG	BCG	BCG	KOTap	KOTap	KOTap
4	7.6E+04	6.2E+04	7.6E+04	4.2E+04	7.0E+04	5.4E+04	4.0E+01	4.0E+01	1.2E+02	4.2E+02	6.6E+02	4.0E+02
11	2.8E+06	7.4E+06	2.4E+06	7.0E+05	5.8E+05	6.8E+05	2.2E+04	8.6E+04	2.2E+04	1.9E+04	2.2E+04	2.3E+04

Table VI.4. CFU/mL values used to calculate the replication rates of *Mtb* and KOTap mutant in the *in vitro* granuloma model (Figure 49).

Donors	Time (day)	*Mtb*		KOTap	
Donor 4	1	1.20E+04	1.23E+04	1.50E+04	1.36E+04
	4	6.00E+04	6.60E+04	7.00E+04	6.50E+04
	8	6.50E+05	5.05E+05	5.60E+05	5.70E+05
Donor 3	1	1.25E+04	6.65E+03	1.00E+04	5.30E+03
	4	7.50E+04	6.80E+04	7.50E+04	5.55E+04
	8	2.10E+05	2.20E+05	2.20E+05	1.40E+05
	11	4.50E+05	3.00E+05	2.00E+05	2.80E+05
Donor 1	1	1.14E+04	1.25E+04	7.23E+03	1.50E+04
	4	8.00E+04	7.40E+04	3.00E+04	3.75E+04
	8	4.00E+05	2.00E+05	1.50E+05	2.15E+05
	11	9.00E+05	8.00E+05	5.00E+05	6.55E+05

Table VI.5. CFU/mL values used to calculate the percentage of RIF-tolerant *Mtb* (**Figure 50**).

Donors	Time (day)	Control				RIF			
		Mtb	*Mtb*	KOTap	KOTap	*Mtb*	*Mtb*	KOTap	KOTap
Donor 4	1-4	8.70E+04	9.10E+04	7.05E+04	9.15E+04	3.05E+03	3.03E+03	4.08E+03	4.68E+03
	8-11	2.53E+05	8.35E+05	2.80E+05	4.38E+05	4.28E+04	9.08E+04	3.90E+04	3.00E+04
Donor 3	1-4	7.00E+04	5.40E+04	8.00E+04	8.85E+04	2.90E+03	2.00E+03	2.50E+03	3.40E+03
	8-11	3.00E+05	2.90E+05	3.00E+05	3.55E+05	7.50E+04	4.33E+04	5.43E+04	5.60E+04
Donor 1	1-4	7.00E+04	7.35E+04	4.50E+04	5.85E+04	3.50E+03	2.10E+03	3.00E+03	2.30E+03
	8-11	8.95E+05	8.50E+05	1.25E+06	5.78E+05	5.85E+04	7.40E+04	8.25E+04	8.30E+04

REFERENCES

REFERENCES

1. World Health Organization. Global Tuberculosis Report 2021. *WHO* (2021).
2. Pai, M. *et al.* Tuberculosis. *Nat. Rev. Dis. Prim.* **2**, 16076 (2016).
3. Daniel, T. M. The history of tuberculosis. *Respir. Med.* **100**, 1862–1870 (2006).
4. Barberis, I., Bragazzi, N. L., Galluzzo, L. & Martini, M. The history of tuberculosis: from the first historical records to the isolation of Koch's bacillus. *J Prev Med Hyg* **58**, E9–E12 (2017).
5. Daniel, T. M. Jean-Antoine Villemin and the infectious nature of tuberculosis. *Int. J. Tuberc. Lung Dis.* **19**, 267–268 (2015).
6. Sakula, A. Robert Koch: centenary of the discovery of the tubercle bacillus, 1882. *Thorax* **37**, 246–51 (1982).
7. Warren, P. The evolution of the sanatorium: the first half-century, 1854-1904. *Can Bull Med Hist.* **23**, 457–476 (2006).
8. Calmette, A. On preventive vaccination of the new-born against tuberculosis by B.C.G. *Br. J. Tuberc.* **22**, 161–165 (1928).
9. Herzog, H. History of tuberculosis. *Respiration* **65**, 5–15 (1998).
10. Ma, Z., Lienhardt, C., McIlleron, H., Nunn, A. J. & Wang, X. Global tuberculosis drug development pipeline: the need and the reality. *Lancet* **375**, 2100–2109 (2010).
11. Bhagwat, A., Deshpande, A. & Parish, T. How Mycobacterium tuberculosis drug resistance has shaped anti-tubercular drug discovery. *Front. Cell. Infect. Microbiol.* **12**, 974101 (2022).
12. Murray, J. F., Schraufnagel, D. E. & Hopewell, P. C. Treatment of Tuberculosis. A Historical Perspective. *Ann. Am. Thorac. Soc.* **12**, 1749–1759 (2015).
13. World Health Organization. Tuberculosis: a global emergency. *WHO* https://apps.who.int/iris/handle/10665/52639 (1993).
14. World Health Organization. The end TB strategy. *WHO* https://www.who.int/publications/i/item/WHO-HTM-TB-2015.19 (2015).
15. World Health Organization. Global Tuberculosis Report 2022. *WHO* (2022).
16. Pai, M., Kasaeva, T. & Swaminathan, S. Covid-19's Devastating Effect on Tuberculosis Care — A Path to Recovery. *N. Engl. J. Med.* **386**, 1490–1493 (2022).
17. Getahun, H., Matteelli, A., Chaisson, R. E. & Raviglione, M. Latent Mycobacterium tuberculosis infection. *N. Engl. J. Med.* **372**, 2127–2135 (2015).
18. Johansen, M. D., Herrmann, J.-L. & Kremer, L. Non-tuberculous mycobacteria and the rise of Mycobacterium abscessus. *Nat. Rev. Microbiol.* **18**, 392–407 (2020).
19. Percival, S. L. & Williams, D. W. Mycobacterium. in *Microbiology of Waterborne Diseases: Microbiological Aspects and Risks.* 177–207 (Academic Press, 2014). doi:10.1016/B978-0-12-415846-7.00009-3.
20. Chiaradia, L. *et al.* Dissecting the mycobacterial cell envelope and defining the composition of the native mycomembrane. *Sci. Rep.* **7**, 12807 (2017).
21. Akira, S., Uematsu, S. & Takeuchi, O. Pathogen recognition and innate immunity. *Cell* **124**, 783–801 (2006).
22. Philips, J. A. & Ernst, J. D. Tuberculosis Pathogenesis and Immunity. *Annu. Rev. Pathol.* **7**, 353–384 (2012).

23. Zuñiga, J. *et al.* Cellular and humoral mechanisms involved in the control of tuberculosis. *Clin. Dev. Immunol.* **2012**, 193923 (2012).
24. Ndlovu, H. & Marakalala, M. J. Granulomas and inflammation: Host-directed therapies for tuberculosis. *Front. Immunol.* **24**, 434 (2016).
25. Armstrong, R. M. & Zahrt, T. C. Mycobacteria Infection and Lipid Droplets: Host and Pathogen Stealing, Sharing and Storing Fat. in *Tuberculosis Host-Pathogen Interactions* 201–229 (Springer, Cham, 2019). doi:10.1007/978-3-030-25381-3_9.
26. Ramakrishnan, L. Revisiting the role of the granuloma in tuberculosis. *Nat. Rev. Immunol.* **12**, 352–366 (2012).
27. Zheng, H. & Abramovitch, R. B. Host–Pathogen Interactions Influencing Mycobacterium tuberculosis Persistence and Drug Tolerance. in *Persister Cells and Infectious Disease* 217–245 (Springer, Cham, 2019). doi:10.1007/978-3-030-25241-0_10.
28. Vilchèze, C. & Kremer, L. Acid-Fast Positive and Acid-Fast Negative Mycobacterium tuberculosis: The Koch Paradox. *Microbiol. Spectr.* **5**, (2017).
29. Balaban, N. Q. *et al.* Definitions and guidelines for research on antibiotic persistence. *Nat. Rev. Microbiol.* **17**, 441–448 (2019).
30. Goossens, S. N., Sampson, S. L. & Van Rie, A. Mechanisms of drug-induced tolerance in mycobacterium tuberculosis. *Clin. Microbiol. Rev.* **34**, e00141-20 (2020).
31. World Health Organization. Global Tuberculosis Report 2019. *WHO* (2019).
32. Behinaein, P. & Cirillo, J. The Silent Plague: Regulation of Latent Tuberculosis Infections. in *Tuberculosis Host Pathogen Interactions* 23–42 (Springer International Publishing, 2019). doi:10.1007/978-3-030-25381-3_2.
33. Gengenbacher, M. & Kaufmann, S. H. E. Mycobacterium tuberculosis: Success through dormancy. *FEMS Microbiol. Rev.* **36**, 514–532 (2012).
34. Kim, M. *et al.* Caseation of human tuberculosis granulomas correlates with elevated host lipid metabolism. *EMBO Mol. Med.* **2**, 258–274 (2010).
35. Cheung, L. S., Srikrishna, G. & Bishai, W. R. Role of Myeloid-Derived Suppressor Cells and Regulatory T-Cells in the Tuberculous Granuloma. in *Tuberculosis Host-Pathogen Interactions* 63–93 (Springer Nature Switzerland, 2019). doi:10.1007/978-3-030-25381-3_4.
36. Kurosu, M. Cell Wall Biosynthesis and Latency During Tuberculosis Infections. in *Tuberculosis Host Pathogen Interactions* 1–21 (Springer Nature Switzerland, 2019). doi:10.1007/978-3-030-25381-3_1.
37. Luies, L. & Preez, I. du. The echo of pulmonary tuberculosis: Mechanisms of clinical symptoms and other disease-induced systemic complications. *Clin. Microbiol. Rev.* **33**, e00036-20 (2020).
38. Martín, C., Marinova, D., Aguiló, N. & Gonzalo-Asensio, J. MTBVAC, a live TB vaccine poised to initiate efficacy trials 100 years after BCG. *Vaccine* **39**, 7277–7285 (2021).
39. Arbues, A. *et al.* Construction, characterization and preclinical evaluation of MTBVAC, the first live-attenuated M. tuberculosis-based vaccine to enter clinical trials. *Vaccine* **31**, 4867–4873 (2013).
40. TBVI. TB vaccine pipeline, 2022. https://www.tbvi.eu/what-we-do/pipeline-of-vaccines/ (2022).
41. Nandlal, L., Perumal, R. & Naidoo, K. Rapid Molecular Assays for the Diagnosis of Drug-Resistant Tuberculosis. *Infect. Drug Resist.* **15**, 4971–4984 (2022).
42. World Health Organization. WHO consolidated guidelines on tuberculosis. Module

3: rapid diagnostics for tuberculosis detection, 2021 update. *WHO* (2021).

43. Nahid, P. *et al.* Official American Thoracic Society/Centers for Disease Control and Prevention/Infectious Diseases Society of America Clinical Practice Guidelines: Treatment of Drug-Susceptible Tuberculosis. *Clin. Infect. Dis.* **63**, e147–e195 (2016).
44. World Health Organization. Guidelines for treatment of drug-susceptible tuberculosis and patient care, 2017 update. *WHO* (2017).
45. World Health Organization. WHO consolidated guidelines on tuberculosis. Module 4: Treatment. Drug-susceptible tuberculosis treatment. *WHO* (2022).
46. World Health Organization. The WHO/IUATLD Global Project on Anti-Tuberculosis Drug Resistance Surveillance. Antituberculosis drug resistance in the world: third global report. *WHO* (2004).
47. World Health Organization. Meeting report of the WHO expert consultation on the definition of extensively drug-resistant tuberculosis. *WHO* (2020).
48. World Health Organization. Global Tuberculosis Report 2018. *WHO* (2018).
49. World Health Organization. Rapid communication: Key changes to the treatment of drug-resistant tuberculosis. *WHO* (2022).
50. World Health Organization. WHO consolidated guidelines on tuberculosis. Module 4: treatment. Drug-resistant tuberculosis treatment. *WHO* (2022).
51. Conradie, F. *et al.* Bedaquiline-Pretomanid-Linezolid Regimens for Drug-Resistant Tuberculosis. *N. Engl. J. Med.* **387**, 810–823 (2022).
52. World Health Organization. WHO consolidated guidelines on tuberculosis. Module 4: treatment. Drug-resistant tuberculosis treatment. *WHO* (2020).
53. Teixeira, M. C. *et al.* New Insights in to the Intrinsic and Acquired Drug Resistance Mechanisms in Mycobacteria. *Front. Microbiol.* **8**, 681 (2017).
54. Singh, R. *et al.* Recent updates on drug resistance in Mycobacterium tuberculosis. *J. Appl. Microbiol.* **128**, 1547–1567 (2020).
55. Ramón-García, S. *et al.* Functional and genetic characterization of the tap efflux pump in Mycobacterium bovis BCG. *Antimicrob. Agents Chemother.* **56**, 2074–2083 (2012).
56. Burian, J. *et al.* The mycobacterial transcriptional regulator whiB7 gene links redox homeostasis and intrinsic antibiotic resistance. *J. Biol. Chem.* **287**, 299–310 (2012).
57. Geiman, D. E., Raghunand, T. R., Agarwal, N. & Bishai, W. R. Differential gene expression in response to exposure to antimycobacterial agents and other stress conditions among seven Mycobacterium tuberculosis whiB-like genes. *Antimicrob. Agents Chemother.* **50**, 2836–2841 (2006).
58. Hernando-Amado, S. *et al.* Multidrug efflux pumps as main players in intrinsic and acquired resistance to antimicrobials. *Drug Resist. Updat.* **28**, 13–27 (2016).
59. Andries, K. *et al.* Acquired resistance of Mycobacterium tuberculosis to bedaquiline. *PLoS One* **9**, e102135 (2014).
60. Hartkoorn, R. C., Uplekar, S. & Cole, S. T. Cross-resistance between clofazimine and bedaquiline through upregulation of MmpL5 in Mycobacterium tuberculosis. *Antimicrob. Agents Chemother.* **58**, 2979–2981 (2014).
61. Milano, A. *et al.* Azole resistance in Mycobacterium tuberculosis is mediated by the MmpS5-MmpL5 efflux system. *Tuberculosis (Edinb).* **89**, 84–90 (2009).
62. Egorova, A., Jackson, M., Gavrilyuk, V. & Makarov, V. Pipeline of anti-Mycobacterium abscessus small molecules: Repurposable drugs and promising novel chemical entities. *Med. Res. Rev.* **41**, 2350–2387 (2021).

63. Hughes, J. P., Rees, S. S., Kalindjian, S. B. & Philpott, K. L. Principles of early drug discovery. *Br. J. Pharmacol.* **162**, 1239–1249 (2011).

64. Hughes, D. & Karlén, A. Discovery and preclinical development of new antibiotics. *Ups. J. Med. Sci.* **119**, 162–169 (2014).

65. Keseru, G. M. & Makara, G. M. Hit discovery and hit-to-lead approaches. *Drug Discov. Today* **11**, 741–748 (2006).

66. Gwynn, M. N., Portnoy, A., Rittenhouse, S. F. & Payne, D. J. Challenges of antibacterial discovery revisited. *Ann. N. Y. Acad. Sci.* **1213**, 5–19 (2010).

67. Matano, L. M., Morris, H. G., Wood, B. M. K., Meredith, T. C. & Walker, S. Accelerating the discovery of antibacterial compounds using pathway-directed whole cell screening. *Bioorg. Med. Chem.* **24**, 6307–6314 (2016).

68. Chung, H. Drug Discovery and Development. *BioAI* https://medium.com/bioai/drug-discovery-and-development-31758bf6cc72.

69. Farha, M. A. & Brown, E. D. Drug repurposing for antimicrobial discovery. *Nat. Microbiol.* **4**, 565–577 (2019).

70. Mukherjee, T. & Boshoff, H. Nitroimidazoles for the treatment of TB: past, present and future. *Futur. Med Chem* **3**, 1427–1454 (2011).

71. Grzelak, E. M. *et al.* Strategies in anti-Mycobacterium tuberculosis drug discovery based on phenotypic screening. *J. Antibiot. (Tokyo).* **72**, 719–728 (2019).

72. Hariguchi, N. *et al.* OPC-167832, a novel carbostyril derivative with potent antituberculosis activity as a DPRE1 inhibitor. *Antimicrob. Agents Chemother.* **64**, e02020-19 (2020).

73. Working Group on New TB Drugs. Drug discovery pipeline. https://www.newtbdrugs.org/pipeline/clinical.

74. Foo, C. S.-Y., Pethe, K. & Lupien, A. Oxidative Phosphorylation-an Update on a New, Essential Target Space for Drug Discovery in Mycobacterium tuberculosis. *Appl. Sci.* **10**, 2339 (2020).

75. Bald, D., Villellas, C., Lu, P. & Koul, A. Targeting Energy Metabolism in Mycobacterium tuberculosis, a New Paradigm in Antimycobacterial Drug Discovery. *MBio* **8**, e00272-17 (2017).

76. Jacobs, W. R. A world without tuberculosis: moving from imagination to reality. *J. Clin. Invest.* **132**, e162688 (2022).

77. Dupont, C. *et al.* Bedaquiline Inhibits the ATP Synthase in Mycobacterium abscessus and Is Effective in Infected Zebrafish. *Antimicrob. Agents Chemother.* **61**, e01225-17 (2017).

78. Singh, S., Bouzinbi, N., Chaturvedi, V., Godreuil, S. & Kremer, L. In vitro evaluation of a new drug combination against clinical isolates belonging to the Mycobacterium abscessus complex. *Clin. Microbiol. Infect.* **20**, O1124–O1127 (2014).

79. Singh, V. & Mizrahi, V. Identification and validation of novel drug targets in Mycobacterium tuberculosis. *Drug Discov. Today* **22**, 503–509 (2017).

80. Hudson, M. A. & Lockless, S. W. Elucidating the Mechanisms of Action of Antimicrobial Agents. *MBio* **13**, e0224021 (2022).

81. Chen, X., Li, Y., Wang, B. & Lu, Y. Identification of Mutations Associated With Macozinone-Resistant in Mycobacterium Tuberculosis. *Curr. Microbiol.* **79**, 205 (2022).

82. O'Neill, A. J. & Chopra, I. Use of Mutator Strains for Characterization of Novel Antimicrobial Agents. *Antimicrob. Agents Chemother.* **45**, 1599–1600 (2001).

83. Pulido, M. R., García-Quintanilla, M., Gil-Marqués, M. L. & McConnell, M. J. Identifying targets for antibiotic development using omics technologies. *Drug Discov. Today* **21**, 465–472 (2016).

84. Venter, H. *et al.* Genome-Wide Transcriptional Responses of Mycobacterium to Antibiotics. *Front. Microbiol.* **10**, 249 (2019).

85. Santos, N. C. D. S. *et al.* Minimum Bactericidal Concentration Techniques in Mycobacterium tuberculosis: A Systematic Review. *Microb. Drug Resist.* **26**, 752–765 (2020).

86. Dartois, V. A. & Rubin, E. J. Anti-tuberculosis treatment strategies and drug development: challenges and priorities. *Nat. Rev. Microbiol.* **20**, 685–701 (2022).

87. Millán-Placer, A. C. Estudios iniciales para la caracterización del modo de acción molecular de una nueva serie química con actividad antimicrobiana. *Master thesis* (2018).

88. Andries, K. *et al.* A diarylquinoline drug active on the ATP synthase of Mycobacterium tuberculosis. *Science.* **307**, 223–227 (2005).

89. Melly, G. & Purdy, G. E. MmpL Proteins in Physiology and Pathogenesis of M. tuberculosis. *Microorganisms* **7**, 70 (2019).

90. Richard, M. *et al.* Mutations in the MAB_2299c TetR Regulator Confer Cross-Resistance to Clofazimine and Bedaquiline in Mycobacterium abscessus. *Antimicrob. Agents Chemother.* **63**, e01316-18 (2019).

91. Wells, R. M. *et al.* Discovery of a siderophore export system essential for virulence of Mycobacterium tuberculosis. *PLoS Pathog.* **9**, e1003120 (2013).

92. Vergara, R. B. Characterization of the MmpL4/MmpS4 efflux system in Mycobacterium bovis and Mycobacterium tuberculosis. (PhD Thesis, University of Zaragoza, 2015).

93. Rodriguez, G. M., Voskuil, M. I., Gold, B., Schoolnik, G. K. & Smith, I. ideR, an essential gene in Mycobacterium tuberculosis: Role of IdeR in iron-dependent gene expression, iron metabolism, and oxidative stress response. *Infect. Immun.* **70**, 3371–3381 (2002).

94. Mobarra, N. *et al.* A review on iron chelators in treatment of iron overload syndromes. *Int. J. Hematol. Stem Cell Res.* **10**, 239–247 (2016).

95. Gomez-Lorenzo, M. G. *et al.* Functional screening of selective mitochondrial inhibitors of Plasmodium. *Int. J. Parasitol. Drugs Drug Resist.* **8**, 295–303 (2018).

96. Kumar Akela, A. & Kumar, A. Bioenergetic Heterogeneity in Mycobacterium tuberculosis Residing in Different Subcellular Niches. *MBio* **12**, e0108821 (2021).

97. Lobritz, M. A. *et al.* Antibiotic efficacy is linked to bacterial cellular respiration. *Proc. Natl. Acad. Sci. U. S. A.* **112**, 8173–8180 (2015).

98. Zeng, S. *et al.* Isoniazid Bactericidal Activity Involves Electron Transport Chain Perturbation. *Antimicrob. Agents Chemother.* **63**, e01841-18 (2019).

99. Shetty, A. & Dick, T. Mycobacterial Cell Wall Synthesis Inhibitors Cause Lethal ATP Burst. *Front. Microbiol.* **9**, 1898 (2018).

100. Lamprecht, D. A. *et al.* Turning the respiratory flexibility of Mycobacterium tuberculosis against itself. *Nat. Commun.* **7**, 12393 (2016).

101. Berube, B. J. & Parish, T. Combinations of Respiratory Chain Inhibitors Have Enhanced Bactericidal Activity against Mycobacterium tuberculosis. *Antimicrob. Agents Chemother.* **62**, e01677-17 (2017).

102. Lechartier, B. & Cole, S. T. Mode of Action of Clofazimine and Combination Therapy with Benzothiazinones against Mycobacterium tuberculosis. *Antimicrob. Agents Chemother.* **59**, 4457–4463 (2015).

103. Vilchèze, C. *et al.* Enhanced respiration prevents drug tolerance and drug resistance in Mycobacterium tuberculosis. *Proc. Natl. Acad. Sci. U. S. A.* **114**, 4495–4500 (2017).

104. Vilchèze, C. & Jacobs, W. R. The Isoniazid Paradigm of Killing, Resistance, and Persistence in Mycobacterium tuberculosis. *J. Mol. Biol.* **431**, 3450–3461 (2019).

105. Vilchèze, C., Hartman, T., Weinrick, B. & Jacobs, W. R. Mycobacterium tuberculosis is extraordinarily sensitive to killing by a vitamin C-induced Fenton reaction. *Nat. Commun.* **4**, 1881 (2013).

106. Siddiqi, N. *et al.* Molecular Characterization of Multidrug-Resistant Isolates of Mycobacterium tuberculosis from Patients in North India. *Antimicrob. Agents Chemother.* **46**, 443–450 (2002).

107. Iwao, Y. & Nakata, N. Roles of the three Mycobacterium smegmatis katG genes for peroxide detoxification and isoniazid susceptibility. *Microbiol. Immunol.* **62**, 158–167 (2018).

108. Lindman, M. & Dick, T. Bedaquiline Eliminates Bactericidal Activity of β-Lactams against Mycobacterium abscessus. *Antimicrob. Agents Chemother.* **63**, e00827-19 (2019).

109. Yang, J. H. *et al.* A White-Box Machine Learning Approach for Revealing Antibiotic Mechanisms of Action. *Cell* **177**, 1649-1661.e9 (2019).

110. Ruth, M. M. *et al.* A bedaquiline/clofazimine combination regimen might add activity to the treatment of clinically relevant non-tuberculous mycobacteria. *J. Antimicrob. Chemother.* **74**, 935–943 (2019).

111. Lee, J. *et al.* Differential in vitro activities of individual drugs and bedaquiline-rifabutin combinations against actively multiplying and nutrient-starved Mycobacterium abscessus. *Antimicrob. Agents Chemother.* **65**, e02179-20 (2021).

112. Jaffré, J. *et al.* Rational Choice of Antibiotics and Media for Mycobacterium avium Complex Drug Susceptibility Testing. *Front. Microbiol.* **11**, 81 (2020).

113. Schoutrop, E. L. M. *et al.* The stability of antimycobacterial drugs in media used for drug susceptibility testing. *Diagn. Microbiol. Infect. Dis.* **92**, 305–308 (2018).

114. Kalia, N. P. *et al.* Exploiting the synthetic lethality between terminal respiratory oxidases to kill Mycobacterium tuberculosis and clear host infection. *Proc. Natl. Acad. Sci. U. S. A.* **114**, 7426–7431 (2017).

115. Scherr, N. *et al.* Targeting the Mycobacterium ulcerans cytochrome bc1:aa3 for the treatment of Buruli ulcer. *Nat. Commun.* **9**, 5370 (2018).

116. Blanco, P., Sanz-García, F., Hernando-Amado, S., Martínez, J. L. & Alcalde-Rico, M. The development of efflux pump inhibitors to treat Gram-negative infections. *Expert Opin. Drug Discov.* **13**, 919–931 (2018).

117. Nishino, K. & Yamaguchi, A. Role of Histone-Like Protein H-NS in Multidrug Resistance of Escherichia coli. *J. Bacteriol.* **186**, 1423–1429 (2004).

118. Ueguchi, C., Seto, C., Suzuki, T. & Mizuno, T. Clarification of the dimerization domain and its functional significance for the Escherichia coli nucleoid protein H-NS. *J. Mol. Biol.* **274**, 145–151 (1997).

119. Rodriguez, G. M., Sharma, N., Biswas, A. & Sharma, N. The Iron Response of Mycobacterium tuberculosis and Its Implications for Tuberculosis Pathogenesis and Novel Therapeutics. *Front. Cell. Infect. Microbiol.* **12**, 876667 (2022).

120. Sritharan, M. Iron Homeostasis in Mycobacterium tuberculosis: Mechanistic Insights into Siderophore-Mediated Iron Uptake. *J. Bacteriol.* **198**, 2399–2409 (2016).

121. Schuessler, D. L. & Parish, T. The Promoter of Rv0560c Is Induced by Salicylate and Structurally-Related Compounds in Mycobacterium tuberculosis. *PLoS One* **7**, e34471 (2012).

122. Warrier, T. *et al.* N-methylation of a bactericidal compound as a resistance mechanism in Mycobacterium tuberculosis. *Proc. Natl. Acad. Sci. U. S. A.* **113**, E4523–E4530 (2016).

123. Arnold, F. M. *et al.* The ABC exporter IrtAB imports and reduces mycobacterial siderophores. *Nature* **580**, 413–417 (2020).

124. Tufariello, J. A. M. *et al.* Separable roles for Mycobacterium tuberculosis ESX-3 effectors in iron acquisition and virulence. *Proc. Natl. Acad. Sci. U. S. A.* **113**, E348–E357 (2016).

125. Tullius, M. V., Nava, S. & Horwitz, M. A. PPE37 is essential for mycobacterium tuberculosis heme-iron acquisition (HIA), and a defective PPE37 in Mycobacterium bovis BCG prevents HIA. *Infect. Immun.* **87**, e00540-18 (2019).

126. Tripathi, A. *et al.* Mycobacterium tuberculosis requires SufT for Fe-S cluster maturation, metabolism, and survival in vivo. *PLoS Pathog.* **18**, e1010475 (2022).

127. Rodriguez, G. M. & Smith, I. Identification of an ABC transporter required for iron acquisition and virulence in Mycobacterium tuberculosis. *J. Bacteriol.* **188**, 424–430 (2006).

128. Bajeli, S. *et al.* Terminal Respiratory Oxidases: A Targetables Vulnerability of Mycobacterial Bioenergetics? *Front. Cell. Infect. Microbiol.* **10**, 589318 (2020).

129. Estorninho, M. *et al.* ClgR regulation of chaperone and protease systems is essential for Mycobacterium tuberculosis parasitism of the macrophage. *Microbiology* **156**, 3445–3455 (2010).

130. He, H., Hovey, R., Kane, J., Singh, V. & Zahrt, T. C. MprAB is a stress-responsive two-component system that directly regulates expression of sigma factors SigB and SigE in Mycobacterium tuberculosis. *J. Bacteriol.* **188**, 2134–2143 (2006).

131. Kurthkoti, K. *et al.* The Capacity of Mycobacterium tuberculosis To Survive Iron Starvation Might Enable It To Persist in Iron-Deprived Microenvironments of Human Granulomas. *MBio* **8**, e01092-17 (2017).

132. Maciag, A. *et al.* Global analysis of the Mycobacterium tuberculosis Zur (FurB) regulon. *J. Bacteriol.* **189**, 730–740 (2007).

133. Li, X. *et al.* A novel stress-inducible CmtR-ESX3-Zn2+ regulatory pathway essential for survival of Mycobacterium bovis under oxidative stress. *J. Biol. Chem.* **295**, 17083–17099 (2020).

134. Voskuil, M. I. *et al.* Inhibition of respiration by nitric oxide induces a Mycobacterium tuberculosis dormancy program. *J. Exp. Med.* **198**, 705–713 (2003).

135. Gouzy, A., Poquet, Y. & Neyrolles, O. Nitrogen metabolism in Mycobacterium tuberculosis physiology and virulence. *Nat. Rev. Microbiol.* **12**, 729–737 (2014).

136. Read, R., Pashley, C. A., Smith, D. & Parish, T. The role of GlnD in ammonia assimilation in Mycobacterium tuberculosis. *Tuberculosis (Edinb).* **87**, 384–390 (2007).

137. Wilburn, K. M., Fieweger, R. A. & VanderVen, B. C. Cholesterol and fatty acids grease the wheels of Mycobacterium tuberculosis pathogenesis. *Pathog. Dis.* **76**, fty021 (2018).

138. Masiewicz, P., Brzostek, A., Wolański, M., Dziadek, J. & Zakrzewska-Czerwińska, J. A novel role of the PrpR as a transcription factor involved in the regulation of methylcitrate pathway in Mycobacterium tuberculosis. *PLoS One* **7**, e43651 (2012).

139. Theriault, M. E. *et al.* Iron limitation in M. tuberculosis has broad impact on central carbon metabolism. *Commun. Biol.* **5**, 685 (2022).

140. Chiarelli, L. R. *et al.* New insight into structure-activity of furan-based salicylate synthase (MbtI) inhibitors as potential antitubercular agents. *J. Enzyme Inhib. Med. Chem.* **34**, 823–828 (2019).

141. Koul, A. *et al.* Delayed bactericidal response of Mycobacterium tuberculosis to bedaquiline involves remodelling of bacterial metabolism. *Nat. Commun. 2014 51* **5**, 3369 (2014).

142. Dhillon, J., Andries, K., Phillips, P. P. J. & Mitchison, D. A. Bactericidal activity of the diarylquinoline TMC207 against Mycobacterium tuberculosis outside and within cells. *Tuberculosis (Edinb).* **90**, 301–305 (2010).

143. Parish, T. In vitro drug discovery models for Mycobacterium tuberculosis relevant for host infection. *Expert Opin. Drug Discov.* **15**, 349–358 (2020).

144. Cohen, N. R., Lobritz, M. A. & Collins, J. J. Microbial persistence and the road to drug resistance. *Cell Host Microbe* **13**, 632–642 (2013).

145. Mandal, S., Njikan, S., Kumar, A., Early, J. V & Parish, T. The relevance of persisters in tuberculosis drug discovery. *Microbiology* **165**, 492–499 (2019).

146. Tomas, M. *et al.* Tolerance and Persistence to Drugs: A Main Challenge in the Fight Against Mycobacterium tuberculosis. *Front. Microbiol.* **11**, 1924 (2020).

147. Du, D. *et al.* Multidrug efflux pumps: structure, function and regulation. *Nat. Rev. Microbiol.* **16**, 523–539 (2018).

148. Aínsa, J. A. *et al.* Molecular cloning and characterization of Tap, a putative multidrug efflux pump present in Mycobacterium fortuitum and Mycobacterium tuberculosis. *J. Bacteriol.* **180**, 5836–5843 (1998).

149. Ramón-García, S., Martín, C., Aínsa, J. A. & De Rossi, E. Characterization of tetracycline resistance mediated by the efflux pump Tap from Mycobacterium fortuitum. *J. Antimicrob. Chemother.* **57**, 252–259 (2006).

150. Adams, K. N. *et al.* Drug tolerance in replicating mycobacteria mediated by a macrophage-induced efflux mechanism. *Cell* **145**, 39–53 (2011).

151. Adams, K. N., Szumowski, J. D. & Ramakrishnan, L. Verapamil, and its metabolite norverapamil, inhibit macrophage-induced, bacterial efflux pump-mediated tolerance to multiple anti-tubercular drugs. *J. Infect. Dis.* **210**, 456–466 (2014).

152. Zhang, M. *et al.* Streptomycin-starved Mycobacterium tuberculosis 18b, a drug discovery tool for latent tuberculosis. *Antimicrob. Agents Chemother.* **56**, 5782–5789 (2012).

153. Arbués, A. *et al.* TNF-α antagonists differentially induce TGFβ1-dependent resuscitation of dormant-like Mycobacterium tuberculosis. *PLoS Pathog.* **16**, e1008312 (2020).

154. Kapoor, N. *et al.* Human Granuloma In Vitro Model, for TB Dormancy and Resuscitation. *PLoS One* **8**, e53657 (2013).

155. Arbués, A., Kammüller, M. & Portevin, D. Generating Three-dimensional Human Granulomas in vitro to Study Mycobacterium tuberculosis-Host Interaction. *Bio Protoc.* **10**, e3820 (2020).

156. Ramón-García, S. *et al.* Synergistic drug combinations for tuberculosis therapy identified by a novel high-throughput screen. *Antimicrob. Agents Chemother.* **55**, 3861–3869 (2011).

157. Chilakapati, J. & Mehendale, H. M. Butyrophenones. in *Encyclopedia of Toxicology: Third Edition* 604–608 (Academic Press, 2014). doi:10.1016/B978-0-12-386454-3.00265-7.

158. Weinstein, E. A. *et al.* Inhibitors of type II NADH:menaquinone oxidoreductase represent a class of antitubercular drugs. *Proc. Natl. Acad. Sci. U. S. A.* **102**, 4548–4553 (2005).

159. Rodrigues, L., Viveiros, M. & Aínsa, J. A. Measuring efflux and permeability in mycobacteria. *Methods Mol. Biol.* **1285**, 227–239 (2015).

160. Barone, J. A. Domperidone: a peripherally acting dopamine2-receptor antagonist. *Ann. Pharmacother.* **33**, 429–440 (1999).

161. Patteet, L. *et al.* Therapeutic drug monitoring of common antipsychotics. *Ther. Drug Monit.* **34**, 629–651 (2012).

162. Dubinsky, B. *et al.* Bromperidol, a new butyrophenone neuroleptic: a review. *Psychopharmacology (Berl).* **78**, 1–7 (1982).

163. Morris, R. P. *et al.* Ancestral antibiotic resistance in Mycobacterium tuberculosis. *Proc. Natl. Acad. Sci. U. S. A.* **102**, 12200–12205 (2005).

164. International Organization for Standardization. Biological evaluation of medical devices. Part 5: tests for in vitro cytotoxicity. ISO 10993-5:2009. International Organization for Standardization, Geneva, Switzerland. (2009).

165. Garton, N. J. *et al.* Cytological and Transcript Analyses Reveal Fat and Lazy Persister-Like Bacilli in Tuberculous Sputum. *PLOS Med.* **5**, e75 (2008).

166. Schuessler, D. L. *et al.* Induced ectopic expression of HigB toxin in Mycobacterium tuberculosis results in growth inhibition, reduced abundance of a subset of mRNAs and cleavage of tmRNA. *Mol. Microbiol.* **90**, 195–207 (2013).

167. Sala, A., Calderon, V., Bordes, P. & Genevaux, P. TAC from Mycobacterium tuberculosis: a paradigm for stress-responsive toxin-antitoxin systems controlled by SecB-like chaperones. *Cell Stress Chaperones* **18**, 129–135 (2013).

168. Armalyte, J., Jurenas, D., Krasauskas, R., Čepauskas, A. & Sužiedeliene, E. The higBA toxin-antitoxin module from the opportunistic pathogen Acinetobacter baumannii - Regulation, activity, and evolution. *Front. Microbiol.* **9**, 732 (2018).

169. Rustad, T. R., Sherrid, A. M., Minch, K. J. & Sherman, D. R. Hypoxia: a window into Mycobacterium tuberculosis latency. *Cell. Microbiol.* **11**, 1151–1159 (2009).

170. Shah, S., Cannon, J. R., Fenselau, C. & Briken, V. A Duplicated ESAT-6 Region of ESX-5 Is Involved in Protein Export and Virulence of Mycobacteria. *Infect. Immun.* **83**, 4349–4361 (2015).

171. Champion, P. A. *et al.* Modular Organization of the ESX-5 Secretion System in Mycobacterium tuberculosis. *Front. Cell. Infect. Microbiol.* **6**, 49 (2016).

172. Wilson, M. *et al.* Exploring drug-induced alterations in gene expression in Mycobacterium tuberculosis by microarray hybridization. *Proc. Natl. Acad. Sci. U. S. A.* **96**, 12833–12838 (1999).

173. Fisher, M. A., Plikaytis, B. B. & Shinnick, T. M. Microarray Analysis of the Mycobacterium tuberculosis Transcriptional Response to the Acidic Conditions Found in Phagosomes. *J. Bacteriol.* **184**, 4025–4032 (2002).

174. Ang, M. L. T. *et al.* EthA/R-independent killing of Mycobacterium tuberculosis by ethionamide. *Front. Microbiol.* **8**, 710 (2017).

175. Baulard, A. R. *et al.* Activation of the pro-drug ethionamide is regulated in mycobacteria. *J. Biol. Chem.* **275**, 28326–28331 (2000).

176. Healy, C., Gouzy, A. & Ehrt, S. Peptidoglycan Hydrolases RipA and Ami1 Are Critical for Replication and Persistence of Mycobacterium tuberculosis in the Host. *MBio* **11**, e03315-19 (2020).

177. Squeglia, F., Moreira, M., Ruggiero, A. & Berisio, R. The Cell Wall Hydrolytic NlpC/P60 Endopeptidases in Mycobacterial Cytokinesis: A Structural Perspective. *Cells* **8**, 609 (2019).

178. Raman, S., Hazra, R., Dascher, C. C. & Husson, R. N. Transcription Regulation by the Mycobacterium tuberculosis Alternative Sigma Factor SigD and Its Role in Virulence. *J. Bacteriol.* **186**, 6605–16 (2004).

179. Saint-Joanis, B. *et al.* Inactivation of Rv2525c, a Substrate of the Twin Arginine Translocation (Tat) System of Mycobacterium tuberculosis, Increases β-Lactam Susceptibility and Virulence. *J. Bacteriol.* **188**, 6669 (2006).

180. England, K., Crew, R. & Slayden, R. A. Mycobacterium tuberculosis septum site determining protein, Ssd encoded by rv3660c, promotes filamentation and elicits an alternative metabolic and dormancy stress response. *BMC Microbiol.* **11**, 79 (2011).

181. Lee, R. E. *et al.* Spectinamides: A New Class of Semisynthetic Anti-Tuberculosis Agents that Overcome Native Drug Efflux. *Nat. Med.* **20**, 152–158 (2014).

182. Omollo, C. *et al.* Developing synergistic drug combinations to restore antibiotic sensitivity in drug-resistant Mycobacterium tuberculosis. *Antimicrob. Agents Chemother.* **65**, e02554-20 (2021).

183. Machado, D. *et al.* Ion Channel Blockers as Antimicrobial Agents, Efflux Inhibitors, and Enhancers of Macrophage Killing Activity against Drug Resistant Mycobacterium tuberculosis. *PLoS One* **11**, e0149326 (2016).

184. Canezin, P. H. *et al.* Intramacrophage Mycobacterium tuberculosis efflux pump gene regulation after rifampicin and verapamil exposure. *J. Antimicrob. Chemother.* **73**, 1770–1776 (2018).

185. Villellas Arilla, M. C. A role of efflux pumps in intrinsic drug resistance and virulence of Mycobacterium tuberculosis. (PhD Thesis, University of Zaragoza, 2013).

186. Tizzano, B. *et al.* Survival of hypoxia-induced dormancy is not a common feature of all strains of the Mycobacterium tuberculosis complex. *Sci. Rep.* **11**, 2628 (2021).

187. Datsenko, K. A. & Wanner, B. L. One-step inactivation of chromosomal genes in Escherichia coli K-12 using PCR products. *Proc. Natl. Acad. Sci. U. S. A.* **97**, 6640–6645 (2000).

188. Brosch, R. *et al.* Use of a Mycobacterium tuberculosis H37Rv Bacterial Artificial Chromosome Library for Genome Mapping, Sequencing, and Comparative Genomics. *Infect. Immun.* **66**, 2221–2229 (1998).

189. Andreu, N. *et al.* Optimisation of bioluminescent reporters for use with mycobacteria. *PLoS One* **5**, e10777 (2010).

190. van Kessel, J. C. & Hatfull, G. F. Recombineering in Mycobacterium tuberculosis. *Nat. Methods* **4**, 147–152 (2007).

191. Lucía Quintana, A. Investigation of new mechanisms of intrinsic antibiotic resistance in mycobacteria. *PhD thesis* (University of Zaragoza, 2010).

192. Tal, N. & Schuldiner, S. A coordinated network of transporters with overlapping specificities provides a robust survival strategy. *Proc. Natl. Acad. Sci. U. S. A.* **106**, 9051–9056 (2009).

193. Montoro, E. *et al.* Comparative evaluation of the nitrate reduction assay, the MTT test, and the resazurin microtitre assay for drug susceptibility testing of clinical isolates of Mycobacterium tuberculosis. *J. Antimicrob. Chemother.* **55**, 500–505 (2005).

194. Odds, F. C. Synergy, antagonism, and what the chequerboard puts between them. *J. Antimicrob. Chemother.* **52**, 1 (2003).

195. van Soolingen, D., de Haas, P. E., Hermans, P. W. & van Embden, J. D. DNA fingerprinting of Mycobacterium tuberculosis. *Methods Enzymol.* **235**, 196–205 (1994).

196. Wards, B. J. & Collins, D. M. Electroporation at elevated temperatures substantially improves transformation efficiency of slow-growing mycobacteria. *FEMS Microbiol. Lett.* **145**, 101–105 (1996).

197. Andrews, S. FastQC A Quality Control tool for High Throughput Sequence Data. https://www.bioinformatics.babraham.ac.uk/projects/fastqc/.

198. Li, H. Aligning sequence reads, clone sequences and assembly contigs with BWA-MEM. *arXiv: Genomics* (2013) doi:10.48550/arxiv.1303.3997.

199. Li, H. *et al.* The Sequence Alignment/Map format and SAMtools. *Bioinformatics* **25**, 2078–2079 (2009).

200. Broad Institute. Picard Tools. http://broadinstitute.github.io/picard.

201. Milne, I. *et al.* Using tablet for visual exploration of second-generation sequencing data. *Brief. Bioinform.* **14**, 193–202 (2013).

202. Koboldt, D. C. *et al.* VarScan: variant detection in massively parallel sequencing of individual and pooled samples. *Bioinformatics* **25**, 2283–2285 (2009).

203. Cingolani, P. *et al.* A program for annotating and predicting the effects of single nucleotide polymorphisms, SnpEff: SNPs in the genome of Drosophila melanogaster strain w1118; iso-2; iso-3. *Fly (Austin).* **6**, 80–92 (2012).

204. Van der Auwera, G. A. & O'Connor, B. *Genomics in the Cloud: Using Docker, GATK, and WDL in Terra*. (O'Reilly Media, Inc., 2020).

205. Babraham Bioinformatics. Trim Galore. https://www.bioinformatics.babraham.ac.uk/projects/trim_galore/.

206. Bray, N. L., Pimentel, H., Melsted, P. & Pachter, L. Near-optimal probabilistic RNA-seq quantification. *Nat. Biotechnol.* **34**, 525–527 (2016).

207. Soneson, C., Love, M. I. & Robinson, M. D. Differential analyses for RNA-seq: transcript-level estimates improve gene-level inferences. *F1000Research* **4**, 1521 (2015).

208. Robinson, M. D., Mccarthy, D. J. & Smyth, G. K. edgeR: a Bioconductor package for differential expression analysis of digital gene expression data. *Bioinformatics* **26**, 139–140 (2010).

209. Ritchie, M. E. *et al.* limma powers differential expression analyses for RNA-sequencing and microarray studies. *Nucleic Acids Res.* **43**, e47 (2015).

210. Maere, S., Heymans, K. & Kuiper, M. BiNGO: a Cytoscape plugin to assess overrepresentation of Gene Ontology categories in Biological Networks. *Bioinformatics* **21**, 3448–3449 (2005).